



JOHANNES GUTENBERG
UNIVERSITÄT MAINZ

Dissertation

Small molecules targeting apoptosis and
parthanatos in sensitive and drug-resistant
tumor cells

Min Zhou

Mainz, August 2023

**Small molecules targeting apoptosis and parthanatos
in sensitive and drug-resistant tumor cells**

**Kumulative Dissertation
zur Erlangung des Grades**

**“Doktor der Naturwissenschaften”
im Promotionsfach Pharmazie**

**am Fachbereich Chemie, Pharmazie und
Geowissenschaften der Johannes Gutenberg-Universität in
Mainz**

**vorgelegt von Min Zhou
geboren am 01.29.1994 in China**

Mainz, August 2023

Betreuer:

Uni.-Prof. Dr. Thomas Efferth

Gutachter Der Arbeit:

Uni.-Prof. Dr. Thomas Efferth

Uni.-Prof. Dr. Kristina Friedland

Datum der mündlichen Prüfung:

04.10.2023

Prüfungskommission:

Uni.-Prof. Dr. Peter Langguth (Vorsitzende)

Uni.-Prof. Dr. Thomas Efferth

Uni.-Prof. Dr. Kristina Friedland

Frau Dr. Xiaohua Lu (Protokoll)

List of publications

Publications as first author

M. Zhou, J.C. Boulos, S. Klauck, T. Efferth, The novel cardiac glycosides ZINC253504760 induces parthanatos-type cell death and G2/M arrest via downregulating MEK1/2 phosphorylation in CCRF-CEM leukemia cells. *Cell Biology and Toxicology* (2023) 1-27.

M. Zhou, J.C. Boulos, H.A. Rudbari, T. Schirmeister, N. Micale, T. Efferth, Two palladium (II) complexes derived from halogen-substituted Schiff bases and 2-picolylamine induce parthanatos-type cell death in sensitive and multi-drug resistant CCRF-CEM leukemia cells. *European Journal of Pharmacology* 956 (2023) 175980.

M. Zhou, J.C. Boulos, E. Omer, S. Klauck, T. Efferth, Modes of action of a novel c-MYC inhibiting 1,2,4-oxadiazol derivative in leukemia and breast cancer cells. *Molecules* 28(15) (2023) 5658.

M. Zhou, A. Varol, T. Efferth, Multi-omics approaches to improve malaria therapy, *Pharmacological Research*. 167 (2021) 105570.

Publications as co-author

M. Elbadawi, J.C. Boulos, M. Dawood, **M. Zhou**, W. Gul, M.A. ElSohly, S.M. Klauck, T. Efferth, The Novel Artemisinin Dimer Isoniazide ELI-XXIII-98-2 Induces c-MYC Inhibition, DNA Damage, and Autophagy in Leukemia Cells, *Pharmaceutics* 15(4) (2023) 1107.

H.A. Rudbari, N. Kordestani, J.V. Cuevas-Vicario, **M. Zhou**, T. Efferth, I. Correia, T. Schirmeister, F. Barthels, M. Enamullah, A.R. Fernandes, Investigation of the influence of chirality and halogen atoms on the anticancer activity of enantiopure palladium (II) complexes derived from chiral amino-alcohol Schiff bases and 2-picolylamine, *New Journal of Chemistry* 46(14) (2022) 6470-6483.

C. Di Chio, **M. Zhou**, T. Efferth, T. Schirmeister, M. Zappalà, R. Ettari, Synthesis and Cytotoxicity of Diarylpentanoids against Sensitive CCRF-CEM and Multidrug-Resistant CEM/ADR5000 Leukemia Cells, *Chemistry & Biodiversity* 19(2) (2022) e202100451.

Conference papers

1. 6th Cancer World Congress, Lisbon, Portugal, Sep 28-30, 2022. Presentation: Cytotoxicity of ZINC253504760 in CCRF-CEM leukemia cells through inhibition of MEK1/2 phosphorylation, G2/M cell cycle arrest, and the induction of parthanatos-type cell death". (Best Flash Oral Presentation of Young Researcher)
2. 7th Cancer World Congress, Palermo, Italy, May 29-31, 2023. Presentation: The mode of action of a 1,2,4-oxadiazole derivative as c-MYC inhibitor in leukemia and breast cancer cells.

Contribution to articles included in the thesis

1. **Title:** The cardiac glycoside ZINC253504760 induces parthanatos-type cell death and G2/M arrest via downregulation of MEK1/2 phosphorylation in leukemia cells.

Contribution:

- 1) Conceptualization and methodology.
- 2) Conduction of experiments including growth inhibition assay, RNA extraction, qRT-PCR, cell cycle, apoptosis, fluorescence microscopy of the microtubule cytoskeleton, protein extraction and western blot, mitochondrial membrane potential, immunofluorescence microscopy of AIF translocation, single cell gel electrophoresis (comet assay), molecular docking, ROS detection, microscale thermophoresis.
- 3) Data curation, visualization, and data presentation of all Figures 1-7.
- 4) Writing the original manuscript.

2. **Title:** Two palladium (II) complexes derived from halogen-substituted Schiff bases and 2-picolylamine induce parthanatos-type cell death in sensitive and multi-drug resistant CCRF-CEM leukemia cells.

Contribution:

- 1) Conceptualization and methodology.
- 2) Conduction of experiments including isolation and cytotoxicity of human peripheral mononuclear cells, apoptosis, mitochondrial membrane potential, protein extraction and western blotting, immunofluorescence microscopy of AIF translocation, immunofluorescence microscopy of AIF and mitochondria staining, single cell gel electrophoresis (comet assay), cytotoxicity in the combination with PARP inhibitor.
- 3) Data curation, visualization, and data presentation of all Figures 1-10.
- 4) Writing the original manuscript.

3. **Title:** Modes of action of a novel c-MYC inhibiting 1,2,4-oxadiazole derivative in leukemia and breast cancer cells.

Contribution:

- 1) Conceptualization and methodology.

- 2) Conduction of experiments including growth inhibition assay, molecular docking, microscale thermophoresis, RNA extraction, qRT-PCR, cell cycle, apoptosis, single cell gel electrophoresis (comet assay), protein extraction and western blotting, doxorubicin uptake assay.
- 3) Data curation, visualization, and data presentation of all Figures 1-11, except Figure 2G.
- 4) Writing the original manuscript.

Erklärung

Hiermit erkläre ich an Eides statt, dass ich diese Arbeit selbständig verfasst und keine anderen als die angegebenen Quellen und Hilfsmittel verwendet habe.

Mainz, 15. 08. 2023

Ort, Datum

周敏

Min Zhou

Acknowledgment

Time is the best gift for me. Five years ago, when I decided to study the anticancer activity of medical plants, I applied to Prof. Dr Thomas Efferth. The following life in Germany, the food, the weather, the environment, the people, everything was new but exciting to me. Now it is my graduation.

My sincere and hearty appreciations go firstly to my supervisor. Prof. Dr. Thomas Efferth, who gave me this cherished opportunity to be a Ph.D candidate, work in an excellent international group, and experienced a rich and wonderful life in Mainz, Germany. It has been a great privilege and joy to study under his guidance and supervision, which brought me into the field of studying pharmaceutical biology about cancer. He constantly guided me in the correct direction with his wisdom and expertise, helped me move into new steps, and we shared progress and challenges regularly. I vividly remember the first time I verified our hypothesis (the treated cells induced parthanatos), how beautiful the sunset was when I reported to him, and how much happy we were! It is my honor to benefit from his personality, diligence, and encouragement, which I will treasure my whole life. My gratitude to Prof. Efferth knows no bounds.

I would like to thank Prof. Dr. Peter Langguth, Prof. Dr. Kristina Friedland, and Prof. Dr. Thomas Efferth for becoming my Ph. D defense committee members, reviewing my thesis, and taking part in my defense.

Thanks to the Chinese Scholar Council (CSC) for the financial support of my Ph. D life in Germany. This scholarship allows me to focus on study without distractions, and it encourages me to improve my overall research skills. Thanks to the teachers of the Generalkonsulat der Volksrepublik China in Frankfurt a. Main for their service to us Chinese students. Many greetings and helps deliver our country's care.

Sincere gratitude should also go to Prof. Dr. Tanja Schirmeister, Dr. Sabine M. Klauck, Prof. Nicola Micale, and Prof. Hadi Amiri Rudbari for their collaborations in my projects. Their detailed feedback and corrections of manuscripts have been supporting me to solve problems and improve my articles in a scientific way. I am thankful to the scientists in IMB for their technical support in flow cytometry and microscopy, their suggestions and clearing up confusion help me gain better lab skills.

I would like to express my warm gratitude to all group members of the Department of Pharmaceutical Biology. Thanks to Dr. Mona Dawood who taught me cell culture and resazurin assay, this was my first lesson beginning in the cell culture room. Thanks to Mohamed Elbadawi who showed me IPA analysis and qRT-PCR, and we discussed potential pathways and targets, as well as many urgent occasions I need help, he was here. Thanks to Dr. Xiaohua Lu for her help in the lab and for my life. Thanks to Joelle C. Boulos for her showing me many important experiments, the efforts we spent in the lab were all about our exciting explorations, and we were happy for each other's nice progress. My cordial thanks to the support and encouragement from Nasim Shahhamzehei, Ejlal Omer, Roxana Damiescu, Chunmei Jin, Matteo Rosellini, Assia Drif, Dr. Rümeyza Yücer, and so forth. There are also many thanks that will not be forgotten to our previous group members Dr. Onat Kadioglu, Dr. Mohamed Elfatih Saeed, Dr. Sara Abdelfatah, Dr. Nuha Mahmoud, and Dr. Nadire Özenver, they were generous in helping me in the early stage of my PhD. I also want to thank our secretary, Ms. Elena Zigutkin and Ms. Christine Böslér-Uzman for their patience and willingness for helping me at the university administration.

Thanks to my Chinese friends who had been in Germany, Dr. Chunlun Hong, Dr. Ge Yan, Dr. Yuanping Hai, Dr. Yuhuan Yuan, and Xizhi Huang.

I would love to extremely express my appreciation to my beloved family, my father, my mother, my twin sister, and my brother-in-law. I thank you from the bottom of my heart for staying healthy, happy, and positive. For four years, I was unable to return home due to the pandemic, missed too much happiness, and felt too much guilty that I could not be with you. But you always give me the greatest hope, inner strength, and faith. I believe that we can finally be reunited.

I would thank my husband Feng Jiang, who accompanies me to Germany and also obtained his doctoral degree in the summer of this year. Thanks for his love. His enthusiasm for life makes me realize how wonderful it is and makes me determined to be the best I can be. We enjoyed life in Germany, we also traveled to 10 countries across Europe, Africa, and North America, and we preserved plenty of precious memories.

Last but not least, I would like to thank time, for witnessing my growth, and making me brave, strong, and committed to my ideals.

Min Zhou 周敏

Mainz, in July 2023

Abstract

Resisting cell death is one of the hallmarks of carcinogenesis, especially when it is relevant to tumor proliferation pathways and oncogene overexpression. Deregulation of cell death mechanisms (*e.g.*, anti-apoptotic modalities) during cancer therapy also contributes to tumors that display multidrug resistance (MDR), which is a challenging obstacle for successful treatments. The aim of this thesis is two parts: 1) which novel cell death mechanisms that bypass apoptosis can be induced by three synthetic compounds (cardenolide derivative, palladium (II) complexes), 2) how does a natural product derivative of 1,2,4-oxadiazole inhibit the oncogene *c-MYC* and promotes apoptosis. These investigations in both drug-sensitive and -resistant cancer cells would be a promising way to overcome tumor resistance to apoptosis.

The compound ZINC253504760 showed potent cytotoxicity to different drug-sensitive and multidrug-resistant cell lines, which showed the most lethal effect in CCRF-CEM cells. Transcriptome-wide mRNA expression profiling and pathway analysis pointed out a canonical pathway involved in G2/M phase cell cycle arrest, which was predicted to be linked with MEK1/2 and ERK in the network analysis. Afterward, G2/M phase arrest was measured by flow cytometry in a time- and concentration-dependent manner, which was supported by the microtubule-destabilizing observation using fluorescence microscopy. Interestingly, apoptosis was not the predominant mode of cell death observed by flow cytometry, nor was it autophagy. Using western blotting, ZINC253504760 induced parthanatos accompanied by p-histone H2A.X, PARP, and PAR accumulation, leading to the translocation of AIF from the cytoplasm to the nucleus. The dissipation of the mitochondrial membrane potential, AIF translocation, and DNA damage were further confirmed by flow cytometry, immunofluorescence microscopy, and alkaline single cell electrophoresis. Moreover, ZINC253504760 inhibited the phosphorylation of MEK1/2, which further affected the activation of ERK. Molecular docking also showed ZINC253504760 as an ATP competitive kinase inhibitor bound to the phosphorylation sites of MEK1 and MEK2. Their binding was confirmed in microscale thermophoresis (MST). Therefore, ZINC253504760 induced parthanatos as a major mode of cell death and downregulated MEK1/2 phosphorylation.

Palladium (II) complexes J4 and J6 induced parthanatos-type cell death in CCRF-CEM and its multidrug-resistant CEM/ADR5000 cells. The biomarker p-histone H2A.X, PARP, and PAR were clearly hyperactivated by J4 and J6, followed by AIF translocated into the nucleus, mitochondrial membrane potential dysfunction, and large-scale DNA fragmentation. Furthermore, J4 and J6 specifically suppressed leukemia cells, but not healthy leukocytes.

Therefore, J4 and J6 triggered parthanatos for cell death, which offers the prospect of more effective treatment of malignancies with drug resistance that are hampered by the inability to cause cell death.

The 1,2,4-oxadiazoles derivative ZINC15675948 showed profound cytotoxicity towards CCRF-CEM and MDA-MB-231-pcDNA3 cells, while it was cross-resistant in P-glycoprotein-overexpressing CEM/ADR5000 cells and BCRP-overexpressing MDA-MB-BCRP cells. MST and molecular docking revealed a strong binding of ZINC15675948 to c-MYC with an interaction close to the c-MYC/MAX interface. C-MYC reporter assay and western blotting showed a downregulation of c-MYC by ZINC15675948 in a concentration-dependent manner. Furthermore, ZINC15675948 induced apoptosis and DNA damage in leukemia and breast cancer cell lines. Autophagy induction was only observed in CCRF-CEM cells. ZINC15675948 also caused G2/M phase or S phase arrest in CCRF-CEM cells or MDA-MB-231-pcDNA3 cells, accompanied by the downregulation of CDK1 or p-CDK2 in western blotting. Additionally, the microarray profiling of MDA-MB-231-pcDNA3 cells revealed an involvement of ubiquitination toward c-MYC, indicated by the upregulation of a novel ubiquitin ligase (ELL2) in the absence of c-MYC expression. Therefore, ZINC15675948 promoted apoptosis in c-MYC-driven cancers by targeting c-MYC.

Zusammenfassung

Die Resistenz gegen den Zelltod ist eines der Kennzeichen der Karzinogenese, insbesondere im Zusammenhang mit der Tumorproliferation und der Überexpression von Onkogenen. Die Deregulierung von Zelltod-Mechanismen (z.B. anti-apoptotische Modalitäten) während der Krebstherapie trägt auch dazu bei, dass Tumore eine Multidrug-Resistenz (MDR) aufweisen, was eine Herausforderung für eine erfolgreiche Behandlung darstellt. Das Ziel dieser Arbeit besteht aus zwei Teilen: 1) ob und welche neuartigen Zelltodmechanismen, welche die Apoptose umgehen, durch drei synthetische Verbindungen (Cardenolid-Derivat, Palladium(II)-Komplexe) induziert werden können, 2) wie ein Derivat des Naturproduktes 1,2,4-Oxadiazol das Onkogen c-MYC hemmt und die Apoptose fördert. Diese Untersuchungen sowohl an medikamentenempfindlichen als auch -resistenten Krebszellen wären ein vielversprechender Weg zur Überwindung der Tumorresistenz gegen Apoptose.

ZINC253504760 zeigte eine starke Zytotoxizität bei verschiedenen medikamentenempfindlichen und -resistenten Zelllinien, wobei die stärkste Wirkung bei CCRF-CEM-Zellen zu beobachten war. Die transkriptomweite mRNA-Expressionsprofilierung und die Analyse der Signalwege wiesen auf einen kanonischen Signalweg hin, der an der Zellzyklus-Arretierung in der G2/M-Phase beteiligt ist und mit MEK1/2 und ERK in der Netzwerk-Analyse verbunden war. Anschließend wurde der G2/M-Phasenstillstand mittels Durchflusszytometrie zeit- und konzentrationsabhängig gemessen, was durch die Beobachtung der Mikrotubuli-Destabilisierung mittels Fluoreszenzmikroskopie unterstützt wurde. Interessanterweise war Apoptose nicht die vorherrschende Form des Zelltods, die mittels Durchflusszytometrie beobachtet wurde, ebenso wenig wie Autophagie. Im Western Blot induzierte ZINC253504760 Parthanatos, begleitet von einer schnellen Akkumulation von p-Histon H2A.X, PARP und PAR, was zu einer Verlagerung von AIF aus dem Zytoplasma in den Zellkern führte. Der Abbau des mitochondrialen Membranpotenzials, die AIF-Translokation und die DNA-Schäden wurden durch Durchflusszytometrie, Immunfluoreszenzmikroskopie und alkalische Einzelzellenelektrophorese bestätigt. Darüber hinaus hemmte ZINC253504760 die Phosphorylierung von MEK1/2, was wiederum die Aktivierung von ERK beeinträchtigte. Molekulares Docking zeigte außerdem, dass ZINC253504760 als ATP-kompetitiver Kinaseinhibitor an die Phosphorylierungsstellen von MEK1 und MEK2 bindet, was durch mikroskalige Thermophorese (MST) bestätigt wurde. Daher induzierte ZINC253504760 Pathanatos als Hauptmodus des Zelltods und regulierte die MEK1/2-Phosphorylierung herunter.

Die Palladium(II)-Komplexe J4 und J6 lösten in CCRF-CEM- und multiresistenten CEM/ADR5000-Zellen einen parthanatischen Zelltod aus. Der Biomarker p-Histon H2A.X, PARP und PAR wurden durch J4 und J6 eindeutig hyperaktiviert, gefolgt von einer Verlagerung von AIF in den Zellkern, einer Störung des mitochondrialen Membranpotenzials und einer großflächigen DNA-Fragmentierung. Darüber hinaus unterdrücken J4 und J6 spezifisch Leukämiezellen, jedoch nicht gesunde Leukozyten. Daher lösten J4 und J6 Parthanatos für den Zelltod aus, was die Aussicht auf eine wirksamere Behandlung bösartiger Erkrankungen mit Arzneimittelresistenz bietet, die durch die Unfähigkeit, den Zelltod herbeizuführen, behindert wird.

Das 1,2,4-Oxadiazol-Derivat ZINC15675948 zeigte eine ausgeprägte Zytotoxizität in CCRF-CEM- und MDA-MB-231-pcDNA3-Zellen, während es in P-Glykoprotein-überexprimierenden CEM/ADR5000-Zellen und BCRP-überexprimierenden MDA-MB-BCRP-Zellen kreuzresistent war. MST und molekulares Docking zeigten eine starke Bindung von ZINC15675948 an c-MYC mit einer Interaktion nahe der c-MYC/MAX-Schnittstelle. C-MYC-Reporter-Assay und Western Blotting zeigten eine konzentrationsabhängige Downregulation von c-MYC durch ZINC15675948. Darüber hinaus induzierte ZINC15675948 Apoptose und DNA-Schäden in Leukämie- und Brustkrebszelllinien. Eine Induktion der Autophagie wurde nur in CCRF-CEM-Zellen beobachtet. ZINC15675948 verursachte auch einen G2/M- oder S-Phasen-Arrest in CCRF-CEM-Zellen oder MDA-MB-231-pcDNA3-Zellen, begleitet von einer Herunterregulation von CDK1 oder p-CDK2 im Western Blotting. Darüber hinaus zeigte das Microarray-Profilung von MDA-MB-231-pcDNA3-Zellen eine Beteiligung der Ubiquitinierung von c-MYC, was durch die Hochregulierung einer neuartigen Ubiquitin-Ligase (ELL2) in Abwesenheit der c-MYC-Expression angezeigt wurde. Daher förderte ZINC15675948 die Apoptose bei c-MYC-gesteuerten Krebsarten, indem es auf c-MYC abzielte.

Table of contents

Acknowledgment	I
Abstract	III
Zusammenfassung	V
Table of contents	VII
1 Introduction	1
1.1 Cancer	1
1.2 Cancer treatment	3
1.2.1 Classical chemotherapy	4
1.2.2 Targeted therapy	6
1.3 Mechanisms of drug resistance	9
1.3.1 Multidrug resistance by ABC transporters	9
1.3.2 Apoptosis resistance	11
1.4 Targeting of cell death pathways for cancer therapy	13
1.4.1 Apoptosis	14
1.4.2 Parthanatos	17
1.4.3 Autophagy and other modes of cell death	18
1.5 The relevance of MEK1/2 for apoptosis in cancer therapy	20
1.5.1 The RAS-RAF-MEK-ERK (MAPK) cascade in cancer	20
1.5.2 MEK1/2 as targets for cancer treatment	22
1.6 The relevance of c-MYC for apoptosis in cancer therapy	24
1.6.1 the c-MYC oncogene in cancer	24
1.6.2 c-MYC as a target for cancer treatment	27
1.7 Parthanatos-inducing compounds in cancer cells	28
2 Objective of the thesis	32
3 Results and discussion	33

3.1 Cardiac glycoside (ZINC253504760), a novel MEK1/2 inhibitor inducing a state-of-art parthanatic cell death and G2/M arrest in leukemia cells	33
3.2 Palladium(II) complexes induced parthanatos-type cell death in CCRF-CEM leukemia and its multidrug-resistant cells.....	34
3.3 1,2,4-oxadiazole derivative (ZINC15675948) as a novel c-MYC inhibitor by inducing DNA damage, cell cycle arrest, and apoptosis in leukemia and breast cancer cells	35
4 Conclusion.....	37
5 Reference.....	38
6. Appendices (published articles)	47
Curriculum Vitae of Min Zhou.....	48

1 Introduction

1.1 Cancer

Cancer is a disease caused by cells dividing uncontrollably and spreading into surrounding tissues. In about two-thirds of the world's countries, cancer is the first or second leading cause of mortality before the age of 70 (**Figure 1**). According to the World Health Organization (WHO), the number of new cases globally was estimated to be 19.3 million, with 10 million cancer death in 2020 (1). Approximately one-half of all cases and 58.3% of cancer death occur in Asia, which reside 60% of the world's population, followed by Europe and America. Female breast cancer (11.7 %), lung cancer (11.4 %), and colon cancer (10.0 %) are the top diagnosed cancer types. Lung cancer (18%) accounts for the highest cancer mortality (1). Some cancers are commonly diagnosed in children and adolescents, including leukemia, brain tumor, and lymphoma.

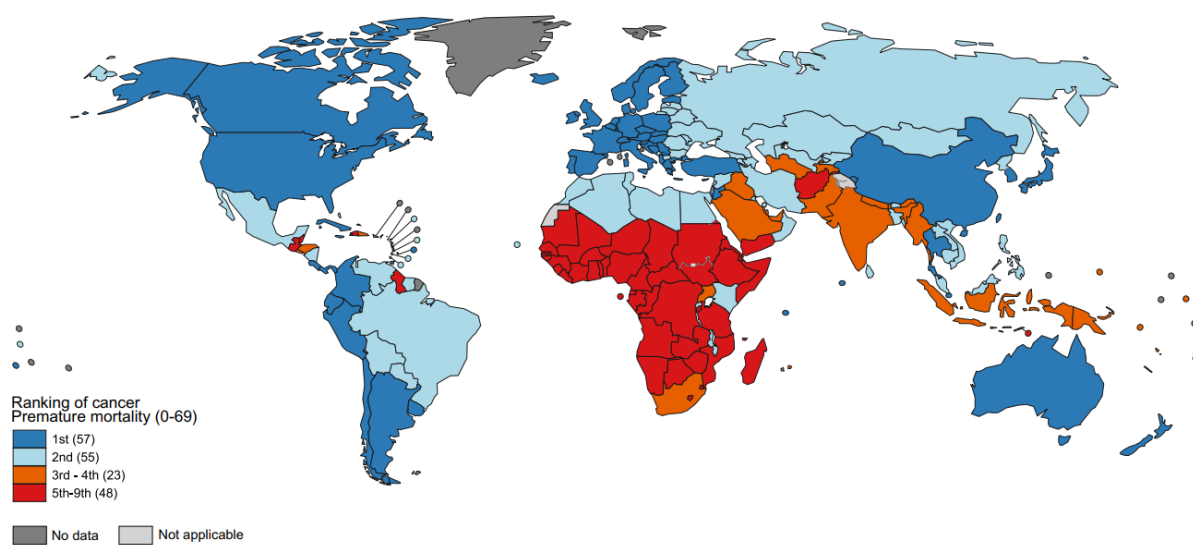


Figure 1. National ranking of cancer as a leading cause of death for people under 70 in 2019. (1)

Cancer has more than 100 different types, they can be broadly divided into six groups from a histological perspective: carcinoma, sarcoma, leukemia, lymphoma, myeloma, and mixed types (2). Carcinoma is a form of cancer that develops from epithelial cells, which are the cells that constitute the tissue that covers the surface of organs, glands, and other structures in the body. Carcinoma accounts for 80-90% of all cancer cases (3). Sarcoma refers to cancer of supporting

and connective tissues, such as bones, muscles, tendons, cartilage, and fat (4). Leukemias (“blood cancers”) are cancers developing in the bone marrow that are often associated with rapidly multiplying immature white blood cells. As a result, the production and function of normal blood cells, including white blood cells, red blood cells, and platelets are hampered. The patient is frequently at risk for infection and fatigue (5). Lymphomas originate in the glands or nodes of the lymphatic system, which is primarily responsible for cleaning bodily fluids and producing white blood cells that fight infections (6). Multiple myeloma is characterized by aberrant clonal plasma cells that possess the potential to expand out of control in the bone marrow. It causes anemia, hypercalcemia, acute kidney injury, and destructive osseous bone lesions (7). The mixed type may be within one or from different categories, such as carcinosarcoma and adenoid cystic carcinoma.

Tumor initiation and progression are a process that normal cells transform into a metastatic cancer cell. Two decades ago, the landmark paper has been highlighted six enabling features (“hallmarks”) concerning the acquired functional capabilities that allow cancer cells to uncontrollably proliferate and survive: sustaining proliferative signaling, resisting cell death, inducing angiogenesis, enabling replicative immortality, evading growth suppressors, and activating invasion and metastasis (8). Since then, it has been evident that tumor is also contributed by reprogramming cellular energy metabolism and avoiding immune destruction. Meanwhile, there are probably two enabling characteristics that facilitate their acquisition for tumorigenesis: genomic instability and tumor-promoting inflammation (9). Furthermore, the latest study proposed four possibly emerging hallmarks and enabling characteristics, involving unlocking phenotypic plasticity, non-mutational epigenetic reprogramming, polymorphic microbiomes, and senescent cells, which could be incorporated into the hallmarks of cancer after further validation (10). The canonical and prospective new additions to the “Hallmarks of cancer” are shown in **Figure 2**. These aberrations have been recognized as essential principle in the treatment of cancer.

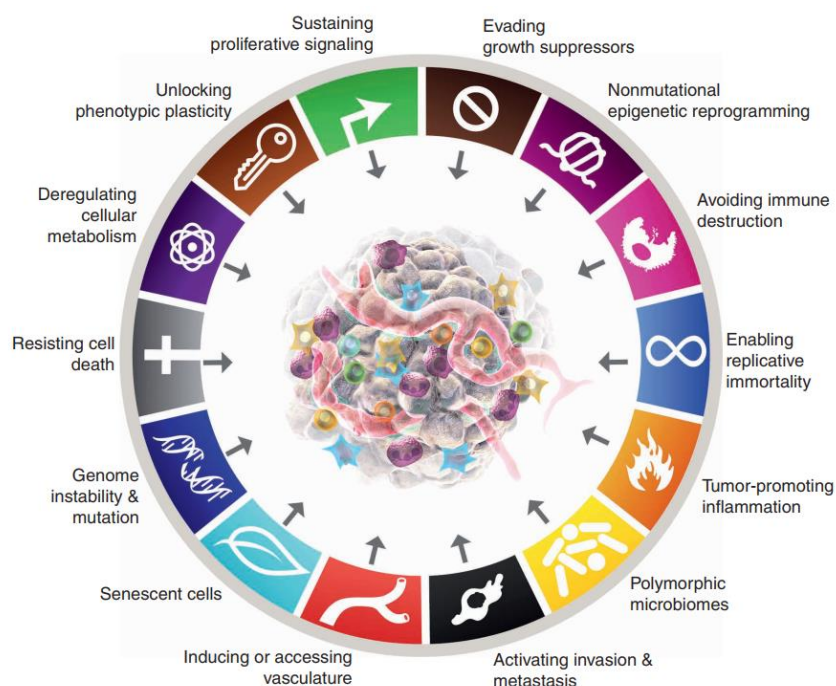


Figure 2. Hallmarks of cancer with new additions. Canonical and prospective new additions to the “Hallmarks of cancer”. (10)

1.2Cancer treatment

The treatment of cancer depends on the cancer types and stages, the patient’s health status, and individual preferences. Currently, the main strategies of cancer treatment include surgery, radiation therapy, chemotherapy, immunotherapy, targeted therapy, and hormone therapy. Cancer surgery involves the removal of the tumor and surrounding tissues. It is the earliest oncological discipline, with descriptions of the removal of breast tumors dating back to ancient Egypt (1600 BC). The surgery for local tumor excision progresses commonly in breast, gastric, colorectal, esophageal, and neurological cancers (11). Surgery also provides prevention of tumorigenesis, including screening-associated surgery for premalignant conditions, and prophylactic surgery in high-risk people with heritable genetic disorders (12). Radiation is a physical agent and aims to target aberrant cancer cells with the maximum radiation dose while minimizing exposure to healthy cells (13). The radiation used is referred to as ionizing radiation. It deposits energy to damage the DNA of the cells and thus block further cell division and lead to cell death (14). Apoptosis and mitotic cell death account for the major types of cell death induced by radiation therapy to exhibit therapeutic effects (13). Immunotherapy provides passive or active immunity to target tumors by reactivating and harnessing the immune system (15). The passive immunotherapy applies effector molecules to direct attack tumor cells, such

as antibodies and genetically engineered T cells (chimeric antigen receptor [CAR]-T). The active immunotherapy is to enhance immune system activation through the modulation of endogenous regulation (16). Hormonal therapy is the administration of exogenous hormones that manipulate the endocrine system in patients with hormone-dependent cancer. Hormones are chemical messengers released by certain endocrine system organs to act on gene expression and cell proliferation (17). A high level of specific hormone therefore raises the probability of neoplastic transformation. Tumors caused by hormonal dysregulation include prostate, endometrial, ovarian and breast cancer, and uterine sarcomas (18). The following paragraphs will focus on classical chemotherapy and targeted chemotherapy.

1.2.1 Classical chemotherapy

In the early 1900s, the use of chemicals to treat disease was defined as “chemotherapy” by the German chemist Paul Ehrlich. During World War II, an accidental leakage of sulfur mustard from a bombed ship led to the discovery that both bone marrow and lymph nodes had significantly declined in those personnel exposed to the mustard gas. Then, the management of lymphomas by nitrogen mustard observed remarkable regression of lymphoid tumors, which brought great initiation to the development of chemotherapy for cancer (19-21). Currently, chemotherapy with cytotoxic anticancer agents is the mainstay of therapy in cancer treatment. Most chemotherapy drugs act by killing or inhibiting the growth of cancer cells through an interaction with DNA or preventing chromosomal replication, this further prevents cell division and leads to programmed cell death (apoptosis) (22). However, due to the poor selectivity for malignant cells over normal tissue, cytotoxic chemotherapy agents cause a series of severe side effects, such as gastrointestinal toxicity, ototoxicity, hepatotoxicity, and nephrotoxicity (23). Chemotherapy drugs are classified into different types:

1) DNA-binding substance: DNA is the most extensive target of anti-cancer compounds. When exogenous chemicals that bind to DNA alter the structure of nucleic acid, which in turn affects DNA-interacting enzymes or transcription factors, disturbing cell cycle and affecting DNA replication, cell division, and cell proliferation (24). The types of DNA-binding substances are as below:

a) Topoisomerase inhibitors: DNA topoisomerases (TOPO) are crucial enzymes that catalyze the modification of DNA topology for DNA replication. Topoisomerase activity is particularly elevated in rapidly dividing cells, such as cancer cells. There are two types of topoisomerases:

type I, which breaks single-stranded DNA, and type II, which cuts double-stranded DNA. Various anticancer drugs act as TOPO poison inhibitors, trapping covalent complexes of human TOPOs, leading to DNA damage and cell death (25).

The DNA topoisomerase I inhibitors (*e.g.*, camptothecin, topotecan, and irinotecan): alternating the DNA topology by breaking the phosphodiester bonds between nucleotides in DNA strands is the fundamental mechanism for this class of anticancer drugs. Camptothecin was the first compound demonstrated to target topoisomerase I. It is a natural product that was isolated from the bark and stem of *Camptotheca acuminata* ('tree of joy'). Clinical-approved topotecan and irinotecan are analogs of camptothecin. DNA topoisomerase I inhibitors are commonly applied in lung cancers, however, they exhibit notable dose-limiting toxicity, and cancer cells develop drug resistance (26).

The DNA topoisomerase II inhibitors include anthracyclines (*e.g.*, doxorubicin, daunorubicin, epirubicin, and idarubicin) and epipodophyllotoxins (*e.g.*, etoposide, etopophos, and teniposide). Cutting both DNA stands is the main mechanism by which DNA topoisomerase II inhibitors disrupt DNA topology. Especially, anthracyclines involve in binding to DNA by inserting a polycyclic aromatic moiety between base pairs, at the same time extending and unwinding the helix. DNA topoisomerase II inhibitors are effective against leukemia, lymphomas, sarcomas, and breast carcinoma. However, they were hampered by the development of drug resistance and cardiotoxicity. Treatment with DNA topoisomerase II inhibitors can cause secondary malignancies such as acute myeloid leukemia (27, 28).

b) Alkylating agents (*e.g.*, chlorambucil, melphalan, cyclophosphamide, and ifosfamide): form covalent bond structures with DNA and cause single-strand or double-strand DNA breaks. These drugs are extensively used in leukemias, lymphomas, and solid tumors. Most alkylating agents cause gastrointestinal side effects and dose-limiting bone marrow toxicity (29).

c) Platinum (*e.g.*, cisplatin, carboplatin, and oxaliplatin) The mechanism of action of cisplatin is mediated by its binding with DNA to generate DNA lesions and block DNA synthesis, which suppresses RNA transcription and arrests the cell cycle, therefore inducing the activation of apoptosis (30). Cisplatin has been widely applied as adjuvant therapy in the treatment of a spectrum of cancers, such as ovarian, cervix, bladder, small and non-small cell lung cancers, Hodgkin's and non-Hodgkin's lymphomas, and melanoma (31). The major toxicities of cisplatin include general cell-damaging effects, nephrotoxicity, hepatotoxicity, neurotoxicity, and hearing loss (32). Despite emerging newer platinum-based complexes, only carboplatin and oxaliplatin received approval for clinical practice.

2) Microtubule inhibitors: this group is referred to as mitotic poisons, because they interfere with microtubule dynamics, leading to chromosomal dysregulation, aberrant spindle formation, and ultimately cell death due to mitotic failure. Microtubule inhibitors are categorized into microtubule-destabilizing agents (*Vinca* alkaloids, *e.g.*, vinblastine and vincristine) and microtubule-stabilizing agents (Taxanes, *e.g.*, paclitaxel and docetaxel). However, they are associated with cardiotoxicity (33).

3) Antimetabolites: The early discovery by Sidney Farber found that aminopterin helped acute lymphoblastic leukemia relief in children and promoted the development of the drug class of antimetabolites (34). Antimetabolites are small molecules structurally similar to nucleotide metabolites, they interfere with critical enzymes that are used for DNA synthesis, thereby causing DNA damage, and induction of apoptosis. Notable examples include folate antagonists (*e.g.*, methotrexate), purine antagonists (*e.g.*, thioguanine, 6-TG), pyrimidine antagonists (*e.g.*, fluorouracil, 5-FU), and other nucleoside analogs (*e.g.*, gemcitabine and cytarabine) (35).

4) Antihormones: some breast cancers are known as hormone-sensitive (or hormone-dependent) breast cancers, are driven by estrogen and progesterone. Various antihormones therapies have been approved by FDA, such as tamoxifen treated in estrogen-positive early-stage breast cancer of premenopausal women, and aromatase inhibitors (*e.g.*, letrozole) used in postmenopausal women. Hot flashes and night sweats are common side effects (36).

1.2.2 Targeted therapy

Targeted therapy refers to blocking specific biological transduction pathways or cancer proteins that are involved in tumor growth, progression, and metastasis. The molecular targets (*e.g.*, receptors, growth factors, kinase cascades, cell cycle proteins, or modulators of apoptosis) present in healthy tissue but are mutated or overexpressed in cancer (37). The aim of targeted therapy is to inhibit one of the capabilities in hallmarks of cancer, impair uncontrolled tumor growth and progression, lead to the death of cancer cells, and avoid undesirable side effects (9). The outstanding clinical success of targeted therapy is witnessed by the Food and Drug Administration (FDA), which has approved a growing number of drugs in the oncology area in recent two decades. The types of targeted therapy can be classified into 1) small molecules; 2) monoclonal antibodies; 3) cancer vaccines; 4) gene therapy.

1) Small molecules

Small molecules are substances with low molecular weight (less than 800 Dalton) that can access cells to interfere with signaling pathways and act on targets inside the cells. They have “ib” as the suffix in the name representing the molecule has inhibitory properties (38). Encouraged by the approval of the first small molecule tyrosine kinase inhibitor (TKI) in 2001, imatinib, involved in the pathogenesis of chronic myeloid leukemia (CML), small molecules for targeted therapy are moving quickly from bench to bedside for both solid tumors and hematological malignancies (39, 40) (**Figure 3**). Currently, there are 68 FDA-approved therapeutic agents that target protein kinase, including receptor tyrosine kinase inhibitors (*e.g.*, the epidermal growth factor receptor, EGFR; vascular endothelial growth factor, VEGF; platelet-derived growth factor, PDGF), serine/threonine kinase inhibitors (*e.g.*, RAF-MEK-ERK; PI3K/AKT/mTOR; cyclin-dependent kinases, CDK;) (41). Furthermore, epigenetic inhibitors (*e.g.*, histone deacetylase, HDACs), non-receptor tyrosine kinase inhibitors (*e.g.*, Bcr-abl1; BTK; JAK), Poly (ADP-ribose) polymerase (PARP) inhibitors have been obtained approval (39). There is a substantial pipeline of valuable targets in the development, such as c-MYC. Two attractive targets MEK1/2 and c-MYC for cancer therapy are shown in details in section 1.5.2 and 1.6.2.

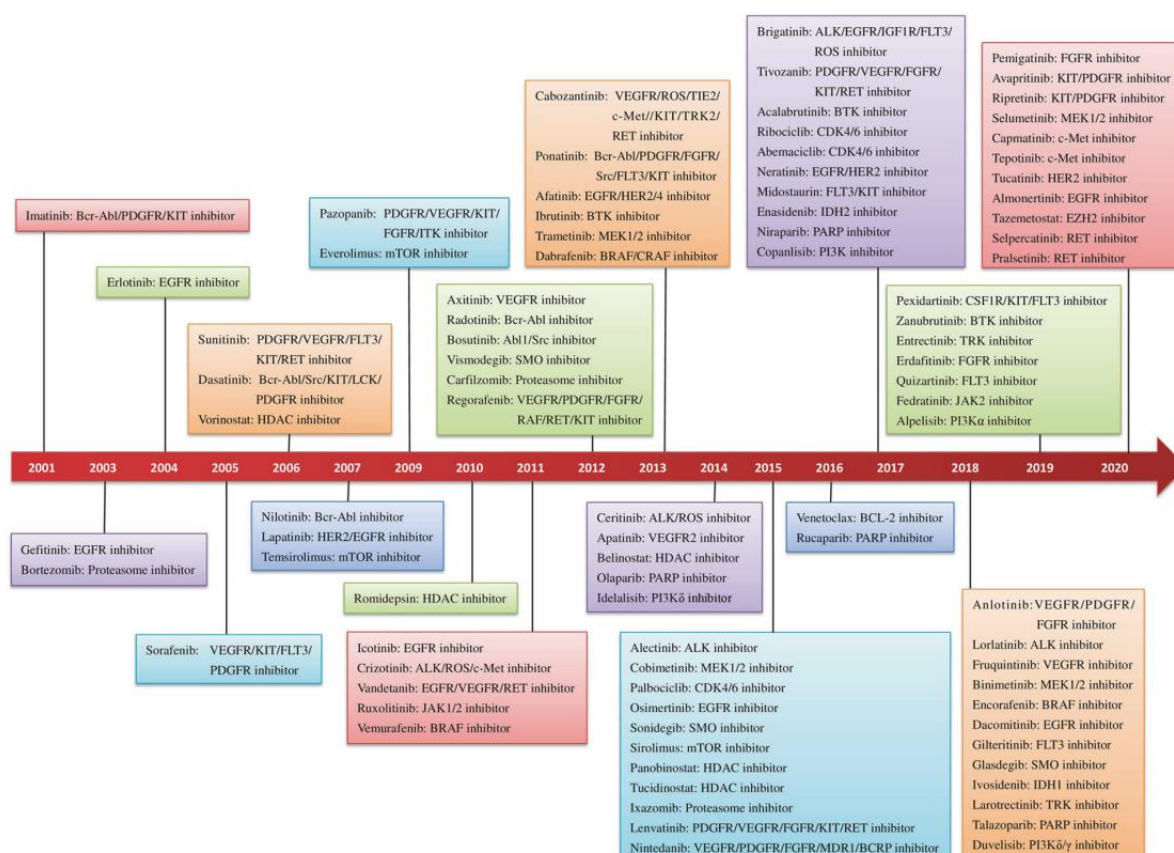


Figure 3. Timetable for approval of small molecule targeted anti-cancer drugs. (39)

2) Monoclonal antibodies

B-lymphocytes become active when a foreign substance enters the body, and antibodies take place in the recognition of epitope regions on the foreign substance (antigen). Monoclonal antibodies (mAbs) are produced in response to a single epitope (42). The use of mAbs for cancer therapy has achieved considerable success in recent years. mAbs specifically target extracellular proteins because they are generally too large to fit inside the cells. After attaching the cells, mAbs can exert their effects either directly or indirectly. The direct mechanism refers to the binding of mAbs to an antigen, cell receptor, or membrane-bound protein, allowing them to exert effects on the specific target to cause cell death (43). While the indirect mechanism refers to after stimulation via the binding of mAbs to cancer-specific antigens, the immune system can respond and further attack cancerous cells. The indirect mechanism is widely applied in immunotherapy (44). Furthermore, immunotherapeutic mAbs depend on whether or not they carry drugs or radioactive substances, can be categorized into self-acting, non-conjugated mAbs (*e.g.*, trastuzumab and alemtuzumab), and conjugated mAbs (*e.g.*, gemtuyumab otogamicin). Conjugated mAbs have been shown to improve drug pharmacokinetic profiles by decreasing volume of distribution and prolonging the distribution and elimination phases (45). Therefore, the application of mAbs is a promising strategy and also lies at the heart of personalized medicine.

3) Cancer vaccines

Cancer vaccines are designed to specifically recognize aberrantly expressed tumor-associated antigens (TAAs), tumor-specific antigens (TSAs), peptides, and antigenic epitopes through CD4⁺ T cells and CD8⁺ T cells. This further stimulates cytotoxic T lymphocytes and helps T cell-mediated immune response against TAAs and TSAs (46, 47). Common therapeutic cancer vaccines include hepatitis C virus (HCV), viral proteins (*e.g.*, human papillomavirus (HPV)), and oncofetal antigens (*e.g.*, carcinoembryonic antigen (CEA)). Several cancer vaccines targeting oncoproteins (*e.g.*, HER2) are in clinical trials. However, given the intricacy of cancer immunology and the optimal vaccine design, clinical translation of cancer vaccine has been challenging (37, 48).

4) Gene therapy

Gene therapy is a treatment of genetic disease by transferring genetic material into the cells of the patients. It acts through one of three mechanisms: (i) blocking the expression of a target gene, (ii) enabling expression of the transferred gene, (iii) modifying a target gene (49). Gene

therapy drugs were biological medicines that are provided as nucleic acids, lipid complexes, viruses, or genetically engineered micro-organisms. There are two dozen of gene therapies officially licensed so far as clinical used drugs (50).

1.3 Mechanisms of drug resistance

In response to therapies, cancer cells modify their dependence on an original particularly hallmark capability and increase dependent on another, this represents drug resistance. Innate or acquired resistance remains a major impediment to effective chemotherapy of cancer (9). Multidrug resistance (MDR) is characterized by drug resistance that develops not only to a single chemotherapeutic drug, but also occurs in a broad range of drugs with different chemical structures and various modes of action (51). Chemotherapy failure has been attributed to a number of reasons. Known mechanisms with clinical relevance represent alternations in intracellular drug concentration (drug efflux/influx pump), inhibition of cell death (apoptosis suppression), enhance DNA repair and gene amplification, change in drug metabolism, and epigenetic alternations (52, 53). This thesis will focus on drug efflux and deregulation of cell death, which are discussed in detail below.

1.3.1 Multidrug resistance by ABC transporters

One of the major causes of MDR is the enhanced overexpression of transmembrane efflux pumps such as ATP-binding cassette (ABC) transporters. ABC transporters are a family of membrane proteins that mediate the ATP-driven transport process. They are found in all domains of life, including bacteria, archaea, fungi, plants, as well as humans (54). Forty-nine human ABC transporters have been found so far and divided into 7 subfamilies (55). The most of molecular architecture of ABC transporters is similar. They consist of a pair of conserved cytoplasmic domains refer as nucleotide-binding domains (NBDs). Substrates can pass through the membrane's lipid bilayer, either be imported into or exported out of the cytoplasm due to the NBD's hydrolysis of ATP, which drives the conformational changes in the associated transmembrane domains (TMDs). Some ABC transporters, termed half-transporters, are composed of only one TMD and NBD (56). ABC transporters are involved in fundamental cellular functions, especially regulating levels of biochemical substances to maintain cellular homeostasis and protect issues from xenobiotics (57).

Overexpression of ABC transporters plays an important role in MDR-cells and confers resistance to anticancer drugs. P-glycoprotein (P-gp, gene symbol *ABCB1*), multidrug resistance-associated protein 1 (MRP1, gene symbol *ABCC1*), and breast cancer resistance protein (BCRP, gene symbol *ABCG2*) are primary determinants of drug resistance in cancer cells. These drug transporters engage in active efflux of drugs and drug conjugates (58). An example of a substrate is transported by P-gp is shown in **Figure 4**.

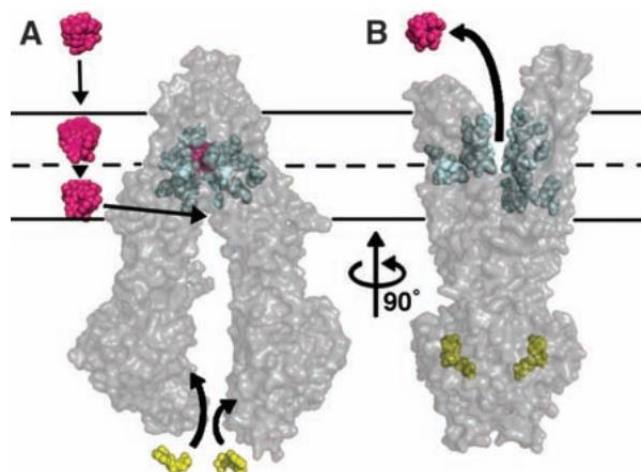


Figure 4. Model of substrate transport by P-gp. (A) From the outside of the cell to the inside leaflet, the substrate (magenta) partitions into the bilayer and enters the drug-binding site (cyan spheres). (B) ATP (yellow) binds to the NBDs and results in a large conformational change, bringing the substrate and drug-binding site to the extracellular space. (59)

P-gp was the first member of ABC transporter identified in cancer. P-glycoprotein-expressing organs (*e.g.*, apical membrane of hepatocytes, kidney proximal tubules, endothelial cells of the blood-brain barrier) are crucial for absorption, distribution, metabolism, and excretion (ADME) pharmacological drugs, which also prevent the accumulation of harmful, carcinogenic compounds from tumorigenesis (55). However, a limited phase I trial reported that enrolled patients with sarcoma pulmonary metastases showed a 3-15-fold rapid increase in *ABCB1* gene expression after around 1 h of doxorubicin treatment (60). In addition, *in vitro* study has indicated P-gp overexpressing CEM/ADR5000 cells were cross-resistant (6.9 ~ 1036-fold) to a number of unrelated anticancer drugs, such as anthracyclines (*e.g.*, doxorubicin idarubicin, epirubicin), *Vinca* alkaloids (*e.g.*, vincristine, vinblastine), taxanes (*e.g.*, docetaxel, paclitaxel), epipodophyllotoxins (*e.g.*, etoposide) (61). A great deal of effort has been expended to identify

potent and selective P-gp inhibitors to overcome multidrug resistance. The first generation of P-gp inhibitors such as verapamil and deverapamil were not specifically for inhibiting P-gp while with a low affinity. The second generation contained more specific inhibitors with less side effect, such as biricodar and valsopodar. The third generation is composed of more potent and selective inhibitors, such as tariquidar and elacridar. The fourth generation obtained with multiple strategies, such as natural products with their derivatives, peptides and lipids (62).

The role of BCRP in drug disposition is highly resembles P-gp in tissue expression and distribution. BCRP substrates include broadly anticancer agents such as camptothecin derivatives, methotrexate, and flavopiridol. Notably, some TKIs including imatinib, gefitinib, and nilotinib are BCRP substrates (63). Many BCRP inhibitors with various chemical structures have been found. The first part is P-gp inhibitors, which are also excellent BCRP inhibitors. The other outstanding BCRP inhibitors include tamoxifen, novobiocin, tryprostatin, and dietary flavonoids such as chrysin (64).

1.3.2 Apoptosis resistance

An underlying hallmark of cancers is resisting cell death. Dysregulated apoptotic signaling enables cancer cells to escape the fate of death, resulting in uncontrolled proliferation, tumor survival, therapeutic resistance, and cancer recurrence (65). To date, apoptosis is still the most common form of cell death induced by radio- and chemotherapy in cancer cells. However, multiple molecular mechanisms can be altered leading to the reduction of apoptosis or acquisition of apoptosis resistance (**Figure 5**), including 1) disrupted balance between proapoptotic and anti-apoptotic proteins; 2) impaired 53 function; 3) overexpression of IAP proteins; 4) reduced caspase function; 5) impaired death receptor signaling (66).

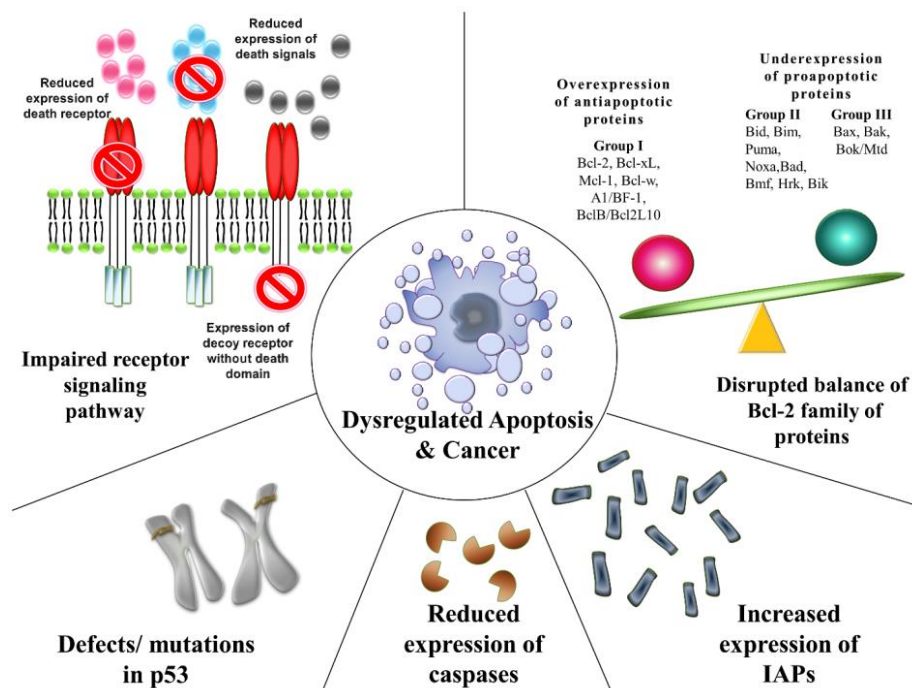


Figure 5. Mechanisms contribute to deregulation of apoptosis. (67)

Table 1. Bcl-2 members classification based on function and the Bcl-2 homology (BH) domains (68).

Function	Bcl-2 homology (BH) domain	Protein
Anti-apoptotic proteins	Contain four BH domains	Bcl-2, Bcl-X _L , Bcl-w, Mcl-1, A1/Bfl-1 and Bcl-B/Bcl2L10
Pro-apoptotic proteins	Restrict to the BH3 domain	Bid, Bim, Puma, Noxa, Bad, Bmf, Bik and Hrk
Pro-apoptotic proteins	Contain four BH domains	Bax, Bak, and Bok/Mtd

First of all, the disruption of balance between proapoptotic and antiapoptotic proteins is a powerful mechanism of tumor growth and drug resistance. Bcl-2 family proteins consist of proapoptotic and antiapoptotic proteins that play a vital role in the regulation of apoptosis. The three groups of Bcl-2 family members are shown in

Table 1. This unbalance can be one or more anti-apoptotic proteins may be overexpressed while one or more pro-apoptotic proteins may be downregulated, or both may be present (67). Secondly, the p53 protein is a well-known tumor suppressor protein encoded by the tumor suppressor gene *TP53*. The most conserved function of p53 is the induction of apoptosis in

response to cellular stress. A set of pro-apoptotic genes (*e.g.*, *Bax*, *Bid*, and *PUMA*) and anti-apoptotic gene *Bcl-X_L* of Bcl-2 family are p53 targets (69-71). However, mutated p53 leads to abnormal activity of p53 and inefficient apoptosis induction (66). Furthermore, dysregulated expression of a group of the inhibitor of apoptosis proteins (IAPs) that are negative regulators of caspase function has been correlated to many cancers. IAPs can bind and inhibit caspase 3, -7, or -9 by promoting their degradation or keeping caspases away from their substrates (72). X-linked IAP (XIAP) is the most widely characterized IAPs and is regarded as the most potent endogenous caspase inhibitor (73). Finally, as section 1.4.1 will show, caspases and death receptor signaling are important plays in initiating and executing apoptosis. Therefore, it is reasonable to believe that reduced expression of caspase and impaired death receptor signaling cannot activate apoptosis.

1.4 Targeting of cell death pathways for cancer therapy

Cell death is an essential physiological process for human health to maintain homeostasis and response to stress (74). The homeostatic balance between survival and death is critical. Aberrant (excessive or deficient) cell death underpins multiple pathologies, including cancer, neurodegeneration, autoimmunity, and injury (75). Tumor cells gain the ability to avoid cell death pathway, which functions as a protective mechanism in normal cells to remove damaged cells. As a consequence, a population of death-resistant cells with accumulating genetic and epigenetic errors contributes to tumorigenesis (76). Thus, cell death has risen in importance as targets for the development of cancer therapies.

Historically, cell death based on morphological alternations is classified into three different forms: (1) type I cell death/apoptosis, (2) type II cell death/autophagy, and (3) type III cell death/necrosis (75). As various types of cell death sprung up, the Nomenclature Committee on Cell Death in 2018 proposed an updated classification of more than 10 types of cell death with an emphasis on the molecular mechanisms involved in the initiation, execution, and propagation (77). Cell death can be categorized into accidental cell death (ACD) and regulated cell death (RCD). ACD is an uncontrolled process of cell death, in which cells are exposed to server physical (*e.g.*, high temperature or pressure), chemical (*e.g.*, extreme variations in pH), or mechanical damages. RCD involves genetically regulated cell death that maintains the stability of the internal environment in an orderly and autonomous manner. When RCD occurs as a physiological program without any external environment disturbance, it is referred to as

programmed cell death (PCD). PCD can be further classified into apoptotic cell death and non-apoptotic cell death. The classification of cell death is shown in **Figure 6**.

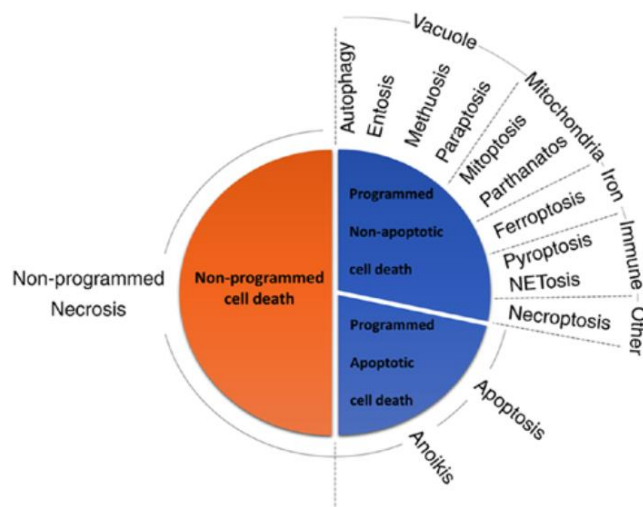


Figure 6. Cell death classification. (78)

1.4.1 Apoptosis

Apoptosis is the most widely studied form of cell death. It is a highly regulated and conserved process with multicellular organisms. The term "apoptosis" was proposed by Kerr and colleagues in 1972 to describe morphological features detected as cells were eliminated during embryonic development (79). From a morphological perspective, apoptotic cells show characteristics including membrane blebbing, cell shrinkage, loss of cytoplasmic organelle positional organization, membrane exposure of phosphatidylserine (PS) on the extracellular side, DNA condensation and fragmentation, and formation of apoptotic bodies (78, 80). They are mechanically induced by the activation of a set of cysteine-aspartic proteases known as caspase. To date, two types of caspases have been defined, the initiator caspase and the executioner caspase. Initiator caspases (caspase-2, -8, -9, and -10) are responsible for initiating caspase activation cascades. Effector caspases (caspase-3, -6, and -7) are in charge of the actual breakdown of the cell by cleaving cellular substrates (81). Furthermore, apoptosis is regulated by the components of the Bcl-2 protein family (see above 1.3.2). There are two major apoptosis pathways: the intrinsic or mitochondria pathway and the extrinsic or death receptor pathway (82). The intrinsic and extrinsic pathways are shown in **Figure 7**.

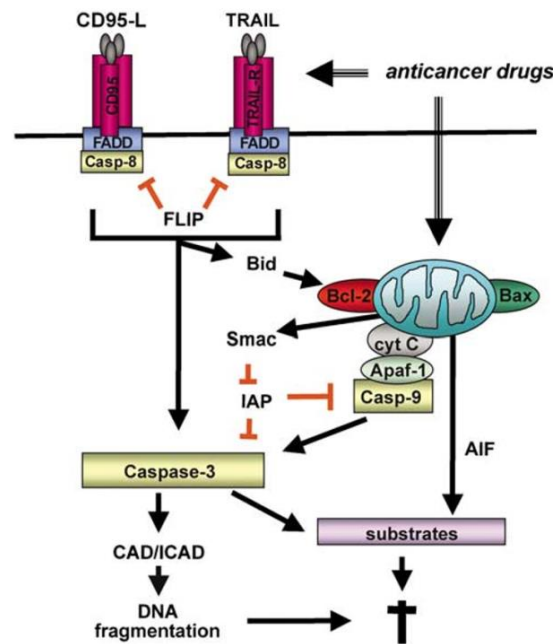


Figure 7. Apoptosis signaling pathways. (82)

1) Intrinsic apoptosis pathway: This pathway is initiated by the cell when it detects damage via numerous intracellular sensors. When cytotoxic stimuli activate proapoptotic molecules (BAX and BAK) to change the mitochondrial outer membrane permeabilization (MOMP), it caused subsequent release of cytochrome *c* from mitochondria to cytoplasm and binds to APAF-1, further triggering apoptosome to activate the formation of caspase 9, and subsequently a cascade of effector caspases (74).

2) Extrinsic apoptosis pathway

Death receptors are members of the tumor necrosis factor (TNF) receptor gene superfamily. They are characterized by a cytoplasmic region known as the “death domain” (FADD), which plays a vital part in transmitting the death signal from the cell’s surface to intracellular signaling pathways (82). The best-studied death receptors are CD95 (APO-1/Fas), TNF receptor 1 (TNFR1), TNF-related apoptosis-inducing ligand-receptor 1 (TRAIL-R1), and TRAIL-R2. The corresponding death receptor ligands include CD95L (FasL), TNF, and TRAIL (83). Upon stimulation and ligation, the signals are transmitted via FADD to activate caspase 8. In ‘type I’ cells (primarily dependent on the extrinsic pathway), activated caspase 8 leads to sufficient activation of downstream effector caspases. While in ‘type II’ cells (primarily dependent on the intrinsic pathway), activator protein Bid enhances the apoptotic signal via the mitochondria, which eventually demands mitochondrial processes for cell execution (84).

Understanding of molecular mechanisms of apoptotic pathways and their deregulations has already provided new avenues for cancer treatment. Therapeutic approaches directly targeting the apoptosis intrinsic pathway (e.g., Bcl-2, Bcl-X_L, Mcl-1 and IAP inhibitors) and extrinsic pathway (e.g., targeting death receptor agonists and targeting p53) are under development, which have brought small molecules into clinical research (85) (**Figure 8**). On the other hand, most of the approaches indirectly induce apoptosis, including targeting oncogenic signaling pathways (e.g., MEK inhibitors) and blocking the deregulated oncogenic downstream effectors (e.g., MYC, CDKs). However, targeting apoptotic pathways is particularly complex due to the abundance of therapeutic targets, each with particular resistance mechanism (85). Instead, much more remains to be explored about other modes of cell death, as shown in section 1.4.2 and 1.4.3.

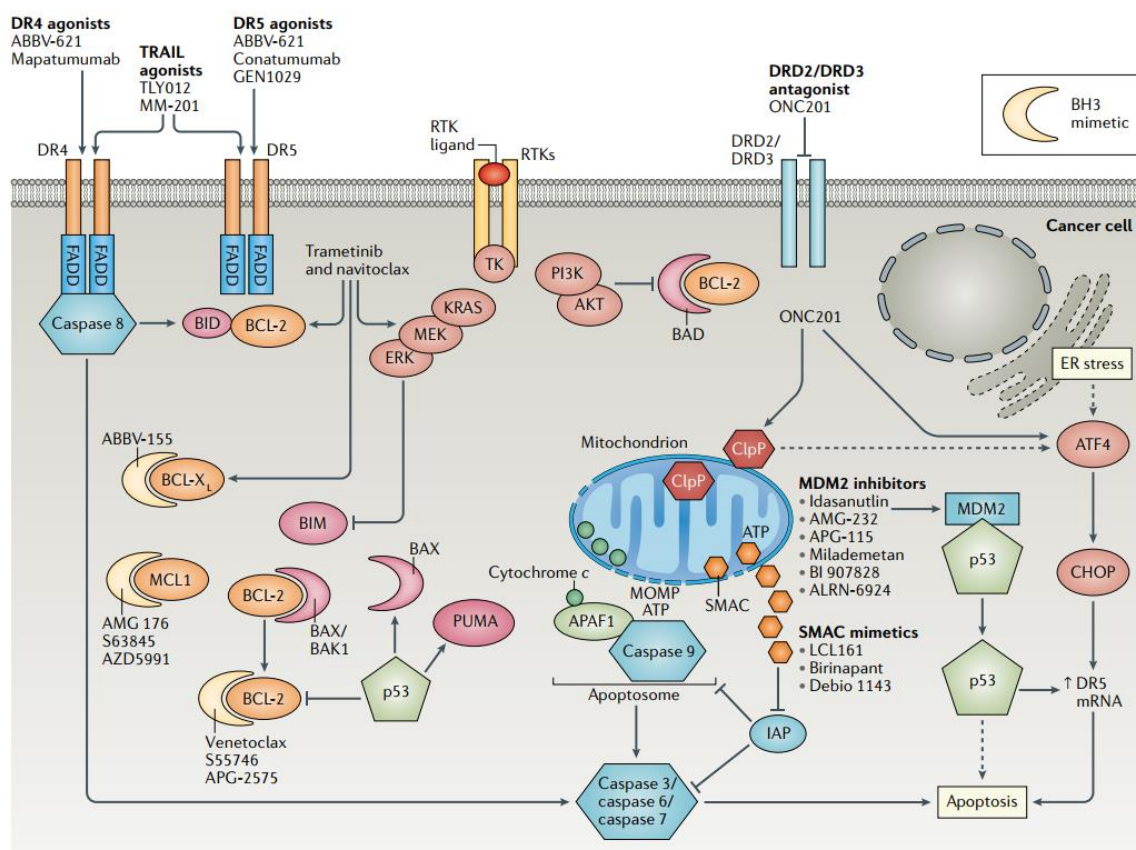


Figure 8. Therapeutic approaches targeting apoptosis pathways in cancer cells. (85)

1.4.2 Parthanatos

Parthanatos known as a PARP-1-dependent cell death, is officially recognized as a non-apoptotic cell death. The word “parthanatos” was coined from *Thanatos*, the personification of death in Greek mythology to illustrate cell death carried on by PAR polymer, which is a product of PARP-1 activation (86). Parthanatos take part in many crucial pathogenic processes, such as Parkinson’s disease, Alzheimer’s disease, ischemia-reperfusion injury after myocardial infarction or brain ischemia. Increasing evidence recently suggests that pathanatos is involved in the regulation of cancer cells (87, 88). Parthanatos is distinctive with classical cell death pathways concerning of its biochemical and morphological characteristics. The biochemical features of parthanatos include rapid activation of PARP-1, synthesis and accumulation of PAR polymer, mitochondria depolarization, nuclear AIF translocation, and perhaps caspase activation at late stage (89). Caspase activation does not engage in parthanatos since caspase inhibitors are unable to protect cells from parthanatic cell death (90). Therefore, parthanatos is a caspase-independent type of cell death. The morphological characteristics of parthanatos include membrane breakdown, shrunken and condensation of the nucleus (87). Unlike apoptosis, parthanatos does not result in the production of apoptotic bodies or small-scale DNA fragmentation (90). Even though parthanatic cells exhibit loss of membrane integrity comparable to necrosis, but it does not cause cell swelling (91). The key steps of parthanatos are illustrated below in **Figure 9**.

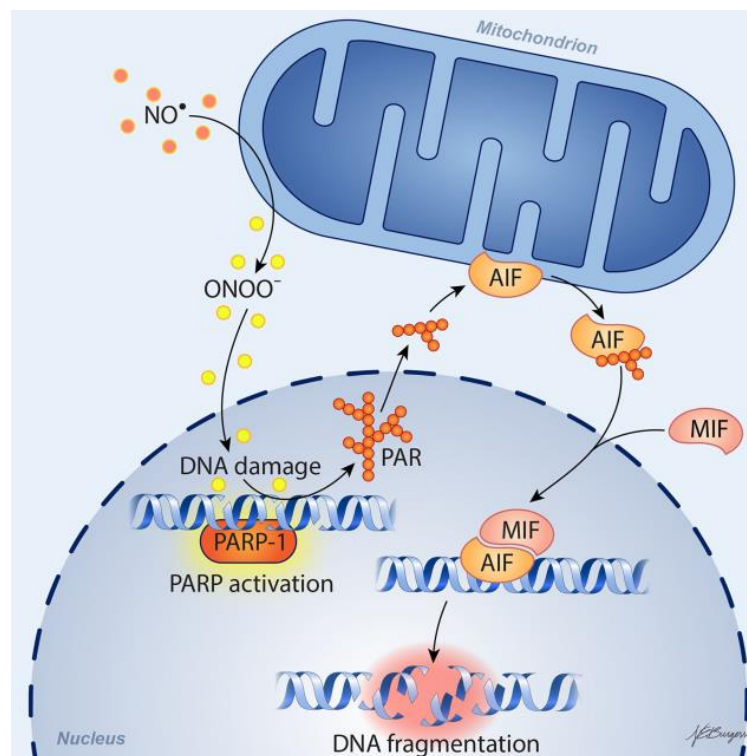


Figure 9. The pathway of parthanatos. (92)

PARP-1 is a fundamental member of the PARP family localized in nuclei. PARP-1 contains four major domains as shown in **Figure 10**. They are 1) two zinc fingers are in charge of detecting DNA breaks, 2) nuclear localization of signal (NLS) containing a caspase-3 cleavage site, 3) an automodification domain with a BRCT motif for protein-protein interactions, 4) a catalytic site has NAD⁺-fold (93). Hence, PARP-1 function ranges from supporting survival (*e.g.*, DNA repair, genomic stability, and transcription) to inducing cell death (94). PARP-1 can be activated by posttranslational modifications such as phosphorylation, acetylation, or ADP ribosylation. In response to DNA damage, PARP-1 binds to PAR to various receptor proteins or on PARP-1 itself (automodification) by using NAD⁺. Mild genomic stress induces PARP-1 activation to repair DNA damage, whereas massive DNA damage generates excessive ADP ribosylation, PARP is overactivated, producing excess PAR (87, 95). PAR is a death signal that translocates to cytosol and induces AIF nuclear translocation (96). AIF is a flavoprotein involved in maintaining mitochondria structure and effecting cell death when it moves to the nucleus. AIF translocates from mitochondria to the nucleus has been recognized as a key factor to mediate parthanatos, where it causes cell death by chromatin condensation and significant DNA fragmentation (50 kb) (91). In addition, cytochrome *c* is also a mitochondria protein as introduced above, which is efficient in stimulation of apoptosis. Studies have reported that AIF release occurs ahead of that of cytochrome *c* upon PARP-1 activation (97). The parthanatos-inducing compounds in cancer are shown in section 1.7.

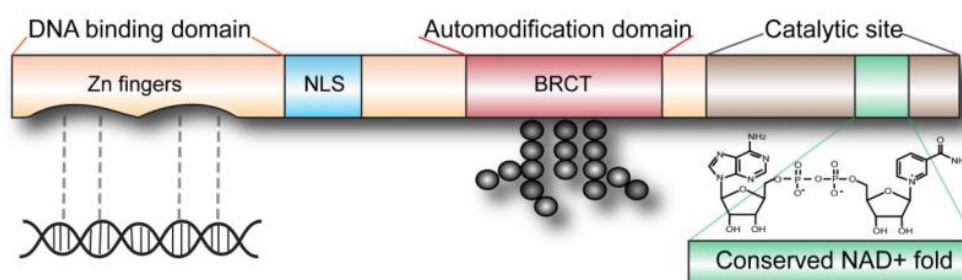


Figure 10. The major domains of PARP-1. (86)

1.4.3 Autophagy and other modes of cell death

Autophagy ("self-eating") is a nonselective, intracellular catabolic degradation process. The Nobel Prize in Medicine in 2016 was awarded to Dr. Yoshinori Ohsumi for the breakthrough in the discovery of autophagy mechanisms (98). There are three types of autophagy: macroautophagy, microautophagy, and chaperone-mediated autophagy, and "autophagy"

typically refers to macroautophagy (99). Autophagy involves cytoplasmic constituents being sequestered in double-membrane autophagosomes. These structures are then fused with lysosomes, which deliver their cargoes for degradation and recycling (100). This process is regulated by around 20 autophagy-related (ATG) proteins. Autophagy has been viewed as a survival mechanism, such as starvation adaption, organelle clearance, removal of microorganisms (101). However, autophagy has double roles in cancer. In the widespread hypothesis, autophagy performs an anticarcinogenic role in primary cells through protection from metabolic stress, further clearing the protein aggregates. While in established tumors, autophagy might provide survival benefits for tumor cells, which further contributes to acquired resistance to chemotherapy (102). Even whether to develop autophagy inducer or inhibitor is debated, recent evidence supported that inhibiting autophagy could be an effective cancer treatment (103).

Pyroptosis is an inflammatory form of PCD triggered by caspase-1/4/5/11 which is activated certain inflammasomes (*e.g.*, NLRP3), leading to the cleaving of gasdermin D (GSDMD) and activation of inactivated cytokines like IL-18 and IL-1 β (104). Morphologically, the nucleus of pyroptotic cells is still intact despite chromatin condensation and DNA fragmentation. The formation of plasma membrane pores allows water influx and generates cell swelling and lysis (105). Pyroptosis has been shown to affect the proliferation, invasion, and metastasis of tumor (106).

Ferroptosis is an iron- and ROS-dependent form of non-apoptotic cell death that was first described in 2012 (107). Morphological characteristics of ferroptosis involved intact cell membrane, decreased or absent mitochondrial crests, fractured mitochondrial outer membrane, and normal nuclear size and chromatin (108). Ferroptosis is initiated by the suppression of cystine glutamate antiporter (system X_c⁻), resulting in a reduction of glutathione (GSH) biosynthesis and phospholipid peroxidase glutathione peroxidase 4 (GPX4) inactivation. Generally, GPX4 converts harmful lipid hydroperoxides (L-OOH) to non-toxic lipid alcohols (L-OH). Inactivation of GPX4 ultimately leads to excessive lipid peroxidation, which interacted with free iron through the Fenton reaction, further forming lipid ROS and leading to cell death (109). Recently a novel FDA-approved drug (*e.g.*, sulfasalazine) shows the induction to ferroptosis, implying ferroptosis has a tumor suppression function and a unique potential for reversing drug resistance (110-112).

More recently, excess concentration of copper (Cu) causes a mitochondrial-induced cell death referred to as cuproptosis. It involves direct binding of Cu to lipoylated components of

tricarboxylic acid (TAC) cycle, resulting in aggregation of lipoylated protein, proteotoxic stress, and subsequent cell death (113). Interestingly, cells in a more respiratory condition may have higher levels of lipoylated enzyme expression, which lead to increased aggregation formation. The finding of cuproptosis suggests inhibiting mitochondrial respiration may be a strategy for cancer cells (114).

Therefore, it is expected that additional regulated forms of nonapoptotic cell death will be discovered, which will increase the likelihood that cancer cells will die in different mechanisms, and overcome the challenges of drug resistance.

1.5 The relevance of MEK1/2 for apoptosis in cancer therapy

1.5.1 The RAS-RAF-MEK-ERK (MAPK) cascade in cancer

Mitogen-activated protein kinase (MAPK) pathways relay, amplify and integrate intracellular signals from a number of cell surface receptors to response cell proliferation, development, differentiation, and apoptosis. In mammalian cells, there are four well-known MAPK cascades: the classical extracellular signal-regulated kinase (ERK) cascade, the c-Jun N-terminal kinase cascade, the p38MAPK cascade, and the ERK5 cascade. Each MAPK cascade consists of a MAPK kinase kinase (MAP3K), a MAPK kinase (MAP2K), and a MAPK (115, 116). Among the MAPK pathways, the RAS-RAF-MEK-ERK axis is the best characterized (**Figure 11**). Mechanically, signal transduction along this pathway is initiated by the binding of different ligands to growth factor receptors such as EGFR. Upon the upstream stimulation, inactivated Ras-GDP converts to activated Ras-GTP and subsequently recruits Raf to the cell membrane for dimerization and activation. Activated Raf phosphorylates and activates the downstream dual-specificity protein kinase MEK. Two Raf-MEK dimers constitute a transient tetramer, to promote MEK activation by Raf. Then, activated MEK dually phosphorylates and activates ERK (117, 118). Hundreds of proteins involved in diverse cellular response have been identified as ERK substrates and ERK-interacted partners. For example, ERK controls G1 to S phase cell cycle checkpoint for preventing the cell from abnormal replication (119). ERK also regulates several pro-survival Bcl-2 proteins such as Bcl-2, Bcl-X_L, and Mcl-1 to achieve cell survival (120).

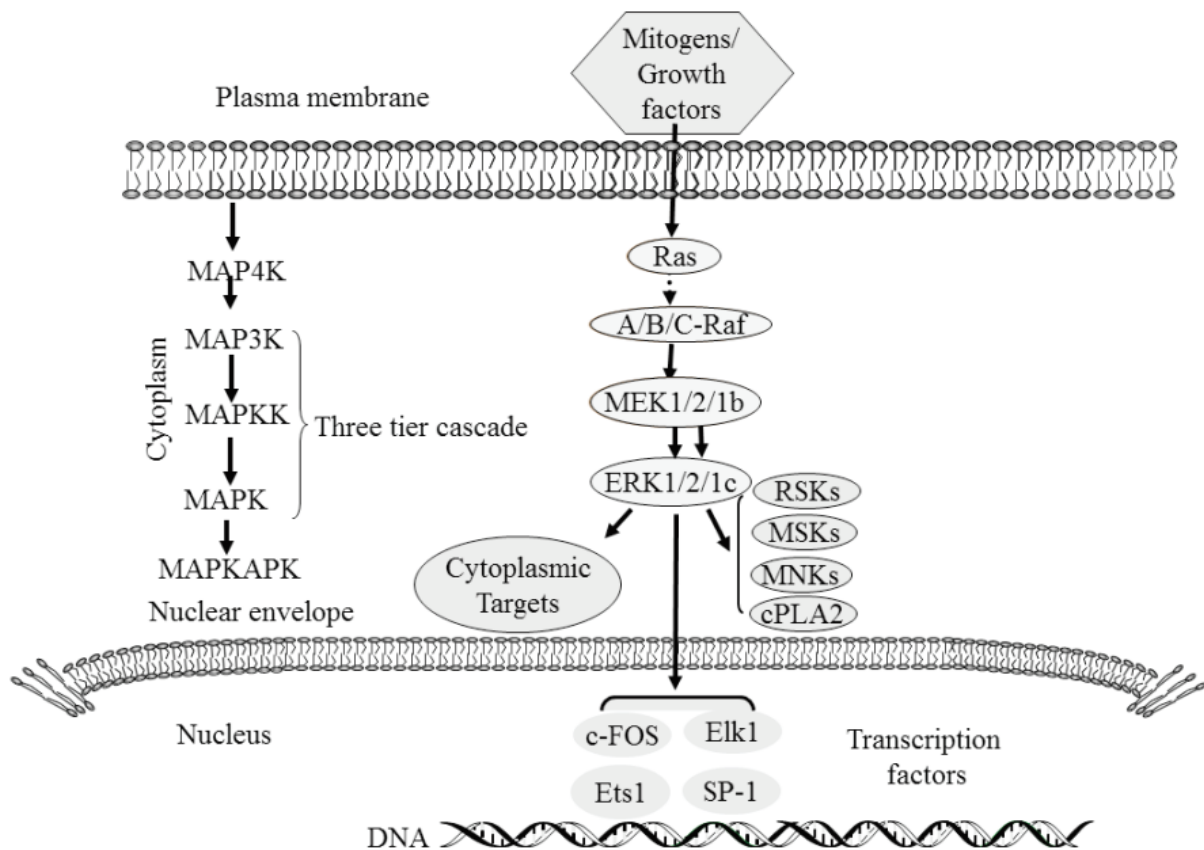


Figure 11. The RAS-RAF-MEK-ERK signaling pathway. (121)

Deregulation of the Ras-Raf-MEK-ERK pathway has been established a thoroughly important role in human cancers. Expressing a constitutively activated mutant form of Ras (*KRAS*, *NRAS*, *HRAS*) and Raf (*ARAF*, *BRAF*, *CRAF*) have been associated with different types of cancers (122). For example, *KRAS* is the most frequently mutated form of *RAS*, which is mutated in more than 20% of all cancers, including pancreatic ductal adenocarcinoma (PDAC), non-small cell lung cancer (NCSLC), and colorectal cancer (CRC) (123). *BRAF* is also commonly mutated in 7%-10% of all cancer such as melanoma and ovarian cancer. Therefore, the efforts to target oncogenic RAS and RAF, have been extensively studied as promising targets for therapeutic development. However, drug resistance inevitably has been developed in patients within 6-7 months of initiating treatment, for example, in advanced melanoma treated with BRAF inhibitor (124, 125). The resistance is typically mediated through rapid recovery of the ERK pathway with several different mechanisms (126).

Activation of ERK pathway has well-documented anti-apoptotic effects, which are related to the inactivation of pro-apoptotic proteins and the induction of anti-apoptotic proteins belonging to the Bcl-2 family (127, 128). For example, in transformed human mammary epithelial cells, Bcl-X_L overexpression is vital for RAS-induced cancer cells and the maintenance of cancer-

initiating cells phenotype (129). On the contrary, suppression of inducible oncogenic *HRAS*^{V12G} expression causes melanoma to regress while triggering an extensive rise in apoptotic cell death (130). While applying RAS downstream MEK inhibitor has been shown promising anticancer potential. For example, the combination of Bcl-2/Bcl-X_L inhibitor, navitoclax, and MEK inhibitor, G-963, resulted in dramatic enhancement of apoptosis in lung and pancreatic tumors harboring KRAS mutation (131). Hence, for maximum ERK pathway inhibition and minimizing resistance, MEK inhibitors are of growing interest as an alternative strategy to block ERK pathway, especially those cancers brought on RAS or RAF dysfunction.

1.5.2 MEK1/2 as targets for cancer treatment

Compared with hot-spot RAS and RAF mutations, the occurrence of MEK mutations is sporadic (around 1% of human cancers) (132). Both MEK and ERK have two isoforms, known as MEK1/2 and ERK1/2. MEK1 and MEK2 share 80% homology, and are encoded by *MAP2K1* and *MAP2K2* genes, respectively. The molecular weight of MEK1 and MEK2 are 44 and 45 kDa, and they exhibit similar functions to activate ERK1 and ERK2. While MEK1 and MEK2 are the only known upstream regulators of ERK1 and ERK2, which serves as “ERK1 and ERK2 gatekeeper” kinases (133). Inhibiting MEK can inhibit ERK activation and its downstream process, resulting in inhibition of cell proliferation and survival.

MEK1 and MEK2 consist of a small N-terminal lobe, which contains an ERK1 and ERK2 docking site, and a big C-terminal lobe, which contains the docking site for upstream activating MAP3Ks (**Figure 12**). At the interface between these lobes, conserved regions are important in ATP binding and hydrolysis, substrate binding, and phosphate transfer. MEK1 is activated by phosphorylation at Ser218 and Ser222, and MEK2 is activated by phosphorylation at Ser222 and Ser226 (117). Moreover, two potential phosphorylation sites are unique to MEK1. In addition to RAS, MEK1 integrates signals from integrins and is phosphorylated at Ser298 (134). MEK1 is also subjected to negative feedback from activated ERK, which is phosphorylated at Thr292. This phosphorylation induces inhibition of the pathway, decreases MEK1 activation, and further conferred to MEK2 via heterodimerization for accelerating MEK2 dephosphorylation as well (135).

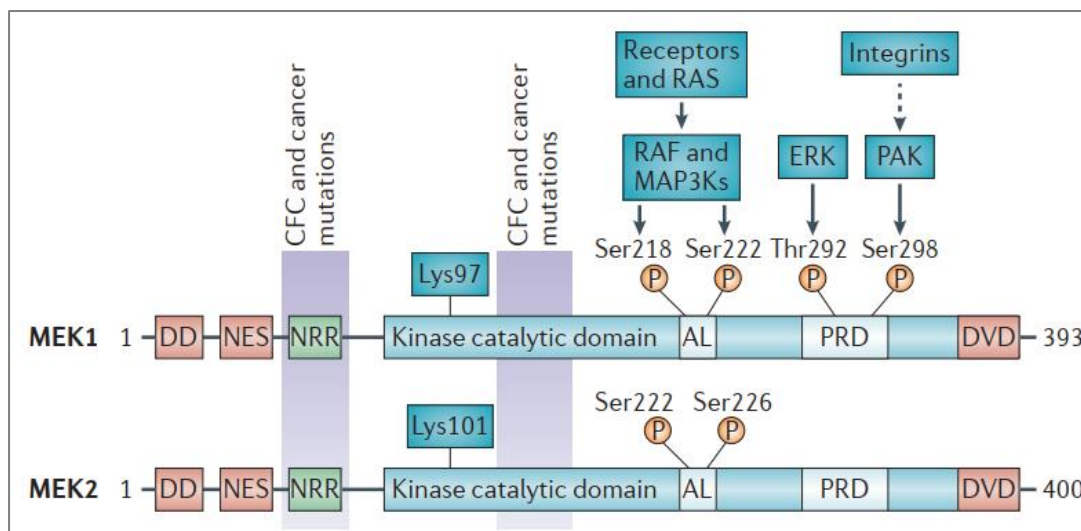


Figure 12. Key functional domains of the human MEK1 and MEK2 proteins are shown in a linear format. (133)

The first synthetic inhibitor of MEK1 and MEK2, PD098059, was reported in 1995 (136). Two other potent inhibitors U0126 (137) and Ro-2210 (138) were subsequently identified from cell-based assays. However, none of them moved to the clinical stage because of their pharmaceutical limitations such as low potency and physical properties. There are currently four FDA-approved clinical utility of MEK inhibitors, trametinib, cobimetinib, binimetinib, and selumetinib. They are all classified as ATP non-competitive, type III allosteric protein kinase inhibitors, which means they bind to a site that is adjacent to, but not on ATP-binding sites on MEK (139). Given resistance occurs to BRAF inhibitors alone, the combinations of MEK inhibitors with first-generations of BRAF inhibitors (*e.g.*, trametinib plus dabrafenib, cobimetinib plus vemurafenib) have been demonstrated enhanced apoptosis than the respective monotherapies in metastatic melanoma, which have revolutionized treatment for many patients and approved by FDA (126). In recent years, a number of novel MEK1/2 inhibitors such as refametinib or pimasertib as monotherapy, as well as the combination of AZD6244 and Akt inhibitor MK-2206 have progressed into clinical trials (140, 141). The novel MEK1/2 inhibitors may take advantage of their role at the central part of the ERK pathway to inform future drug development, or to find potential combinations with other targeted agents or conventional cytotoxic drugs.

1.6 The relevance of c-MYC for apoptosis in cancer therapy

1.6.1 the c-MYC oncogene in cancer

The *MYC* (known as c-MYC) oncogene is a “global” transcription factor. It controls the expression of the genes that are essential to a vast range of biological events, including proliferation, differentiation, programmed cell death, and immune regulation (142). *C-MYC* was the first gene to be discovered in *myc* family due to its homology to the oncogene *v-myc* of the avian myelocytomatosis virus (143). Two additional paralogs were found later: MYCN (*N-myc*) was first identified in human neuroblastomas (144), and MYCL (*L-myc*) was originally observed in human small cell lung cancer (145). Subsequently, both MYCN and MYCL were identified in many tissues and tumor types. MYCN and MYCL share function with c-MYC despite having a more restricted tissue expression pattern than c-MYC (146). All three MYC proteins frequently deregulate and contribute to human cancers.

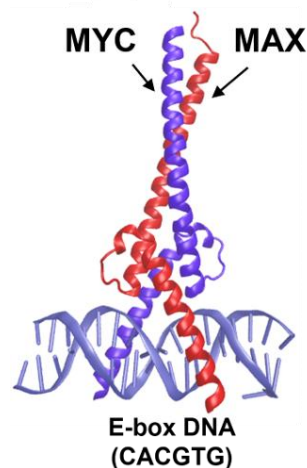


Figure 13. Crystal structure of the a MYC/MAX heterodimer binds to a canonical E-box (PDB code: 1NKP).

C-MYC encompasses a C-terminal domain (CTD), an N-terminal transactivation domain (NAD), and a central region (142). The C-terminal domain contains a basic region helix-loop-helix leucine zipper (bHLHLZ) motif and promotes dimerize with its obligatory partner, the MYC-associated protein X (MAX) protein. The MYC/MAX heterodimers bind to the canonical E-box sequence 5'-CACGTG-3' in promoters and enhance MYC-regulated genes (147) (**Figure 13**). The N-terminal domain contains conserved transcriptional regulation elements called “MYC boxes” (MBI and II). The control of c-MYC stability and activity in response to

cell growth signals involves two important phosphorylation sites, threonine 58 (T58) and serine 62 (62), which are located in MBI (148). The central region comprises a nuclear localization signal (NLS), and other conserved MYC boxes (MBIII and MB IV) (149). In addition, c-MYC mRNA is innately unstable, with a short half-life of 30 min. The stability and degradation of c-MYC protein are also subjected to other various of post-translational modifications, including ubiquitination, SUMOylation, methylation, acetylation, and glycosylation (150, 151).

c-MYC expression is tightly controlled in healthy adult tissue. However, approximately 70% of all human malignancies exhibit deregulated c-MYC activity, which is frequently associated with a poor clinical outcome, an elevated risk of recurrence, aggressive biological behavior, and an advanced stage of disease (148). Generally, *c-MYC* overexpression does not result from gene point mutations. Aberrant *c-MYC* expression is involved in gene amplification, chromosomal translocation, enhanced cell signaling, retroviral promoter insertion, altered protein degradation and mutation (152). Of these mechanisms, gene amplification is the most widely mechanism of c-MYC deregulation in solid tumors. The Cancer Genome Atlas Program (TCGA) in 2018 showed *c-MYC* gene amplification contributes to ovarian cancer (33.2%), breast cancer (15.0%), pancreatic cancer (12.6%) and lung cancer (8.4%) (153). Depending on biochemical features of tumors, *c-MYC* gene amplification is more prevalent in certain cancer types. For example, in the comparison with ER+ (estrogen receptor α positive) or HER2+ (human epidermal growth factor receptor 2 positive) breast cancers, *c-MYC* is markedly elevated in triple-negative breast cancer (TNBC) (154). While the translocation of *c-MYC* gene into the T cell receptor locus or immunoglobulin is of the key events in the development of hematological malignancies such as acute lymphoblastic leukemia (ALL) and Burkitt's lymphoma (155). Upstream oncogenic signaling from EGFR, ALK, Wnt, NOTCH, TGF, Hedgehog and Hippo pathways also drive irregular c-MYC expression in many cancer cells (156).

c-MYC activation alone is generally insufficient to cause non-malignant cells to undergo neoplastic transformation. The tumorigenesis function of oncogenic c-MYC is limited by numerous physiological mechanisms including cell cycle arrest, apoptosis, and/or cellular senescence (157). C-MYC has an intrinsic function involved in cell death, which induces apoptosis requiring its DNA binding functions and dimerization with MAX. C-MYC does not act as a death effector but instead acts to sensitize cells to a variety of apoptotic stimuli such as hypoxia, genotoxic stress, and death receptor signaling. Plenty of evidence supports the view that this apoptotic sensitization substantially restraints the oncogenic potential of c-MYC (158). The prosurvival Bcl-2 pathway and the proapoptotic p53 pathway are primarily interrelated in cancer cells, which respond to c-MYC activation by proliferation or by inducing apoptosis (159,

160) (**Figure 14**). For example, Bax is one of the transcriptional targets of c-MYC and the main regulator of c-MYC-dependent apoptosis. Expression of c-MYC induces Bax upregulation and further releases cytochrome *c* from mitochondria. However, Bak is prevented from activating in response to c-MYC by the overexpression of Bcl-X_L (161). C-MYC is also known as stimuli participates in the extrinsic apoptosis pathway to sensitize cells to Fas-induced and TNF- α induced cell death. As introduced above, caspase 8 is a crucial initiator caspase downstream of FADD. The expression of caspase 8 can be enhanced directly or indirectly by c-MYC even with neutralizing antibodies against Fas ligand and TNF- α , therefore increasing the susceptibility of apoptosis (162). Furthermore, stable p53 in normal cells can interact with pro-apoptotic genes such as Puma, Noxa, Apaf-1, and Bax, and suppress anti-apoptotic genes including Bcl-2, Bcl-X_L, and Mcl-1. While ectopic MYC expression upregulates a tumor suppressor ARF, which further inhibits MDM2-mediated degradation of p53. Therefore c-MYC expression indirectly promotes p53 expression and triggers apoptosis (163). However, the oncogenic potential of c-MYC is released when continuous abnormal *c-MYC* expression occurs correlated with loss of stress response checkpoints such as p53 and Bcl-X_L, or activation of mitogenic signals such as RAS. In these circumstances, oncogenic c-MYC binds to canonical E-boxes at promoters, amplifying the output of current gene expression, simultaneously, also invasive non-canonical, lower-affinity E-boxes at promoters in a concentration-dependent manner, causing previously silent genes to be ectopically deregulated. Through this mechanism, c-MYC activated multiple genes to initiate and maintain all the “hallmarks” of cancer (153, 164, 165).

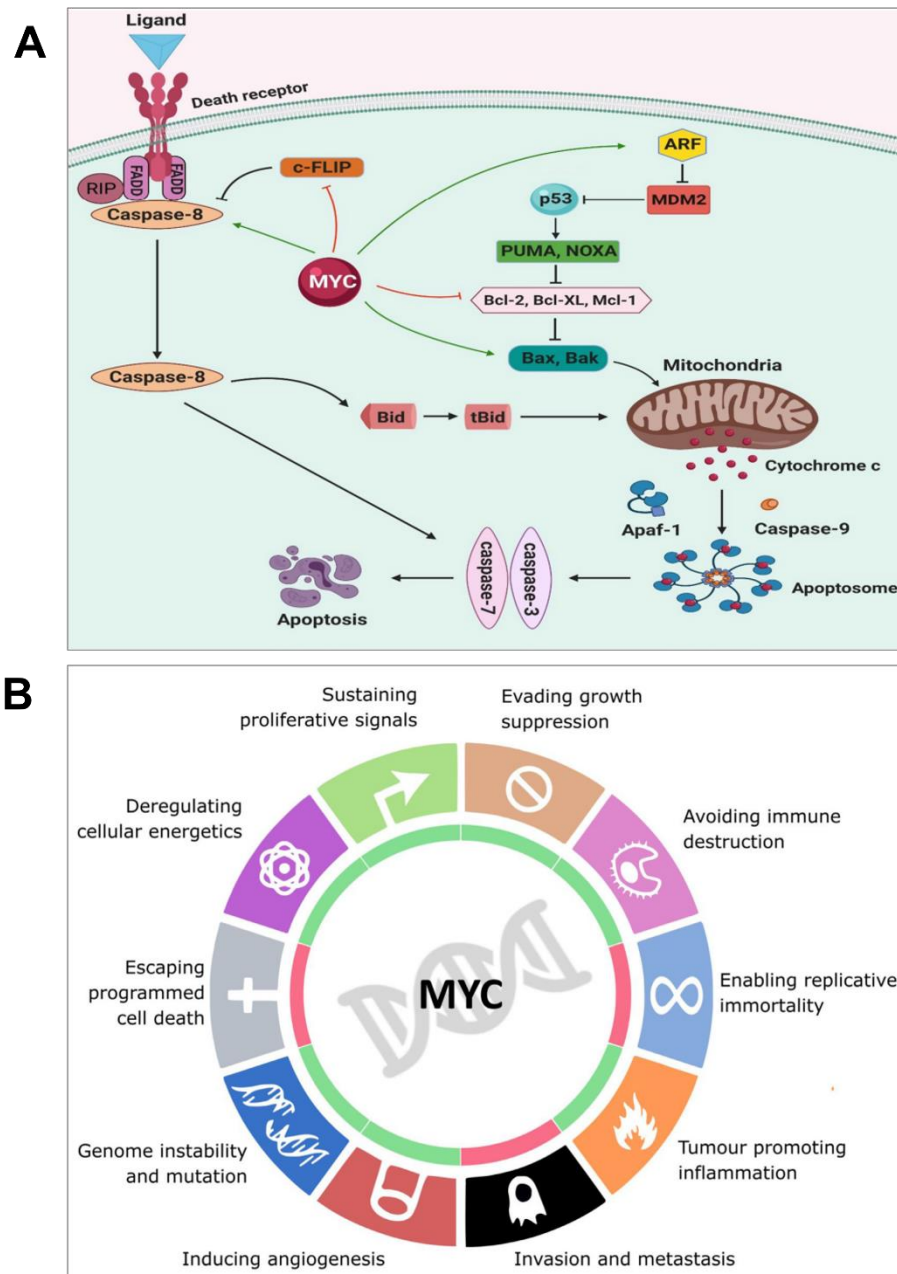


Figure 14. The relevance of c-MYC with apoptosis in the normal cells and c-MYC contributes to cancer. (A) c-MYC and apoptosis pathway. C-MYC expression can sensitize cells to a variety of proapoptotic stimuli (163). (B) Oncogenic level of c-MYC regulates all hallmarks of cancer (164).

1.6.2 c-MYC as a target for cancer treatment

c-MYC is a well-established therapeutic target. Experiments have shown that turning off c-MYC expression can regress tumor development. However, c-MYC has been considered to be

“undruggable”. Due to the large size of the c-MYC/MAX bHLHZ interface, and c-MYC lacks catalytic activity, unlike the other oncoprotein (*e.g.*, BRAF, EGFR, HEK2) with enzymatic pocket, many drugs are difficult to bind c-MYC with high affinity. This reality makes it extremely challenging in developing effective c-MYC inhibitors (166). Therapeutically, c-MYC has not yet been successfully targeted. Despite these challenges, direct inhibition of c-MYC and indirect inhibition of c-MYC are the major strategies and have been evaluated by a series of potential c-MYC inhibitors.

Direct inhibition is inhibiting c-MYC/MAX dimerization and E-box binding. Small molecules and peptides, as well as applying RNA interferences to downregulate c-MYC translation, have effectively blocked c-MYC activity (167). 10058-F4, 10075-G4, and 10075-A4 are the early identified compounds disrupting c-MYC/MAX interaction (168). The bHLHLZ of MYC represented the most studied structure for drug design of MYC inhibitors so far, aiming to bind to c-MYC/MAX dimer and prevent it from binding to DNA (169). Recently, OmoMYC as a 90 amino acid MYC mini-mutant attracted great attention. OmoMYC consists of the bHLHLZ domain and competes with c-MYC for binding to DNA by excluding c-MYC/MAX heterodimers and preventing the transcription of target genes. Among the different types of OmoMYC, OMO-1, and OMO-103 have progressed into clinical trials (170). In addition, given the short-life of c-MYC and its stability is regulated by ubiquitination, the field of proteolysis-targeting chimeras (PROTACs) is expanding. A promising result has shown pan-BETi PROTAC ARC-771 decreased c-MYC expression and caused xenograft tumor regression in prostate cancer mouse models (171).

Indirect inhibition is concerning c-MYC-related synthetic lethal interactions, which means the genes are the important mediators of c-MYC in the c-MYC-driven tumor cells (157). Diverse potential targets have been identified, including cyclin-dependent kinases (CDKs) related to cell cycle, ATR and CDHK1 related to DNA repair (172, 173). Moreover, one advantage of this group of novel synthetic lethal targets may already holding a clinical approved inhibitor that could be promptly utilized in c-MYC driven malignancies.

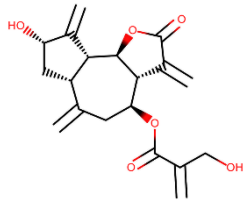
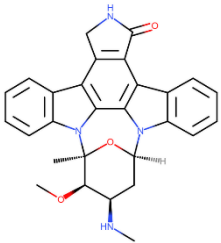
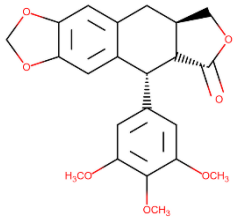
1.7 Parthanatos-inducing compounds in cancer cells

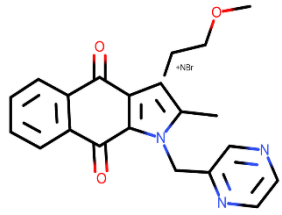
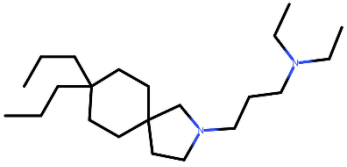
Mechanisms for bypassing the apoptosis signaling pathways have received considerable attention to cause the death of cancer cells. Parthanatos, as described above, is a recently discovered cell death mechanism related to cancer. The first discovery of parthanatos induced

by chemicals was in fibroblasts, exposed to N-methyl-N'-nitro-N-nitrosoguanidine (MNNG), a DNA-alkylating agent. This groundbreaking study also confirmed parthanatos is a caspase-dependent mode of cell death (90). Several evidence reported small molecules inducing parthanatos have shown promise as anticancer strategies. They are summarized in **Table 2**.

Interestingly, two known anticancer agents were found to be parthanatos-inducing compounds. For example, saurosporine was demonstrated to trigger AIF release and downstream DNA fragmentation in non-small-cell carcinomas (NSCLC2) cells, which are resistant to induce apoptosis by conventional anticancer treatment (174). Saurosporine is a microbial alkaloid isolated in 1977, followed by the approval for clinical use as a broadly selective and potent protein kinase inhibitor (175). Atiprimod is a kinase inhibitor against multiple myelomas. It was found to lead to cell death in an AIF-mediated pathway, but caspase-independent. However, some investigations were not accounted for here. For example, flavopiridol, a pan CDK inhibitor to kill cholangiocarcinoma cells, showed that the cell death mechanism was caspase-dependent, which raises the potential that might be parthanatos but lacks sufficient evidence. More verifications of biochemical relevant events are still required (176). Natural products have also induced parthanatos, such as cynaropicrin, isolated from edible plant (*Cynara scolymus*) (177), and deoxypodophyllotoxin, isolated from traditional plant (*Anthriscus sylvestris*) (178). These studies not only indicated parthanatos was triggered by the active compounds, but also affected deregulated proliferation pathways or transcription factors that are related to tumor progression. Therefore, parthanatos deserves to be investigated by established anticancer agents or natural products as a potential treatment for cancer drug resistance.

Table 2. Cancer therapeutic agents that inducing parthanatos verified *in vitro* and/or *in vivo*.

Compound (resource)	Chemical structure	Parthanatos-related biochemical events	Study model	Reference
Cynaropicrin (natural product)		γ H2AX upregulation, PARP and PAR hyperactivation, AIF translocation, Mitochondria membrane potential dysfunction, PARP-dependent cell death	Multiple myeloma, AMO1; T-ALL tumor xenograft zebrefish	(177)
Staurosporine (natural product)		Mitochondria membrane potential dysfunction, AIF release, nuclear fragmentation	Non-small-cell lung carcinomas, U1810	(174)
Deoxydopodophyllotoxin (natural product)		Upregulation of PARP and PAR, nuclear translocation of AIF	Glioma, C6, SHG-44	(178)

<p>YM155 (synthetic compound)</p>	 <p>The chemical structure of YM155 is a complex molecule. It features a central benzimidazole ring system. One of the benzimidazole nitrogens is substituted with a 2-pyridylmethyl group. The other benzimidazole nitrogen is substituted with a 2-(2-methoxyethyl)ethyl group. The benzimidazole ring is fused to a benzene ring. Two carbonyl groups are attached to the benzimidazole ring, one at the 2-position and one at the 4-position. The 2-position carbonyl is also attached to a benzene ring. The 4-position carbonyl is also attached to a benzene ring. The 2-position carbonyl is also attached to a benzene ring. The 4-position carbonyl is also attached to a benzene ring.</p>	<p>γH2AX expression, PARP and PAR overexpression, AIF translocation</p>	<p>Esophageal squamous-cell carcinoma, KYSE410</p>	<p>(179)</p>
<p>Atiprimod (synthetic compound)</p>	 <p>The chemical structure of Atiprimod is a complex molecule. It features a central benzimidazole ring system. One of the benzimidazole nitrogens is substituted with a 2-pyridylmethyl group. The other benzimidazole nitrogen is substituted with a 2-(2-methoxyethyl)ethyl group. The benzimidazole ring is fused to a benzene ring. Two carbonyl groups are attached to the benzimidazole ring, one at the 2-position and one at the 4-position. The 2-position carbonyl is also attached to a benzene ring. The 4-position carbonyl is also attached to a benzene ring. The 2-position carbonyl is also attached to a benzene ring. The 4-position carbonyl is also attached to a benzene ring.</p>	<p>AIF release, caspase-independent cell death</p>	<p>Mantle cell lymphoma, MCL; CB-17SCID mice</p>	<p>(180)</p>

2 Objective of the thesis

Although enormous advances in cancer biology and rapid growth in the designs of new chemotherapy agents, cancer cell resistance against the anticancer agent is still a challenging process that leads to major treatment failures. The cytotoxicity of antineoplastic drugs depends mainly on their ability to induce cell death, especially apoptosis. However, cancer cells are constantly evolving and adapting, allowing them the capacity to evade cell death, and the activation of oncogene, which confers the cells a selective growth advantage. Hence, the first part of this thesis focuses on a state-of-art cell death mechanism, parthanatos, induced by new synthetic derivatives, and investigates their underlying molecular modes of action. The other part of this thesis aimed to study a natural product derivative as a potential c-MYC inhibitor.

ZINC253504760 is a synthetic cardenolide that is structurally similar to cardiac glycoside (CG) such as digitoxin. In recent years, CG exhibited potential anticancer effects with many potential mechanisms and has been attracted interest in cancer drug discovery. This study aimed to 1) investigate the cytotoxicity of ZINC253504760 towards different drug-sensitive and -resistant cancer cells, 2) explore the major mode of cell death, 3) verify the potential affected target and pathway *in vitro* and *in silico* informed by microarray-based mRNA profiling.

J4 and J6 are two synthetic and characterized palladium (II) complexes, and were designed to be novel metal-based small molecules to overcome drug resistance. Despite displaying excellent cytotoxicity in drug-sensitive leukemia cells, J4 and J6 have not been shown to significantly induce apoptotic cell death. The aim of this study was continuously to find out the predominant mode of cell death induced by J4 and J6, as well as to verify whether the cell death mechanism efficiently works in multi-drug resistant cells.

ZINC15675948 is a natural product derivative of 1,2,4-oxadiazole. The compounds, 10074-G5 and 10075-A4 possess oxadiazole scaffold, are well-known c-MYC inhibitors. The aim of this study was 1) explore whether c-MYC is the potential target of ZINC15675948, 2) investigate the downstream cellular functions when c-MYC was affected.

3 Results and discussion

3.1 Cardiac glycoside (ZINC253504760), a novel MEK1/2 inhibitor inducing a state-of-art parthanatic cell death and G2/M arrest in leukemia cells

Cardiac glycosides have been identified as leading compounds in cancer treatment recently. The Raf-MEK-ERK signaling cascade is a well-characterized MAPK pathway that is aberrantly activated in human cancers. MEK currently being the only activator of ERK, making it an attractive target. In the present study, a cardiac glycoside compound ZINC253504760 displayed potent cytotoxicity to five pairs of drug-sensitive and -resistant cell lines except for MDA-MB-BCRP. CCRF-CEM cells were the most sensitive to ZINC253504760 with an IC_{50} value of $0.022 \pm 0.002 \mu\text{M}$, which were selected as the study model for further investigation. Transcriptome-wide mRNA expression profiling and pathway analysis pointed out the canonical pathway involved in “G2/M cell cycle arrest”, which was predicted to be connected with downregulations of MEK1/2 and ERK. Afterward, G2/M arrest was remarkably observed by flow cytometry in a time- and concentration-dependent manner. The results were confirmed by fluorescence microscopy that ZINC253504760 affected microtubule polymerization. A series of genes affected by ZINC253504760 in G2/M arrest was verified by the upregulation of HIPK2, PPM1D, CDK1, Wee1, CKS1, CKS2, and the downregulation of p53 and CDK7 using qRT-PCR. Interestingly, apoptosis was not the major mode of cell death observed on flow cytometry, nor was it autophagy. While ZINC253504760 resulted in mitochondrial membrane potential collapse. Western blotting showed caspase 3 expression but not its cleaved form. These results indicated the mode of cell death was caused by mitochondria dysfunction and were caspase 3-independent. Therefore, we further focused on a novel caspase-independent cell death mechanism parthanatos. The key features of ZINC253504760-induced parthanatos were confirmed by PARP activation, PAR accumulation, and AIF translocation by western blotting. AIF translocation from cytoplasm to nucleus was captured using immunofluorescence microscopy. Sing cell gel electrophoresis (comet assay) supported ZINC253504760 caused parthanatos and eventually the cells die from large-scale DNA damage. Moreover, ZINC253504760 inhibited phosphorylation of MEK1/2 upon treatment for 24 h, which further affected the activation of ERK. Molecular docking also showed ZINC253504760 as an ATP

competitive kinase inhibitor bound to the phosphorylation sites on MEK1 (SER218) and MEK2 (SER222). Their binding was confirmed in microscale thermophoresis.

Further reading: Appendix I

The cardiac glycoside ZINC253504760 induces parthanatos-type cell death and G2/M arrest via downregulation of MEK1/2 phosphorylation in leukemia cells

Min Zhou, Joelle C. Boulos, Sabine M. Klauck, Thomas Efferth

3.2 Palladium(II) complexes induced parthanatos-type cell death in CCRF-CEM leukemia and its multidrug-resistant cells

Due to severe-side effects and the development of drug resistance with platinum complexes, palladium complexes as innovative anticancer drugs are emerging. The aim of this study was to reveal the major mode of cell death of two synthetic palladium (II) complexes with halogen-substitute Schiff bases and 2-picolylamine (pic), one with double chlorine-substitution, another with double iodine-substitution. Their profound cytotoxicity and G2/M arrest in CCRF-CEM leukemia cells had been investigated in previous study (IC₅₀ value of J4: 1.78 μ M, IC₅₀ value of J6: 2.39 μ M), but none of them significantly induce apoptotic cell death (181). In the present study, surprisingly, PARP-dependent parthanatic cell death was primarily induced by the two palladium(II) complexes, evidenced by PARP, PAR, and p-histone H2A.X overactivation by western blotting, mitochondrial membrane potential sharply dysfunction, AIF translocation from cytoplasm to nucleus by immunofluorescence microscopy, and DNA fragmentation in a concentration-dependent manner using alkaline single cell gel electrophoresis. The induction of parthanatos was also observed in P-gp overexpressing CEM/ADR5000 cells. PARP inhibitor PJ34 indicated cell viability was maintained in combination with PJ34 plus J4 or J6. Furthermore, J4 and J6 were unable to induce other cell death mechanisms such as autophagy, apoptosis, or necrosis, verified by western blotting and flow cytometry. Both J4 and J6 showed less cytotoxicity on human peripheral blood mononuclear cells (PBMCs) than leukemia cells.

Further reading: Appendix II

Two palladium (II) complexes derived from halogen-substituted Schiff bases and 2-picoplylamine induce parthanatos-type cell death in sensitive and multi-drug resistant CCRF-CEM leukemia cells

Min Zhou, Joelle C. Boulos, Ejlal A. Omer, Hadi Amiri Rudbari, Tanja Schirmeister, Nicola Micale, Thomas Efferth

3.3 1,2,4-oxadiazole derivative (ZINC15675948) as a novel c-MYC inhibitor by inducing DNA damage, cell cycle arrest, and apoptosis in leukemia and breast cancer cells

The *MYC* oncogene contributes many hallmarks of cancer in various highly aggressive human cancers, such as acute leukemia and triple-negative breast cancer. 1,2,4-oxadiazole is one of the well-known oxadiazoles attracting increasing interest for their anticancer activities. In this study, (6*S*)-*N*-(4-methylphenyl)-6-(3-naphthalen-2-yl-1,2,4-oxadiazol-5-yl)-3,4,6,7-tetrahydroimidazo[4,5-*c*]pyridine-5-carboxamide, code name ZINC15675948, exhibited profound cytotoxicity in CCRF-CEM leukemia and MDA-MB-231-pcDNA3 breast cancer cells with IC₅₀ values at $0.008 \pm 0.001 \mu\text{M}$ and $0.08 \pm 0.004 \mu\text{M}$, respectively. Particularly, ZINC15675948 displayed a strong binding to c-MYC/MAX interaction site in molecular docking (LEB: -9.91 kcal/mol , pKi: $0.055 \mu\text{M}$), compared with and microscale thermophoresis (K_d: $1.18 \pm 0.1 \mu\text{M}$). C-MYC reporter assay, western blotting, and qRT-PCR showed downregulation of c-MYC by ZINC15675948 in a concentration-dependent manner. For mechanistic studies of ZINC15675948, microarray hybridization and signaling pathway analyses predicted several cellular functions were commonly affected by ZINC15675948 in both CCRF-CEM cells and MDA-MB-231-pcDNA3 cells compared with their control samples, including “cellular growth and proliferation”, “DNA replication, recombination and repair”, “cell cycle”, as well as “cell death and survival”. The “cell cycle”, and “cell death and survival” networks of ZINC15675948 treated CCRF-CEM cells indeed revealed downregulation of *c-MYC* gene, implying they were downstream of c-MYC inhibition. However, the microarray profiling of MDA-MB-231-pcDNA3 cells revealed an involvement of ubiquitination toward c-MYC, indicated by the upregulation of a novel ubiquitin ligase (*ELL2*) in the absence of *c-MYC*

expression. DNA damage was significantly induced by ZINC15675948 indicated by “comet tail” in single cell gel electrophoresis. ZINC15675948 arrested CCRF-CEM cells in G2/M phase and MDA-MB-231-pcDNA3 cells in S phase. Furthermore, ZINC15675948 induced apoptosis in both of the cell lines. Autophagy induction was only observed in CCRF-CEM cells. We propose ZINC15675948 as a novel c-MYC inhibitor for leukemia and breast cancer treatment.

Further reading: Appendix III

Modes of action of a novel c-MYC inhibiting 1,2,4-oxadiazole derivative in leukemia and breast cancer cells

Min Zhou, Joelle C. Boulos, Ejlal A. Omer, Sabine M. Klauck, Thomas Efferth

4 Conclusion

Programmed cell death especially apoptosis is an important barrier to prevent cancer development. Cancer cells evolve multiple strategies to evade apoptosis. Therefore, resisting cell death is not only a hallmark to initiate tumors, but also a challenge for overcoming multi-drug resistance. This thesis reported three promising compounds that induce the novel mode of cell death termed parthanatos rather than apoptosis in leukemia cells to better attack drug resistance, and one potential compound that promotes apoptotic cell death in leukemia and breast cancer cells by inhibiting oncogene *c-MYC*.

The synthetic derivative of cardiac glycoside compounds (CGs) (ZINC253504760) might be a potential therapeutic agent for blocking the RAS-RAF-MEK-ERK signaling pathway in CCRF-CEM leukemia cells. ZINC253504760 inhibited MEK1/2 phosphorylation, which further affected downstream ERK. G2/M phase arrest was significantly induced in a time- and concentration-dependent manner. Importantly, ZINC253504760 triggered parthanatos-type cell death. A series of *in vitro* investigations confirmed that this compound induced PARP and PAR hyperactivation, and nuclear AIF translocation, mitochondrial membrane potential collapse. This study will promote novel modes of cell death as an alternative strategy for cancer treatment.

Two synthetic palladium (II) complexes (J4 and J6) containing double chlorine-/iodine substituted Schiff base and 2-picolyamine showed induction of parthanatos as their primary cell death in CCRF-CEM leukemia cells and its subline P-gp overexpressing cells. J4 and J6 overactivated p-histone H2A.X, PARP, and PAR, followed by AIF translocation from mitochondria to the nucleus, leading to large DNA fragmentation and eventually parthanatic cell death. The investigation of cell death mechanism of J4 and J6 will motivate further designs on the development of palladium-based complexes as cancer therapy, especially to kill cancer cells in other cell death modes that insufficiently induce apoptosis.

The 1,2,4-oxadiazole derivative (ZINC15675948) may provide a novel treatment for c-MYC-driven CCRF-CEM and MDA-MB-231-pcDNA cells. ZINC15675948 bound to c-MYC/MAX interface and further affected c-MYC activity. As downstream of c-MYC inhibition, ZINC15675948 induced remarkable DNA damage, cell cycle arrest, and apoptosis in both cell lines. In addition, ZINC15675948 also induced autophagy in leukemia cells. This study will help to continue targeting apoptosis, as *c-MYC* oncogene is one of the master regulators for gene expression of apoptosis.

5 Reference

1. Sung H, *et al.* (2021) Global Cancer Statistics 2020: GLOBOCAN Estimates of Incidence and Mortality Worldwide for 36 Cancers in 185 Countries. *CA: a cancer journal for clinicians* 71(3):209-249.
2. Carbone A (2020) Cancer Classification at the Crossroads. *Cancers* 12(4).
3. Murali R, Soslow RA, & Weigelt B (2014) Classification of endometrial carcinoma: more than two types. *The Lancet. Oncology* 15(7):e268-278.
4. HaDuong JH, Martin AA, Skapek SX, & Mascarenhas L (2015) Sarcomas. *Pediatric clinics of North America* 62(1):179-200.
5. Minciacchi VR, Kumar R, & Krause DS (2021) Chronic Myeloid Leukemia: A Model Disease of the Past, Present and Future. *Cells* 10(1).
6. Jiang M, Bennani NN, & Feldman AL (2017) Lymphoma classification update: T-cell lymphomas, Hodgkin lymphomas, and histiocytic/dendritic cell neoplasms. *Expert review of hematology* 10(3):239-249.
7. Cowan AJ, *et al.* (2022) Diagnosis and Management of Multiple Myeloma: A Review. *Jama* 327(5):464-477.
8. Hanahan D & Weinberg RA (2000) The hallmarks of cancer. *Cell* 100(1):57-70.
9. Hanahan D & Weinberg RA (2011) Hallmarks of cancer: the next generation. *Cell* 144(5):646-674.
10. Hanahan D (2022) Hallmarks of Cancer: New Dimensions. *Cancer discovery* 12(1):31-46.
11. Wyld L, Audisio RA, & Poston GJ (2015) The evolution of cancer surgery and future perspectives. *Nature reviews. Clinical oncology* 12(2):115-124.
12. Lippman SM & Hawk ET (2009) Cancer prevention: from 1727 to milestones of the past 100 years. *Cancer research* 69(13):5269-5284.
13. Baskar R, Lee KA, Yeo R, & Yeoh KW (2012) Cancer and radiation therapy: current advances and future directions. *International journal of medical sciences* 9(3):193-199.
14. Bernier J, Hall EJ, & Giaccia A (2004) Radiation oncology: a century of achievements. *Nature Reviews Cancer* 4(9):737-747.
15. Baxevanis CN, Perez SA, & Papamichail M (2009) Cancer immunotherapy. *Critical reviews in clinical laboratory sciences* 46(4):167-189.
16. Sanmamed MF & Chen L (2018) A Paradigm Shift in Cancer Immunotherapy: From Enhancement to Normalization. *Cell* 175(2):313-326.
17. Fairchild A, *et al.* (2015) Hormonal therapy in oncology: a primer for the radiologist. *AJR. American journal of roentgenology* 204(6):W620-630.
18. Henderson BE & Feigelson HS (2000) Hormonal carcinogenesis. *Carcinogenesis* 21(3):427-433.
19. DeVita VT, Jr. & Chu E (2008) A history of cancer chemotherapy. *Cancer research* 68(21):8643-8653.
20. Krumbhaar EB & Krumbhaar HD (1919) The Blood and Bone Marrow in Yellow Cross Gas (Mustard Gas) Poisoning: Changes produced in the Bone Marrow of Fatal Cases. *The Journal of medical research* 40(3):497-508.493.
21. DeVita VT, Jr. (1978) The evolution of therapeutic research in cancer. *The New England journal of medicine* 298(16):907-910.
22. Lind MJ (2011) Principles of cytotoxic chemotherapy. *Medicine* 39(12):711-716.
23. Oun R, Moussa YE, & Wheate NJ (2018) The side effects of platinum-based chemotherapy drugs: a review for chemists. *Dalton transactions (Cambridge, England : 2003)* 47(19):6645-6653.

24. Portugal J (2018) Challenging transcription by DNA-binding antitumor drugs. *Biochemical pharmacology* 155:336-345.
25. Delgado JL, Hsieh CM, Chan NL, & Hiasa H (2018) Topoisomerases as anticancer targets. *The Biochemical journal* 475(2):373-398.
26. Hartmann JT & Lipp HP (2006) Camptothecin and podophyllotoxin derivatives: inhibitors of topoisomerase I and II - mechanisms of action, pharmacokinetics and toxicity profile. *Drug safety* 29(3):209-230.
27. Minotti G, Menna P, Salvatorelli E, Cairo G, & Gianni L (2004) Anthracyclines: molecular advances and pharmacologic developments in antitumor activity and cardiotoxicity. *Pharmacological reviews* 56(2):185-229.
28. Jang JY, Kim D, & Kim ND (2023) Recent Developments in Combination Chemotherapy for Colorectal and Breast Cancers with Topoisomerase Inhibitors. *International Journal of Molecular Sciences* 24(9):8457.
29. Godzieba M & Ciesielski S (2020) Natural DNA Intercalators as Promising Therapeutics for Cancer and Infectious Diseases. *Current cancer drug targets* 20(1):19-32.
30. Siddik ZH (2003) Cisplatin: mode of cytotoxic action and molecular basis of resistance. *Oncogene* 22(47):7265-7279.
31. Florea AM & Büsselberg D (2011) Cisplatin as an anti-tumor drug: cellular mechanisms of activity, drug resistance and induced side effects. *Cancers* 3(1):1351-1371.
32. Ghosh S (2019) Cisplatin: The first metal based anticancer drug. *Bioorganic chemistry* 88:102925.
33. Joshi AM, *et al.* (2021) Microtubule Inhibitors and Cardiotoxicity. *Current Oncology Reports* 23(3):30.
34. Farber S & Diamond LK (1948) Temporary remissions in acute leukemia in children produced by folic acid antagonist, 4-aminopteroyl-glutamic acid. *The New England journal of medicine* 238(23):787-793.
35. Luengo A, Gui DY, & Vander Heiden MG (2017) Targeting Metabolism for Cancer Therapy. *Cell chemical biology* 24(9):1161-1180.
36. Plummer C, *et al.* (2019) Treatment specific toxicities: Hormones, antihormones, radiation therapy. *Seminars in oncology* 46(6):414-420.
37. Lee YT, Tan YJ, & Oon CE (2018) Molecular targeted therapy: Treating cancer with specificity. *Eur J Pharmacol* 834:188-196.
38. Joo WD, Visintin I, & Mor G (2013) Targeted cancer therapy--are the days of systemic chemotherapy numbered? *Maturitas* 76(4):308-314.
39. Zhong L, *et al.* (2021) Small molecules in targeted cancer therapy: advances, challenges, and future perspectives. *Signal transduction and targeted therapy* 6(1):201.
40. Chabner BA & Roberts TG (2005) Chemotherapy and the war on cancer. *Nature Reviews Cancer* 5(1):65-72.
41. Roskoski Jr R (2022) Properties of FDA-approved small molecule protein kinase inhibitors: A 2022 update. *Pharmacological Research* 175:106037.
42. Kimiz-Gebologlu I, Gulce-Iz S, & Biray-Avcı C (2018) Monoclonal antibodies in cancer immunotherapy. *Molecular biology reports* 45(6):2935-2940.
43. van de Donk NW, *et al.* (2016) Clinical efficacy and management of monoclonal antibodies targeting CD38 and SLAMF7 in multiple myeloma. *Blood* 127(6):681-695.
44. Weiner LM, Surana R, & Wang S (2010) Monoclonal antibodies: versatile platforms for cancer immunotherapy. *Nature Reviews Immunology* 10(5):317-327.
45. Dosio F, Brusa P, & Cattell L (2011) Immunotoxins and anticancer drug conjugate assemblies: the role of the linkage between components. *Toxins* 3(7):848-883.
46. Morse MA, Gwin WR, 3rd, & Mitchell DA (2021) Vaccine Therapies for Cancer: Then and Now. *Targeted oncology* 16(2):121-152.

47. Lin MJ, *et al.* (2022) Cancer vaccines: the next immunotherapy frontier. *Nature Cancer* 3(8):911-926.
48. Burke EE, Kodumudi K, Ramamoorthi G, & Czerniecki BJ (2019) Vaccine Therapies for Breast Cancer. *Surgical oncology clinics of North America* 28(3):353-367.
49. Tang R & Xu Z (2020) Gene therapy: a double-edged sword with great powers. *Molecular and Cellular Biochemistry* 474(1):73-81.
50. Ma CC, Wang ZL, Xu T, He ZY, & Wei YQ (2020) The approved gene therapy drugs worldwide: from 1998 to 2019. *Biotechnology advances* 40:107502.
51. Gottesman MM & Pastan I (1993) Biochemistry of multidrug resistance mediated by the multidrug transporter. *Annual review of biochemistry* 62:385-427.
52. Mansoori B, Mohammadi A, Davudian S, Shirjang S, & Baradaran B (2017) The Different Mechanisms of Cancer Drug Resistance: A Brief Review. *Advanced pharmaceutical bulletin* 7(3):339-348.
53. Assaraf YG, *et al.* (2019) The multi-factorial nature of clinical multidrug resistance in cancer. *Drug resistance updates : reviews and commentaries in antimicrobial and anticancer chemotherapy* 46:100645.
54. Efferth T (2001) The human ATP-binding cassette transporter genes: from the bench to the bedside. *Current molecular medicine* 1(1):45-65.
55. Efferth T & Volm M (2017) Multiple resistance to carcinogens and xenobiotics: P-glycoproteins as universal detoxifiers. *Archives of toxicology* 91(7):2515-2538.
56. Locher KP (2016) Mechanistic diversity in ATP-binding cassette (ABC) transporters. *Nat Struct Mol Biol* 23(6):487-493.
57. Nobili S, *et al.* (2020) Role of ATP-binding cassette transporters in cancer initiation and progression. *Seminars in cancer biology* 60:72-95.
58. Sharom FJ (2008) ABC multidrug transporters: structure, function and role in chemoresistance. *Pharmacogenomics* 9(1):105-127.
59. Aller SG, *et al.* (2009) Structure of P-glycoprotein reveals a molecular basis for poly-specific drug binding. *Science (New York, N.Y.)* 323(5922):1718-1722.
60. Abolhoda A, *et al.* (1999) Rapid activation of MDR1 gene expression in human metastatic sarcoma after in vivo exposure to doxorubicin. *Clinical cancer research : an official journal of the American Association for Cancer Research* 5(11):3352-3356.
61. Efferth T, *et al.* (2008) Prediction of broad spectrum resistance of tumors towards anticancer drugs. *Clinical cancer research : an official journal of the American Association for Cancer Research* 14(8):2405-2412.
62. Palmeira A, Sousa E, Vasconcelos MH, & Pinto MM (2012) Three decades of P-gp inhibitors: skimming through several generations and scaffolds. *Current medicinal chemistry* 19(13):1946-2025.
63. DeGorter MK, Xia CQ, Yang JJ, & Kim RB (2012) Drug transporters in drug efficacy and toxicity. *Annual review of pharmacology and toxicology* 52:249-273.
64. Mao Q & Unadkat JD (2015) Role of the breast cancer resistance protein (BCRP/ABCG2) in drug transport--an update. *Aaps j* 17(1):65-82.
65. Mohammad RM, *et al.* (2015) Broad targeting of resistance to apoptosis in cancer. *Seminars in cancer biology* 35 Suppl(0):S78-s103.
66. Pistritto G, Trisciuglio D, Ceci C, Garufi A, & D'Orazi G (2016) Apoptosis as anticancer mechanism: function and dysfunction of its modulators and targeted therapeutic strategies. *Aging* 8(4):603-619.
67. Wong RS (2011) Apoptosis in cancer: from pathogenesis to treatment. *Journal of experimental & clinical cancer research : CR* 30(1):87.
68. Youle RJ & Strasser A (2008) The BCL-2 protein family: opposing activities that mediate cell death. *Nature Reviews Molecular Cell Biology* 9(1):47-59.

69. Yu J, Wang Z, Kinzler KW, Vogelstein B, & Zhang L (2003) PUMA mediates the apoptotic response to p53 in colorectal cancer cells. *Proceedings of the National Academy of Sciences of the United States of America* 100(4):1931-1936.
70. Thornborrow EC, Patel S, Mastropietro AE, Schwartzfarb EM, & Manfredi JJ (2002) A conserved intronic response element mediates direct p53-dependent transcriptional activation of both the human and murine bax genes. *Oncogene* 21(7):990-999.
71. Song G, Wang W, & Hu T (2011) p53 facilitates BH3-only BID nuclear export to induce apoptosis in the irreparable DNA damage response. *Medical hypotheses* 77(5):850-852.
72. Schimmer AD (2004) Inhibitor of apoptosis proteins: translating basic knowledge into clinical practice. *Cancer research* 64(20):7183-7190.
73. Tu H & Costa M (2020) XIAP's Profile in Human Cancer. *Biomolecules* 10(11).
74. Strasser A & Vaux DL (2020) Cell Death in the Origin and Treatment of Cancer. *Molecular cell* 78(6):1045-1054.
75. Galluzzi L, et al. (2007) Cell death modalities: classification and pathophysiological implications. *Cell death and differentiation* 14(7):1237-1243.
76. Cerella C, Teiten MH, Radogna F, Dicato M, & Diederich M (2014) From nature to bedside: pro-survival and cell death mechanisms as therapeutic targets in cancer treatment. *Biotechnology advances* 32(6):1111-1122.
77. Galluzzi L, et al. (2018) Molecular mechanisms of cell death: recommendations of the Nomenclature Committee on Cell Death 2018. *Cell Death & Differentiation* 25(3):486-541.
78. Yan G, Elbadawi M, & Efferth T (2020) Multiple cell death modalities and their key features (Review). *World Acad Sci J* 2(2):39-48.
79. Kerr JF, Wyllie AH, & Currie AR (1972) Apoptosis: a basic biological phenomenon with wide-ranging implications in tissue kinetics. *British journal of cancer* 26(4):239-257.
80. Xu X, Lai Y, & Hua ZC (2019) Apoptosis and apoptotic body: disease message and therapeutic target potentials. *Bioscience reports* 39(1).
81. McIlwain DR, Berger T, & Mak TW (2013) Caspase functions in cell death and disease. *Cold Spring Harbor perspectives in biology* 5(4):a008656.
82. Fulda S & Debatin KM (2006) Extrinsic versus intrinsic apoptosis pathways in anticancer chemotherapy. *Oncogene* 25(34):4798-4811.
83. Walczak H (2013) Death receptor-ligand systems in cancer, cell death, and inflammation. *Cold Spring Harbor perspectives in biology* 5(5):a008698.
84. Ozören N & El-Deiry WS (2002) Defining characteristics of Types I and II apoptotic cells in response to TRAIL. *Neoplasia (New York, N.Y.)* 4(6):551-557.
85. Carneiro BA & El-Deiry WS (2020) Targeting apoptosis in cancer therapy. *Nature Reviews Clinical Oncology* 17(7):395-417.
86. David KK, Andrabi SA, Dawson TM, & Dawson VL (2009) Parthanatos, a messenger of death. *Frontiers in bioscience (Landmark edition)* 14(3):1116-1128.
87. Andrabi SA, Dawson TM, & Dawson VL (2008) Mitochondrial and nuclear cross talk in cell death: parthanatos. *Annals of the New York Academy of Sciences* 1147:233-241.
88. Zhou Y, et al. (2021) Parthanatos and its associated components: Promising therapeutic targets for cancer. *Pharmacol Res* 163:105299.
89. Fatokun AA, Dawson VL, & Dawson TM (2014) Parthanatos: mitochondrial-linked mechanisms and therapeutic opportunities. *British journal of pharmacology* 171(8):2000-2016.
90. Yu SW, et al. (2002) Mediation of poly(ADP-ribose) polymerase-1-dependent cell death by apoptosis-inducing factor. *Science (New York, N.Y.)* 297(5579):259-263.
91. Wang Y, Dawson VL, & Dawson TM (2009) Poly(ADP-ribose) signals to mitochondrial AIF: A key event in parthanatos. *Experimental Neurology* 218(2):193-202.

92. Koehler RC, Dawson VL, & Dawson TM (2021) Targeting Parthanatos in Ischemic Stroke. *Frontiers in neurology* 12:662034.
93. Amé JC, Spenlehauer C, & de Murcia G (2004) The PARP superfamily. *BioEssays : news and reviews in molecular, cellular and developmental biology* 26(8):882-893.
94. Pascal JM (2018) The comings and goings of PARP-1 in response to DNA damage. *DNA repair* 71:177-182.
95. Bürkle A & Virág L (2013) Poly(ADP-ribose): PARadigms and PARadoxes. *Molecular aspects of medicine* 34(6):1046-1065.
96. Andrabi SA, et al. (2006) Poly(ADP-ribose) (PAR) polymer is a death signal. *Proceedings of the National Academy of Sciences of the United States of America* 103(48):18308-18313.
97. Daugas E, et al. (2000) Mitochondrio-nuclear translocation of AIF in apoptosis and necrosis. *FASEB journal : official publication of the Federation of American Societies for Experimental Biology* 14(5):729-739.
98. Levine B & Klionsky DJ (2017) Autophagy wins the 2016 Nobel Prize in Physiology or Medicine: Breakthroughs in baker's yeast fuel advances in biomedical research. *Proceedings of the National Academy of Sciences of the United States of America* 114(2):201-205.
99. Mizushima N & Klionsky DJ (2007) Protein turnover via autophagy: implications for metabolism. *Annual review of nutrition* 27:19-40.
100. Mizushima N (2007) Autophagy: process and function. *Genes & development* 21(22):2861-2873.
101. Mizushima N (2005) The pleiotropic role of autophagy: from protein metabolism to bactericide. *Cell death and differentiation* 12 Suppl 2:1535-1541.
102. Choi AM, Ryter SW, & Levine B (2013) Autophagy in human health and disease. *The New England journal of medicine* 368(7):651-662.
103. Onorati AV, Dyczynski M, Ojha R, & Amaravadi RK (2018) Targeting autophagy in cancer. *Cancer* 124(16):3307-3318.
104. Fang Y, et al. (2020) Pyroptosis: A new frontier in cancer. *Biomedicine & pharmacotherapy = Biomedecine & pharmacotherapie* 121:109595.
105. Wang H, et al. (2022) The emerging role of pyroptosis in pediatric cancers: from mechanism to therapy. *Journal of hematology & oncology* 15(1):140.
106. Tong X, et al. (2022) Targeting cell death pathways for cancer therapy: recent developments in necroptosis, pyroptosis, ferroptosis, and cuproptosis research. *Journal of hematology & oncology* 15(1):174.
107. Dixon SJ, et al. (2012) Ferroptosis: an iron-dependent form of nonapoptotic cell death. *Cell* 149(5):1060-1072.
108. Xie Y, et al. (2016) Ferroptosis: process and function. *Cell death and differentiation* 23(3):369-379.
109. Stockwell BR, et al. (2017) Ferroptosis: A Regulated Cell Death Nexus Linking Metabolism, Redox Biology, and Disease. *Cell* 171(2):273-285.
110. Liu J, et al. (2022) Iron plays a role in sulfasalazine-induced ferroptosis with autophagic flux blockage in K7M2 osteosarcoma cells. *Metallomics : integrated biometal science* 14(5).
111. Zhang C, Liu X, Jin S, Chen Y, & Guo R (2022) Ferroptosis in cancer therapy: a novel approach to reversing drug resistance. *Mol Cancer* 21(1):47.
112. Zhao L, et al. (2022) Ferroptosis in cancer and cancer immunotherapy. *Cancer communications (London, England)* 42(2):88-116.
113. Tsvetkov P, et al. (2022) Copper induces cell death by targeting lipoylated TCA cycle proteins. *Science (New York, N.Y.)* 375(6586):1254-1261.

114. Kahlson MA & Dixon SJ (2022) Copper-induced cell death. *Science (New York, N.Y.)* 375(6586):1231-1232.
115. Montagut C & Settleman J (2009) Targeting the RAF-MEK-ERK pathway in cancer therapy. *Cancer letters* 283(2):125-134.
116. Zhang W & Liu HT (2002) MAPK signal pathways in the regulation of cell proliferation in mammalian cells. *Cell research* 12(1):9-18.
117. Barbosa R, Acevedo LA, & Marmorstein R (2021) The MEK/ERK Network as a Therapeutic Target in Human Cancer. *Molecular cancer research : MCR* 19(3):361-374.
118. Roberts PJ & Der CJ (2007) Targeting the Raf-MEK-ERK mitogen-activated protein kinase cascade for the treatment of cancer. *Oncogene* 26(22):3291-3310.
119. Voisin L, Saba-El-Leil MK, Julien C, Frémin C, & Meloche S (2010) Genetic demonstration of a redundant role of extracellular signal-regulated kinase 1 (ERK1) and ERK2 mitogen-activated protein kinases in promoting fibroblast proliferation. *Molecular and cellular biology* 30(12):2918-2932.
120. Balmano K & Cook SJ (2009) Tumour cell survival signalling by the ERK1/2 pathway. *Cell Death & Differentiation* 16(3):368-377.
121. Guo YJ, *et al.* (2020) ERK/MAPK signalling pathway and tumorigenesis. *Experimental and therapeutic medicine* 19(3):1997-2007.
122. Samatar AA & Poulikakos PI (2014) Targeting RAS-ERK signalling in cancer: promises and challenges. *Nature reviews. Drug discovery* 13(12):928-942.
123. Haigis KM (2017) KRAS Alleles: The Devil Is in the Detail. *Trends in cancer* 3(10):686-697.
124. Proietti I, *et al.* (2020) Mechanisms of Acquired BRAF Inhibitor Resistance in Melanoma: A Systematic Review. *Cancers* 12(10).
125. Sosman JA, *et al.* (2012) Survival in BRAF V600-mutant advanced melanoma treated with vemurafenib. *The New England journal of medicine* 366(8):707-714.
126. Subbiah V, Baik C, & Kirkwood JM (2020) Clinical Development of BRAF plus MEK Inhibitor Combinations. *Trends in cancer* 6(9):797-810.
127. Pylayeva-Gupta Y, Grabocka E, & Bar-Sagi D (2011) RAS oncogenes: weaving a tumorigenic web. *Nature reviews. Cancer* 11(11):761-774.
128. Raimondi V, *et al.* (2022) A personalized molecular approach in multiple myeloma: the possible use of RAF/RAS/MEK/ERK and BCL-2 inhibitors. *Exploration of targeted anti-tumor therapy* 3(4):463-479.
129. Carné Trécesson S, *et al.* (2017) BCL-X(L) directly modulates RAS signalling to favour cancer cell stemness. *Nature communications* 8(1):1123.
130. Chin L, *et al.* (1999) Essential role for oncogenic Ras in tumour maintenance. *Nature* 400(6743):468-472.
131. Tan N, *et al.* (2013) Bcl-2/Bcl-xL inhibition increases the efficacy of MEK inhibition alone and in combination with PI3 kinase inhibition in lung and pancreatic tumor models. *Molecular cancer therapeutics* 12(6):853-864.
132. Ullah R, Yin Q, Snell AH, & Wan L (2022) RAF-MEK-ERK pathway in cancer evolution and treatment. *Seminars in cancer biology* 85:123-154.
133. Caunt CJ, Sale MJ, Smith PD, & Cook SJ (2015) MEK1 and MEK2 inhibitors and cancer therapy: the long and winding road. *Nature Reviews Cancer* 15(10):577-592.
134. Eblen ST, *et al.* (2004) Mitogen-activated protein kinase feedback phosphorylation regulates MEK1 complex formation and activation during cellular adhesion. *Molecular and cellular biology* 24(6):2308-2317.
135. Kocieniewski P & Lipniacki T (2013) MEK1 and MEK2 differentially control the duration and amplitude of the ERK cascade response. *Physical biology* 10(3):035006.

136. Alessi DR, Cuenda A, Cohen P, Dudley DT, & Saltiel AR (1995) PD 098059 Is a Specific Inhibitor of the Activation of Mitogen-activated Protein Kinase Kinase in Vitro and in Vivo(*). *Journal of Biological Chemistry* 270(46):27489-27494.
137. Duncia JV, *et al.* (1998) MEK inhibitors: the chemistry and biological activity of U0126, its analogs, and cyclization products. *Bioorganic & medicinal chemistry letters* 8(20):2839-2844.
138. Williams DH, *et al.* (1998) Ro 09-2210 exhibits potent anti-proliferative effects on activated T cells by selectively blocking MKK activity. *Biochemistry* 37(26):9579-9585.
139. Pan Y & Mader MM (2022) Principles of Kinase Allosteric Inhibition and Pocket Validation. *Journal of Medicinal Chemistry* 65(7):5288-5299.
140. Singh VJ, Sharma B, & Chawla PA (2021) Recent developments in mitogen activated protein kinase inhibitors as potential anticancer agents. *Bioorganic chemistry* 114:105161.
141. Do K, *et al.* (2015) Biomarker-driven phase 2 study of MK-2206 and selumetinib (AZD6244, ARRY-142886) in patients with colorectal cancer. *Investigational new drugs* 33(3):720-728.
142. Dang CV (2012) MYC on the path to cancer. *Cell* 149(1):22-35.
143. Vennstrom B, Sheiness D, Zabielski J, & Bishop JM (1982) Isolation and characterization of c-myc, a cellular homolog of the oncogene (v-myc) of avian myelocytomatosis virus strain 29. *Journal of virology* 42(3):773-779.
144. Stanton LW, Schwab M, & Bishop JM (1986) Nucleotide sequence of the human N-myc gene. *Proceedings of the National Academy of Sciences of the United States of America* 83(6):1772-1776.
145. Nau MM, *et al.* (1985) L-myc, a new myc-related gene amplified and expressed in human small cell lung cancer. *Nature* 318(6041):69-73.
146. Nesbit CE, Tersak JM, & Prochownik EV (1999) MYC oncogenes and human neoplastic disease. *Oncogene* 18(19):3004-3016.
147. Amati B, *et al.* (1993) Oncogenic activity of the c-Myc protein requires dimerization with Max. *Cell* 72(2):233-245.
148. Meyer N & Penn LZ (2008) Reflecting on 25 years with MYC. *Nature Reviews Cancer* 8(12):976-990.
149. Conacci-Sorrell M, McFerrin L, & Eisenman RN (2014) An overview of MYC and its interactome. *Cold Spring Harbor perspectives in medicine* 4(1):a014357.
150. Farrell AS & Sears RC (2014) MYC degradation. *Cold Spring Harbor perspectives in medicine* 4(3).
151. Chen Y, Sun X-X, Sears RC, & Dai M-S (2019) Writing and erasing MYC ubiquitination and SUMOylation. *Genes & Diseases* 6(4):359-371.
152. Duffy MJ, O'Grady S, Tang M, & Crown J (2021) MYC as a target for cancer treatment. *Cancer treatment reviews* 94:102154.
153. Lourenco C, *et al.* (2021) MYC protein interactors in gene transcription and cancer. *Nature Reviews Cancer* 21(9):579-591.
154. Fallah Y, Brundage J, Allegakoen P, & Shajahan-Haq AN (2017) MYC-Driven Pathways in Breast Cancer Subtypes. *Biomolecules* 7(3).
155. Boxer LM & Dang CV (2001) Translocations involving c-myc and c-myc function. *Oncogene* 20(40):5595-5610.
156. Gabay M, Li Y, & Felsher DW (2014) MYC activation is a hallmark of cancer initiation and maintenance. *Cold Spring Harbor perspectives in medicine* 4(6).
157. Dhanasekaran R, *et al.* (2022) The MYC oncogene — the grand orchestrator of cancer growth and immune evasion. *Nature Reviews Clinical Oncology* 19(1):23-36.
158. Prendergast GC (1999) Mechanisms of apoptosis by c-Myc. *Oncogene* 18(19):2967-2987.

159. Prendergast GC (1999) Mechanisms of apoptosis by c-Myc. *Oncogene* 18(19):2967-2987.
160. McMahon SB (2014) MYC and the control of apoptosis. *Cold Spring Harbor perspectives in medicine* 4(7):a014407.
161. Juin P, *et al.* (2002) c-Myc functionally cooperates with Bax to induce apoptosis. *Molecular and cellular biology* 22(17):6158-6169.
162. Järvinen K, Hotti A, Santos L, Nummela P, & Hölttä E (2011) Caspase-8, c-FLIP, and caspase-9 in c-Myc-induced apoptosis of fibroblasts. *Experimental Cell Research* 317(18):2602-2615.
163. Ahmadi SE, Rahimi S, Zarandi B, Chegeni R, & Safa M (2021) MYC: a multipurpose oncogene with prognostic and therapeutic implications in blood malignancies. *Journal of hematology & oncology* 14(1):121.
164. Llombart V & Mansour MR (2022) Therapeutic targeting of "undruggable" MYC. *EBioMedicine* 75:103756.
165. Vita M & Henriksson M (2006) The Myc oncoprotein as a therapeutic target for human cancer. *Seminars in cancer biology* 16(4):318-330.
166. Beaulieu ME & Soucek L (2019) Finding MYCure. *Molecular & cellular oncology* 6(5):e1618178.
167. Madden SK, de Araujo AD, Gerhardt M, Fairlie DP, & Mason JM (2021) Taking the Myc out of cancer: toward therapeutic strategies to directly inhibit c-Myc. *Mol Cancer* 20(1):3.
168. Yin X, Giap C, Lazo JS, & Prochownik EV (2003) Low molecular weight inhibitors of Myc-Max interaction and function. *Oncogene* 22(40):6151-6159.
169. Sammak S, *et al.* (2019) Crystal Structures and Nuclear Magnetic Resonance Studies of the Apo Form of the c-MYC:MAX bHLHZip Complex Reveal a Helical Basic Region in the Absence of DNA. *Biochemistry* 58(29):3144-3154.
170. Massó-Vallés D & Soucek L (2020) Blocking Myc to Treat Cancer: Reflecting on Two Decades of Omomyc. *Cells* 9(4).
171. Raina K, *et al.* (2016) PROTAC-induced BET protein degradation as a therapy for castration-resistant prostate cancer. *Proceedings of the National Academy of Sciences* 113(26):7124-7129.
172. Hydbring P & Larsson LG (2010) Cdk2: a key regulator of the senescence control function of Myc. *Aging* 2(4):244-250.
173. Krüger K, *et al.* (2018) Multiple DNA damage-dependent and DNA damage-independent stress responses define the outcome of ATR/Chk1 targeting in medulloblastoma cells. *Cancer letters* 430:34-46.
174. Gallego MA, *et al.* (2004) Apoptosis-inducing factor determines the chemoresistance of non-small-cell lung carcinomas. *Oncogene* 23(37):6282-6291.
175. Gani OA & Engh RA (2010) Protein kinase inhibition of clinically important staurosporine analogues. *Natural product reports* 27(4):489-498.
176. Saisomboon S, *et al.* (2019) Antitumor effects of flavopiridol, a cyclin-dependent kinase inhibitor, on human cholangiocarcinoma in vitro and in an in vivo xenograft model. *Heliyon* 5(5):e01675.
177. Boulos JC, *et al.* (2023) Cynaropicrin disrupts tubulin and c-Myc-related signaling and induces parthanatos-type cell death in multiple myeloma. *Acta Pharmacologica Sinica*.
178. Ma D, *et al.* (2016) Deoxypodophyllotoxin triggers parthanatos in glioma cells via induction of excessive ROS. *Cancer letters* 371(2):194-204.
179. Zhao N, *et al.* (2015) YM155, a survivin suppressant, triggers PARP-dependent cell death (parthanatos) and inhibits esophageal squamous-cell carcinoma xenografts in mice. *Oncotarget* 6(21):18445-18459.

180. Wang M, *et al.* (2007) Atiprimod inhibits the growth of mantle cell lymphoma in vitro and in vivo and induces apoptosis via activating the mitochondrial pathways. *Blood* 109(12):5455-5462.

6. Appendices (published articles)



The cardiac glycoside ZINC253504760 induces parthanatos-type cell death and G2/M arrest via downregulation of MEK1/2 phosphorylation in leukemia cells

Min Zhou · Joelle C. Boulos · Sabine M. Klauck · Thomas Efferth

Received: 23 February 2023 / Accepted: 23 May 2023
© The Author(s) 2023

Abstract Overcoming multidrug resistance (MDR) represents a major obstacle in cancer chemotherapy. Cardiac glycosides (CGs) are efficient in the treatment of heart failure and recently emerged in a new role in the treatment of cancer. ZINC253504760, a synthetic cardenolide that is structurally similar to well-known GCs, digitoxin and digoxin, has not been investigated yet. This study aims to investigate the cytotoxicity of ZINC253504760 on MDR cell lines and its molecular mode of action for cancer treatment. Four drug-resistant cell lines (P-glycoprotein-, ABCB5-, and EGFR-overexpressing cells, and TP53-knockout cells) did not show cross-resistance to ZINC253504760 except BCRP-overexpressing cells. Transcriptomic profiling indicated that cell death and survival as well as cell cycle (G2/M damage) were the top cellular functions affected by ZINC253504760 in

CCRF-CEM cells, while CDK1 was linked with the downregulation of MEK and ERK. With flow cytometry, ZINC253504760 induced G2/M phase arrest. Interestingly, ZINC253504760 induced a novel state-of-the-art mode of cell death (parthanatos) through PARP and PAR overexpression as shown by western blotting, apoptosis-inducing factor (AIF) translocation by immunofluorescence, DNA damage by comet assay, and mitochondrial membrane potential collapse by flow cytometry. These results were ROS-independent. Furthermore, ZINC253504760 is an ATP-competitive MEK inhibitor evidenced by its interaction with the MEK phosphorylation site as shown by molecular docking *in silico* and binding to recombinant MEK by microscale thermophoresis *in vitro*. To the best of our knowledge, this is the first time to describe a cardenolide that induces parthanatos in leukemia cells, which may help to improve efforts to overcome drug resistance in cancer.

Supplementary Information The online version contains supplementary material available at <https://doi.org/10.1007/s10565-023-09813-w>.

M. Zhou · J. C. Boulos · T. Efferth (✉)
Department of Pharmaceutical Biology, Institute of Pharmaceutical and Biomedical Sciences, Johannes Gutenberg University-Mainz, Staudinger Weg 5, 55128 Mainz, Germany
e-mail: efferth@uni-mainz.de

S. M. Klauck
Division of Cancer Genome Research, German Cancer Research Center (DKFZ), German Cancer Consortium (DKTK), National Center for Tumor Disease (NCT), 69120 Heidelberg, Germany

Keywords Cardiac glycosides · Leukemia · MEK inhibitors · Parthanatos · Synthetic derivative · Transcriptomics

Abbreviations

AIF	apoptosis-inducing factor
ATM	ataxia-telangiectasia mutated
ATR	ataxia-telangiectasia mutated and Rad3-related
BCRP	breast cancer resistance protein
BSA	bovine serum albumin

CDK1	cyclin-dependent kinase 1
CGs	cardiac glycosides
DAPI	4'6-diamidino-2-phenylindole
DSB	double-strand break
ERK	extracellular signal-regulated kinase
IPA	Ingenuity Pathway Analysis
JC-1	5,5'6,6'-trtrachloro-1,1'3,3'-tetraethylbenzimidazolylcarbocyanine iodide
K_d	dissociation constant
MAPK	mitogen-activated protein kinase
MDR	multidrug resistance
MEK	mitogen-activated protein kinase kinase
MEKi	MEK inhibitors
MMP	mitochondrial membrane potential
MNNG	N-methyl-N' nitro-N-nitrosoguanidine
MST	microscale thermophoresis
NAD	nicotinamide adenine dinucleotide
PAR	poly(ADP-ribose)
PARP1	poly(ADP-ribose) polymerase 1
PBS	phosphate-buffer saline
PI	propidium iodide
PS	phosphatidylserine
qRT-PCR	quantitative reverse transcription PCR
ROS	reactive oxygen species

Introduction

Cancer is one of the leading causes of death worldwide. Although chemotherapy made great progress as a major therapeutic strategy in oncology, the development of multidrug resistance (MDR) still limits drug efficiency and the successful treatment of patients.

Cardiac glycosides (CGs) are a class of steroid-like naturally derived products (Prassas and Diamandis 2008). CG-containing herbs have been used in folk medicine by native people of the ancient Egyptian culture, and Arab physicians treated heart and malignant diseases (Gurel et al. 2017). In the year 1785, extracts from *Digitalis purpurea* containing CGs were first described for medical use in the Western world by William Withering (Bessen 1986). Nowadays, more than 100 CGs have been identified in plants and animals (Mijatovic et al. 2007). *Digitalis*-based drugs such as digitoxin and digoxin are still in clinical use as oral medications for treating heart failure and atrial arrhythmias. In the case of myocardial fibrosis, CGs bind to and inhibit Na^+/K^+ -ATPase, allowing calcium to elevate contraction and improve myocardial contraction

and cardiac pump activity (Newman et al. 2008; Prassas and Diamandis 2008). Chemically, CGs consist of a steroid core, with a sugar portion at position 3 and an unsaturated lactone ring at position 17 (Fig. 1a). The two CGs classes are cardenolides and bufadienolides, both of which have unsaturated five- or six-membered rings, respectively (El-Seedi et al. 2019a).

Since the 1980s, Stenkvist *et al.* noted that breast cancer cells from women who received *Digitalis* therapy showed a lower risk of recurrence compared with untreated patients, suggesting CGs may have strong anticancer effects (Stenkvist et al. 1979, 1982). During the past three decades, the interest in developing CG as an anticancer drug has been steadily growing. The initial anticancer mechanism of CGs is binding to Na^+/K^+ -ATPase and altering signal transduction pathways to affect the growth of human malignant tumor cells, in particular glioblastoma, melanoma, and non-small cell lung cancer where Na^+/K^+ -ATPase is vastly expressed (Silva et al. 2021). This makes CGs promising chemotherapeutic candidates for anticancer treatment (Ayogu and Odoh 2020). Subsequently, other modes of action of CGs have been elucidated, including activation of ERK1/2, increased expression of cell cycle inhibitor p21 (Yuan et al. 2019), inhibition of Akt and PI3K pathway, and inhibition of transcription factors such as NF- κ B (Prassas and Diamandis 2008). Different types of cancer cells, such as leukemia (Zeino et al. 2015a, b; Saeed et al. 2016), breast (Li et al. 2021), melanoma (Smolarczyk et al. 2018), lung (Hu et al. 2021), pancreatic (Ha et al. 2021), liver (Reddy et al. 2019), and kidney carcinoma (Nolte et al. 2017) induced cell death upon treatment with CGs. A series of synthetic CGs analogs raised interest because some of them showed improved anticancer properties through structural modification (Ren et al. 2020; Ainembabazi et al. 2022; Wang et al. 2017). Their synthetic route, structure-activity relationship (SAR), and the screening of anticancer activity are still in progress, and their potential modes of action are not fully elucidated yet and need further investigation.

The mitogen-activated protein kinase (MAPK) cascades are key signaling pathways in transmitting signals from cell surface receptors into the inside of the cell to regulate numerous cellular activities, including cell proliferation, survival, and differentiation (Roberts and Der 2007). The Ras-Raf-MEK-ERK signaling is the most extensively studied pathway, which is aberrantly activated in nearly one-third of all human cancers (Kun

et al. 2021). MEK is playing a central role in transmitting signals from Raf to ERK, making it an attractive drug target. MEK has two isoforms, MEK1 and MEK2 (Barbosa et al. 2021). The activation segments of protein kinase commonly contain phosphorylation sites. The activation of MEK1 by Raf requires the phosphorylation of two serine residues, S218 and S222 (Zheng and Guan 1994). The corresponding residues on MEK2 are S222 and S226. While both serine residues are necessary for activation, the dephosphorylation of either one would fully inactivate MEK (Roskoski 2012). MEK mutations are rare in cancer. (Ullah et al. 2022). However, constitutive MEK activation has been observed in 50 tumor cell lines (Hoshino et al. 1999), resulting in cell transformation and, eventually, tumorigenesis (Cowley et al. 1994; Mansour et al. 1994). Currently, there are four FDA-approved MEK inhibitors (MEKi), *i.e.*, trametinib, cobimetinib, binimetinib, and selumetinib (Frémin and Meloche 2010; Singh et al. 2021). Tumor cells driven by mutated Raf are sensitive to MEKi *in vitro* and *in vivo*. Significantly, the combinations of Raf and MEK inhibitors (*e.g.*, dabrafenib and trametinib, vemurafenib and cobimetinib) were particularly successful in BRAF^{V600E} mutant melanoma and showed better efficiency than using a Raf inhibitor alone (Flaherty et al. 2012). More importantly, MEK is the only known activator of ERK up to date, which can inhibit ERK activation and downstream molecules, thereby inhibiting cell proliferation and survival (Caunt et al. 2015). This makes MEK a prime target suppressing cell signaling. Therefore, targeting MEK is a rational solution to efficiently silence the MAPK signaling pathway in cancers.

Parthanatos is a programmed cell death mode that depends on poly(ADP-ribose) polymerase 1 (PARP1) hyperactivation independent of caspase activity. Mechanically, PARP is rapidly activated by DNA damage, such as ultraviolet light, reactive oxygen species (ROS), or alkylating agents (*e.g.*, *N*-methyl-*N*'-nitro-*N*-nitrosoguanidine (MNNG)). PARP produces excess poly(ADP-ribose) (PAR), which migrates from the nucleus to the cytoplasm. PAR binds to mitochondrial membrane proteins, causing apoptosis-inducing factor (AIF) to translocate from mitochondria to the nucleus, which eventually leads to large-scale fragmentation and chromatin condensation. Simultaneously, PARP overactivation causes nicotinamide adenine dinucleotide (NAD⁺) and ATP depletion, which further leads to mitochondrial depolarization.

All these steps trigger parthanatos, which is distinct from apoptosis and necrosis. Parthanatos has been involved in retinal disease, ischemia-reperfusion injury, and neurodegenerative diseases including Alzheimer's disease and Parkinson's disease (Wang and Ge 2020). Applying PARP inhibitors to suppress parthanatos opens new treatment possibilities in these diseases. Several cancer cells such as glioma cells have a greater level of PARP and are negatively correlated with patient survival rates (Galia et al. 2012). Instead, parthanatos through hyperactivation of PARP has been induced by chemotherapies in esophageal cancer and glioma cells (Zhao et al. 2015; Ma et al. 2016), suggesting parthanatos as a promising strategy to kill cancer cells.

We recently screened a series of phytochemicals against MDR cancer cells, digitoxin and digoxin were ranked at the top with promising growth-inhibitory potential, suggesting CG compounds have the crucial benefit to anticancer effect (Khalid et al. 2022). The aim of this study was to explore the anticancer activity of a modified CG compound ZINC253504760 that could be a potential anticancer agent. We investigated the cytotoxicity of ZINC253504760 toward MDR cancer cells and studied the molecular mode of action. ZINC253504760 revealed the highest sensitivity in CCRF-CEM leukemic cells. After microarray-based mRNA profiling, we applied flow cytometry to investigate cell cycle, apoptosis and mitochondrial membrane potential. Molecular docking, western blotting and immunofluorescence were used to confirm the potential targets and the major mode of cell death.

Material and methods

Compound

Compound ZINC253504760 (IPUAC name: 3-[(3S,5S,8S,9R,10S,12R,13S,14S,17S)-3-[(2S,4R,5R,6R)-5-[(2R,4R,5R,6R)-5-[(2S,4S,5S,6R)-4,5-dihydroxy-6-methyloxan-2-yl]oxy-4-hydroxy-6-methyloxan-2-yl]oxy-4-hydroxy-6-methyloxan-2-yl]oxy-12,14-dihydroxy-10,13-dimethyl-1,2,3,4,5,6,7,8,9,11,12,15,16,17-tetradecahydrocyclopenta[a]henanthrene-17-yl]-2H-furan-5-one) was purchased from SPECS (Zoetermeer, Netherlands) (#SPECS AP-163/40806811). The chemical structure is shown in Fig. 1A. The stock solution (20 mM) was prepared in DMSO and stored at -20 °C.

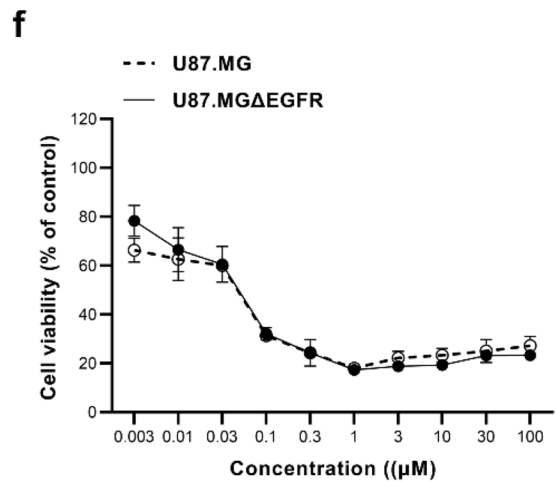
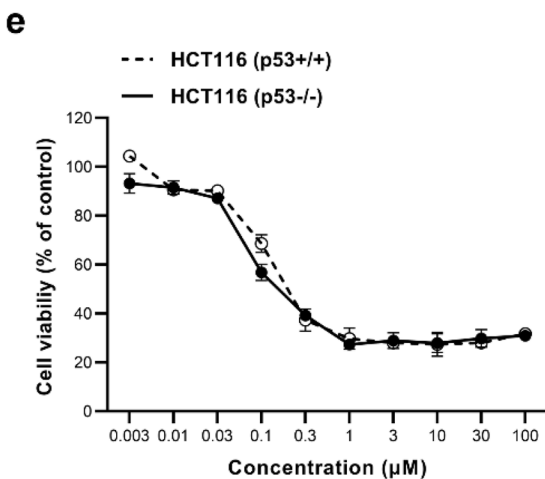
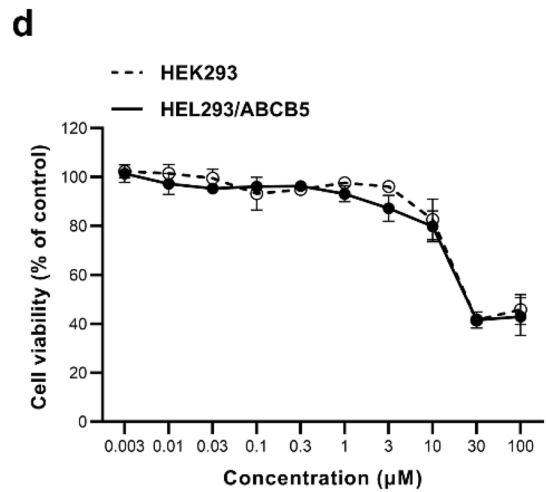
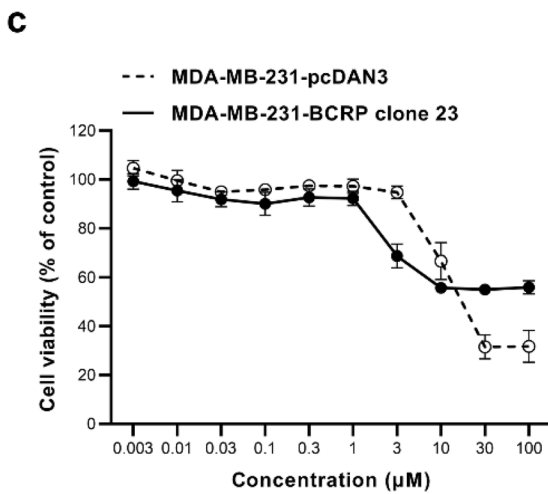
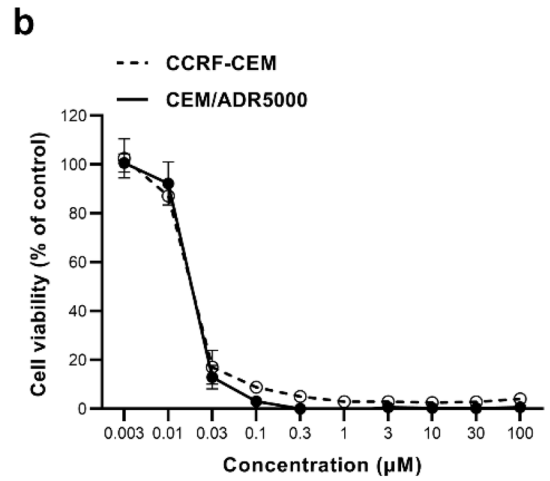
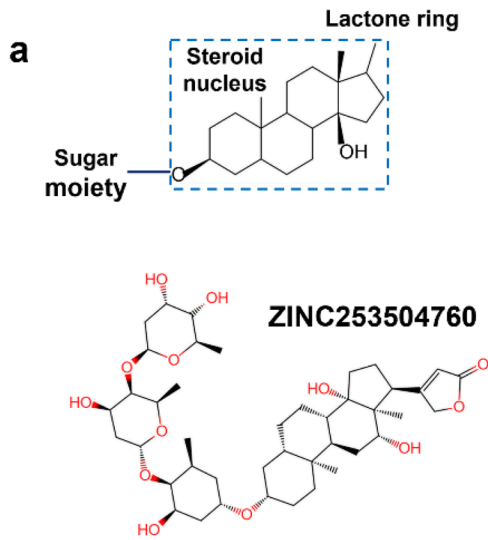


Fig. 1 Dose-response curves of ZINC253504760 towards drug-sensitive and drug-resistant cell lines as determined by the resazurin assay. **a** Steroid nucleus, the core structure of cardiac glycoside, and the chemical structure of ZINC253504760. **b** Growth inhibition of ZINC253504760 towards CCRF-CEM and ABCB1/P-glycoprotein expressing CEM/ADR5000 leukemia cell lines. **c** Growth inhibition of MDA-MB-231-pcDNA3 and their transduced MDA-MB-231-BCRP clone 23 breast cancer cell lines. **d** Growth inhibition of HEK293 and their transduced HEK293/ABCB5 human embryonic kidney cancer cell lines. **e** Growth inhibition of HCT116 (p53^{+/+}) and p53^{-/-} knockout HCT116 (p53^{-/-}) colon cancer cell lines. **f** Growth inhibition of U87MG wild-type and their transfected U87MG. ΔEGFR glioblastoma cell lines. The results are mean values ± SD of three independent experiments

Cell culture

The source and culture of cell lines used in this study were reported before (Saeed et al. 2019; Doyle et al. 1998; Rudbari et al. 2022; Dawood et al. 2020b). Two leukemia cell lines, drug-sensitive CCRF-CEM and multidrug-resistant CEM/ADR5000 were cultured in RPMI 1640 medium. Doxorubicin (5,000 ng/mL) has been added to CEM/ADR5000 cells every 14 days to maintain the resistance.

Human HEK293 embryonic kidney cells and HEK293/ABCB5, breast cancer cells MDA-MB-231-pcDNA3 and MDA-MB-231-BCRP clone 23, wild-type colon cancer cells HCT116 (p53^{+/+}) and HCT116 (p53^{-/-}), glioblastoma multiform cells U87MG and U87MG.ΔEGFR was maintained in DMEM medium (Invitrogen, Darmstadt, Germany). Both media were supplied with 10% fetal bovine serum (FBS) and 1% penicillin-streptomycin (Invitrogen, Darmstadt, Germany). Cells were cultured at 37 °C in a humidified environment with 5% CO₂. In addition, 400 µg/mL geneticin was continuously added to resistant cells HCT116 (p53^{-/-}) and U87MG.ΔEGFR, and 800 ng/mL geneticin for MDA-MB-231-BCRP clone 23 every two weeks. Cells in the logarithmic growth phase were used in the experiments.

Growth inhibition assay

The growth inhibitory activity of ZINC253504760 was determined with the resazurin reduction assay (Saeed et al. 2018). A 100 µL medium containing suspension cells (1 × 10⁴ cells/well) or adherent cells (5 × 10³ cells/well) was seeded in a 96-well plate. Cells were treated with a series of concentrations of ZINC253504760 diluted in 100 µL medium.

Following 72 h of incubation, 20 µL 0.01% resazurin (Promega, Mannheim, Germany) was added and incubated at 37 °C for 4 h. The fluorescence signal was measured with the Infinite M200 Pro-plate reader (Tecan, Crailsheim, Germany). The experiment was repeated in triplicates independently and with six replicates of each concentration. The growth inhibitory effect of treatment was presented as the percentage of cell viability, plotted as a dose-response curve. The fifty percent inhibition concentration (IC₅₀) value was calculated from the dose-response curve using Microsoft Excel 2021. The figures were generated using Prism 8 GraphPad Software (GraphPad Software Inc., San Diego, CA, USA).

RNA extraction

The procedure of RNA extraction has been previously reported (Mahmoud et al. 2018). One million CCRF-CEM cells were treated in duplicates with 1-fold IC₅₀ of ZINC253504760 or DMSO (solvent control) and incubated for 24 h, followed by total RNA extraction with InviTrap[®] Spin Universal RNA Mini Kit (Invitex Molecular, Berlin, Germany). The lysis solution was prepared as 350 µL Lysis Solution TR containing 1% β-mercaptoethanol for each sample. The RNA concentrations were quantified by a Nanodrop spectrophotometer (Nanodrop Technologies, Wilmington, DE, USA).

Microarray gene expression profiling and Ingenuity Pathway Analysis (IPA)

The duplicate extracted total RNA was further used in microarray hybridizations, which were carried out using Affymetrix GeneChips[®] with human Clariom[™] S assays (Affymetrix, Santa Clara, CA, USA) at the Genomics and Proteomics Core Facility at the German Cancer Research Center (DKFZ, Heidelberg).

The differential gene expressions between the control and ZINC253504760-treated groups were analyzed by applying Chipster software as we previously reported (Hegazy et al. 2021; Kadioglu et al. 2021). Robust Multi-array Average (RMA) method was used to normalize the data. Genes were filtered using the percentage to exclude genes with a standard deviation of 0.5 from the gene mean. Then, the missing value were removed. The subsequent assessment of significantly deregulated genes used empirical Bayes t-test ($p < 0.05$) (accessed in July 2021).

The significantly deregulated genes were analyzed with the Ingenuity Pathway Analysis (IPA) software (Qiagen, Redwood City, CA, USA) (accessed in August 2021). The core analysis tool was used to generate the canonical pathway, cellular functions, and networks that were affected by ZINC253504760 treatment.

qRT-PCR

The primers design and protocol were previously reported (Mahmoud et al. 2018). One microgram of extracted RNA was converted into cDNA with the Luna Script™ RT SuperMix Kit (New England Biolabs, Frankfurt, Germany). The cDNA sample, both extracted from untreated cells (DMSO, 24 h) and treated cells (IC₅₀, 24 h), were used for the verifications in qRT-PCR. Four genes, including two top-upregulated genes (*CD82* and *H2AC18*) and two top-downregulated genes (*HSP90AA1* and *HSP90ABI*), were chosen to validate the microarray results. Eight genes (*HIPK2*, *PPM1D*, *CDK1*, *Wee1*, *CKS1*, *CKS2*, *TP53*, and *CDK7*) involved in cell cycle regulation were selected to verify the mechanism. Primer sequences are presented in Supplementary Table S1. The real-time quantitative polymerase chain reaction (qRT-PCR) was carried out with the CFX384™ Touch Real-Time PCR Detection System (Bio-Rad, Munich, Germany). The expressions were normalized using *GAPDH* as an internal control gene. The 2^{ΔΔCt} method was applied to calculate the fold change of each gene between treated cells and untreated cells (Livak and Schmittgen 2001).

Cell cycle analysis and detection of apoptosis

The cell cycle analysis was previously described using propidium iodide (PI) staining (Abdelfatah et al. 2020; Rudbari et al. 2022). CCRF-CEM cells (1 × 10⁶ cells/well) were treated with ZINC253504760 at 0.5 × IC₅₀, IC₅₀, 2 × IC₅₀ and 4 × IC₅₀, DMSO (solvent control) or doxorubicin (positive control), respectively. After corresponded incubation (24 h, 48 h or 72 h), cells were fixed with ethanol and stored at -20 °C for 24 h. Then, samples were centrifuged (4000 rpm, 10 min) and re-suspended in 500 μL cold PBS containing 20 μg/mL RNase (Roche Diagnostics, Mannheim, Germany), followed by staining with 50 μg/mL PI (Sigma-Aldrich, Darmstadt, Germany). The measurement was performed using a BD Accuri™ C6 Flow Cytometer (Becton-Dickinson, Heidelberg, Germany). The results were analyzed using FlowJo software (Celeza, Olten, Switzerland). Cells were firstly gated

based on forward and side scatter properties (FSC-A/SSC-A), the single cells were gated (FL2-A/FL2-H) in a linear manner to remove doublets or debris.

Annexin V/PI staining was applied to detect and quantify apoptotic and necrotic cells (Reutelingsperger and van Heerde 1997; Vermes et al. 1995). The protocol has been recently reported by us (Saeed et al. 2022; Rudbari et al. 2022). The same amount of CCRF-CEM cells was treated with ZINC253504760 at different concentrations, DMSO (negative control), or vincristine (positive control, 5 μM) for 24, 48 or 72 h. Cells were stained with Annexin V and PI (BioVersion/Bio-cat, Heidelberg, Germany) in the dark, and further analyzed using a BD Accuri™ C6 Flow Cytometer. All experiments were performed three times.

Fluorescence microscopy of the microtubule cytoskeleton

Briefly, human U2OS osteosarcoma cells were seeded in μ-Slide 8 Well (30,000 cells/well) (ibidi, Gräfelfing, Germany) and kept overnight to allow cells to adhere to the plate. Then cells were treated with ZINC253504760 (IC₅₀, 2 × IC₅₀, and 4 × IC₅₀) or DMSO as a negative control. After 24 h, cells were washed with PBS, fixed with 4% paraformaldehyde, and stained with 1 μg/mL of 4'-diamidino-2-phenylindole (DAPI, Sigma-Aldrich, Darmstadt, Germany) in the dark. Subsequently, the slides were immersed in Mounting Medium (ibidi, Gräfelfing, Germany). Imaging was carried out using an AF7000 widefield fluorescence microscope (Leica Microsystems, Wetzlar, Germany). Images were analyzed with Image J software (National Institute of Health, Bethesda, MD, USA). The methods have been described by us (Boulos et al. 2021).

Western blotting

CCRF-CEM cells were treated with ZINC253504760 for the indicated times, cells were washed twice with PBS. Total proteins were extracted with M-PER Mammalian Protein Extraction Reagent (Thermo Fisher Scientific, Darmstadt, Germany). Nuclear and cytoplasmic proteins were extracted using NE-PER Nuclear and Cytoplasmic Extraction Reagents kit (Thermo Fisher Scientific). CER I, CER II, and NER reagents were added as the volume ratio at 200:11:100 μL following the manufacturer's instructions. Both lysis buffer contained 1% Halt Protease Inhibitor Cocktail and phosphatase inhibitor (Thermo

Fisher Scientific). Protein concentrations were quantified by a Nanodrop spectrophotometer.

Equal amounts of protein extracts (30 µg) were separated by 10% SDS-PAGE and blotted onto a polyvinylidene fluoride membrane (ROTIPVDF®). The membrane was blocked in TBST buffer containing 5% bovine serum albumin (BSA) for 1 h. Afterward, the membranes were incubated with specific primary antibodies (anti-p44/42 MAPK (Erk1/2) rabbit antibody (1:1000, Cell Signaling Technology, Leiden, The Netherlands), anti-phospho-p44/42 MAPK (Erk1/2) (Thr202/Tyr204) rabbit antibody (1:1000, Cell Signaling Technology), anti-MEK1/2 rabbit antibody (1:1000, Cell Signaling Technology), anti-phospho-MEK1/2 (Ser217/221) rabbit antibody (1:1000, Cell Signaling Technology), anti-AIF rabbit antibody (1:1000, Cell Signaling Technology), anti-Lamin B1 monoclonal antibody (1:10000, Proteintech, Planegg-Martinsried, Germany), anti-PAR mouse antibody (1:1000, Merck, Darmstadt, Germany), anti-caspase 3/p17/p19 polyclonal antibody (1:1000, Proteintech), anti-PARP rabbit antibody (1:1000, Cell Signaling Technology), anti-phospho-histone H2A.X (Ser139) antibody (1:1000, Cell Signaling Technology), anti-GAPDH rabbit antibody (1:1000, Cell Signaling Technology), anti-β-actin rabbit antibody (1:1000, Cell Signaling Technology), anti-p62, SQSTM1 polyclonal antibody (1:1000, Proteintech), or anti-Beclin 1 polyclonal antibody (1:1000, Proteintech) overnight at 4 °C. Finally, the membrane was incubated in anti-mouse IgG or anti-rabbit IgG, HRP-linked antibody (1:2000, Cell Signaling Technology) for 1 h at room temperature. Horseradish peroxidase (HRP) substrate (Luminata™ Classic, Merck Millipore, Schwalbach, Germany) was used to detect the immunoreactive band. The protein was visualized by an Alpha Innotech FluorChem Q system (Biozym, Oldendorf, Germany). The bands were quantified using Image J software (National Institutes of Health). Relative protein expression was normalized to GAPDH or β-actin.

Analysis of mitochondrial membrane potential (MMP)

To analyze the mitochondrial membrane potential, 5,5',6,6'-trtrachloro-1,1',3,3'-tetraethylbenzimidazolylcarbocyanine iodide (JC-1; Biomol, Hamburg, Germany) staining was used as previously reported (Özenver et al. 2018). Briefly, aliquots of 10⁴ CCRF-CEM cells were seeded in a 96-well plate and treated with 0.5-, 1-, 2- and 4-fold IC₅₀ of ZINC253504760, or DMSO as a negative control, or vinblastine (1 µM) as a positive control, respectively, for 24 h. Cells were

stained with 10 µL diluted JC-1 per well (1 µL JC-1 in stock: 9 µL medium) and incubated at 37 °C for 15 min in the dark. Subsequently, cells were washed with 200 µL Cell-based assay buffer (Biomol, Hamburg, Germany) and centrifuged at 400 × g for 5 min twice. Finally, cells were suspended with 100 µL Cell-based assay buffer and detected using a BD LSR Fortessa SORP equipment. JC-1 is the most specific fluorescence probe for measuring changes in mitochondrial membrane potential. J-aggregates or monomers are the two detectable forms with emissions of JC-1 and can be detected by flow cytometry (Smiley et al. 1991). In healthy cells with higher membrane potential, J aggregates emit red fluorescence at 520-570 nm and were collected using a 586/15 bandpass filter. While the fluorescence properties of the probe are altered according to the aggregation. In lower membrane potential, JC-1 is predominantly a monomer (dead cells) that emits green fluorescence at 488 nm and was collected using a 530/30 bandpass filter. All experiments were performed in triplicates. The FSC files were analyzed by the FlowJo software (Celeza).

Immunofluorescence microscopy of AIF translocation

Three concentrations of ZINC253504760 (IC₅₀, 2 × IC₅₀, or 4 × IC₅₀) or DMSO alone were treated in CCRF-CEM cells for 12 h. Cells were harvested and washed once with washing buffer (1% FBS in PBS) and kept on ice. Then, 10,000 cells of each sample were cytospinned on cover slides (Thermo Fisher Scientific, Dreieich, Germany). Subsequently, cells were fixed with 4% paraformaldehyde, then permeabilized with 1% Triton X-100 in PBS. Afterward, samples were kept in the blocking buffer containing 10% FBS and 1% BSA for 1 h. The primary antibody AIF (1:400, Cell Signaling Technology) was diluted in PBS and applied to the slides overnight in a humidified chamber at 4 °C. After rinsing three times with washing buffer, the secondary antibody (1:700) was applied to the samples for 1 h in the dark at room temperature. Then, 1 µg/mL DAPI was added to the samples for 5 min to stain cell nuclei. At last, cells were rinsed five times with washing buffer and immersed in the Mounting Medium (ibidi). Images were taken by a Leica AF7000 widefield fluorescence microscope (Leica Microsystems) and analyzed using ImageJ software (National Institutes of Health).

Single cell gel electrophoresis (comet assay)

The comet assay is one of the common methods for evaluating DNA damage. Under electrophoresis, damaged DNA or denatured cleaved DNA fragments migrate from the intact cells, creating a “comet tail” under the microscope. The Oxiselect™ Comet Assay Kit (3-Well Slides) (Cell Biolabs/Biocat, Heidelberg, Germany) was applied to perform the comet assay as recently described by us (Elbadawi et al. 2023). Briefly, CCRF-CEM cells were plated in a 6-well plate (10^6 cells per well). Cells were treated with ZINC253504760 at 0.088 μ M, 0.15 μ M, and DMSO (negative control), respectively, for 3 h. H_2O_2 (50 μ M) as positive control was added to the cells for 1 h. Collected cells were centrifuged at $3,000 \times g$ for 10 min. A ratio of 1:6 was used to mix cells (10^5 cells/ml) suspended in cold PBS with melting agarose at 37 °C. After samples were spread on comet slides and dried, the pre-chilled lysis buffer and pre-chilled alkaline electrophoresis solution buffer were applied to the slides in the dark. Slides were then placed horizontally in alkaline electrophoresis solution buffer in the electrophoresis chamber. Twenty Volts of voltage were delivered to the chamber for 20 min. After that, the slides were washed by pre-chilled distilled water twice, followed by cold 70% ethanol. Vista Green DNA dye was diluted at a ratio of 1:10,000 in TE buffer and added in the slides (100 μ L/well). DNA damage was observed by EVOS digital inverted microscope (Life technologies GmbH, Darmstadt, Germany). Fifty comets in each treatment were randomly selected and analyzed by OpenComet in Image J software (National Institutes of Health). Tail DNA% was measured as a parameter for DNA damage (Gyori et al. 2014).

Molecular docking

The PDB files of MEK1 and MEK2 were downloaded from the RCSB Protein Data Bank (PDB codes: 1S9J and 1S9I, respectively) (Ohren et al. 2004). ZINC253504760 and trametinib in SDF format were downloaded from the ZINC 15 database (ZINC253504760) and PubChem, respectively, and were converted to PDB files. In addition, considering GCs in human metabolism are normally hydrolyzed to their deglycosylated congeners by removing sugar moiety (Jortani and Valdes 1997), therefore, the deglycosylated form of ZINC253504760 was also performed by molecular docking. The *in silico* binding of ZINC253504760 and its deglycosylated form, and

trametinib to MEK1 and MEK2 was carried out using AutoDock 4.2.6 (The Scripps Research Institute, CA, USA) (Saeed et al. 2018). AutoDockTools 1.5.6 was used for converting the proteins and ligands to PDBQT format. The grid box was set to cover the whole protein. Visual Molecular Dynamics (VMD) software was used to create the visualization of interactions.

ROS detection

Briefly, CCRF-CEM cells (2×10^6 cells/well) were seeded and treated with ZINC253504760 at different indicated concentrations or DMSO (negative control) for 12 h, and 24 h, respectively. Cells were harvested and washed with PBS, then resuspended in 1 mL PBS and incubated with 10 μ M 2'-7-dichlorodihydrofluorescein diacetate ($H_2DCFH-DA$) (Sigma-Aldrich, Germany) at 37 °C for 30 min. 10 μ L H_2O_2 at the stock concentration (positive control) (Sigma-Aldrich, Germany) was treated in cells during the incubation at 15 min. The measurement was performed on a BD Accuri™ C6 Flow Cytometer (Becton-Dickinson). Histograms were analyzed using FlowJo software (Celeza). All the experiments were repeated three times independently. The protocol was described by us (Wu and Efferth 2015).

Microscale thermophoresis

The ligand-protein interactions between ZINC253504760 and MEK1 or MEK2 were performed by microscale thermophoresis (MST) as described (Dawood et al. 2020a). The recombinant human MEK1 protein (Abcam, Berlin, Germany) and the MEK2 protein (Sino Biological, Beijing, China) were labeled using the Monolith™ NT.115 Protein Labeling Kit BLUE-NHS (NanoTemper Technologies, Munich, Germany). Subsequently, the MEK1 protein (1530 nmol/L) and the MEK2 protein (990.1 nmol/L) were titrated against 16 different concentrations of ZINC253504760 in assay buffer. The fluorescence signal measurement was performed using a Monolith NT.115 instrument (NanoTemper Technologies) and the samples were loaded to the standard glass capillaries. The results were shown with 60% LED power and 10% MST power for MEK1, 40% LED power and 10% MST power for MEK2. The curves of ZINC253504760 binding to both proteins were generated using MO. affinity analysis software (NanoTemper Technologies), and the dissociation constant (K_d) was calculated.

Results

Cytotoxicity assay

ZINC253504760 revealed cytotoxicity against a panel of drug-sensitive and -resistant cell lines with IC_{50} values in the range from $0.022 \pm 0.002 \mu\text{M}$ (CCRF-CEM) to $25.95 \pm 0.26 \mu\text{M}$ (HEK293) (Fig. 1 and Table 1). Except for MDA-MB-231-BCRP clone 23 that was cross-resistant, the other four drug-resistant cell lines did not show cross-resistance to ZINC253504760. The resistant ratios were 0.95 (CEM/ADR5000), 0.99 (HEK293/ABC5), 0.81 (HCT116 p53^{-/-}), and 0.98 (U87.MGΔEGFR), respectively. Evidently, ZINC253504760 induced cytotoxicity on both leukemia cells and glioblastoma cells in the nanomolar range.

Among the panel of cell lines tested, ZINC253504760 exerted the most lethal effect with the lowest IC_{50} value in CCRF-CEM cells, we used CCRF-CEM as a model to explore the molecular modes of action of ZINC253504760.

Microarray hybridization and pathway analysis

Gene expression analysis was performed to investigate the potential mode of action of ZINC253504760. Therefore, total RNA was isolated to conduct transcriptome-wide microarray assays after CCRF-CEM cells were exposed to ZINC253504760 at the IC_{50} value ($0.022 \mu\text{M}$) or DMSO as negative control for 24 h. The genes that were differentially expressed were further subjected to IPA for signaling pathway analysis.

IPA predicted that the “mitotic role of polo-like kinase” and “cell cycle: G2/M DNA damage” could be potential molecular mechanisms among the panel of canonical pathways (Fig. 2a). “Cancer and hematological disease” appeared as important diseases affected by ZINC253504760 (Fig. 2b). Notably, the top cellular function in Fig. 2c indicated that ZINC253504760 may affect “cell death and survival”, “DNA replication, recombination, and repair”, “cell cycle”, as well as “cellular growth and proliferation”. Moreover, there were a total of 916 genes that were deregulated between treated and untreated cells according to the expression fold change values. Among them, 368 genes were downregulated, while 548 genes were upregulated (Supplementary Tables S2 and S3). The technical verification was quantified with four selected genes (*CD82*, *H2AC18*, *HSP90AA1*, and *HSP90ABI*) with real-time RT-PCR to validate the microarray results (Fig. 2d). The top

Table 1 IC_{50} values of ZINC253504760 in different drug-sensitive and drug-resistant cell lines

Cell lines	IC_{50} (μM)	Resistance ratio
CCRF-CEM	0.022 ± 0.002	0.95
CEM/ADR5000	0.021 ± 0.001	
MDA-MB-231-pcDNA3	18.76 ± 3.50	> 5.33
MDA-MB-231-BCRP clone 23	> 100	
HEK293	25.95 ± 0.26	0.99
HEK293/ABC5	25.57 ± 1.52	
HCT116 (p53 ^{+/+})	0.22 ± 0.03	0.81
HCT116 (p53 ^{-/-})	0.18 ± 0.03	
U87MG	0.055 ± 0.004	0.98
U87MG.ΔEGFR	0.054 ± 0.01	

upregulated genes *CD82* and *H2AC18* in the microarray data were upregulated in qRT-PCR. *HSP90AA1* and *HSP90ABI*, the top two downregulated genes in the microarray data also showed downregulation in qRT-PCR. The correlation coefficient (R) between mRNA expression values measured by microarray and qRT-PCR was 0.95 (Pearson correlation test), which indicated a high correlation between the two methods (Fig. 2e).

The IPA-based network analysis revealed that caspase 3 expression was increased (Fig. 3a). Fig. 3b shows the increased expression of the cell cycle biomarkers including *CDK1*, *Wee1*, *Cyclin A*, and *Cdc25c*, while *MAP2K1/2* (*MEK1/2*) and *ERK1/2* were downregulated. Therefore, we conducted cell cycle and apoptosis experiments, and explored the cell death mechanisms of ZINC253504760. We chose *MAP2K1/2* (*MEK1/2*) to further investigate whether these two proteins are targets of ZINC253504760. Moreover, Fig. 3c shows the network of top downregulated genes *HSP90AA1* and *HSP90ABI* associated with the decreased expression of *c-Src*.

Cell cycle analysis

To study cell cycle arrest, CCRF-CEM cells were treated with ZINC253504760 and incubated for three different timepoints. Fig. 4a shows that after 24 h treatment, the G2/M phase peak was elevated at all concentrations tested. After 48 and 72 h treatment, the arrest of cells in the G2/M phase was even more evident, and the increased percentages of the G2/M cell fraction were

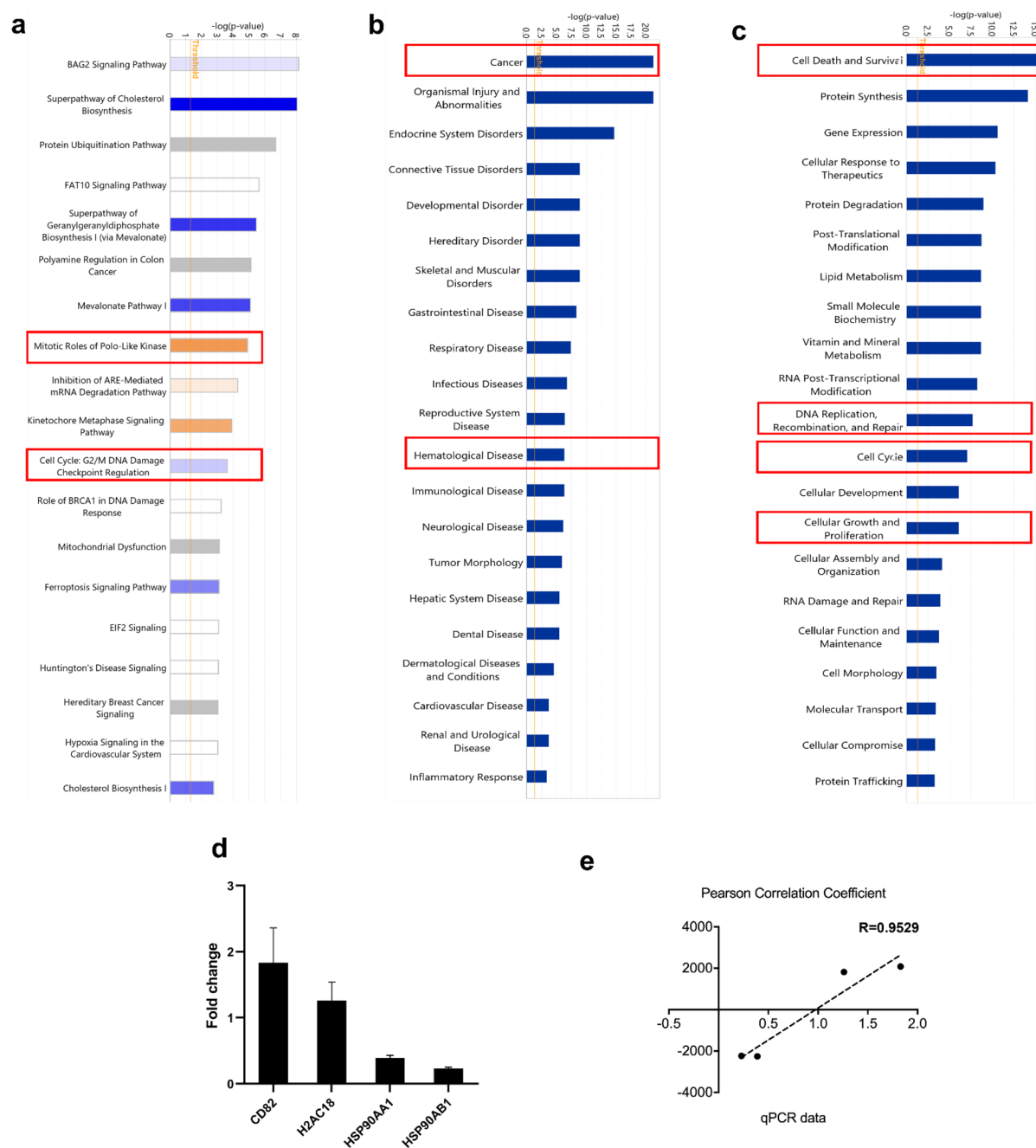


Fig. 2 Microarray gene expression profiling and Ingenuity Pathway Analysis (IPA) in CCRF-CEM cells treated with ZINC253504760. **a** Top canonical, **b** disease, and **c** cellular functional pathways affected by ZINC253504760 were marked

by the red boxes. **d** Technical verification of four selected genes by qRT-PCR analysis in CCRF-CEM cells treated with IC_{50} of ZINC253504760 for 24 h. **e** Person correlation coefficient of microarray and qRT-PCR data

statistically significant compared to untreated cells ($p < 0.05$). Therefore, the flow cytometric analyses verified the IPA prediction of G2/M cell cycle arrest.

To further confirm this result, 8 genes of the G2/M arrest pathway that were deregulated in the microarray analysis were selected for biological verification

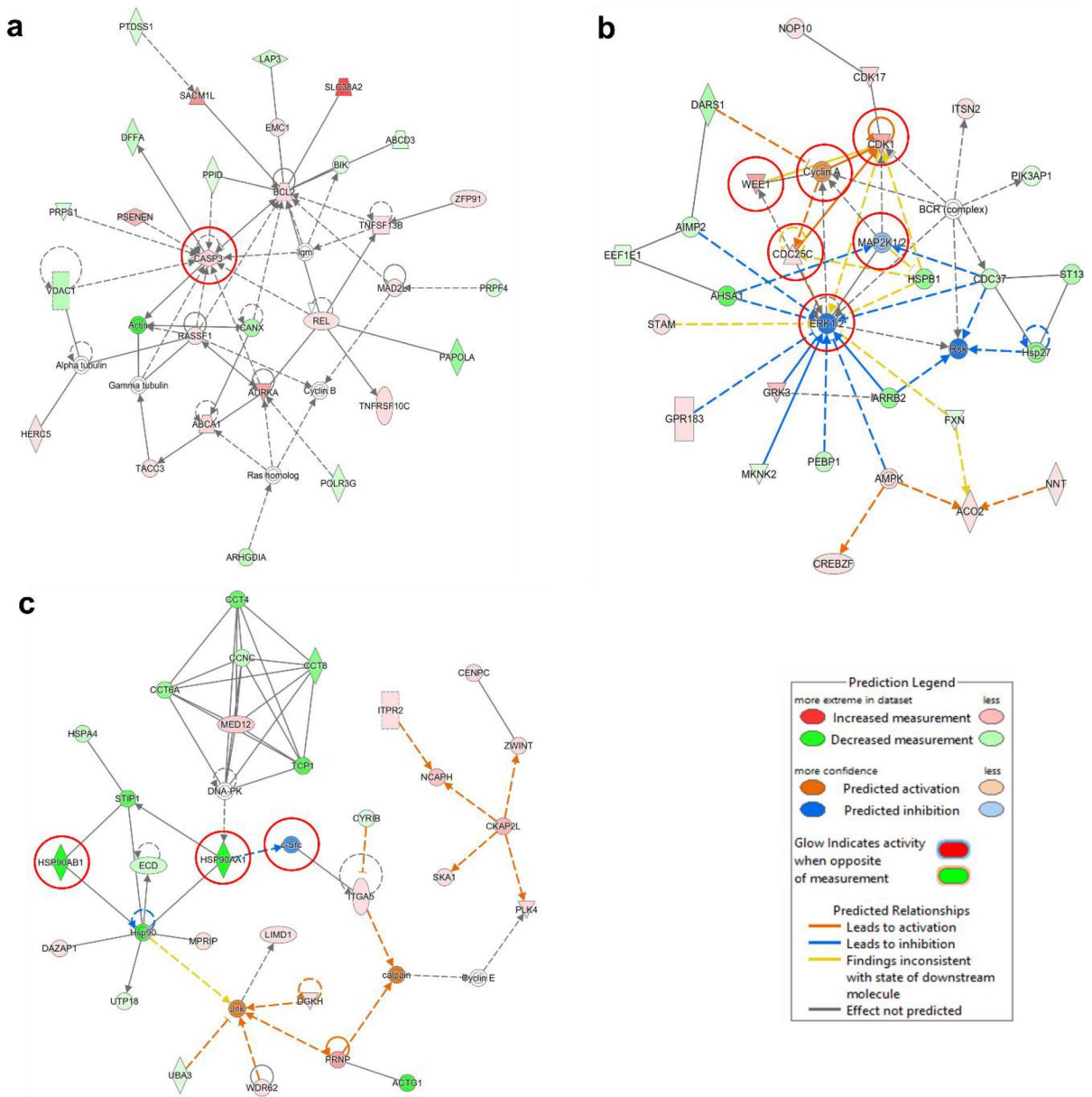


Fig. 3 Prediction of functional networks by transcriptome-wide microarray and IPA analysis of ZINC253504760-treated CCRF-CEM cells. **a** The red circles highlight the upregulation of caspase 3, **b** The red circles highlight the genes related to

the cell cycle linked with the downregulation of *MEK1/2* and *ERK*, and **c** The red circles highlight the downregulation of *Src* linked with the downregulation of *HSP90AA1* and *HSP90AB1*

using qRT-PCR. As shown in Fig. 4b, *HIPK2*, *PPM1D*, *CDK1*, *Wee1*, *CKS1*, and *CKS2* were upregulated, whereas *TP53* and *CDK7* were downregulated compared with housekeeping gene *GAPDH*. These results were consistent between qRT-PCR and microarray data.

Influence on microtubules

The G2/M arrest caused by ZINC253504760 raises the question of how this compound impacts on the microtubules. Tubulin Alpha 1b (TUBA1B) is a microtubule protein (Liu et al. 2017). A characteristic microtubule

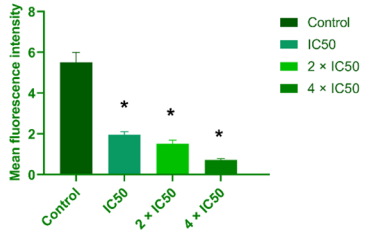
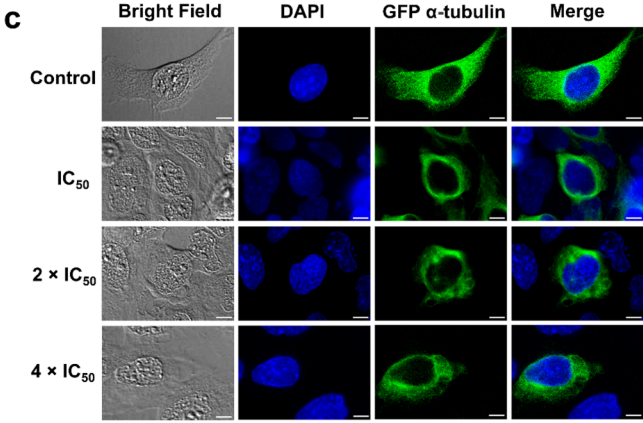
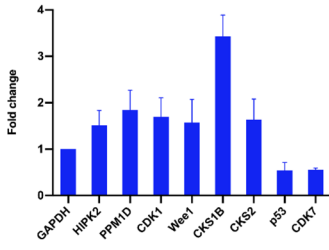
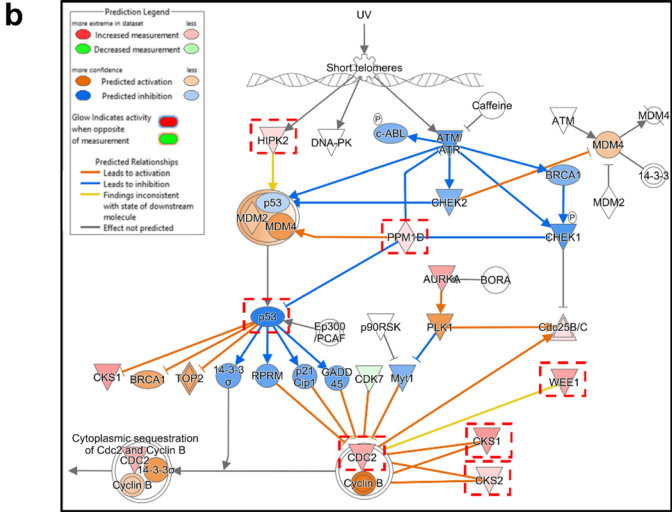
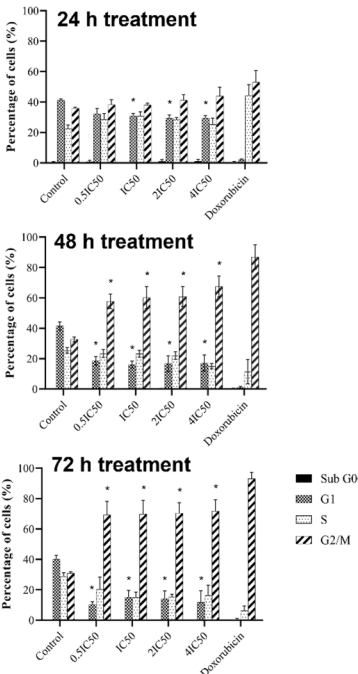
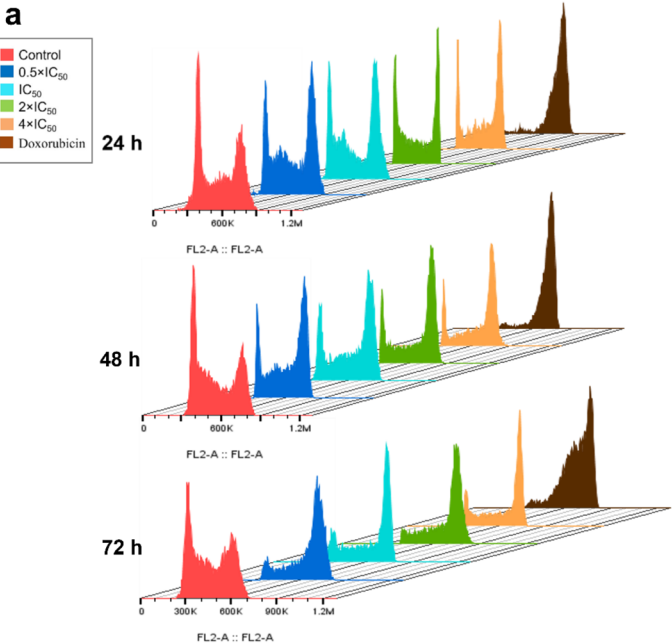


Fig. 4 Cell cycle analysis and influence on microtubules. **a** Flow cytometric cell cycle analysis in CCRF-CEM cells treated with different concentrations of ZINC253504760, or DMSO (control), or doxorubicin (positive control) for 24, 48, or 72 h. **b** The cell cycle genes (red dotted boxes) predicted from transcriptome-wide microarray and IPA treated with ZINC253504760 after 24 h for biological verification by qRT-PCR. The results are represented as mean values \pm SD of three independent experiments. **c** Immunofluorescence analysis of U2OS cells treated with ZINC253504760, or DMSO (control), and stained for DAPI (blue) and α -tubulin-GFP (green) after 24 h. The graph shows the mean fluorescence intensity of U2OS cells expressing α -tubulin-GFP tubulin. Statistics analysis was done by paired student's t-test, * $p < 0.05$, if compared with untreated cells

pattern was visible in the human U2OS cell line that endogenously expresses the fluorescent fusion protein (GFP-TUBA1B, Green Fluorescent Protein (GFP) gene attached to the genomic TUBA1B gene). Therefore, U2OS cells were treated with different concentrations of ZINC253504760. Fig. 4c illustrates the effect of ZINC253504760 observed on the cellular microtubule network. In untreated U2OS cells, the microtubules extended continuously in the cytoplasm and polymerized to form an extensive intracellular network in addition to the nucleus. By contrast, ZINC253504760 significantly disrupted microtubule distribution and reduced the mass of the microtubule network. Specifically, the reduced microtubules aggregated around the nucleus, but the aggregation diminished with increasing concentrations of the treatment, finally resulting in dense microtubules being less present in the cell periphery. The thickness of microtubules weakened compared to untreated cells. It is the same effects as vincristine (positive control) as we reported (Khalid et al. 2022). Hence, these results further strengthened the observation that ZINC253504760 induced G2/M phase arrest in the cell cycle.

Apoptosis and autophagy detection

As cell death and survival appeared in IPA as the first cellular function, we aimed to investigate the mode of cell death induced by ZINC253504760. Apoptosis by annexin V-PI staining on the flow cytometer was first investigated. As shown in Fig. 5a, the percentage of late apoptotic cells showed a slight increase in a time- and concentration-dependent manner after treating CCRF-CEM cells with ZINC253504760 ($0.5 \times IC_{50}$, IC_{50} , $2 \times IC_{50}$, and $4 \times IC_{50}$) for 24 h, 48 h, or 72 h, respectively. At 48 h, the late apoptotic cells were in the range

of 4.18%-11.1%. At 72 h, the fractions of late apoptotic cells were 7.98%-13.1%. Vincristine induced late apoptotic cell death with 14.3% after 24 h treatment, subsequently increased to 74.2% after 72 h. It can be clearly seen that the fraction of late apoptotic cells treated with ZINC253504760 was not significant at all times and concentrations tested. More than 80% of cells were non-apoptotic.

Next, we investigated whether autophagy was related to cell death, and the expression level of p62 and Beclin was measured by western blotting. Fig. 5b shows that p62 and Beclin were both downregulated. Especially after 48 h, the decline of both biomarkers was more significant.

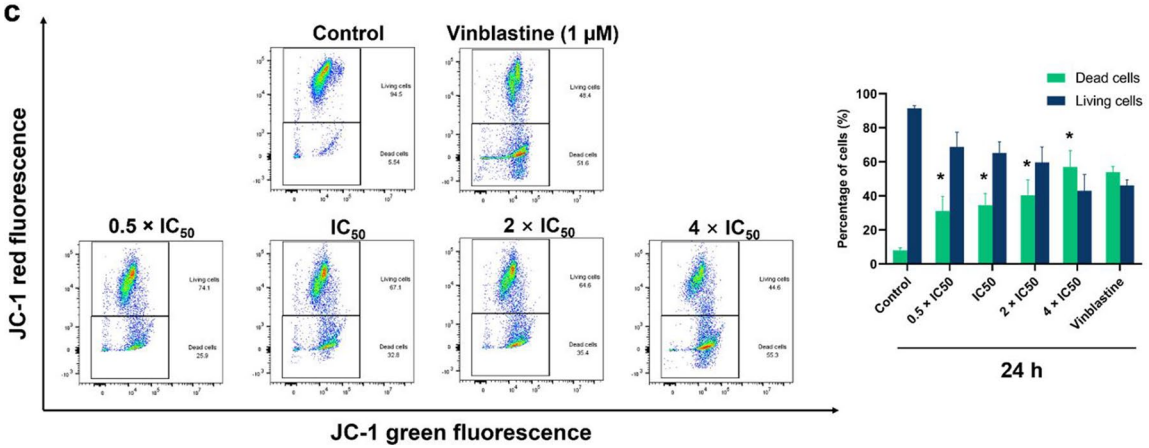
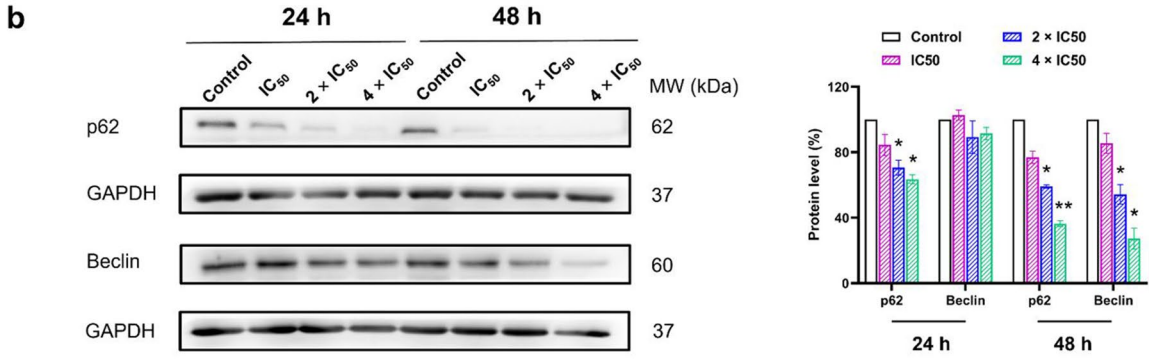
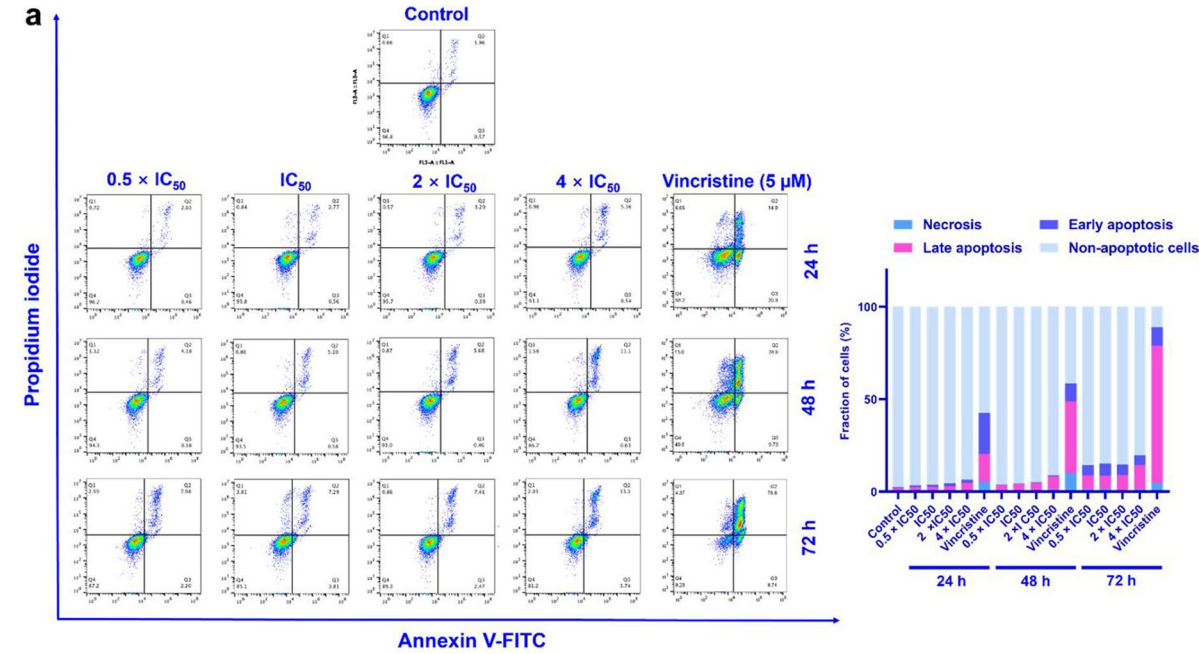
Therefore, these results did not provide evidence that apoptosis or autophagy were the predominant modes of cell death, and other cell death modes may contribute to the cytotoxicity observed in the resazurin assays with ZINC253504760.

Assessment of mitochondrial membrane potential

Mitochondria are essential for ATP generation for life and are the key players of cell death under cell stress conditions. Even if the major form of cell death regulated by mitochondria is apoptosis, other types of cell death also have been implicated with mitochondria (Bock and Tait 2020). Therefore, we investigated the MMP to understand whether it is affected. CCRF-CEM cells were treated with different concentrations of ZINC253504760 or vinblastine (positive control, $1 \mu\text{M}$) and measured by a flow cytometry after 24 h. As shown in Fig. 5c, the percentages of dead cells, which shift from red fluorescence (unaltered potential) to green fluorescence (defective potential), were in a range of 31.1%-57.0%. All treatments showed significant percentages of dead cells compared with untreated cells ($p < 0.05$). Especially, the $4 \times IC_{50}$ treated sample showed a comparable effect (57.0%) to vinblastine (53.9%). Hence, we conclude that ZINC253504760 caused mitochondrial dysfunction leading to cell death.

Western blot analysis of parthanatos

To investigate other forms of cell death, we first examined caspase 3 since the functional network in IPA software showed its upregulation (Fig. 3a). As depicted in Fig. 6a, caspase 3 expressions appeared



◀**Fig. 5** Assessment of apoptosis, autophagy and mitochondrial membrane potential. **a** Flow cytometric analysis in CCRF-CEM cells treated with different concentrations of ZINC253504760, or DMSO (control) or vincristine (positive control) for 24, 48 or 72 h. The graph shows the mean fraction of CCRF-CEM cells. The data represent as mean \pm SD of three independent experiments. **b** Western blot analysis of the proteins involved in autophagy in CCRF-CEM cells treated with different concentrations of ZINC253504760 for 24 or 48 h. Data represent relative expression intensity to GAPDH. Statistics analysis was done by paired student's t-test, * $p \leq 0.05$, ** $p \leq 0.001$, if compared to DMSO untreated cells. Data represent as mean values \pm SEM of three independent experiments. **c** Representative images of JC-1 fluorescence with flow cytometry of mitochondrial membrane potential in CCRF-CEM cells treated with different concentrations of ZINC253504760 or DMSO (control), or vinblastine (positive control) for 24 h. Statistical results of the dead cells defined as MMP collapse after 24 h treatment. Statistics analysis was done by paired student's t-test, * $p \leq 0.05$, if compared to DMSO untreated cells. The statistical analysis shows mean values \pm SD of three independent experiments

but not its cleaved form, which means the mode of cell death was caspase 3-independent. Therefore, we further focused on parthanatos as a novel caspase-independent mode of programmed cell death. The expressions of biomarkers in the parthanatos pathway were examined. As shown in Fig. 6a, the expression level of PARP (116 kDa) significantly increased upon increasing ZINC253504760 concentrations. PAR also showed an increased expression. Then, we measured the nuclear and cytoplasmic AIF localization (Fig. 6b). Notably, the AIF expression decreased in the cytoplasm while increasing in the nucleus compared with the control group. Moreover, the level of p-histone H2A.X increased in a dose-dependent manner. In addition, ZINC253504760 also led to increased PARP cleavage (89 kDa), which appeared to be inconsistent with the absence of cleaved-caspase 3 expressions, we give discussions below. Taken together, these results suggest that ZINC253504760 caused parthanatos as predominant form of cell death.

Immunofluorescence microscopy of apoptosis-inducing factor translocation

AIF is released from mitochondria and rapidly translocated to the nucleus, where it induces large-scale DNA fragmentation (50 kb) and chromatin condensation. This translocation can be captured by confocal immunofluorescence microscopy. Fig. 6c indicates that AIF was almost all extensively localized at the cytoplasm

of control CCRF-CEM cells. However, if cells were treated with ZINC253504760 with IC_{50} , $2 \times IC_{50}$, or $4 \times IC_{50}$ for 12 h, AIF accumulated in the nucleus, which was consistent with the western blotting results. These AIF translocation findings further confirmed that ZINC253504760 induced a parthanatos-type cell death.

Single cell gel electrophoresis (comet assay)

AIF enters the nucleus, triggers cell death by binding to DNA and leads to DNA fragmentation. For this reason, we examined DNA damage at the level of individual cells by the alkaline comet assay. ZINC253504760 induced comet tails in CCRF-CEM cells upon treatment with different concentrations for 3 h (Fig. 6d). The median value (percentage of tail DNA) from 50 randomly selected cells was 5.2% with a range from 2.4% to 97.5% at a concentration of 0.088 μ M. Only a few cells were damaged. Upon treatment with 0.15 μ M, the median value reached 39.4% with a range from 3.9% to 96.2%, evidencing that DNA damage and the number of damaged cells increased in a concentration-dependent manner. This finding further supports the hypothesis that ZINC253504760 caused parthanatos and implies that eventually the cells die from large-scale DNA damage.

Assessment of oxidative stress

ROS are well recognized as DNA damage mediators. Since ZINC253504760 resulted in a parthanatos, G2/M phase arrest, collapse of mitochondrial membrane potential and a minor fraction of apoptosis, we further investigated whether they were induced via ROS generation. Compared with H_2O_2 that showed a high fold change of ROS production, ZINC253504760-treated samples did not show ROS generation at 12 h or 24 h (Supplementary Fig. S4). Therefore, ZINC253504760 did not induce ROS-dependent mitochondrial apoptosis pathway, and the induction of parthanatos and G2/M phase arrest were not ROS-dependent.

Western blotting of MEK

Since MEK1/2 and ERK were predicted to be downregulated and linked with G2/M cell cycle arrest in CCRF-CEM cells using IPA-based evaluation of the microarray data, we further evaluated their expression and phosphorylation status by western blotting. Upon treatment for

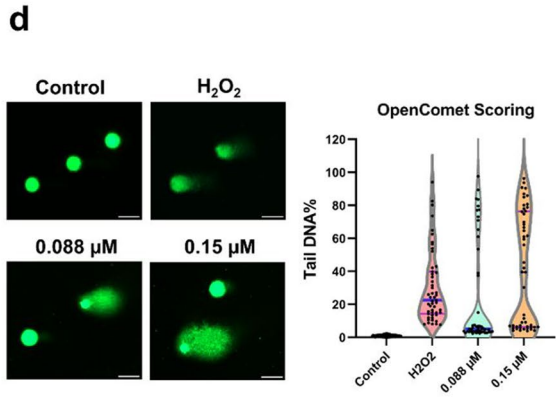
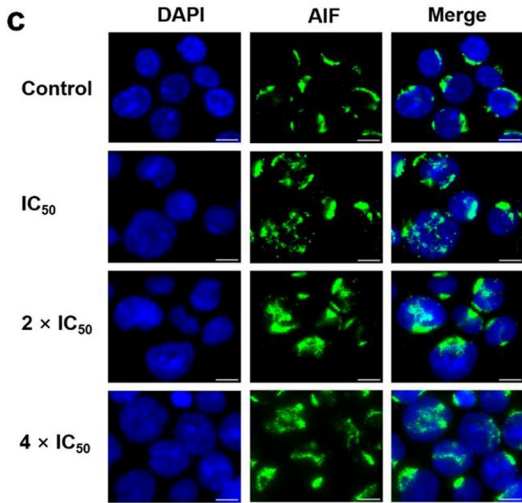
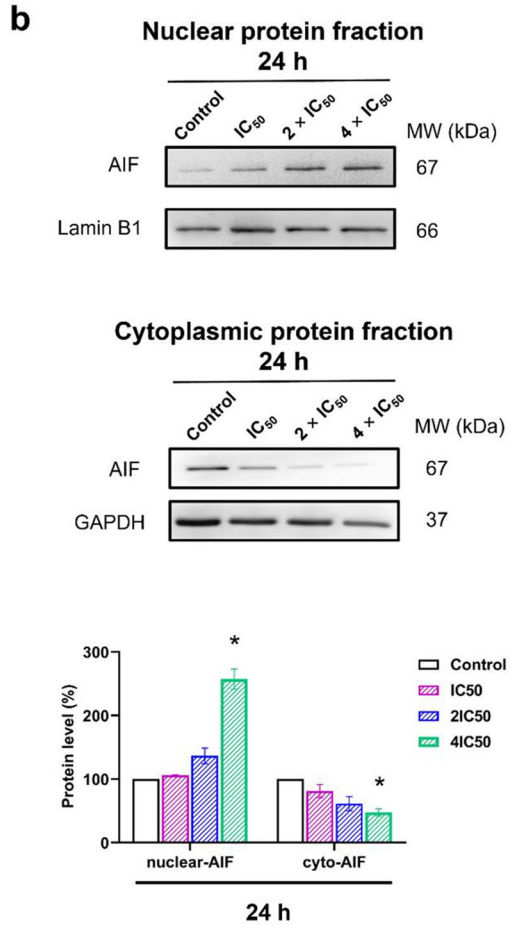
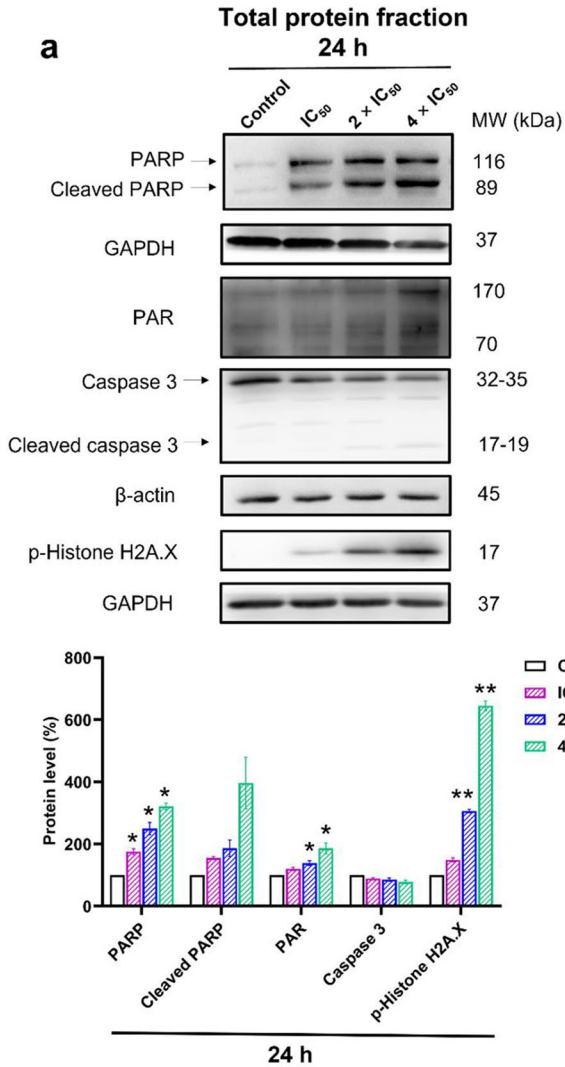


Fig. 6 Induction of parthanatos as major mode of cell death by ZINC253504760. **a** Western blot analysis in total protein of parthanatos-related biomarkers (caspase 3, p-Histone H2A.X, PARP, and PAR) treated with different concentrations of ZINC253504760 for 24 h in CCRF-CEM cells. **b** The expression of AIF in the nucleus and the cytoplasm. Statistics analysis was done by paired student's t-test, * $p \leq 0.05$, ** $p \leq 0.001$, if compared to DMSO untreated cells. The bars represent the mean values \pm SEM of three independent experiments. **c** Detection of AIF translocation from the cytoplasm to the nucleus detected by immunofluorescence microscopy. CCRF-CEM cells treated with different concentrations of ZINC253504760 or DMSO (control) for 12 h and stained with antibody AIF to visualize AIF protein. Nuclear AIF (green) translocated into the nucleus (blue) was obvious. **d** Detection of DNA damage by alkaline comet assay in CCRF-CEM cells. Cells incubated in different concentrations with ZINC253504760 for 3 h and 50 μ M of H₂O₂ (positive control) for 1 h. The parameter tail DNA% was measured from 50 randomly selected cells shown in the violin plot.

24 h, ZINC253504760 significantly downregulated the phosphorylation level of p-MEK1/2, while neither significant effect on MEK 1/2 nor downregulation of ERK protein expression was observed upon treatment, indicating that ZINC253504760 inhibited MEK1/2 phosphorylation (Fig. 7a). After 48 h treatment, ZINC253504760 further downregulated ERK and p-ERK through a more significant downregulation of p-MEK1/2, indicating that ZINC253504760 inhibited ERK protein expression through inhibiting p-MEK1/2. However, there were still no noticeable changes observed on MEK1/2. The significant decrease of MEK1/2 expression with $4 \times IC_{50}$ at 48 h may result from cell death. Therefore, these data suggested that ZINC253504760 inhibited the phosphorylation of MEK1/2.

Molecular docking

To further investigate the possible interaction of ZINC253504760 with MEK1 and MEK2, molecular *in silico* docking studies were performed. Trametinib was used as a known allosteric inhibitor of MEK1/2 to compare the binding affinities with those of ZINC253504760 (Roskoski 2017). ZINC253504760 showed binding affinity (lowest binding energy) to MEK1 (-8.15 ± 0.3 kcal/mol) and MEK2 (-7.85 ± 0.4 kcal/mol), which were approximately the same as trametinib (Supplementary Table S5). As shown in Fig. 7b, five amino acid residues of MEK1 appeared to interact with both ZINC253504760 and trametinib,

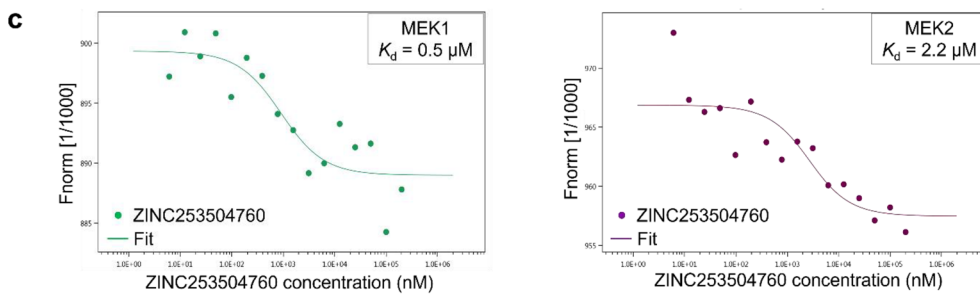
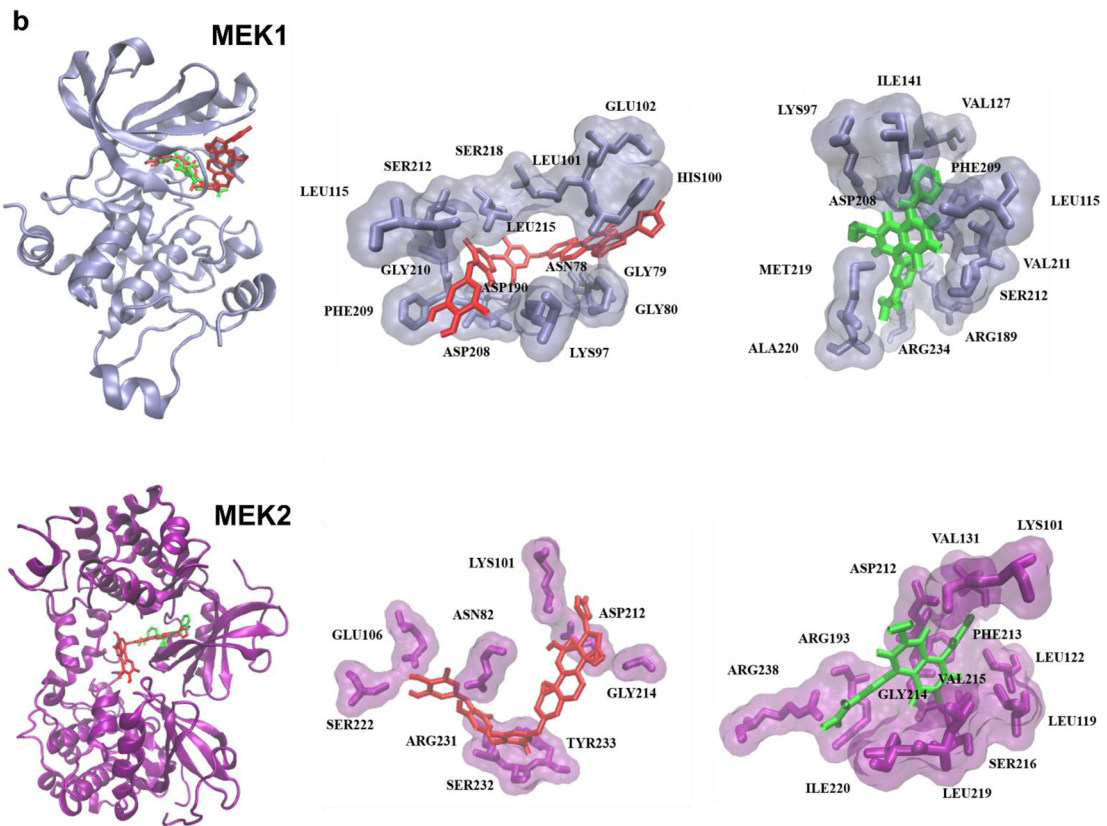
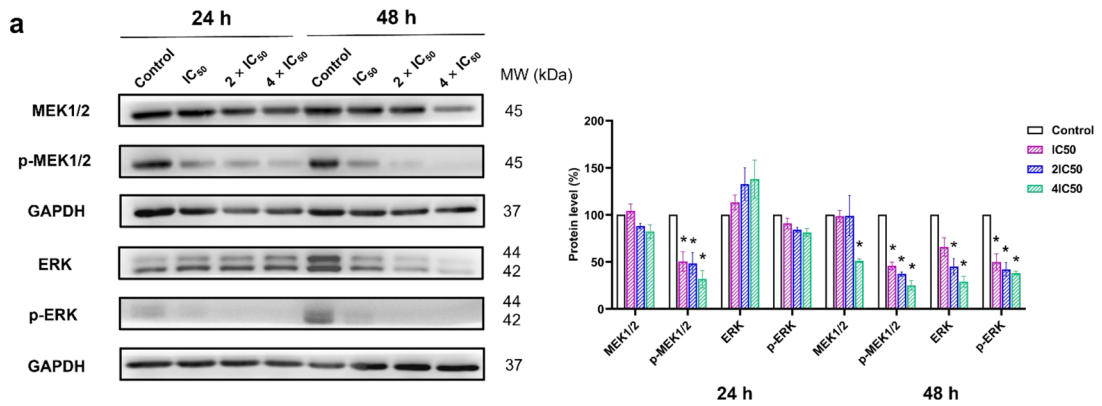
i.e., LYS97, LEU115, ASP208, PHE209, and SER212. Remarkably, ZINC253504760 bound to SER218, which is one of the important phosphorylation sites on MEK1. Regarding MEK2 (chain B), LYS101, ASP212, and GLY214 interacted with both ZINC253504760 and trametinib. Similarly, ZINC253504760 bound to another important phosphorylation site on MEK2, SER222. Therefore, we conclude that ZINC253504760 is an ATP-competitive inhibitor and hereby affects MEK1 and MEK2 phosphorylation. Furthermore, the binding affinity of the deglycosylated form of ZINC253504760 to MEK1 was -6.26 ± 0.05 kcal/mol, and to MEK2 was -6.57 ± 0.005 kcal/mol (Supplementary Table S5), which were closed to the glycosylated form of ZINC253504760. Even though the interacting amino acids of deglycosylated form did not dock to phosphorylated sites on MEK1 or MEK2, they were at similar sites compared with trametinib.

Detection of MEK1/2-compound binding by microscale thermophoresis

The *in vitro* interaction of ZINC253504760 with MEK1/2 was confirmed by MST (Fig. 7c). The measured concentration-dependent fluorescence signals indicated an interaction between the fluorescently labeled MEK1 and MEK2 protein with the compound. ZINC253504760 bound to MEK1 with a K_d value of 0.5 μ M and to MEK2 with a K_d value of 2.2 μ M.

Discussion

Natural products have been regarded as a ‘‘treasure box’’, which greatly contributed to pharmacological research and drug development (Newman and Cragg 2020). Cardiac glycosides (CGs) are one of the leading naturally derived classes of anticancer drug candidates (Kumar and Jaitak 2019). To further develop cardenolides, the aim of the present study was to explore the molecular mode of action of a cardenolide, ZINC253504760. This is a synthetic CG compound with structural similarity to digitoxin and digoxin. Digitoxin and digoxin have been discussed as new anticancer agents (El-Seedi et al. 2019b; Menger et al. 2013), indicating the likelihood that ZINC253504760 might also show anticancer activity.



◀**Fig. 7** Inhibition of MEK1/2 phosphorylation. **a** Western blotting analysis of the effect of ZINC253504760 on MAPK signaling in CCRF-CEM cells. GAPDH was used as the loading control. Digitalized graphs of affected protein levels are shown below. The bars represent mean values \pm SEM of three independent experiments. Statistics analysis was calculated by paired student's t-test, * $p \leq 0.05$, ** $p \leq 0.001$. **b** Visualization of docking results. MEK1 (PDB code:1s9j, ice-blue) and MEK2 (PDB code:1s9i, purple) are presented in a new cartoon format. Ligands are presented in bond format with different colors. ZINC253504760 (red) and trametinib (green). **c** Binding of ZINC253504760 with MEK1 and MEK2 as determined by microscale thermophoresis. MonolithTM NT analysis software was used to determine the fitted K_d on MEK1 and MEK2, and to plot the ZINC253504760 fit curve

We demonstrated that this compound was not involved in the major mechanism of resistance. It is worth to point out that cross-resistance to ZINC253504760 was only observed in BCRP-overexpressing cells, multidrug resistance (except BCRP), making it attractive for further investigations. Previously, we examined the cytotoxicity of a library of 66 CGs that inhibited the efflux function of P-glycoprotein and overcame MDR (Zeino et al. 2015b).

As a next step, we selected drug-sensitive CCRF-CEM leukemia cells as model to unravel the modes of action, since the resazurin assay revealed that ZINC253504760 showed the lowest nanomolar concentration against CCRF-CEM cells. In contrast, the viabilities in embryonic kidney cells (HEK293 and HEK293/ABC5) and breast cancer cells (MDA-MB-231-pcDNA3) were still more than 20% treated with 100 μ M of ZINC253504760, which clearly means these cells lines did not exhibit significant lethality to ZINC253504760. While in glioblastoma multiform cells (U87MG and U87MGEGFR), the viabilities already decreased to 80% at 0.003 μ M, which means ZINC253504760 may begin to kill cells in lower concentrations, while its IC_{50} value was the second only to leukemia cells. Leukemia remains a malignancy in children and adults due to the frequent relapses after treatment (Siegel et al. 2022). A variety of studies reported that CGs including digitoxin, bufalin, ouabain, and perovoside, which showed already profound cytotoxicity in leukemia cells (Masuda et al. 1995; Jing et al. 1994; Feng et al. 2016; Zeino et al. 2015a). Importantly, several CGs indicated that the execution of apoptosis in leukemia cells and did not affect normal blood cells, suggesting that CGs may possess at least some specific tumor-specificity (Ayogu and Odoh 2020).

Cell death was initially categorized into three types: type I (apoptosis), type II (autophagy) and type III

(necrosis). Meanwhile, novel cell death modes have been attracting attention for intervention in disease mechanisms. PARP is activated by DNA strand nicks and breaks and takes part in different pathways of DNA damage repair. Different from mild DNA damage that stimulates PARP to repair damage, parthanatos is uniquely induced by severe DNA damage. It is important to point out that PARP activation is required for AIF translocation. AIF failed to translocate into the nucleus in PARP-knockout fibroblasts after MNNG treatment (Yu et al. 2002). Furthermore, PAR has been identified as an AIF-releasing factor. AIF activity was abrogated by PAR glycohydrolase, an enzyme that plays an important role in the degradation of PAR (Yu et al. 2006). Our western blot analysis revealed elevated full length-PARP (116 kDa) and increased PAR expression in a concentration-dependent manner by ZINC253504760, following decreased cytoplasmic but increased nuclear AIF expression. AIF translocation represents a key event in response to PARP-mediated cell death (Susin et al. 1999). Immunofluorescence microscopy showed that AIF indeed accumulated in the nucleus of treated cells. Currently, the mechanism of AIF release can be explained in two ways: (1) PAR translocates to the cytoplasm, interacts with mitochondria, and binds to AIF (Wang et al. 2011). (2) PAR formation consumes the NAD^+ stores, which leads to a disruption of the MMP and AIF release (Andrabi et al. 2006). Mitochondria act as death centers under cellular stress conditions to release apoptogenic factors including AIF and cytochrome *c* (Andrabi et al. 2008). In our study, flow cytometric analyses showed that ZINC253504760-treated cells lost their MMP in a concentration-dependent manner. Therefore, our experiments support the view that AIF translocated to the nucleus because of the massive PAR accumulation and the loss of the MMP. The phosphorylation of the histone variant H2A.X represents an immediate response to DNA double-strand breaks (DSB) and has been widely applied for the detection of DNA damage (Rahmanian et al. 2021). Our data showed the p-histone H2A.X levels rose instantly upon treatment with increasing drug concentrations. To further validate this result, DNA damage was also investigated by the alkaline comet assay, which indeed revealed increased percentages of tail DNA induced by ZINC253504760. Taken together, from the key features of parthanatos, we demonstrated that ZINC253504760 resulted in rapid PARP activation, PAR accumulation, mitochondrial depolarization, AIF translocation, and large-scale DNA

fragmentation. These data are consistent with the other reports where parthanatos was induced in cancer cells (Zhao et al. 2015; Ma et al. 2016). Parthanatos is the major mode of cell death of ZINC253504760 in CCRF-CEM leukemia cells. It contributes to the growth inhibition of ZINC253504760 in the resazurin assay and explains the appearance of the cell death and survival pathway predicted by the microarray-based Ingenuity Pathway Analysis.

Even if parthanatos is different from other modes of cell death regarding their morphological and molecular pathways, they interact with each other and exert cross-talks. Firstly, parthanatos may interact with apoptosis. Early studies have been demonstrated that PARP activation and AIF activity can be maintained in the presence of wide-ranging caspase inhibitor Z-VAD-fmk in MNNG treated wild-type fibroblasts, suggesting that parthanatos is a caspase-independent cell death mode (Susin et al. 1999; Yu et al. 2002), while recent emerging evidence indicates that caspases also can be activated in parthanatos (Yu et al. 2002). In our study, the PARP fragment (89 kDa) and caspase 3 participated in ZINC253504760-induced cell death. PARP is a switch point that directs cell death toward either apoptosis or parthanatos. Parthanatos starts in the overactivation of PARP and results in the deletion of energy stores, while apoptosis is initiated by cleaved PARP with abundant energy (Zhou et al. 2021). Hence, the switch of PARP might be cross-dynamic. Meanwhile, we observed the expression of cleaved PARP without cleaved caspase 3. In fact, it has been reported that PARP cleavage was not defective in the absence of caspase 3 (Slee et al. 2001). Our results supported this study. Since we did not find significant late apoptosis of ZINC253504760 treatment, we propose here, ZINC253504760 induced parthanatos as the major mode of cell death and with a minor role of apoptosis in leukemia cells. Furthermore, AIF may interact with caspase. As mentioned above, both AIF and cytochrome *c* are released from mitochondria. Cytochrome *c* redistributes into the cytosol and triggers the activation of caspase 3 or caspase 9. Kinetic studies revealed the order of action that the mitochondrial release of AIF occurred earlier than that of cytochrome *c* (Daugas et al. 2000b). This means that AIF release initiates stage I of chromatin condensation (caspase-independent), and in stage II cell death relies on the activation of caspase by cytochrome *c* (caspase-dependent) (Daugas et al. 2000a). Along this line, we assume that upon treatment with ZINC253504760 for 24 h

(stage I), parthanatos is the predominant mode of cell death, when AIF translocates into the nucleus. In stage II (after 24 h or more), caspase 3 was gradually activated, while a small fraction of apoptosis was induced in dying cells. Furthermore, ZINC253504760 did not induce ROS-dependent parthanatos or mitochondrial apoptosis in CCRF-CEM cells, this finding is different with parthanatos induced in glioma cells (Ma et al. 2016). Finally, autophagy biomarkers including Beclin and p62 were decreased in a time- and concentration-dependent manner, suggesting that ZINC253504760 did not induce autophagy in CCRF-CEM cells. Thus, ZINC253504760-induced parthanatos did not correlate to autophagy. Our finding is consistent with parthanatos induced in esophageal cancer (Zhao et al. 2015).

Using flow cytometry, we observed that ZINC253504760 induced G2/M phase arrest, and this result was consistent with the microarray-based pathway prediction. We also further verified a number of genes involved in the cell cycle using qRT-PCR. G2/M phase arrest is one of the main cellular responses to DNA damage that prevents the transmission of damaged DNA to undergo mitosis without repair of DNA lesions. It is worth to mention that ATM (ataxia-telangiectasia mutated) and ATR (ataxia-telangiectasia mutated and Rad3-related) kinase are the required sensors to recognize DNA damage and to phosphorylate their target proteins, such as p53 and H2AX (Sancar et al. 2004). In the present study, HIPK2, a damage-activated checkpoint kinase that is activated by ATM was upregulated after treatment (Hofmann et al. 2013), indicating that ZINC253504760 induced DNA damage. PPM1D, a p53-induced protein after chemical stimulation, deactivates p53 by dephosphorylating ATM/ATR following DNA damage. Therefore, PPM1D has been categorized as an oncogene, since it suppresses the DNA repair function (Lu et al. 2004, 2005). This may explain our results that PPM1D was upregulated while p53 was downregulated. CDK7 along with cyclin H comprises the CDK-activating kinase (CAK), which is necessary to activate CDKs by providing the T-loop phosphorylation (Sava et al. 2020). In our experiment, the downregulation of CDK7 by ZINC253504760 during G2 phase actually disrupts cyclin B1-CDK1 assembling and blocks cells to enter mitosis (Larochelle et al. 2007). However, a connection between CDK7 and p53 was not predicted by our microarray data. CDK7 and p53 have been raised questions because they both share functional similarities regarding cell cycle regulation, transcription, and DNA repair. P53 can be phosphorylated by CDK7-Cyclin

H in a p36^{MAT1}-dependent manner both *in vitro* and *in vivo* (Ko et al. 1997). Hence, it is understandable in our study that CDK7 was downregulated if p53 was also downregulated. Moreover, in our study, CDK1 was upregulated both in microarray and qRT-PCR experiments, which seems to be conflicting with G2/M phase arrest at first sight. In fact, even though the cyclin B1-CDK1 complex is inactive in the G2/M phase, it still can be activated at the start of prophase, and cyclin B1-CDK1 activity reaches its maximum shortly after the nuclear envelope breakdown (Gavet and Pines 2010). This period maintains the cells in their mitotic state. Therefore, we assume that our experiments at 24 h captured this mitotic moment of CDK1 upregulation. On the other hand, cyclinB1-CDK1 was inactivated after cyclin B1 degradation in arrested cells (Porter and Donoghue 2003). The change from the active to the inactive cyclinB1-CDK1 complex has been described as hysteresis (Pomerening et al. 2003). Regarding our results, this may be another reason that CDK7 was already downregulated while CDK1 was still upregulated and active. CKS1 and CKS2 are proposed to physically link with cyclinB1-CDK1 for further phosphorylation to their substrates (Ellederova et al. 2019). The upregulation of CKS1 and CKS2 was consistent with the upregulation of CDK1. Furthermore, Wee1 is a kinase which negatively regulates CDK1 by catalyzing the phosphorylation on Thr14 and Tyr15 and which inhibits CDK1 activity (Du et al. 2020). Our data showed that Wee1 was upregulated by ZINC253504760, while CDK1 remained upregulated under hysteresis and inactivated cyclin B1-CDK1. Furthermore, the ATR-CHEK1-CDC25 pathway was predicted by IPA to be affected by ZINC253504760. This is a classical pathway activated following DNA damage and arrest in the G2 phase (Calonge and O'Connell 2008). Due to our limited treatment time (24 h) and concentration (IC₅₀), this pathway was only predicted by IPA software without expression of fold change, but our validation by qRT-PCR of the eight genes is sufficient to support cell cycle G2/M arrest induced by ZINC253504760.

Microtubules have multiple functions in cellular processes, especially regarding the formation of mitotic spindles during cell cycle, making them vital therapeutic targets in cancer treatment (Dumontet and Jordan 2010). The microtubule-targeting antimetabolic drugs can be divided into microtubule-destabilizing agents (*e.g.*, *Vinca* alkaloids and colchicine), and microtubule-stabilizing agents (*e.g.*, taxanes). Both drug classes block mitosis (Wang et al. 2016). We found that ZINC253504760 interfered with tubulin

polymerization in U2OS cells expressing an α -tubulin-GFP construct. In brief, our data obtained from flow cytometry, qRT-PCR, and fluorescence microscopy of the microtubule cytoskeleton supported the view that ZINC253504760 induced G2/M phase arrest and blocked the cellular entry into mitosis.

A wide of human tumors are under the control of MAPK pathway for growth and survival (Sebolt-Leopold and Herrera 2004). Since the downregulation of MEK1/2 and ERK was associated with G2/M cell cycle arrest biomarkers as predicted by IPA, we confirmed that ZINC253504760 indeed resulted in G2/M phase arrest. Therefore, we also investigated the hypothesis that ZINC253504760 can downregulate MEK1/2 *in vitro*, supposing that MEK1/2 might be a target of ZINC253504760 in CCRF-CEM cells. Indeed, our study revealed that p-MEK1/2 was downregulated in a concentration- and time-dependent manner, which further affected p-ERK and ERK. While ERK was still upregulated after 24 h, MEK1/2 dephosphorylation was still ongoing and ERK was downregulated after 48 h. Next, we carried out molecular docking to understand the mode of binding of ZINC253504760 to MEK1 and MEK2. As expected, ZINC253504760 bound to the phosphorylation sites, SER218 on MEK1 and SER222 on MEK2. In human MEK1, the substitution of either SER218 or SER222 abrogates the MEK1 activation, implying that both serines are required for phosphorylation (Zheng and Guan 1994). Our results supported this finding. Therefore, we conclude that ZINC253504760 contributed to MEK1/2 inactivation, which further led to downstream ERK downregulation and inhibition of cell proliferation. In addition, the lowest binding energy of deglycosylated form of ZINC253504760 to MEK1/2 was similar to that of glycosylated form. Regarding the fact that the bioactivity of GCs decreases with the loss of sugar, the monitor of bioactive metabolites of GCs needs to be studied in the future, and if necessary, concomitant administration such as metabolic enzyme inhibitors or other drugs (*e.g.*, quinidine increased absorption of digoxin) might be options to increase CGs bioavailability (Pedersen et al. 1983; Jortani and Valdes 1997). Moreover, the ATP-binding pocket on kinases has been classified into many types (Pan and Mader 2022). MEK1/2 is one of the most thoroughly investigated kinases for type III allosteric inhibitors. The four FDA-approved MEK1/2 are all ATP-noncompetitive kinase inhibitors (Roskoski 2017; Lu et al. 2020). Our results showed trametinib as a known allosteric inhibitor

bound adjacent to the ATP binding site which supported previous studies and proved that our molecular docking approach was correct. Finally, the molecular interactions of ZINC253504760 with MEK1/2 have been confirmed by MST, and the fit curves proved once again that ZINC253504760 could bind to MEK1 and MEK2. Taken together, our *in vitro* and *in silico* results indicated that ZINC253504760 bound to MEK1/2 and inhibited MEK1/2 phosphorylation.

Interestingly, numerous studies revealed the characteristic molecular mechanisms of CGs in cancer cells. First and foremost, apoptotic cell death has been described in most cases (e.g., UNBS1450) (Juncker et al. 2011). Immunogenetic cell death was also induced by CGs (e.g., oleandrin) (Li et al. 2021; Menger et al. 2012). In the present investigation, ZINC253504760 predominantly induced parthanatic cell death rather than apoptosis. Our finding opened a new door for further studies on the cell death mode of CGs and pointed to the potential of ZINC253504760 to treat anti-apoptosis- and drug-resistant cancers. Moreover, ZINC253504760 arrested CCRF-CEM leukemia cells in the G2/M phase of the cell cycle. This result is comparable to reports from many other CGs, such as proscillaridin A-treated glioblastoma cells (Denicolai et al. 2014), ouabain-treated melanoma cells (Wang et al. 2021), and lanatoside C-treated breast, lung, or liver cancer cells (Reddy et al. 2019). Based on this fact, the induction of parthanatos and G2/M phase arrest in cell cycle are the best evidence to support that ZINC253504760 leads to DNA damage. In addition, Src is a non-receptor protein tyrosine kinase, the activation of the Src-EGFR-MAPK pathway is one of the accepted potential mechanisms of the anticancer effects of CGs (Prassas and Diamandis 2008; Kometiani et al. 2005). Our functional network identified from the transcriptomic analysis (Fig. 3c) showed that c-Src protein, as well as the top affected genes *Hsp90AA1* and *Hsp90 AB1* were downregulated after ZINC253504760 treatment. Luo et al have demonstrated that c-Src was weakly affected by the chaperone Hsp90 (Luo et al. 2017). Therefore, our study revealed the molecular mode of action of ZINC253504760 resulting from DNA damage, parthanatic cell death and G2/M arrest.

Last but not least, CG compounds have a narrow therapeutic window and show different toxicities. In the future, the selectivity and toxicity of ZINC253504760 should be investigated in more

detail. In the light of developing CG compounds for the treatment of malignant diseases, studies based on pharmacokinetic properties, toxicological mechanisms and further structural modifications should be conducted to achieve reduced toxicity of CG compounds. Personalized medicine by investigating gene polymorphisms is also a strategy to delineate applicable populations with increased efficacy and less toxicity (Zhai et al. 2022).

Conclusion

Taken together, in this study we described the mechanism of a new synthetic cardenolide compound, ZINC253504760. This compound displayed cytotoxicity against different multidrug-resistant cell lines with overexpression of ABC transporters (P-glycoprotein, ABCB5), overexpression of the activated oncogene Δ EGFR, or a knock-out of the tumor suppressor TP53. Starting from microarray-based mRNA expression profiling, we demonstrated that ZINC253504760 induced parthanatos-type cell death and G2/M phase arrest in CCRF-CEM cells, both resulting from DNA damage. ZINC253504760 induced the overexpression of PARP and PAR and nuclear AIF translocation, and disrupted the mitochondrial membrane potential, all of which are steps triggering parthanatos. Furthermore, ZINC253504760 blocked the MAPK pathway by inhibiting MEK1/2 phosphorylation in a time- and concentration-dependent manner. ZINC253504760 bound to MEK1 and MEK2 at their phosphorylated sites, as demonstrated by microscale thermophoresis and molecular docking. To the best of our knowledge, parthanatos was shown for the first time to be induced by a cardenolide compound. These results provide a basis for further exploring ZINC253504760 as an alternative strategy to treat cancer cells that have the ability to escape apoptosis and are drug-resistant. Further assessments of ZINC253504760 are warranted regarding its toxicity.

Acknowledgement We gratefully acknowledge the Microarray Unit of the Genomics and Proteomics Core Facility, German Cancer Research Center (DKFZ), for providing excellent Expression Profiling service. We thank Microscope Core Facility and Flow Cytometry Core Facility at the Institute of Molecular Biology (IMB, Mainz, Germany) for their kind training and technical support for microscopy and flow cytometry related experiments. We are grateful for the PhD stipend of the Chinese Scholarship Council to M.Z., and the stipend of the Sibylle Kalkhof-Rose-Foundation to J.C.B.

Author contributions Min Zhou: Data curation, Methodology, Investigation, Conceptualization, Writing – original draft, Writing – review & editing. Joelle C. Boulos: Conceptualization, Methodology, Investigation. Sabine M. Klauk: Conceptualization, Methodology, Investigation, Software, Data curation, Writing – review & editing. Thomas Efferth: Project administration, Supervision, Conceptualization, Writing – review & editing.

Funding Open Access funding enabled and organized by Projekt DEAL.

Data availability The authors declare that the data supporting the findings of this study are available within the paper. All other data are available from the corresponding author upon reasonable request.

Code availability Not applicable.

Declarations

Competing interests The authors declare no competing interests.

Conflict of interest The authors declare there is no conflict of interest.

Ethical approval Not applicable.

Consent for publication All authors have agreed to publish this manuscript.

Consent to participate Not applicable.

Human and animal rights This article does not contain any studies with human or animal subjects.

Open Access This article is licensed under a Creative Commons Attribution 4.0 International License, which permits use, sharing, adaptation, distribution and reproduction in any medium or format, as long as you give appropriate credit to the original author(s) and the source, provide a link to the Creative Commons licence, and indicate if changes were made. The images or other third party material in this article are included in the article's Creative Commons licence, unless indicated otherwise in a credit line to the material. If material is not included in the article's Creative Commons licence and your intended use is not permitted by statutory regulation or exceeds the permitted use, you will need to obtain permission directly from the copyright holder. To view a copy of this licence, visit <http://creativecommons.org/licenses/by/4.0/>.

References

- Abdelfatah S, Fleischer E, Klinger A, Wong VKW, Efferth T. Identification of inhibitors of the polo-box domain of polo-like kinase 1 from natural and semisynthetic compounds. *Invest New Drugs*. 2020;38(1):1–9. <https://doi.org/10.1007/s10637-019-00752-0>.
- Ainembabazi D, Geng X, Gavande NS, Turchi JJ, Zhang Y. Synthesis and Biological Evaluation of Cardiac Glycosides for Cancer Therapy by Targeting the DNA Damage Response. *ChemMedChem*. 2022:e202200415. <https://doi.org/10.1002/cmdc.202200415>.
- Andrabi SA, Dawson TM, Dawson VL. Mitochondrial and nuclear cross talk in cell death: parthanatos. *Ann N Y Acad Sci*. 2008;1147:233–41. <https://doi.org/10.1196/annals.1427.014>.
- Andrabi SA, Kim NS, Yu SW, Wang H, Koh DW, Sasaki M, et al. Poly(ADP-ribose) (PAR) polymer is a death signal. *Proc Natl Acad Sci U S A*. 2006;103(48):18308–13. <https://doi.org/10.1073/pnas.0606526103>.
- Ayogu JI, Odoh AS. Prospects and Therapeutic Applications of Cardiac Glycosides in Cancer Remediation. *ACS Comb Sci*. 2020;22(11):543–53. <https://doi.org/10.1021/acscombsci.0c00082>.
- Barbosa R, Acevedo LA, Marmorstein R. The MEK/ERK Network as a Therapeutic Target in Human Cancer. *Mol Cancer Res*. 2021;19(3):361–74. <https://doi.org/10.1158/1541-7786.Mcr-20-0687>.
- Bessen HA. Therapeutic and toxic effects of digitalis: William Withering, 1785. *J Emerg Med*. 1986;4(3):243–8. [https://doi.org/10.1016/0736-4679\(86\)90048-X](https://doi.org/10.1016/0736-4679(86)90048-X).
- Bock FJ, Tait SWG. Mitochondria as multifaceted regulators of cell death. *Nat Rev Mol Cell Biol*. 2020;21(2):85–100. <https://doi.org/10.1038/s41580-019-0173-8>.
- Boulos JC, Saeed MEM, Chatterjee M, Bülbül Y, Crudo F, Marko D, et al. Repurposing of the ALK Inhibitor Crizotinib for Acute Leukemia and Multiple Myeloma Cells. *Pharmaceuticals (Basel)*. 2021;14(11). <https://doi.org/10.3390/ph14111126>.
- Calonge TM, O'Connell MJ. Turning off the G2 DNA damage checkpoint. *DNA Repair (Amst)*. 2008;7(2):136–40. <https://doi.org/10.1016/j.dnarep.2007.07.017>.
- Caunt CJ, Sale MJ, Smith PD, Cook SJ. MEK1 and MEK2 inhibitors and cancer therapy: the long and winding road. *Nature Reviews Cancer*. 2015;15(10):577–92. <https://doi.org/10.1038/nrc4000>.
- Cowley S, Paterson H, Kemp P, Marshall CJ. Activation of MAP kinase kinase is necessary and sufficient for PC12 differentiation and for transformation of NIH 3T3 cells. *Cell*. 1994;77(6):841–52. [https://doi.org/10.1016/0092-8674\(94\)90133-3](https://doi.org/10.1016/0092-8674(94)90133-3).
- Daugas E, Nochy D, Ravagnan L, Loeffler M, Susin SA, Zamzami N, et al. Apoptosis-inducing factor (AIF): a ubiquitous mitochondrial oxidoreductase involved in apoptosis. *FEBS Lett*. 2000;476(3):118–23. [https://doi.org/10.1016/s0014-5793\(00\)01731-2](https://doi.org/10.1016/s0014-5793(00)01731-2).
- Daugas E, Susin SA, Zamzami N, Ferri KF, Irinopoulou T, Larochette N, et al. Mitochondrio-nuclear translocation of AIF in apoptosis and necrosis. *Faseb j*. 2000;14(5):729–39.
- Dawood M, Fleischer E, Klinger A, Bringmann G, Shan L, Efferth T. Inhibition of cell migration and induction of apoptosis by a novel class II histone deacetylase inhibitor, MCC2344. *Pharmacol Res*. 2020a;160:105076. <https://doi.org/10.1016/j.phrs.2020.105076>.
- Dawood M, Hegazy MF, Elbadawi M, Fleischer E, Klinger A, Bringmann G, et al. Vitamin K(3) chloro derivative (VKT-2) inhibits HDAC6, activates autophagy and apoptosis, and inhibits aggresome formation in hepatocellular carcinoma

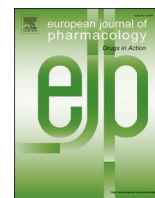
- cells. *Biochem Pharmacol.* 2020b;180:114176. <https://doi.org/10.1016/j.bcp.2020.114176>.
- Denicolai E, Baeza-Kallee N, Tchoghandjian A, Carré M, Colin C, Jiglaire CJ, et al. Proscillaridin A is cytotoxic for glioblastoma cell lines and controls tumor xenograft growth in vivo. *Oncotarget.* 2014;5(21):10934–48. <https://doi.org/10.18632/oncotarget.2541>.
- Doyle LA, Yang W, Abruzzo LV, Krogmann T, Gao Y, Rishi AK, et al. A multidrug resistance transporter from human MCF-7 breast cancer cells. *Proc Natl Acad Sci U S A.* 1998;95(26):15665–70. <https://doi.org/10.1073/pnas.95.26.15665>.
- Du X, Li J, Luo X, Li R, Li F, Zhang Y, et al. Structure-activity relationships of Wee1 inhibitors: A review. *Eur J Med Chem.* 2020;203:112524. <https://doi.org/10.1016/j.ejmech.2020.112524>.
- Dumontet C, Jordan MA. Microtubule-binding agents: a dynamic field of cancer therapeutics. *Nat Rev Drug Discov.* 2010;9(10):790–803. <https://doi.org/10.1038/nrd3253>.
- El-Seedi HR, Khalifa SAM, Taher EA, Farag MA, Saeed A, Gamal M, et al. Cardenolides: Insights from chemical structure and pharmacological utility. *Pharmacol Res.* 2019;141:123–75. <https://doi.org/10.1016/j.phrs.2018.12.015>.
- El-Seedi HR, Khalifa SAM, Taher EA, Farag MA, Saeed A, Gamal M, et al. Cardenolides: Insights from chemical structure and pharmacological utility. *Pharmacol Res.* 2019;141:123–75. <https://doi.org/10.1016/j.phrs.2018.12.015>.
- Elbadawi M, Boulos JC, Dawood M, Zhou M, Gul W, ElSohly MA, et al. The Novel Artemisinin Dimer Isoniazide ELI-XXIII-98-2 Induces c-MYC Inhibition, DNA Damage, and Autophagy in Leukemia Cells. *Pharmaceutics.* 2023;15(4):1107. <https://www.mdpi.com/1999-4923/15/4/1107>.
- Ellederova Z, Rincon Sd, Koncicka M, Susor A, Kubelka M, Sun D, et al. Cks1 Germ Line Exclusion Is Essential for the Transition from Meiosis to Early Embryonic Development. *Mol Cell Biol.* 2019;39(13):e00590-18. <https://doi.org/10.1128/MCB.00590-18>.
- Feng Q, Leong WS, Liu L, Chan W-I. Peruvoside, a Cardiac Glycoside, Induces Primitive Myeloid Leukemia Cell Death. *Molecules.* 2016;21(4):534. <https://www.mdpi.com/1420-3049/21/4/534>.
- Flaherty KT, Infante JR, Daud A, Gonzalez R, Kefford RF, Sosman J, et al. Combined BRAF and MEK inhibition in melanoma with BRAF V600 mutations. *N Engl J Med.* 2012;367(18):1694–703. <https://doi.org/10.1056/NEJMoa1210093>.
- Frémin C, Meloche S. From basic research to clinical development of MEK1/2 inhibitors for cancer therapy. *J Hematol Oncol.* 2010;3:8. <https://doi.org/10.1186/1756-8722-3-8>.
- Galia A, Calogero AE, Condorelli R, Frassetta F, La Corte A, Ridolfo F, et al. PARP-1 protein expression in glioblastoma multiforme. *Eur J Histochem.* 2012;56(1):e9. <https://doi.org/10.4081/ejh.2012.e9>.
- Gavet O, Pines J. Progressive activation of CyclinB1-Cdk1 coordinates entry to mitosis. *Dev Cell.* 2010;18(4):533–43. <https://doi.org/10.1016/j.devcel.2010.02.013>.
- Gurel E, Karvar S, Yucesan B, Eker I, Sameuallah M. An Overview of Cardenolides in Digitalis - More Than a Cardiotonic Compound. *Curr Pharm Des.* 2017;23(34):5104–14. <https://doi.org/10.2174/1381612823666170825125426>.
- Gyori BM, Venkatachalam G, Thiagarajan PS, Hsu D, Clement MV. OpenComet: an automated tool for comet assay image analysis. *Redox Biol.* 2014;2:457–65. <https://doi.org/10.1016/j.redox.2013.12.020>.
- Ha DP, Tsai YL, Lee AS. Suppression of ER-stress induction of GRP78 as an anti-neoplastic mechanism of the cardiac glycoside Lanatoside C in pancreatic cancer: Lanatoside C suppresses GRP78 stress induction. *Neoplasia.* 2021;23(12):1213–26. <https://doi.org/10.1016/j.neo.2021.10.004>.
- Hegazy MF, Dawood M, Mahmoud N, Elbadawi M, Sugimoto Y, Klauck SM, et al. 2 α -Hydroxyalantolactone from *Pulicaria undulata*: activity against multidrug-resistant tumor cells and modes of action. *Phytomedicine.* 2021;81:153409. <https://doi.org/10.1016/j.phymed.2020.153409>.
- Hofmann TG, Glas C, Bitomsky N. HIPK2: A tumour suppressor that controls DNA damage-induced cell fate and cytokinesis. *Bioessays.* 2013;35(1):55–64. <https://doi.org/10.1002/bies.201200060>.
- Hoshino R, Chatani Y, Yamori T, Tsuruo T, Oka H, Yoshida O, et al. Constitutive activation of the 41-/43-kDa mitogen-activated protein kinase signaling pathway in human tumors. *Oncogene.* 1999;18(3):813–22. <https://doi.org/10.1038/sj.onc.1202367>.
- Hu Q-Y, Zhang X-K, Wang J-N, Chen H-X, He L-P, Tang J-S, et al. Malayoside, a cardenolide glycoside extracted from *Antiaris toxicaria* Lesch, induces apoptosis in human non-small lung cancer cells via MAPK-Nur77 signaling pathway. *Biochem Pharmacol.* 2021;190:114622. <https://doi.org/10.1016/j.bcp.2021.114622>.
- Jing Y, Ohizumi H, Kawazoe N, Hashimoto S, Masuda Y, Nakajo S, et al. Selective inhibitory effect of bufalin on growth of human tumor cells in vitro: association with the induction of apoptosis in leukemia HL-60 cells. *Jpn J Cancer Res.* 1994;85(6):645–51. <https://doi.org/10.1111/j.1349-7006.1994.tb02408.x>.
- Jortani SA, Valdes R Jr. Digoxin and its related endogenous factors. *Crit Rev Clin Lab Sci.* 1997;34(3):225–74. <https://doi.org/10.3109/10408369708998094>.
- Juncker T, Cerella C, Teiten MH, Morceau F, Schumacher M, Ghelfi J, et al. UNBS1450, a steroid cardiac glycoside inducing apoptotic cell death in human leukemia cells. *Biochem Pharmacol.* 2011;81(1):13–23. <https://doi.org/10.1016/j.bcp.2010.08.025>.
- Kadioglu O, Klauck SM, Fleischer E, Shan L, Efferth T. Selection of safe artemisinin derivatives using a machine learning-based cardiotoxicity platform and in vitro and in vivo validation. *Arch Toxicol.* 2021;95(7):2485–95. <https://doi.org/10.1007/s00204-021-03058-4>.
- Khalid SA, Dawood M, Boulos JC, Wasfi M, Drif A, Bahramimehr F, et al. Identification of Gedunin from a Phytochemical Depository as a Novel Multidrug Resistance-Bypassing Tubulin Inhibitor of Cancer Cells. *Molecules.* 2022;27(18). <https://doi.org/10.3390/molecules27185858>.
- Ko LJ, Shieh SY, Chen X, Jayaraman L, Tamai K, Taya Y, et al. p53 is phosphorylated by CDK7-cyclin H in a p36MAT1-dependent manner. *Mol Cell Biol.* 1997;17(12):7220–9. <https://doi.org/10.1128/mcb.17.12.7220>.
- Kometiani P, Liu L, Askari A. Digitalis-induced signaling by Na⁺/K⁺-ATPase in human breast cancer cells. *Mol Pharmacol.* 2005;67(3):929–36. <https://doi.org/10.1124/mol.104.007302>.
- Kumar A, Jaitak V. Natural products as multidrug resistance modulators in cancer. *Eur J Med Chem.*

- 2019;176:268–91. <https://doi.org/10.1016/j.ejmech.2019.05.027>.
- Kun E, Tsang YTM, Ng CW, Gershenson DM, Wong KK. MEK inhibitor resistance mechanisms and recent developments in combination trials. *Cancer Treat Rev*. 2021;92:102137. <https://doi.org/10.1016/j.ctrv.2020.102137>.
- Larochelle S, Merrick KA, Terret ME, Wohlbold L, Barboza NM, Zhang C, et al. Requirements for Cdk7 in the assembly of Cdk1/cyclin B and activation of Cdk2 revealed by chemical genetics in human cells. *Mol Cell*. 2007;25(6):839–50. <https://doi.org/10.1016/j.molcel.2007.02.003>.
- Li X, Zheng J, Chen S, Meng F-D, Ning J, Sun S-L. Oleandrin, a cardiac glycoside, induces immunogenic cell death via the PERK/eIF2 α /ATF4/CHOP pathway in breast cancer. *Cell Death Dis*. 2021;12(4):314. <https://doi.org/10.1038/s41419-021-03605-y>.
- Liu YB, Sun YY, Zhang JL, Zhu YS, Dai YP, D J, et al. Up-regulation of TUBA1B promotes astrocyte proliferation after spinal cord injury in adult rats. *Int J Exp Pathol*. 2017;10(2):1094–103
- Livak KJ, Schmittgen TD. Analysis of Relative Gene Expression Data Using Real-Time Quantitative PCR and the 2- $\Delta\Delta$ CT Method. *Methods*. 2001;25(4):402–8. <https://doi.org/10.1006/meth.2001.1262>.
- Lu X, Bocangel D, Nannenga B, Yamaguchi H, Appella E, Donehower LA. The p53-induced oncogenic phosphatase PPM1D interacts with uracil DNA glycosylase and suppresses base excision repair. *Mol Cell*. 2004;15(4):621–34. <https://doi.org/10.1016/j.molcel.2004.08.007>.
- Lu X, Nannenga B, Donehower LA. PPM1D dephosphorylates Chk1 and p53 and abrogates cell cycle checkpoints. *Genes Dev*. 2005;19(10):1162–74. <https://doi.org/10.1101/gad.1291305>.
- Lu X, Smaill JB, Ding K. New Promise and Opportunities for Allosteric Kinase Inhibitors. *Angew Chem Int Ed Engl*. 2020;59(33):13764–76. <https://doi.org/10.1002/anie.201914525>.
- Luo Q, Boczek EE, Wang Q, Buchner J, Kaila VRI. Hsp90 dependence of a kinase is determined by its conformational landscape. *Sci Rep*. 2017;7(1):43996. <https://doi.org/10.1038/srep43996>.
- Ma D, Lu B, Feng C, Wang C, Wang Y, Luo T, et al. Deoxypodophyllotoxin triggers parthanatos in glioma cells via induction of excessive ROS. *Cancer Lett*. 2016;371(2):194–204. <https://doi.org/10.1016/j.canlet.2015.11.044>.
- Mahmoud N, Saeed MEM, Sugimoto Y, Klauk SM, Greten HJ, Efferth T. Cytotoxicity of nimbolide towards multidrug-resistant tumor cells and hypersensitivity via cellular metabolic modulation. *Oncotarget*. 2018;9(87):35762–79. <https://doi.org/10.18632/oncotarget.26299>.
- Mansour SJ, Matten WT, Hermann AS, Candia JM, Rong S, Fukasawa K, et al. Transformation of mammalian cells by constitutively active MAP kinase kinase. *Science*. 1994;265(5174):966–70. <https://doi.org/10.1126/science.8052857>.
- Masuda Y, Kawazoe N, Nakajo S, Yoshida T, Kuroiwa Y, Nakaya K. Bufalin induces apoptosis and influences the expression of apoptosis-related genes in human leukemia cells. *Leuk Res*. 1995;19(8):549–56. [https://doi.org/10.1016/0145-2126\(95\)00031-i](https://doi.org/10.1016/0145-2126(95)00031-i).
- Menger L, Vacchelli E, Adjemian S, Martins I, Ma Y, Shen S, et al. Cardiac glycosides exert anticancer effects by inducing immunogenic cell death. *Sci Transl Med*. 2012;4(143):143ra99. <https://doi.org/10.1126/scitranslmed.3003807>.
- Menger L, Vacchelli E, Kepp O, Eggermont A, Tartour E, Zitvogel L, et al. Trial watch: Cardiac glycosides and cancer therapy. *Oncoimmunology*. 2013;2(2):e23082. <https://doi.org/10.4161/onci.23082>.
- Mijatovic T, Van Quaquebeke E, Delest B, Debeir O, Darro F, Kiss R. Cardiotonic steroids on the road to anti-cancer therapy. *Biochim Biophys Acta*. 2007;1776(1):32–57. <https://doi.org/10.1016/j.bbcan.2007.06.002>.
- Newman DJ, Cragg GM. Natural Products as Sources of New Drugs over the Nearly Four Decades from 01/1981 to 09/2019. *J Nat Prod*. 2020;83(3):770–803. <https://doi.org/10.1021/acs.jnatprod.9b01285>.
- Newman RA, Yang P, Pawlus AD, Block KI. Cardiac glycosides as novel cancer therapeutic agents. *Mol Interv*. 2008;8(1):36–49. <https://doi.org/10.1124/mi.8.1.8>.
- Nolte E, Wach S, Silva IT, Lukat S, Ekici AB, Munkert J, et al. A new semisynthetic cardenolide analog 3 β -[2-(1-amantadine)-1-on-ethylamine]-digitoxigenin (AMANTADIG) affects G2/M cell cycle arrest and miRNA expression profiles and enhances proapoptotic survivin-2B expression in renal cell carcinoma cell lines. *Oncotarget*. 2017;8(7):11676–91. <https://doi.org/10.18632/oncotarget.14644>.
- Ohren JF, Chen H, Pavlovsky A, Whitehead C, Zhang E, Kuffa P, et al. Structures of human MAP kinase kinase 1 (MEK1) and MEK2 describe novel noncompetitive kinase inhibition. *Nat Struct Mol Biol*. 2004;11(12):1192–7. <https://doi.org/10.1038/nsmb859>.
- Özener N, Saeed M, Demirezer L, Efferth T. Aloe-emodin as drug candidate for cancer therapy. *Oncotarget*. 2018;9(25):17770–96. <https://doi.org/10.18632/oncotarget.24880>.
- Pan Y, Mader MM. Principles of Kinase Allosteric Inhibition and Pocket Validation. *J Med Chem*. 2022;65(7):5288–99. <https://doi.org/10.1021/acs.jmedchem.2c00073>.
- Pedersen KE, Christiansen BD, Klitgaard NA, Nielsen-Kudsk F. Effect of quinidine on digoxin bioavailability. *Eur J Clin Pharmacol*. 1983;24(1):41–7. <https://doi.org/10.1007/bf00613925>.
- Pomerening JR, Sontag ED, Ferrell JE. Building a cell cycle oscillator: hysteresis and bistability in the activation of Cdc2. *Nat Cell Biol*. 2003;5(4):346–51. <https://doi.org/10.1038/ncb954>.
- Porter LA, Donoghue DJ. Cyclin B1 and CDK1: nuclear localization and upstream regulators. *Prog Cell Cycle Res*. 2003;5:335–47.
- Prassas I, Diamandis EP. Novel therapeutic applications of cardiac glycosides. *Nat Rev Drug Discov*. 2008;7(11):926–35. <https://doi.org/10.1038/nrd2682>.
- Rahmanian N, Shokrzadeh M, Eskandani M. Recent advances in γ H2AX biomarker-based genotoxicity assays: A marker of DNA damage and repair. *DNA Repair (Amst)*. 2021;108:103243. <https://doi.org/10.1016/j.dnarep.2021.103243>.
- Reddy D, Kumavath R, Ghosh P, Barh D. Lanatoside C Induces G2/M Cell Cycle Arrest and Suppresses Cancer Cell Growth by Attenuating MAPK, Wnt, JAK-STAT, and PI3K/AKT/mTOR Signaling Pathways. *Biomolecules*. 2019;9(12). <https://doi.org/10.3390/biom9120792>.
- Ren Y, Ribas HT, Heath K, Wu S, Ren J, Shriwas P, et al. Na(+)/K(+)-ATPase-Targeted Cytotoxicity of

- (+)-Digoxin and Several Semisynthetic Derivatives. *J Nat Prod.* 2020;83(3):638–48. <https://doi.org/10.1021/acs.jnatprod.9b01060>.
- Reutelingsperger CPM, van Heerde WL. Annexin V, the regulator of phosphatidylserine-catalyzed inflammation and coagulation during apoptosis. *Cell Mol Life Sci CMLS.* 1997;53(6):527–32. <https://doi.org/10.1007/s000180050067>.
- Roberts PJ, Der CJ. Targeting the Raf-MEK-ERK mitogen-activated protein kinase cascade for the treatment of cancer. *Oncogene.* 2007;26(22):3291–310. <https://doi.org/10.1038/sj.onc.1210422>.
- Roskoski R Jr. MEK1/2 dual-specificity protein kinases: structure and regulation. *Biochem Biophys Res Commun.* 2012;417(1):5–10. <https://doi.org/10.1016/j.bbrc.2011.11.145>.
- Roskoski R Jr. Allosteric MEK1/2 inhibitors including cobimetanib and trametinib in the treatment of cutaneous melanomas. *Pharmacol Res.* 2017;117:20–31. <https://doi.org/10.1016/j.phrs.2016.12.009>.
- Rudbari HA, Kordestani N, Cuevas-Vicario JV, Zhou M, Efferth T, Correia I, et al. Investigation of the influence of chirality and halogen atoms on the anticancer activity of enantiopure palladium (II) complexes derived from chiral amino-alcohol Schiff bases and 2-picolyamine. *New J Chem.* 2022;46(14):6470–83.
- Saeed MEM, Boulos JC, Mücklich SB, Leich E, Chatterjee M, Klauk SM, et al. Disruption of Lipid Raft Microdomains, Regulation of CD38, TP53, and MYC Signaling, and Induction of Apoptosis by Lomitapide in Multiple Myeloma Cells. *Cancer Genomics Proteomics.* 2022;19(5):540–55. <https://doi.org/10.21873/cgp.20339>.
- Saeed MEM, Mahmoud N, Sugimoto Y, Efferth T, Abdel-Aziz H. Molecular Determinants of Sensitivity or Resistance of Cancer Cells Toward Sanguinarine. *Front Pharmacol.* 2018;9:136. <https://doi.org/10.3389/fphar.2018.00136>.
- Saeed MEM, Meyer M, Hussein A, Efferth T. Cytotoxicity of South-African medicinal plants towards sensitive and multidrug-resistant cancer cells. *J Ethnopharmacol.* 2016;186:209–23. <https://doi.org/10.1016/j.jep.2016.04.005>.
- Saeed MEM, Rahama M, Kuete V, Dawood M, Elbadawi M, Sugimoto Y, et al. Collateral sensitivity of drug-resistant ABCB5- and mutation-activated EGFR overexpressing cells towards resveratrol due to modulation of SIRT1 expression. *Phytomedicine.* 2019;59:152890. <https://doi.org/10.1016/j.phymed.2019.152890>.
- Sancar A, Lindsey-Boltz LA, Unsal-Kaçmaz K, Linn S. Molecular mechanisms of mammalian DNA repair and the DNA damage checkpoints. *Annu Rev Biochem.* 2004;73:39–85. <https://doi.org/10.1146/annurev.biochem.73.011303.073723>.
- Sava GP, Fan H, Coombes RC, Buluwela L, Ali S. CDK7 inhibitors as anticancer drugs. *Cancer Metastasis Rev.* 2020;39(3):805–23. <https://doi.org/10.1007/s10555-020-09885-8>.
- Sebolt-Leopold JS, Herrera R. Targeting the mitogen-activated protein kinase cascade to treat cancer. *Nat Rev Cancer.* 2004;4(12):937–47. <https://doi.org/10.1038/nrc1503>.
- Siegel RL, Miller KD, Fuchs HE, Jemal A. Cancer statistics, 2022. *CA Cancer J Clin.* 2022;72(1):7–33. <https://doi.org/10.3322/caac.21708>.
- Silva CID, Gonçalves-de-Albuquerque CF, Moraes BPT, Garcia DG, Burth P. Na/K-ATPase: Their role in cell adhesion and migration in cancer. *Biochimie.* 2021;185:1–8. <https://doi.org/10.1016/j.biochi.2021.03.002>.
- Singh VJ, Sharma B, Chawla PA. Recent developments in mitogen activated protein kinase inhibitors as potential anticancer agents. *Bioorg Chem.* 2021;114:105161. <https://doi.org/10.1016/j.bioorg.2021.105161>.
- Slee EA, Adrain C, Martin SJ. Executioner Caspase-3, -6, and -7 Perform Distinct, Non-redundant Roles during the Demolition Phase of Apoptosis*. *J Biol Chem.* 2001;276(10):7320–6. <https://doi.org/10.1074/jbc.M008363200>.
- Smiley ST, Reers M, Mottola-Hartshorn C, Lin M, Chen A, Smith TW, et al. Intracellular heterogeneity in mitochondrial membrane potentials revealed by a J-aggregate-forming lipophilic cation JC-1. *Proc Natl Acad Sci U S A.* 1991;88(9):3671–5. <https://doi.org/10.1073/pnas.88.9.3671>.
- Smolarczyk R, Cichoń T, Pilny E, Jarosz-Biej M, Poczka A, Kułach N, et al. Combination of anti-vascular agent - DMXAA - and HIF-1 α inhibitor - digoxin inhibits the growth of melanoma tumors. *Sci Rep.* 2018;8(1):7355. <https://doi.org/10.1038/s41598-018-25688-y>.
- Stenkvist B, Bengtsson E, Dahlqvist B, Eriksson O, Jarkrans T, Nordin B. Cardiac glycosides and breast cancer, revisited. *N Engl J Med.* 1982;306(8):484.
- Stenkvist B, Bengtsson E, Eriksson O, Holmquist J, Nordin B, Westman-Naeser S. Cardiac glycosides and breast cancer. *Lancet.* 1979;1(8115):563. [https://doi.org/10.1016/s0140-6736\(79\)90996-6](https://doi.org/10.1016/s0140-6736(79)90996-6).
- Susin SA, Lorenzo HK, Zamzami N, Marzo I, Snow BE, Brothers GM, et al. Molecular characterization of mitochondrial apoptosis-inducing factor. *Nature.* 1999;397(6718):441–6. <https://doi.org/10.1038/17135>.
- Ullah R, Yin Q, Snell AH, Wan L. RAF-MEK-ERK pathway in cancer evolution and treatment. *Semin Cancer Biol.* 2022;85:123–54. <https://doi.org/10.1016/j.semcancer.2021.05.010>.
- Vermes I, Haanen C, Steffens-Nakken H, Reutelingsperger C. A novel assay for apoptosis. Flow cytometric detection of phosphatidylserine expression on early apoptotic cells using fluorescein labelled Annexin V. *J Immunol Methods.* 1995;184(1):39–51. [https://doi.org/10.1016/0022-1759\(95\)00072-i](https://doi.org/10.1016/0022-1759(95)00072-i).
- Wang DD, Li XS, Bao YZ, Liu J, Zhang XK, Yao XS, et al. Synthesis of MeON-neoglycosides of digoxigenin with 6-deoxy- and 2,6-dideoxy-d-glucose derivatives and their anticancer activity. *Bioorg Med Chem Lett.* 2017;27(15):3359–64. <https://doi.org/10.1016/j.bmcl.2017.06.008>.
- Wang L, Cai W, Han B, Zhang J, Yu B, Chen M. Ouabain Exhibited Strong Anticancer Effects in Melanoma Cells via Induction of Apoptosis, G2/M Phase Arrest, and Migration Inhibition. *Oncotargets Ther.* 2021;14:1261–73. <https://doi.org/10.2147/ott.S283548>.
- Wang X, Ge P. Parthanatos in the pathogenesis of nervous system diseases. *Neuroscience.* 2020;449:241–50. <https://doi.org/10.1016/j.neuroscience.2020.09.049>.
- Wang X, Tanaka M, Krstin S, Peixoto HS, Wink M. The Interference of Selected Cytotoxic Alkaloids with the Cytoskeleton: An Insight into Their Modes of Action. *Molecules.* 2016;21(7). <https://doi.org/10.3390/molecules21070906>.
- Wang Y, Kim NS, Haince J-F, Kang HC, David KK, Andrabi SA, et al. Poly(ADP-Ribose) (PAR) Binding to Apoptosis-Inducing Factor Is Critical for PAR Polymerase-1-Dependent Cell Death (Parthanatos). *Sci Signal.* 2011;4(167):ra20-ra20. <https://doi.org/10.1126/scisignal.2000902>.

- Wu C-F, Efferth T. Miltirone Induces G2/M Cell Cycle Arrest and Apoptosis in CCRF-CEM Acute Lymphoblastic Leukemia Cells. *J Nat Prod*. 2015;78(6):1339–47. <https://doi.org/10.1021/acs.jnatprod.5b00158>.
- Yu SW, Andrabi SA, Wang H, Kim NS, Poirier GG, Dawson TM, et al. Apoptosis-inducing factor mediates poly(ADP-ribose) (PAR) polymer-induced cell death. *Proc Natl Acad Sci U S A*. 2006;103(48):18314–9. <https://doi.org/10.1073/pnas.0606528103>.
- Yu SW, Wang H, Poitras MF, Coombs C, Bowers WJ, Federoff HJ, et al. Mediation of poly(ADP-ribose) polymerase-1-dependent cell death by apoptosis-inducing factor. *Science*. 2002;297(5579):259–63. <https://doi.org/10.1126/science.1072221>.
- Yuan B, Shimada R, Xu K, Han L, Si N, Zhao H, et al. Multiple cytotoxic effects of gamabufotalin against human glioblastoma cell line U-87. *Chem Biol Interact*. 2019;314:108849. <https://doi.org/10.1016/j.cbi.2019.108849>.
- Zeino M, Brenk R, Gruber L, Zehl M, Urban E, Kopp B, et al. Cytotoxicity of cardiotonic steroids in sensitive and multidrug-resistant leukemia cells and the link with Na(+)/K(+)-ATPase. *J Steroid Biochem Mol Biol*. 2015;150:97–111. <https://doi.org/10.1016/j.jsbmb.2015.03.008>.
- Zeino M, Paulsen MS, Zehl M, Urban E, Kopp B, Efferth T. Identification of new P-glycoprotein inhibitors derived from cardiotonic steroids. *Biochem Pharmacol*. 2015;93(1):11–24. <https://doi.org/10.1016/j.bcp.2014.10.009>.
- Zhai J, Dong X, Yan F, Guo H, Yang J. Oleandrin: A Systematic Review of its Natural Sources, Structural Properties, Detection Methods, Pharmacokinetics and Toxicology. *Front Pharmacol*. 2022;13:822726. <https://doi.org/10.3389/fphar.2022.822726>.
- Zhao N, Mao Y, Han G, Ju Q, Zhou L, Liu F, et al. YM155, a survivin suppressant, triggers PARP-dependent cell death (parthanatos) and inhibits esophageal squamous-cell carcinoma xenografts in mice. *Oncotarget*. 2015;6(21):18445–59. <https://doi.org/10.18632/oncotarget.4315>.
- Zheng CF, Guan KL. Activation of MEK family kinases requires phosphorylation of two conserved Ser/Thr residues. *Embo J*. 1994;13(5):1123–31. <https://doi.org/10.1002/j.1460-2075.1994.tb06361.x>.
- Zhou Y, Liu L, Tao S, Yao Y, Wang Y, Wei Q, et al. Parthanatos and its associated components: Promising therapeutic targets for cancer. *Pharmacol Res*. 2021;163:105299. <https://doi.org/10.1016/j.phrs.2020.105299>.

Publisher's note Springer Nature remains neutral with regard to jurisdictional claims in published maps and institutional affiliations.



Two palladium (II) complexes derived from halogen-substituted Schiff bases and 2-picolylamine induce parthanatos-type cell death in sensitive and multi-drug resistant CCRF-CEM leukemia cells

Min Zhou^a, Joelle C. Boulos^a, Ejlal A. Omer^a, Hadi Amiri Rudbari^b, Tanja Schirmeister^c, Nicola Micale^d, Thomas Efferth^{a,*}

^a Department of Pharmaceutical Biology, Institute of Pharmaceutical and Biomedical Sciences, Johannes Gutenberg University-Mainz, Staudinger Weg 5, 55128, Mainz, Germany

^b Department of Chemistry, University of Isfahan, Isfahan, 81746-73441, Iran

^c Department of Medicinal Chemistry, Institute of Pharmaceutical and Biomedical Sciences, Johannes Gutenberg University-Mainz, Staudinger Weg 5, 55128, Mainz, Germany

^d Department of Chemical, Biological, Pharmaceutical and Environmental Sciences, University of Messina, Viale Ferdinando Stagno D'Alcontres 31, 1-98166, Messina, Italy

ARTICLE INFO

Keywords:

Cell death
Drug design
Leukemia
Metallo drugs
Palladium-based complex
Parthanatos

ABSTRACT

The use of cisplatin and its derivatives in cancer treatment triggered the interest in metal-containing complexes as potential novel anticancer agents. Palladium (II)-based complexes have been synthesized in recent years with promising antitumor activity. Previously, we described the synthesis and cytotoxicity of palladium (II) complexes containing halogen-substituted Schiff bases and 2-picolylamine. Here, we selected two palladium (II) complexes with double chlorine-substitution or double iodine-substitution that displayed the best cytotoxicity in drug-sensitive CCRF-CEM and multidrug-resistant CEM/ADR5000 leukemia cells for further biological investigation. Surprisingly, these compounds did not significantly induce apoptotic cell death. This study aims to reveal the major mode of cell death of these two palladium (II) complexes. We performed annexin V-FITC/PI staining and flow cytometric mitochondrial membrane potential measurement followed by western blotting, immunofluorescence microscopy, and alkaline single cell electrophoresis (comet assay). J4 and J6 still induced neither apoptosis nor necrosis in both leukemia cell lines. They also insufficiently induced autophagy as evidenced by Beclin and p62 detection in western blotting. Interestingly, J4 and J6 induced a novel mode of cell death (parthanatos) as mainly demonstrated in CCRF-CEM cells by hyper-activation of poly(ADP-ribose) polymerase 1 (PARP) and poly(ADP-ribose) (PAR) using western blotting, flow cytometric measurement of mitochondrial membrane potential collapse, nuclear translocation of apoptosis-inducing factor (AIF) by immunofluorescence microscopy, and DNA damage by alkaline single cell electrophoresis (comet assay). AIF translocation was also observed in CEM/ADR5000 cells. Thus, parthanatos was the predominant mode of cell death induced by J4 and J6, which explains the high cytotoxicity in CCRF-CEM and CEM/ADR5000 cells. J4 and J6 may be interesting drug candidates and deserve further investigations to overcome resistance of tumors against apoptosis. This study will promote the design of further novel palladium (II)-based complexes as chemotherapeutic agents.

1. Introduction

Cancer is still a major public health problem worldwide. According to the American Cancer Society, there were an estimated 18.1 million people diagnosed with cancer globally in 2020, and the number is expected to reach 28 million by 2040 (Sung et al., 2021).

Leukemia represents a group of malignancies with genetic errors that occur in normal cell regulatory processes and causes uncontrolled cell proliferation of hematopoietic stem cells in the bone marrow (Davis et al., 2014). The incidence rate of leukemia has been increasing by 1% per year from 2009 to 2018. In 2022, an estimated 60,650 new leukemia cases were reported in the USA, and an estimated 24,000 deaths from this disease (Siegel et al., 2022). Importantly, leukemia is the most

* Corresponding author.

E-mail address: efferth@uni-mainz.de (T. Efferth).

<https://doi.org/10.1016/j.ejphar.2023.175980>

Received 26 May 2023; Received in revised form 29 July 2023; Accepted 8 August 2023

Available online 9 August 2023

0014-2999/© 2023 Elsevier B.V. All rights reserved.

Abbreviations

AIF	Apoptosis-inducing factor
Bcl-2	B-cell CLL/Lymphoma 2
DMSO	Dimethyl sulfoxide
JC-1	5,5',6,6'-tetrachloro-1,1',3,3'-tetraethylbenzimidazolylcarbocyanine iodide
LC/MS	Liquid chromatography-mass spectrometry
NAD	Nicotine amide adenine dinucleotide
PAR	Poly(ADP-ribose)
PARP	Poly(ADP-ribose) polymerase 1
PBMCs	Human peripheral mononuclear cells
PBS	Phosphate-buffered saline
P-gp	P-glycoprotein
PI	Propidium iodide

frequent type of cancer in children. Leukemia is mainly classified into four subtypes based on the cell types and the rate of growth: acute lymphoblastic leukemia (ALL), acute myeloid leukemia (AML), chronic myeloid leukemia (CML), and chronic lymphocytic leukemia (CLL). The most frequently identified risk factors of leukemia are genetic syndromes (e.g., Down syndrome and neurofibromatosis), family history, radiation (e.g., occupational and therapeutic exposure), chemical contamination (e.g., benzene and household pesticide exposure), and lifestyle factors such as smoking (Bispo et al., 2020). In previous decades, evolving therapeutic strategies in leukemia have been developed, such as radiotherapy, bone marrow or stem cell transplantation, immunotherapy, and CAR-T cells (Döhner et al., 2021). Chemotherapy is the most common treatment modality, typical chemotherapeutic agents include doxorubicin, daunorubicin, cytosine arabinoside, etoposide, and vincristine.

Metal ions are essential cellular components and play critical roles in living systems (Frezza et al., 2010). They are frequently found in enzyme catalytic domain and involve many biochemical processes, such as carrying oxygen, electron transfer, catalysis as well as regulating metabolism. Historically, metal-containing compounds have been traditionally used in remedies or medicines to treat a variety of disorders (Orvig and Abrams, 1999). Cisplatin, *cis*-[Pt(NH₃)₂Cl₂] was the first platinum-based chemotherapeutic anticancer agent approved by the Food and Drug Administration (FDA) in 1978, which was a landmark and opened a new era for platinum (II)- and other metal-based compounds as potential anticancer candidates (Desoize and Madoulet, 2002; Ndagi et al., 2017). Cisplatin has been widely applied as adjuvant therapy in the treatment of a large spectrum of cancers. However, its clinical use is hampered due to the notable dose-dependent toxicity and drug resistance (Florea and Büsselberg, 2011; Ghosh, 2019). Therefore, the research interests in medical inorganic chemistry have been extended to other metal ions.

Palladium is frequently applied in medicine, e.g., for dental applications (Kielhorn et al., 2002), for ¹⁰³Pd radioactive plaque radiotherapy of intraocular melanoma (Finger et al., 2002), and for nanoparticles (Miller et al., 2017; Shibuya et al., 2019). Since palladium (II) is a d⁸ system compound close to platinum (II), the remarkable structural similarities between Pd (II) and Pt (II) have triggered the development of Pd (II) complexes with the aim to obtain more effective and less toxic compounds (Lazarević et al., 2017). With the aid of coordination chemistry, properties such as solubility, reactivity, toxicity, or activity can be controlled by joining different types of ligands (Abu-Surrah and Abdalla, 2008). In the past two decades, the interest in Pd (II) complexes as potential anticancer agents has considerably increased (Ferraro et al., 2022; Scattolin et al., 2021). The aquation and ligand-exchange rate of Pd (II) complexes are 10⁵ times faster than that of Pt (II) complexes, which means that Pd (II) complexes have a better

water-solubility making them more attractive (Coskun et al., 2013; Kapdi and Fairlamb, 2014). A plethora of Pd (II) complexes was synthesized with remarkable progress in the antitumor activity *in vitro* and *in vivo* as well as in the understanding of the underlying structure-activity relationships (SAR) (Alam and Huq, 2016). Many of these Pd(II) complexes displayed fewer side effects and exhibited powerful cytotoxicity against various tumor cell lines, some of which were even greater than cisplatin and its platinum analogues (El-Morsy et al., 2014; Ilić et al., 2014; Kovala-Demertzi et al., 2007). For example, a series of comprehensive studies have evaluated Pd(II) dinuclear complexes with spermine (Pd₂Spm) and showed promising anti-invasive as well as anti-proliferative activities in human breast cancer cells. Furthermore, *in vivo* pharmacokinetic studies revealed that the overall tissue accumulation of palladium was lower than platinum, suggesting that Pd(II)-based agents may have less adverse effects (Batista de Carvalho et al., 2016; Vojtek et al., 2021). Remarkably, a recent development is the approval of TOOKAD® Soluble (Padeliporfin, WST11), a palladium-based photosensitizer to treat low-risk prostate cancer with vascular targeted photodynamic therapy (VTP) in Israel, Mexico, and European countries (McFarland et al., 2020). Impressively, clinical phase III results showed that 24 months after VTP, 49% of men in the treatment had negative prostate biopsy compared with only 14% of the men on active surveillance (Azzouzi et al., 2017). Palladium has, thus, raised increasing interest in the development of pharmaceuticals. Furthermore, multiple modes of action of Pd (II) complexes have been identified, including inhibition of cancer cell metabolism, angiogenesis modulation, as well as mitochondria dysfunctions and apoptosis (Carneiro et al., 2020; Qin et al., 2018; Reigosa-Chamorro et al., 2021; Scattolin et al., 2020).

In our previous study, we synthesized and characterized 8 new pure chiral Pd (II) complexes (four enantiopure pairs) with halogen-substituted Schiff bases and 2-picolyamine (pic) (Fig. 1A). The anti-proliferative activity of these Pd (II) complexes was evaluated on two human leukemia cell lines, the drug-sensitive cell line CCRF-CEM cell line and its multidrug-resistant CEM/ADR5000 sub-line (Rudbari et al., 2022). Afterward, the two most active compounds (Fig. 1B), one with double chlorine-substitution (J4) and another one with double iodine-substitution (J6) were subject to detect cell cycle and apoptosis (annexin V-FITC/propidium iodide (PI) staining) in flow cytometry in CCRF-CEM cells. Our results revealed that all Pd (II) complexes showed outstanding growth inhibition activity with IC₅₀ value in the micromolar range in leukemia cell lines. The active compounds J4 and J6 both arrested the cell cycle at G₂/M phase in CCRF-CEM cells without inducing apoptosis or necrosis. With the limited evidence at that time, we only assumed that they may act as non-apoptotic cell death. Since our designed Pd (II) complexes in the combination of Schiff bases and an auxiliary ligand (pic) exhibited optimal stability, solubility, and noteworthy IC₅₀. We assumed that they may be promising compounds for anticancer agents and, therefore, worth further investigation.

Tumor cells that are unable to induce apoptosis and autophagy are also resistant to chemotherapy. Apoptosis is currently the most common mechanism for tumor cells to die in response to chemotherapy. However, tumor cells evolved many de-regulating apoptosis signaling routes, especially activation of anti-apoptotic systems to allow development and progression (Mohammad et al., 2015). For example, B-cell CLL/Lymphoma 2 (Bcl-2) and its relative Bcl-2 family proteins function as controlling outer mitochondrial membrane integrity and apoptosis. They are classified into proapoptotic Bcl-2 proteins (Bax and Bak) and anti-apoptotic Bcl-2 proteins (A1, Bcl-2, Bcl-X_L, and Bcl-w) (Chipuk et al., 2010). Tumor cells achieve anti-apoptosis through increasing expression of antiapoptotic Bcl-2 proteins and downregulation of proapoptotic Bcl-2 proteins, which is one of the hallmarks of cancer (Hanahan and Weinberg, 2011). Indeed, overexpression of Bcl-2 and Bcl-xL induced paclitaxel resistance in AML HL-60 cells (Huang et al., 1997). It is worth noting that the Beclin autophagy protein was initially isolated as a Bcl-2-interacting protein (Liang et al., 1998). Increased apoptosis

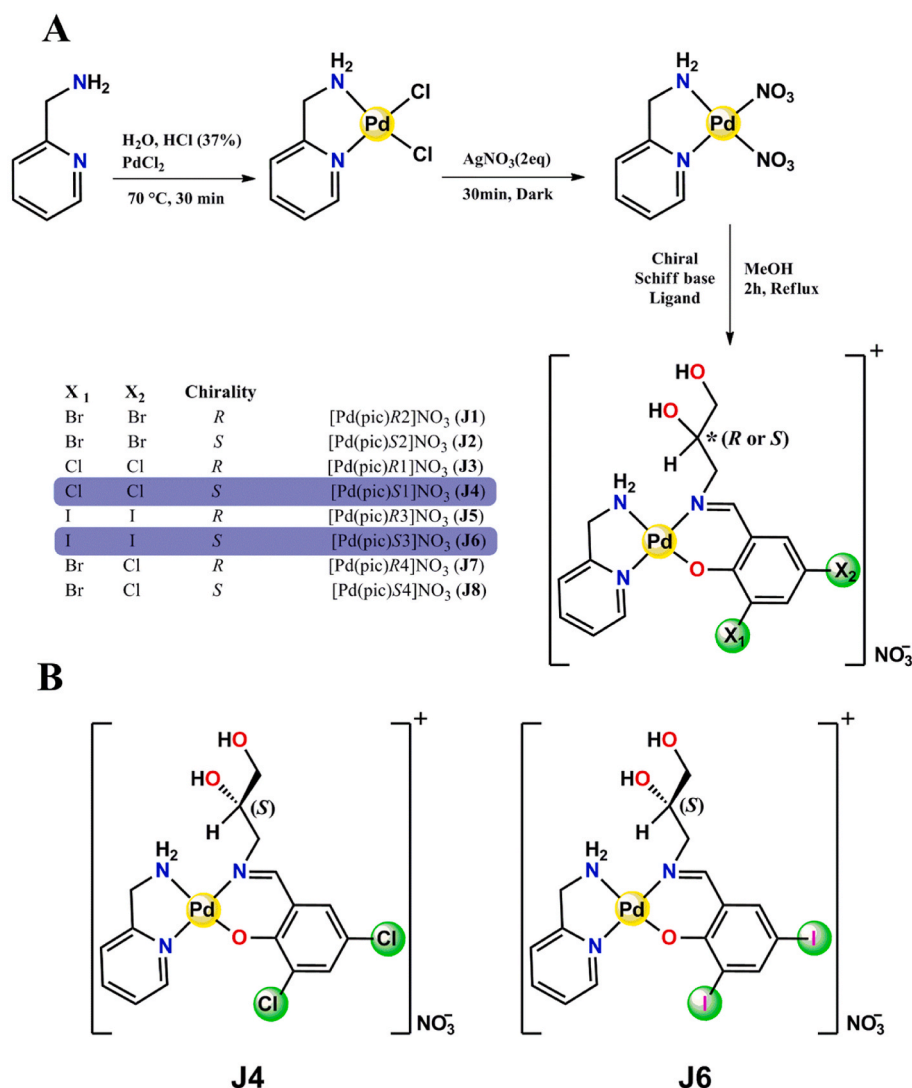


Fig. 1. Synthesis of Pd (II) complexes. (A) Synthetic route of enantiopure Pd(pic) Schiff base complexes. (B) J4 and J6. Based on reference (Rudbari et al., 2022).

resistance via Bcl-2 family members also inhibits autophagy by binding to Beclin and, therefore, protects cells from autophagic cell death (Sinha and Levine, 2008). Even though the role of autophagy in cancer is controversial, Bcl-2 homologs to some extent participate in oncogenesis by inhibiting apoptosis and autophagy. Other mechanisms contribute to evasion of apoptosis including reduced caspase expression, mutations in p53, increased expression of inhibitor of apoptosis proteins, and impaired receptor signaling pathways (Wong, 2011). Therefore, anti-cancer compounds that kill cancer cells by different modes of cell death than apoptosis or autophagy may provide exquisite opportunities to improve the tumor cell killing rates.

In recent years, multiple novel modes of cell death have been identified and provided new clues to tackle human diseases, especially the problem of drug resistance in cancer. Parthanatos is a non-apoptotic form of cell death and has been recently identified in cancer cells in response to different small molecules (Boulos et al., 2023; Ma et al., 2016; Zhao et al., 2015; Zhou et al., 2023). Mechanically, parthanatos does not require caspases for activation. It leads to an enhanced synthesis of poly (ADP-ribose) (PAR) by poly(ADP-ribose) polymerase 1 (PARP1), causing nuclear translocation of apoptosis-inducing factor (AIF), DNA fragmentation, chromatin condensation, and eventually cell death (Andrabi et al., 2006; Fatokun et al., 2014). Targeting parthanatos may offer alternative avenues for cancer management (Zhou et al.,

2021).

The aim of this study is to continue our previous work to get a deeper insight into the mechanism of cell death of the two Pd (II) complexes J4 and J6 in leukemia cells. To understand the induction of cell death response to multidrug-resistant cells, we extended the investigation toward both drug-sensitive CCRF-CEM and multidrug-resistant CEM/ADR5000 cells. We firstly performed annexin V-FITC/PI staining with these two compounds using flow cytometry to verify the absence of apoptosis and necrosis. Then, we investigated autophagy and other mechanisms by means of western blotting and immunofluorescence microscopy. This study on different modes of cell death provides an explanation for the strong cytotoxicity of our Pd (II) complexes toward leukemia cells. The induction of parthanatos in otherwise apoptosis- and autophagy-resistant tumor cells represents a novel therapy concept and eventually stimulates the development of novel metal-based drugs in cancer chemotherapy.

2. Materials and methods

2.1. Compounds

The palladium (II)-based complexes were synthesized and characterized as previously reported. The purity of J4 and J6 accessed by liquid

chromatography-mass spectrometry (LC/MS) was around 90% in different assay media at both timepoints (0 h and 24 h), indicating that the compounds were stable (supplementary file of this reference (Rudbari et al., 2022) <https://www.rsc.org/suppdata/d2/nj/d2nj00321j/d2nj00321j1.pdf>). The synthetic route and their structures are shown in Fig. 1. Stock solution of palladium (II)-based complexes (20 mM) were prepared in dimethyl sulfoxide (DMSO) and stored at -20°C . The cytotoxicity of palladium (II)-based complexes J4 or J6 as well as doxorubicin as positive control in sensitive CCRF-CEM and multidrug-resistant CEM/ADR5000 leukemia cells were previously reported (Rudbari et al., 2022) and presented in Table 1.

2.2. Cell culture

The CCRF-CEM cell line is a human acute lymphoblastic leukemia T lymphocyte line. It was originally isolated from the peripheral blood of a three-year- and eleven-month-old female ALL patient (Foley et al., 1965). Our CCRF-CEM cells were kindly provided by Prof. Axel Sauerbrey (Department of Pediatrics, University of Jena, Germany). CEM/ADR5000 cells were treated with doxorubicin (5000 ng/mL) every other week to sustain P-glycoprotein overexpression. The molecular profile of CEM/ADR5000 cells has been described (Efferth et al., 2003; Kadioglu et al., 2016; Kimmig et al., 1990). The cells were grown in RPMI 1640 medium supplemented with 10% fetal bovine serum (FBS) and 1% penicillin (1000 U mL⁻¹)/streptomycin (100 µg mL⁻¹) (Life Technologies, Darmstadt, Germany). Cells were incubated at 37°C , 90% humidity, and a 5% CO₂ atmosphere. Cells were passaged every three days. All the experiments were performed during the cell growth phase.

2.3. Isolation and cytotoxicity of human peripheral mononuclear cells (PBMCs)

Human peripheral mononuclear cells (PBMCs) were isolated from three healthy donors using Histopaque® as previously described (Dawood et al., 2020). Briefly, 3 mL fresh whole blood was layered carefully over 3 mL of Histopaque® and centrifuged at $400\times g$ for 30 min at room temperature. Subsequently, the interface containing PBMCs was transferred into a clean tube and mixed gently with 10 mL phosphate-buffered saline (PBS, Invitrogen). Cells were centrifuged at $250\times g$ for 10 min several times, then resuspended in Panserin 413 medium (PAN-Biotech, Aidenbach, Germany) supplemented with 2% phytohemagglutinin M (PHA-M, Life Technologies, Darmstadt, Germany). Afterward, the growth inhibition effect was measured using resazurin reduction assay. PBMCs cells (10⁴/well) were seeded into 96-well plates and treated with different concentrations of J4 or J6 ranging from 0.01 to 30 µM for 72 h. Then 20 µL 0.01% resazurin (Promega, Mannheim, Germany) were added and incubated for 4 h at 37°C . The Infinite M200 Pro-plate reader (Tecan, Crailsheim, Germany) was applied to measure the fluorescence intensity. The figure was generated using Prism 8 GraphPad Software (Graphpad Software Inc.,

Table 1

Antiproliferative activity (IC₅₀ values) of compounds J4, J6, and doxorubicin (positive control) towards the drug-sensitive CCRF-CEM leukemia cell line and its multidrug-resistant sub-line CEM/ADR5000. The data have been previously published (Rudbari et al., 2022) and are shown here for illustration only.

Compound	CCRF-CEM (IC ₅₀)		CEM/ADR5000 (IC ₅₀)		Degree of resistance ^a
	Mean	SD	Mean	SD	
J4	1.78	0.20	7.24	4.06	4.06
J6	2.39	0.90	4.87	2.04	2.04
Doxorubicin	0.01	–	26.56	2.31	2656

^a The degree of resistance was determined by dividing the IC₅₀ value against multidrug-resistant CEMADR5000 cells by the IC₅₀ value against drug-sensitive CCRF-CEM cells.

San Diego, CA, USA).

2.4. Apoptosis

Apoptosis was detected with an Annexin V-FITC apoptosis kit (Bio Version/Biotec, Heidelberg, Germany) using flow cytometry. CCRF-CEM and CEM/ADR5000 cells (1 × 10⁶/well) were seeded into a 6-well plate and treated with J4 or J6 at a concentration of 4 × IC₅₀ for 48 h. DMSO or cisplatin (5 µM) were used as negative and positive controls. Cells were collected to remove medium and centrifuged with 1 mL cold PBS or 1 ml 1 × binding buffer (Bio Version), respectively. Afterward, cells were resuspended in 1 × binding buffer, then each sample was stained with 2.5 µL annexin V/FITC and incubated at 4°C for 15 min in the dark. Subsequently, cells were again stained with 10 µL propidium iodide (PI). The measurements were performed using a BD Accuri™ C6 Flow Cytometry (BD Biosciences, Germany) with 20,000 events in each sample. All experiments were repeated three times. The results were analyzed with FlowJo (Celeza, Switzerland). The protocol has been described by us (Dawood et al., 2020).

2.5. Analysis of mitochondrial membrane potential (MMP)

The effects of J4 and J6 on the mitochondrial membrane potential (MMP) were analyzed by 5,5',6,6'-tetrachloro-1,1',3,3'-tetraethylbenzimidazolylcarbocyanine iodide (JC-1; Cayman Chemical, Ann Arbor, Michigan, USA) staining as described before (Lu et al., 2020). JC-1 dye is widely used to monitor mitochondrial integrity. Based on the usage of two lasers, one is to excite green fluorescence of JC-1 monomers at 488 nm (dead cells) and the other one is to excite red fluorescence of JC-1 aggregates at 520–570 nm (healthy cells). The red fluorescence disappears if the cells lose their mitochondrial membrane potential (De Biasi et al., 2015). Briefly, CCRF-CEM cells (1 × 10⁴ cells/well) were seeded in a 96-well flat-bottom plate in a volume of 200 µL and treated with DMSO as negative control, vinblastine (2 µM, positive control), IC₅₀ or 2 × IC₅₀ of J4 or J6 for 24 h. After treatment, cells were incubated at 37°C in dark for 15 min with JC-1 diluted solution (1:10 in culture medium, 10 µL/well). Then, cells were centrifuged with 200 µL cell-based assay buffer (Cayman Chemical) at $400\times g$ for 5 min twice. Cells were re-suspended in 100 µL cell-based assay buffer and measured in a BD LSR Fortessa SORP equipment. For each sample, 10⁴ cells were counted. The green JC-1 signal (488 nm excitation) was detected using a 530/30 nm bandpass filter. The red JC-1 (520–570 nm) signal was measured using a 586/15 bandpass filter. All experiments were performed at least in triplicate. Data were analyzed using FlowJo software (Celeza, Olten Switzerland).

2.6. Protein extraction and western blotting

CCRF-CEM and CEM/ADR5000 cells (5 × 10⁶ cells/flask) were treated with J4 or J6 at different concentrations (0.5 × IC₅₀, IC₅₀, and 2 × IC₅₀) for 24 h and then washed with PBS. The total protein extraction was performed with M-PER Mammalian Protein Extraction Reagent (Thermo Fisher Scientific, Darmstadt, Germany) (Mahmoud et al., 2022). Cells were suspended in 100 µL extraction reagent containing 1% Halt Protease Inhibitor Cocktail and phosphatase inhibitor (Thermo Fisher Scientific). The lysates were shaken for 30 min at 4°C in the dark and centrifuged for 15 min at 14,000 rpm. The concentrations of protein were determined using a NanoDrop 1000 spectrophotometer (Thermo Scientific). A quantity of 30 µg protein was separated by 10% SDS-PAGE gel electrophoresis followed by transfer to polyvinylidene difluoride (PVDF) membrane. The membrane was blocked using 5% BSA for 1 h at room temperature. The membrane was incubated with diluted primary antibodies overnight at 4°C against PARP rabbit antibody (1:1000, Cell Signaling, PAR mouse antibody (1:1000, Merck), phospho-histone H2A.X (Ser139) antibody (1:1000, Cell Signaling), caspase 3/p17/p19 polyclonal antibody (1:1000, Proteintech), AIF rabbit antibody (1:700, Cell

Signaling), anti-p62, SQSTM1 polyclonal antibody (1:1000, Proteintech), Beclin 1 polyclonal antibody (1:1000, Proteintech), anti-Lamin B1 monoclonal antibody (1:10,000, Proteintech), GAPDH rabbit antibody (1:1000, Cell Signaling), β -actin rabbit antibody (1:1000, Cell Signaling). Finally, the membrane was incubated with secondary anti-rabbit IgG HRP-linked antibody or anti-mouse IgG HRP-linked antibody (1:2000, Cell Signaling) for 1 h at room temperature. The membrane was treated with Luminata™ Classico Western HRP substrate (Merk Millipore Darmstadt, Germany), and then the bands were visualized using an Alpha Innotech FluorChem Q System (Biozym, Oldendorf, Germany). The protein expression was quantified using ImageJ software (National Institute of Health, United States).

The NE-PER Nuclear and Cytoplasmic Extraction Reagents kit (Thermo Scientific) was used to extract nuclear and cytoplasmic protein (Zhou et al., 2023). CER I, CER II and NER reagents were added in the following volume ratios: 200:11:100 μ L, along with 1% Halt Protease Inhibitor Cocktail and phosphatase inhibitor. Then, the lysates were vortexed according to the manufacturer's instructions. Finally, the cytoplasmic protein or nuclear protein was centrifuged at 16,000 \times g for 5 or 10 min. The nuclear and cytoplasmic proteins were measured as described above.

2.7. Immunofluorescence microscopy of AIF translocation

CCRF-CEM and CEM/ADR5000 cells (1×10^6 cells/well) were treated with two different concentrations of J4 or J6 ($0.5 \times IC_{50}$ or IC_{50}) or DMSO (negative control) for 24 h. The cells were harvested, washed with washing buffer (1% FBS in PBS), and resuspended with 1 mL washing buffer. Cell suspension (200 μ L) containing 10,000 cells was transferred onto the slides (Super®frost plus slides, VWR International GmbH, Darmstadt, Germany) by centrifugation at 1000 rpm for 5 min. The slides were fixed with 3.7% paraformaldehyde (Sigma-Aldrich, Darmstadt, Germany) for 15 min at room temperature, then rinsed for 3×5 min with washing buffer. Subsequently, the cells were permeabilized with 0.5% Triton X-100 (AppliChem, Darmstadt, Germany) in PBS for 5 min. After rinsing 3×5 min with washing buffer, cells were blocked with blocking buffer (1% BSA + 1% FBS in PBS) for 1 h. Then, the cells were rinsed again with washing buffer for 3×5 min and incubated with the primary antibody against AIF (1:400, Cell Signaling) in a humidified chamber at 4 °C overnight. The next day, antibodies were removed, and the slides were rinsed for 3×5 min with washing buffer. The anti-rabbit IgG secondary antibody Alexa Fluor® 488-conjugate (1:700, Cell Signaling) was added and incubated for 2 h at room temperature in the dark. The slides were rinsed 3×5 min with washing buffer, and nuclear staining was done using 1μ g mL⁻¹ 4',6-diamidino-2-phenylindole (DAPI) diluted in PBS for 5 min. Finally, cells were rinsed with washing buffer for 5×5 min and mounted (ibidi, Gräfelfing, Germany) with coverslips (24 \times 32 mm, VWR international). AIF was visualized by an AF7000 widefield fluorescence microscope (Leica Microsystems, Wetzlar, Germany) controlled by the LAS-X software (version x, Leica Microsystems). The microscope was equipped with a 63 \times (oil) objective, LED light source (SOLA, lumencor), and a sCMOS camera (Flash 4.0, Hamamatsu). Fluorophores were detected with band-pass filters for DAPI (ex. BP 360/40, FT400, em. BP 470/40) and Alexa488 (ex BP 480/40, FT505, em. BP 527/30). The obtained images were further analyzed with Image J software (Mahmoud et al., 2022).

2.8. Immunofluorescence microscopy of AIF and mitochondria staining

CCRF-CEM and CEM/ADR5000 cells (10^6 cells/well) were seeded into a 6-well plate. After 24 h incubation, cells were harvested and washed with washing buffer (800 rpm, 5 min), followed by incubation for 15 min at 37 °C with 100 nM MitoTracker® Deep Red (Invitrogen) as manufacturer's instruction. Cells were centrifuged and then fixed with 3.7% paraformaldehyde (Sigma-Aldrich) for 15 min at room temperature. The washing buffer was used to wash cells twice. Subsequently,

50,000 cells were counted and cytospinned onto slides, followed by the permeabilization and blocking process as described above. The primary antibody AIF, secondary antibody, and DAPI were incubated with cells at the indicated time. Images were taken using Stellaris 8 Falcon confocal microscope (Leica Microsystems) controlled by LASX software (version 4.5.0). The microscope was equipped with a 100 \times /NA1.4 oil objective (HC PL APO CS2), a white light laser (WWL), laser diodes (405 nm) and hybrid detectors. Fluorophores were detected with spectral detection for DAPI (ex. 405 nm, em. 430–484 nm), Alexa Fluor 488 (ex. 488 nm WWL, em. 494–650 nm), MitoTracker® Deep Red (ex. 641 nm WWL, em. 650–750 nm).

2.9. Single cell gel electrophoresis (comet assay)

The comet assay is a sensitive and rapid method for detecting DNA damage. The extent of DNA damage present in the cells directly affects DNA migration (Kumaravel et al., 2009). The OxiSelect™ Comet Assay Kit (Cell Biolabs/Biocat, Heidelberg, Germany) was used to detect DNA damage according to the manufacturer's instructions (Özenver et al., 2018). Briefly, CCRF-CEM cells (1×10^6 cells/well) were treated with 0.5- or 1-fold IC_{50} of J4 or J6, or DMSO (negative control) for 24 h. Cells were harvested, centrifuged at 3000 rpm for 10 min, and resuspended with 1 mL cold PBS (4 °C). After counting cells, 1×10^5 cells/mL were combined with milting agarose at a ratio of 1:6 and then applied to OxiSelect™ Comet Assay slides. The slides were kept at 4 °C in the dark for 30 min to be solidified. Next, slides were treated with pre-chilled lysis buffer (NaCl 14.6 g, EDTA solution 20 mL, $10 \times$ lysis solution, pH 10.0, fulfill to 100 mL with distilled water, stored at 4 °C) for 1 h and alkaline electrophoresis solution buffer (NaOH 12 g, EDTA solution 2 mL, fulfill to 100 mL with distilled water, stored at 4 °C) for 40 min in the dark. Subsequently, alkaline electrophoresis solution buffer was added to the chamber, electrophoresis was performed with horizontally placed slides with a voltage of 20 V for 20 min. The slides were washed with pre-chilled distilled water for 2×5 min, and then fixed with 70% ethanol for another 5 min. Diluted Vista Green DNA dye (1: 10,000 in TE buffer (121.14 mg, EDTA 200 μ L, pH 7.5, fulfill to 100 mL distilled water)) was applied on the slides (100 μ L/well) in the dark. The slides were photographed with an EVOS digital inverted microscope (Life Technologies GmbH, Darmstadt, Germany). At least 50 cells were randomly selected and analyzed with OpenComet (Image J). The tail DNA percentage was used to present DNA damage (Gyori et al., 2014).

2.10. Confirmation of parthanatos using PARP inhibitor

Since PARP overexpression is an important biomarker of parthanatos, this cell death mechanism was verified using PARP inhibitor evidenced by cell viability. The protocol was recently reported by us (Boulos et al., 2023). CCRF-CEM and CEM/ADR5000 cells (10^4 /well) were seeded in 100 μ L medium in 96-well plates. Cells were treated with 100 μ L medium containing J4 or J6 of a concentration at $0.5 \times IC_{50}$ and IC_{50} , which are 0.89 μ M and 1.78 μ M of J4 in CCRF-CEM cells, 3.62 μ M and 7.24 μ M of J4 in ADR/CEM5000 cells, 1.195 μ M and 2.39 μ M of J6 in CCRF-CEM cells, and 2.435 μ M and 4.87 μ M of J6 in CEM/ADR5000 cells. These treatments were additionally also combined with the PARP inhibitor PJ34 (10 μ M) (Sigma-Aldrich, Darmstadt, Germany). The plates were incubated at 37 °C for 24 h as the detected timepoint of parthanatos. The cell viability was measured using resazurin reduction assay as described above. The experiments were repeated three times with four replicates in each plate.

3. Results

3.1. Cytotoxicity on human peripheral mononuclear cells (PBMCs)

To study the cytotoxicity of J4 and J6 towards normal cells, human peripheral mononuclear cells (PBMCs) were isolated from healthy

donors. As shown in Fig. 2, the cell viability did not decrease upon a series of increasing concentrations of J4 or J6, which means that PBMCs were not affected by J4 and J6. Taken together with the previously reported antiproliferative activity on drug-sensitive CCRF-CEM and -resistant CEM/ADR5000 cells (see Table 1), J4 and J6 specifically inhibited leukemia cells but not healthy leukocytes.

3.2. Detection of apoptosis, necrosis, and autophagy

Our previous investigation revealed that J4 and J6 exerted cytotoxicity in CCRF-CEM cells without inducing apoptotic cell death at different concentrations and timepoints (Rudbari et al., 2022). As a first step to illustrate the mode of cell death of J4 and J6, the detection of apoptosis by annexin V-FITC/PI staining was carried out to verify our previous results. After treatment with J4 or J6 at $4 \times IC_{50}$ for 48 h (Fig. 3), 86.9% of cells treated with J4 were non-apoptotic in CCRF-CEM cells, J6 also showed 81.03% of non-apoptotic cells. Fractions of 95.9% or 88.9% of CEM/ADR5000 cells remained non-apoptotic upon treatment with J4 or J6. However, over 90% of living cells appeared upon DMSO treatment in both cell lines. Cisplatin as a positive control induced 42.9% late apoptosis in CCRF-CEM cells and 24.7% early apoptosis in CEM/ADR5000 cells. J4 or J6 induced only minor fractions of apoptosis. This validation experiment was consistent with our previous investigation (Rudbari et al., 2022) and proved that J4 or J6 did not significantly kill CCRF-CEM and CEM/ADR5000 cells by apoptosis or necrosis.

Afterward, to investigate whether J4 and J6 induce autophagy as the mode of cell death, we measured the expression level of p62 and Beclin after treatment for 24 h. Fig. 4 shows that in CCRF-CEM cells, J4 gradually increased p62 expression and decreased Beclin expression, while J6 downregulated p62 and upregulated Beclin. It seems that J6 may induce autophagy, but the expression of these biomarkers was not significant for both compounds. In CEM/ADR5000 cells treated with J4 or J6, the expression of p62 and Beclin showed slight variations but without significant differences compared to control. Therefore, autophagy was not the major mode of cell death of J4 and J6. These two compounds presumably kill CCRF-CEM and CEM/ADR5000 cells by other cell death mechanisms. To evaluate the primary mode of cell death

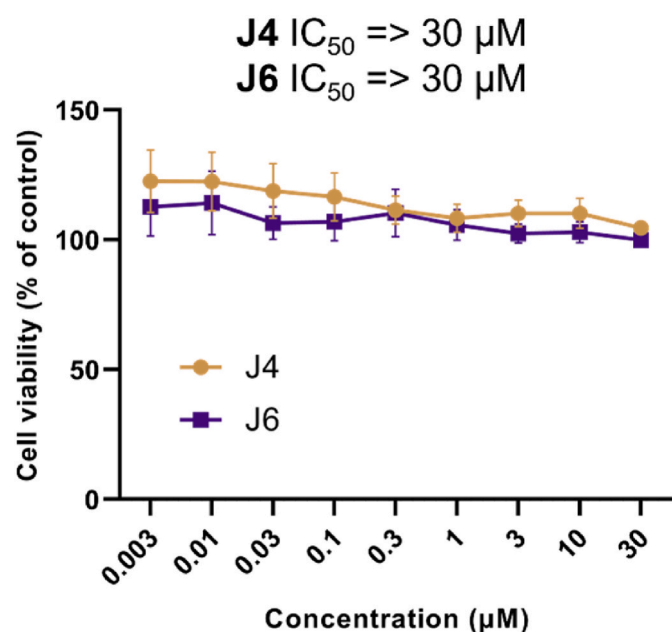


Fig. 2. Cytotoxicity of compounds J4 and J6 toward human peripheral mononuclear cells (PBMCs). The PBMCs were isolated from three healthy donors and the measurements were carried out after incubation with a series of concentrations of J4 or J6 for 72 h.

induced by J4 and J6, we used CCRF-CEM cells as a study model. The effects in CEM/ADR5000 cells were then confirmed in the key steps.

3.3. Mitochondrial membrane potential (MMP)

Even though apoptosis was not observed with J4 or J6, some types of cell death are regulated by mitochondria. Hence, we further detected the mitochondrial membrane potential of J4 or J6, to understand if it could be positively affected in CCRF-CEM cells. Cells were treated at IC_{50} or 2-fold IC_{50} with J4 or J6 for 24 h. Subsequently, the cells were stained with JC-1 and analyzed by flow cytometry. Fig. 5 shows that J4, J6, as well as vinblastine altered the MMP to different extents, as indicated by the sharp shift of red fluorescence of JC-1 to green fluorescence. The percentages of reduced MMP with J4 were up to 94.8%–95.6%, and with J6 were 90.47%–95.7%, which was more significant than that of vinblastine displaying a 54.9% alternation. Therefore, these findings suggested that both J4 and J6 can cause mitochondrial dysfunction, and we assume that they may induce other forms of programmed cell death regulated by mitochondria.

3.4. Western blotting

To study the predominant mode of cell death induced by J4 and J6, the protein expression level of poly (ADP-ribose) (PAR) polymerase-1 (PARP-1) and caspase 3 were firstly measured by western blotting analysis in CCRF-CEM cells (Fig. 6A). Significantly increased levels of both full-length PARP (116 kDa) and cleaved PARP (89 kDa) were observed upon increasing J4 or J6 concentrations. Caspase 3 and cleaved caspase 3 were expressed but the differences were not significant in comparison to untreated cells, implying that the mode of cell death was caspase-independent. Afterward, we concentrated on another potential mode of cell death that does not rely on caspase: parthanatos. As assumed, poly (ADP-ribose) (PAR) and p-histone H2A.X showed an obviously increased expression. Then, we detected the expression levels of apoptosis-inducing factor (AIF) in the nucleus and cytoplasm, respectively (Fig. 6B–C). Notably, AIF was upregulated in the nucleus in a concentration-dependent manner, particularly J6 treated with $2 \times IC_{50}$ was very significant ($p = 0.007$). Cytoplasmic AIF showed a slight decrease with J4 and steady expression with J6. These results suggest that J4 and J6 predominantly induced parthanatos as the major mechanism of cell death.

3.5. Nuclear localization of AIF

Translocation of AIF, which occurs downstream of PAR over-expression, is a critical step of parthanatos. Using immunofluorescent imagining, the localization of AIF was monitored upon 24 h treatment with J4 or J6 to verify whether AIF can translocate to the nucleus. The experiments were carried out in both CCRF-CEM and CEM/ADR5000 cells. Fig. 7 indicates that J4 and J6 treated independently with 0.5- or 1-fold IC_{50} showed a nuclear fraction of AIF besides that at the cytoplasm in both leukemia cell lines, while AIF was on the edge of the nucleus and only localized at the cytoplasm in the untreated cells. Therefore, these findings of CCRF-CEM cells were consistent with the results from western blotting, confirming that both J4 and J6 caused the translocation of AIF from the cytoplasm into the nucleus, further leading to parthanatic cell death. Similarly, the observed translocation of AIF in CEM/ADR5000 cells indicated parthanatos as the principal mode of cell death induced by J4 or J6.

3.6. AIF and mitochondria staining

Non-stimulated AIF resides in mitochondria (Yu et al., 2002). We found that AIF was translocated from the cytosol into the nucleus of CCRF-CEM and CEM/ADR5000 cells by treatment with J4 and J6. As shown in Fig. 8 and Supplementary Video 1, the triple

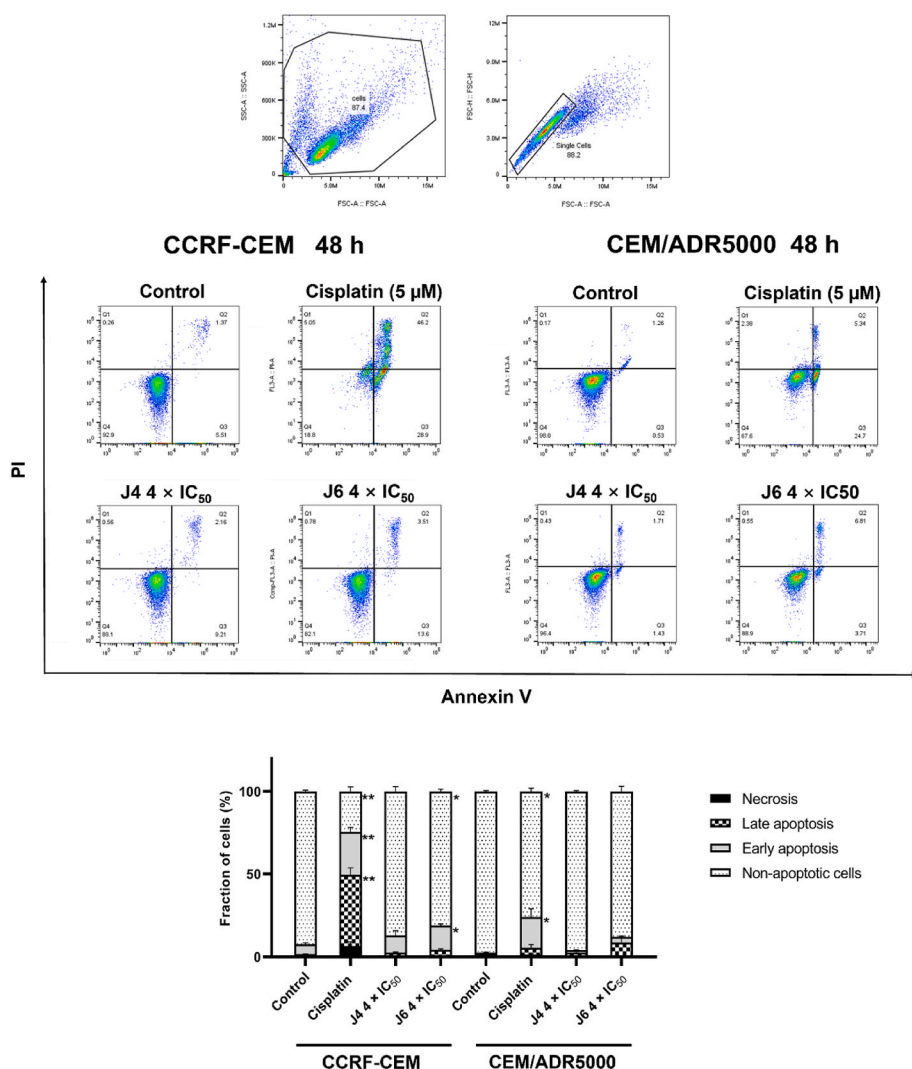


Fig. 3. Assessment of apoptosis. CCRF-CEM leukemia cells and their multidrug-resistant CEM/ADR5000 subline treated with palladium (II)-based compounds J4 or J6, DMSO (negative control), and cisplatin (positive control) after 48 h. Samples were stained by annexin V-FITC/PI and detected on flow cytometry. The $4 \times IC_{50}$ was 7.12 μM for J4 and 9.56 μM for J6 in CCRF-CEM cells. In CEM/ADR5000 cells, $4 \times IC_{50}$ was 29.0 μM for J4, and 19.5 μM for J6. Q1 and Q2: necrotic cells or late apoptotic cells exhibit annexin V+/PI+; Q3: early apoptotic cells exhibit annexin V+/PI-; Q4: non-apoptotic cells exhibit annexin V-/PI-. The graph presents the mean fraction of CCRF-CEM cells. The data represent as mean values \pm SD of three independent experiments. The statistical significance was calculated by the Student's t-test, * $p < 0.05$, ** $p < 0.01$ compared with DMSO.

immunofluorescence staining of untreated cells shows that AIF was present with mitochondria and outside of the nucleus. This confocal microscopical experiment illustrated the migration of AIF localization.

3.7. Single cell gel electrophoresis (comet assay)

As a result of nuclear AIF translocation, DNA fragmentation and chromatin condensation were observed. Since the protein expression levels of p-histone H2AX in CCRF-CEM cells treated with J4 and J6 were shown at 24 h, we also performed comet assay and detected DNA damage at the same timepoint. As shown in Fig. 9, the cells with J4 or J6 treatment at a concentration of IC_{50} showed slight tails-like patterns. Furthermore, the mean value (percentage of tail DNA) of J4 at $2 \times IC_{50}$ was increased to 9.3%, and J6 at $2 \times IC_{50}$ also significantly showed a mean value of 41.3%. The DNA damage extent of H_2O_2 was less than J6 with a mean value of 26%. No effects were observed in untreated cells (DMSO). Therefore, J4 and J6 induced DNA damage in a concentration-dependent manner followed by AIF translocation, which further induced cell death.

3.8. Confirmation of parthanatos using PARP inhibitor

Parthanatos is a PARP-dependent cell death form (Yu et al., 2006). In a series of experiments, we identified key events of parthanatos induced by J4 and J6 in leukemia cells. The known PARP inhibitor PJ34 was

further applied for the confirmation of parthanatos. As shown in Fig. 10, cells treated with J4 or J6 alone resulted in lower percentages of visible cells, while J4 or J6 in combination with PJ34 clearly prevented cell death. The cell viability of J4 treated in CEM/ADR5000 cells at a concentration of IC_{50} combined with PJ34 ($p = 0.01$), as well as J6 treated at a concentration of IC_{50} combined with PJ34 in both CCRF-CEM ($p = 0.008$), and CEM/ADR5000 ($p = 0.008$) cells are particularly significant compared with only J4 or J6. Therefore, PJ34 maintained cell survival in the presence of J4 or J6, supporting that indeed parthanatos was the primary mode of cell death.

4. Discussion

Cells die through a variety of mechanisms that can be categorized into non-programmed cell death as unexpected cell injury and programmed cell death. Programmed cell death can be further classified into apoptotic cell death and non-apoptotic cell death (e.g., autophagy, entosis, pyroptosis, mitoptosis, ferroptosis, and necroptosis) (Yan et al., 2020). Previously, we synthesized a set of Pd (II) complexes, and the best two of them (J4 and J6) revealed excellent cytotoxicity in CCRF-CEM leukemia cells resulting in G2/M cell cycle arrest but without inducing apoptotic cell death (Rudbari et al., 2022). In continuation of this work on Pd (II) complexes, the goal of this study was to pinpoint the principal mode of cell death induced by these two palladium-based complexes in drug-sensitive CCRF-CEM and its multidrug-resistant CEM/ADR5000

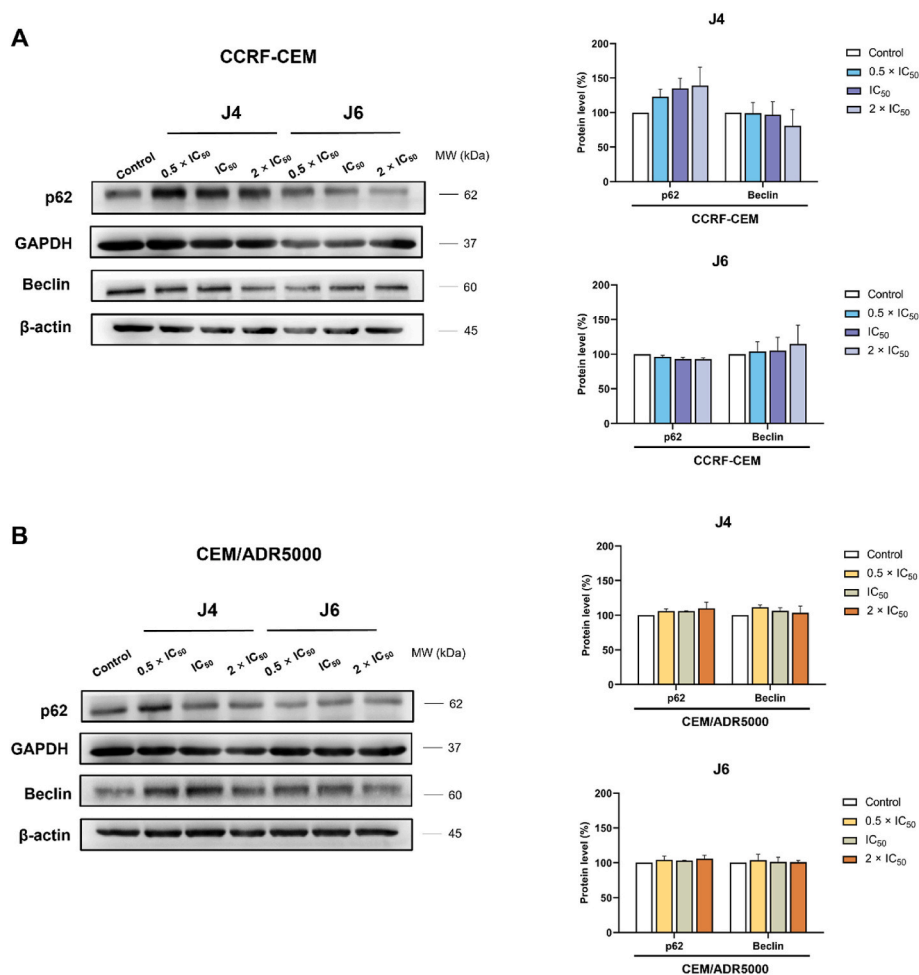


Fig. 4. Western blot analysis of biomarkers related to autophagy. CCRF-CEM and CEM/ADR5000 leukemia cells treated with palladium (II)-based compounds J4 or J6 after 24 h. (A) p62 and Beclin were detected by western blotting in CCRF-CEM cells. (B) p62 and Beclin in CEM/ADR5000 cells. Graphs show quantification of protein expression levels with J4 and J6. The expression of p62 and Beclin was normalized to GAPDH or β -actin. The histograms present the mean value \pm SD of three independent experiments. Statistics analysis was done by paired Student's t-test.

subline. Our current finding illustrated that parthanatos was the major mode of cell death as evidenced by rapid accumulation of PARP and PAR, dissipation of mitochondrial membrane potential, nuclear AIF translocation, and DNA fragmentation. Additionally, the cytotoxicity on PBMCs cells revealed that both J4 and J6 were less toxic toward PBMCs. We previously reported that J4 and J6 were more specific on eliminating leukemia cells (Rudbari et al., 2022). This difference in activity towards leukemia cells and normal leukocytes is consistent with the recently described safety profile that palladium nanoparticles showed mitigated toxicity compared to formulations with conventional chemotherapeutic drugs (Miller et al., 2017).

Initially, cell death was divided into three types: apoptosis (Type I), autophagy (Type II), and necrosis (Type III) (Green and Llambi, 2015). Apoptosis is characterized as a series of well-organized distinct steps and biochemical modifications including cell shrinkage, phosphatidylserine (PS) exposure, DNA condensation and fragmentation, as well as mitochondrial membrane potential alternation. The initiation of apoptosis is dependent on the activation of caspases (Elmore, 2007). In our study, we analyzed apoptosis with two methods. First, using annexin V-FITC/PI staining, CCRF-CEM and CEM/ADR5000 cells treated with J4 or J6 at a concentration of $4 \times IC_{50}$ for 48 h still did not show significant apoptotic cells or necrotic cells were induced, which is in accord with our previously reported results (Rudbari et al., 2022). Annexin V and PI uptake is one of the most widely used assays to measure apoptosis and necrosis. PS located at the outer layer of the plasma membrane are bound to annexin V, and DNA fragments that are released from apoptotic nuclei are stained by PI (Crowley et al., 2016; Riccardi and Nicoletti, 2006). In contrast to other studies, several Pd (II) complexes recently have been described as inducers of apoptosis as proved by annexin V-FITC/PI

staining (Ari et al., 2014; Coskun et al., 2013). As a second independent method, we further determined the expression level of caspase 3, cleaved caspase 3, and cleaved PARP by western blotting in CCRF-CEM cells. Fig. 5A indicates that J4 or J6 induced the expression of both caspase 3 and cleaved caspase 3, while almost equal expression levels appeared as negative control. Cleaved caspase 3 could be related to the small apoptotic fraction observed in flow cytometry, indicating that J4 or J6 induced a minor cell fraction with apoptotic cell death but it was not the major mode of cell death. Along this line, PARP-1 as one of the downstream substrates of caspases can be cleaved as an 89 kDa fragment during apoptotic cell death (Soldani and Scovassi, 2002). As expected, we observed expression levels of cleaved PARP which were in accordance with cleaved caspase 3. In our study, cleaved PARP by both J4 and J6 reached significant expression levels in a concentration-dependent manner. The expression of cleaved PARP and cleaved caspase 3 was also found in human breast cancer cell lines treated with other Pd (II) complexes (Ari et al., 2013). PARP-1 can be also cleaved even in the absence of caspase 3 (Jänicke et al., 1998). However, it is important to note that the expression of caspase 3 was not significant, implying that the major mode of cell death may not rely on caspases. Among the various forms of cell death, one caspase-independent mode has been addressed as parthanatos (Kang et al., 2004; Yu et al., 2002). Therefore, we conclude that J4 and J6 induced apoptosis only in a minor cell fraction, and we further investigated if CCRF-CEM and CEM/ADR5000 cells would be killed through parthanatos.

PARP-1 is the best-known nuclear enzyme of the PARP superfamily. It is a 116 kDa protein that serves as a DNA damage sensor. In the presence of moderate DNA damage, PARP uses nicotinic amide adenine dinucleotide (NAD^+) as a substrate to catalyze the addition of

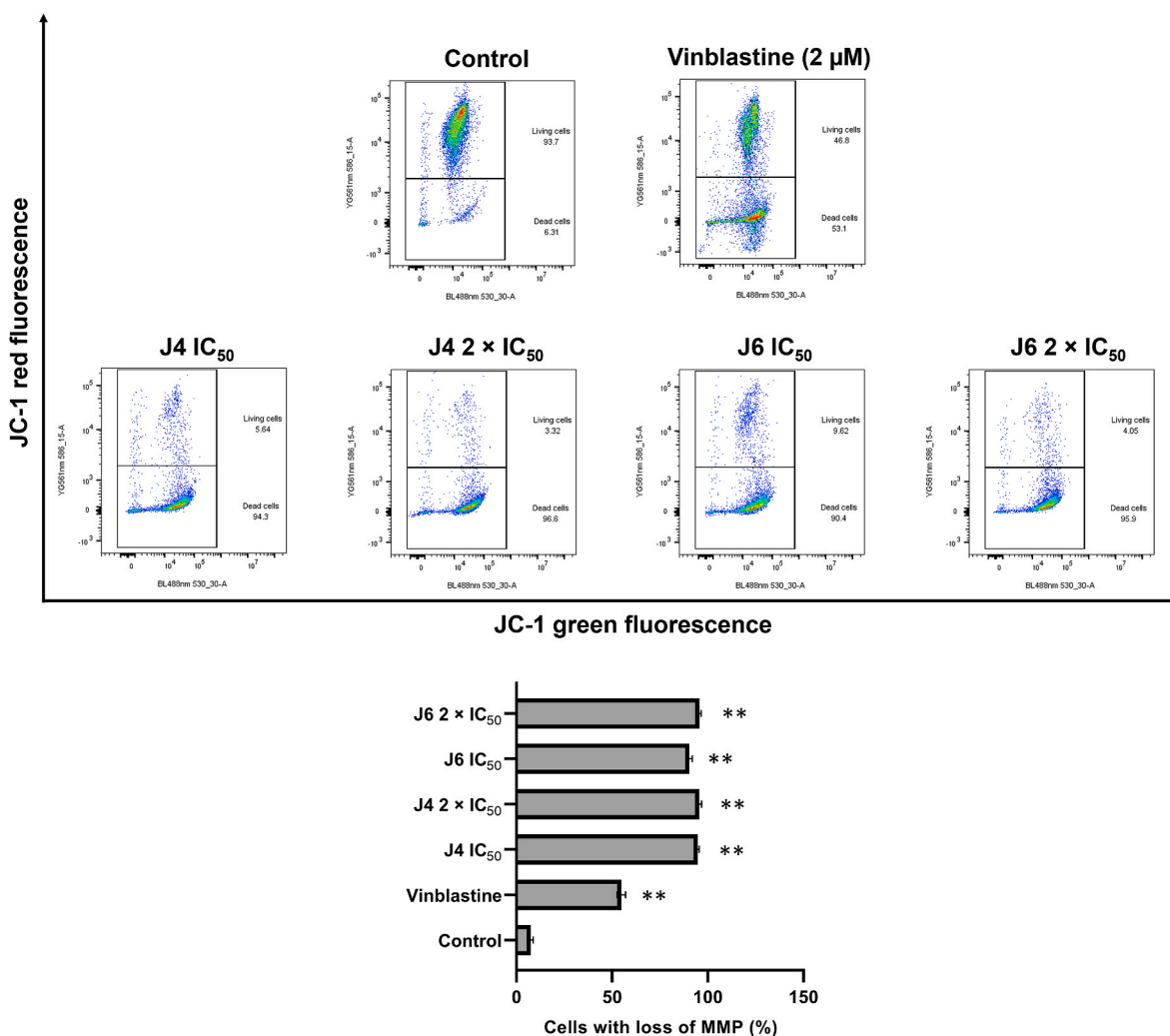


Fig. 5. Assessment of mitochondrial membrane potential. Representative images of JC-1 fluorescence with flow cytometry of mitochondrial membrane potential in CCRF-CEM cells treated with palladium (II)-based compounds J4 or J6, DMSO (negative control) or vinblastine (positive control) for 24 h. The IC_{50} was 1.78 μM for J4 and 2.39 μM for J6. $2 \times IC_{50}$ was 3.56 μM for J4 and 4.78 μM for J6. Death of cells were defined as MMP collapse after 24 h treatment. The graph presents percentages of CCRF-CEM cells. The statistical analysis was done by paired Student's t-test, $**p \leq 0.01$, if compared to DMSO untreated cells. Mean values \pm SD were derived from three independent experiments.

monoADP-ribose or PAR to various acceptor proteins or to PARP itself. This early event fosters the recruitment of DNA repair proteins and nucleases to damaged sites and promotes DNA damage repair (Wang et al., 2019). Whereas in toxin-exposed cells with considerable DNA damage, PARP becomes hyper-activated, leading to PAR production, which translocates to the cytosol, from where it affects the translocation of AIF to the nucleus and results in large-scale DNA fragmentation and chromatin condensation. These steps trigger the PARP-dependent and caspase-independent parthanatos (Andrabi et al., 2008; Fatokun et al., 2014). It acts through unique biochemical features which differ from that of apoptosis. Parthanatos has been associated with ischemic reperfusion injury after brain ischemia or myocardial infarction (Eliasson et al., 1997; Harraz et al., 2008; Zhang et al., 2019), neurodegenerative disease (Kam et al., 2018), and retinal disease (Greenwald and Pierce, 2019).

Our western blotting analyses in CCRF-CEM cells showed that PARP was rapidly overactivated upon J4 or J6 treatment, which stimulates mass PAR production and indicates the initiation of parthanatos. The overactivation of PARP depletes NAD^+ , which is also required for the synthesis of PAR. In turn, increased PARP and PAR cause mitochondrial dysfunction. Mitochondrial depolarization could be reversed by PARP inhibitor or supplementation with NAD^+ (Jang et al., 2017).

Interestingly, our mitochondrial depolarization experiments showed a sharp dissipation of the mitochondrial membrane potential by J4 and J6. At the same time, we verified that the cell viability was increased if J4 or J6 was combined with the PARP inhibitor PJ34, indicating that the mode of cell death was PARP-independent. Following PARP and PAR overexpression as well as mitochondrial damage, AIF is released from the mitochondrial outer membrane layer and translocated through the cytosol into the nucleus. AIF is a mitochondrial effector regulating cell death and survival. Reducing AIF abundance or blocking AIF release protects cells against parthanatos (Wang et al., 2009). Therefore, AIF is a commitment protein in this form of cell death. PARP, PAR, and AIF regulate parthanatos in a tightly coordinated manner. Genetic deletion of PARP caused a failure of AIF to translocate into the nucleus (Yu et al., 2002). Furthermore, AIF is a PAR-binding protein (Wang et al., 2011), and AIF-release activity is abolished if cells are treated with PAR glycohydrolase, which can degrade PAR. This demonstrates that PAR is a releasing signal of AIF (Andrabi et al., 2006a; Yu et al., 2006). Hence, PARP activation and PAR formation are fundamental for AIF translocation into the nucleus. Our results of nuclear AIF by western blotting in CCRF-CEM cells indeed showed that AIF was released from mitochondria and translocated to the nucleus. Immunofluorescence microscopy demonstrated as well that AIF accumulated in the nucleus, which

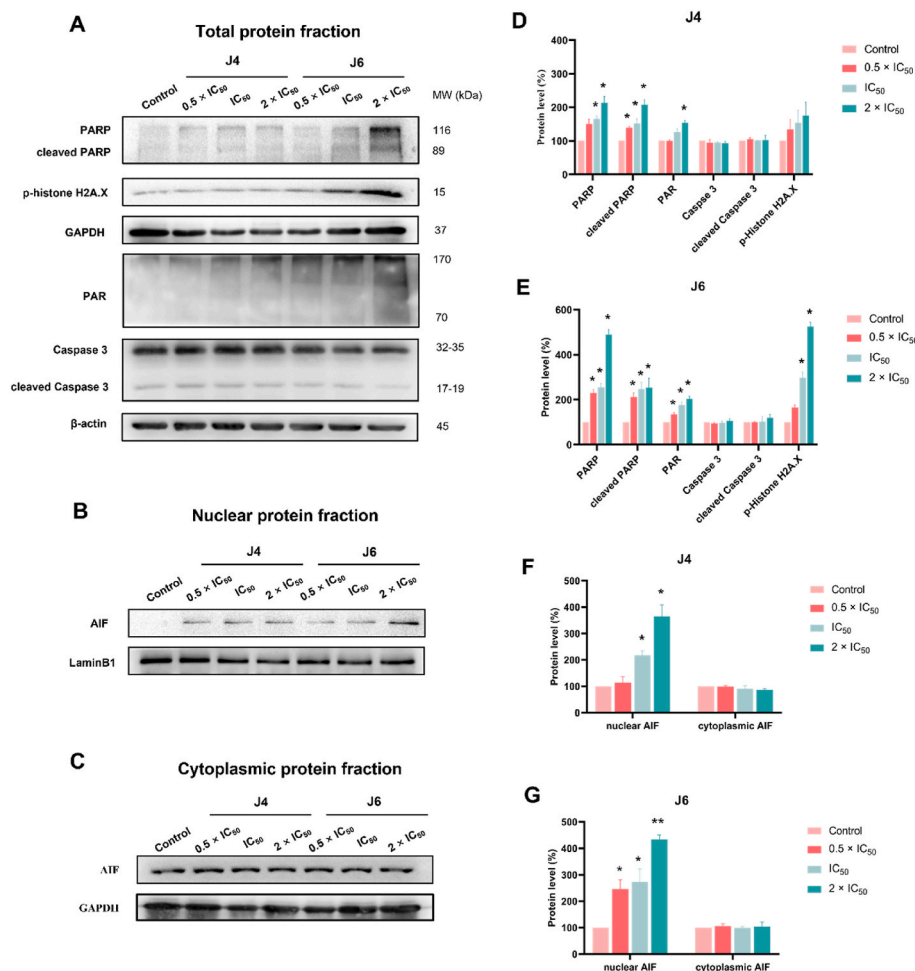


Fig. 6. Western blot analysis of parthanatos-related proteins. CCRF-CEM cells were treated with palladium (II)-based compounds J4 or J6 treated for 24 h. (A) The protein expression of full-length PARP, cleaved PARP, p-histone H2AX, PAR, caspase 3, and cleaved caspase 3 in total protein. (B) The protein expression of AIF in nuclear protein. (C) The protein expression of AIF in cytoplasmic protein. (D), (E), (F), and (G) Quantification of protein expression levels. Data represent relative expression intensity to GAPDH or β -actin. Statistical significance used paired Student's t-test in comparison to control (DMSO), * $p \leq 0.05$, ** $p \leq 0.01$. The data represent as mean values \pm SD of three independent experiments.

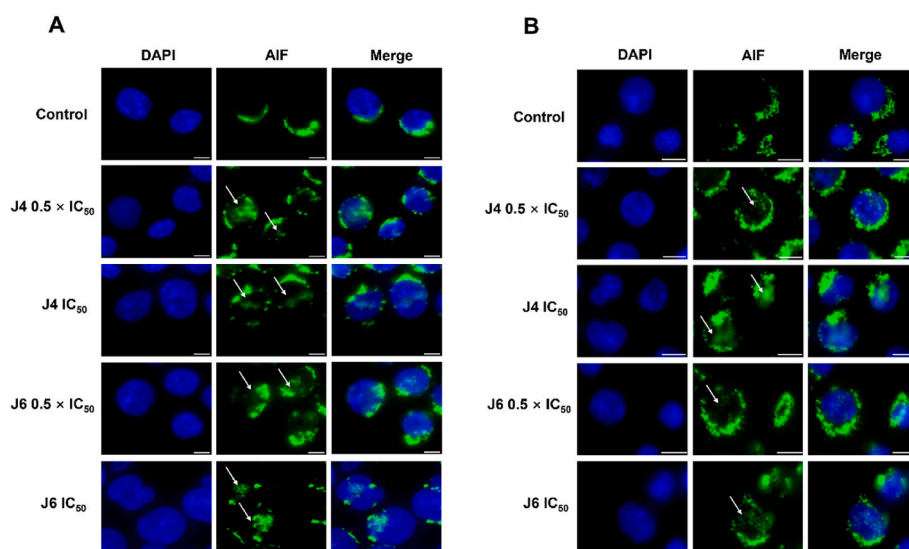


Fig. 7. Detection of AIF translocation from the cytoplasm into the nucleus by immunofluorescence microscopy. Cells were treated with different concentrations of palladium (II)-based compounds J4 or J6, or DMSO (control) for 24 h. (A) CCRF-CEM cells (Scale bar: 50 μ m) and (B) CEM/ADR5000 cells (Scale bar: 80 μ m). Samples stained with AIF primary antibody to visualize AIF protein. Images were merged with DAPI (blue) as cell nucleus to indicate AIF (green) translocation.

particularly supported that J4 and J6 induced parthanatos also in CEM/ADR5000 cells. Moreover, AIF induces large-scale DNA fragmentation after translocation, but apoptosis only causes small-scale DNA fragmentation, which means that AIF induces more critical DNA damage

(Fatokun et al., 2014). The phosphorylation of histone variant H2AX is an early cellular response to DNA double-strand breaks induction and is a sensitive biomarker and commonly used to monitor DNA damage initiation (Mah et al., 2010). Our results on p-histone H2A.X expression

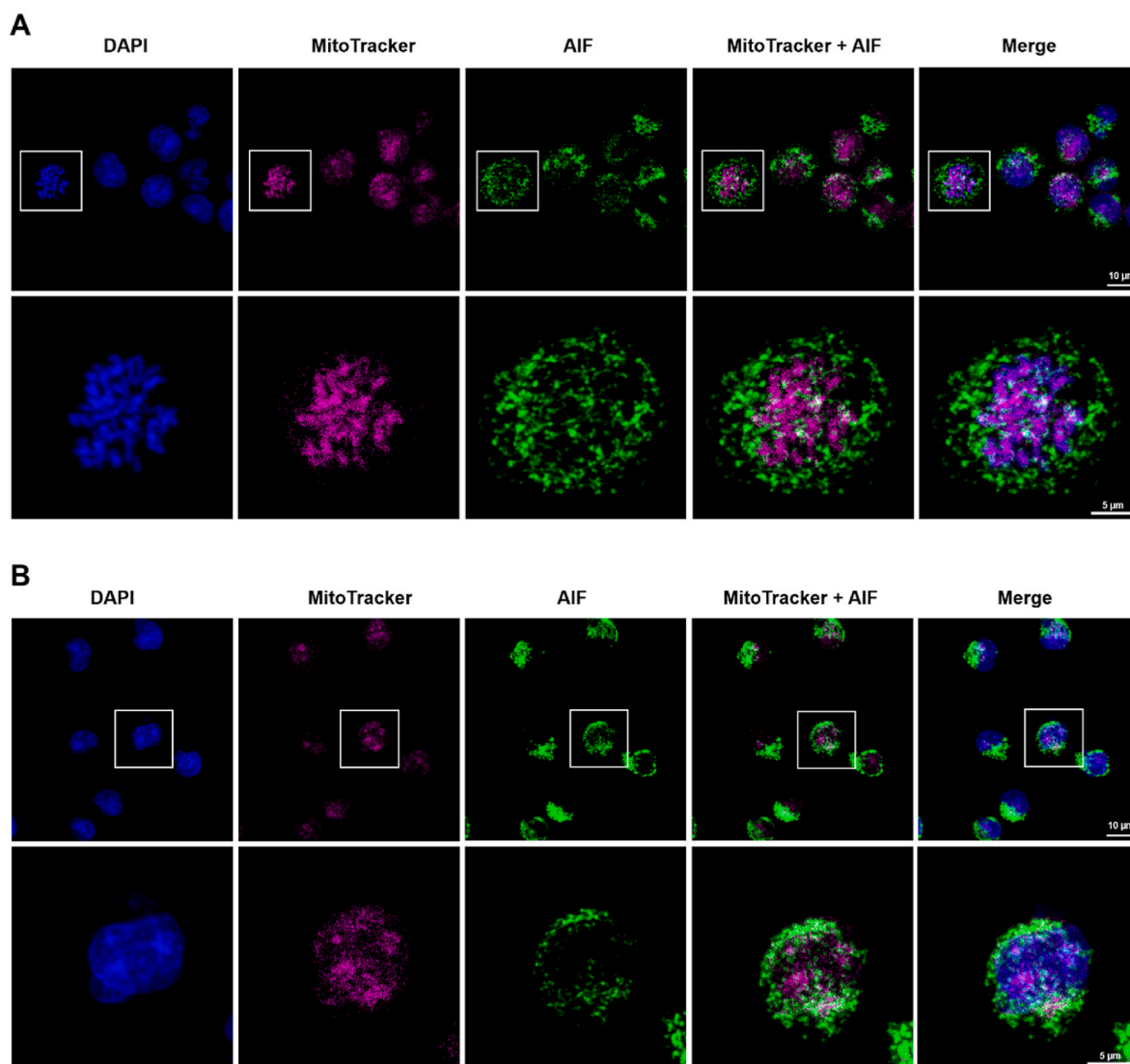


Fig. 8. The mitochondrial localization of AIF in (A) CCRF-CEM cells and (B) CEM/ADR5000 cells. Cells were stained with AIF (green), MitoTracker® Deep Red (magenta) to show mitochondria, and DAPI (blue) to show the nucleus. See also Supplementary Video 1.

in CCRF-CEM cells showed a continuous upregulation upon the treatments, especially with J6, and the comet assay revealed the formation of J4- and J6-induced DNA tails in a concentration-dependent manner. In addition, parthanatos as caspase-independent cell death cannot be rescued by pan-caspase inhibitors. However, the activation of caspase was found in some studies after AIF release (Yu et al., 2002). Our western blotting also showed caspase 3 expression. In parallel to AIF, mitochondria contain different apoptogenic factors including cytochrome C, pro-caspase 2, 3, and 9 to engage in the degradation of apoptosis. AIF can initiate the release of cytochrome c, which further activates caspases. The activation of caspase after the executioner phase of AIF may assist in cell disintegration (Susin et al., 1999). Therefore, we conclude that parthanatos is the most relevant mode of cell death induced by the two Pd (II) complexes, J4 and J6.

The crosstalk between apoptosis and autophagy is intricate. If cells are under stress, autophagy can activate a cytoprotective switch by inactivating apoptosis to help cancer cells to escape cell death (Gump and Thorburn, 2011). Hence, we also focused on autophagy to understand whether autophagy contributes to death or even protects cells from apoptosis by J4 and J6. Autophagy is a programmed self-digesting mechanism, which is characterized by the formation of double-membrane vesicles (autophagosomes) that engulfs impaired

cellular proteins and organelles and deliver the infusion with the lysosome (Levy et al., 2017). This lysosomal degradation pathway is a highly controlled process that is regulated by multiple signaling events. It involves a set of about 16–20 core conserved autophagy-related genes (ATGs), which initiate the formation of the autophagosome (Levine and Kroemer, 2019). Human Beclin, an ortholog of the Atg6/vacuolar protein sorting (Vps)-30 protein in yeast, is important for the localization of autophagic proteins to the phagophore, which interacts with the class III phosphatidylinositol 3-kinase (PI3K) complex and several cofactors (He and Levine, 2010). By means of gene-transfer techniques, autophagic bodies have been identified in *beclin-1*-transformed yeast that were hardly seen in non-transformed yeast, confirming that Beclin induces autophagy (Liang et al., 1999). Our data revealed that J4 decreased the expression of Beclin 1, while J6 increased it in CCRF-CEM cells. The effects of Beclin in CEM/ADR5000 cells were minor (Fig. 3). On the other hand, sequestosome 1 (SQSTM1/p62) is an autophagy receptor and a selective substrate for autophagy. P62 interacts with light chain 3 (LC3) for attachment to the autophagosomes, and thereby delivers polyubiquitin cargos to the lysosome system for degradation (Islam et al., 2018). A widely accepted notion is that the activation of autophagy suppresses the expression of p62, as p62 degrades together with the target cargos (Liu et al., 2016). Our results showed that p62

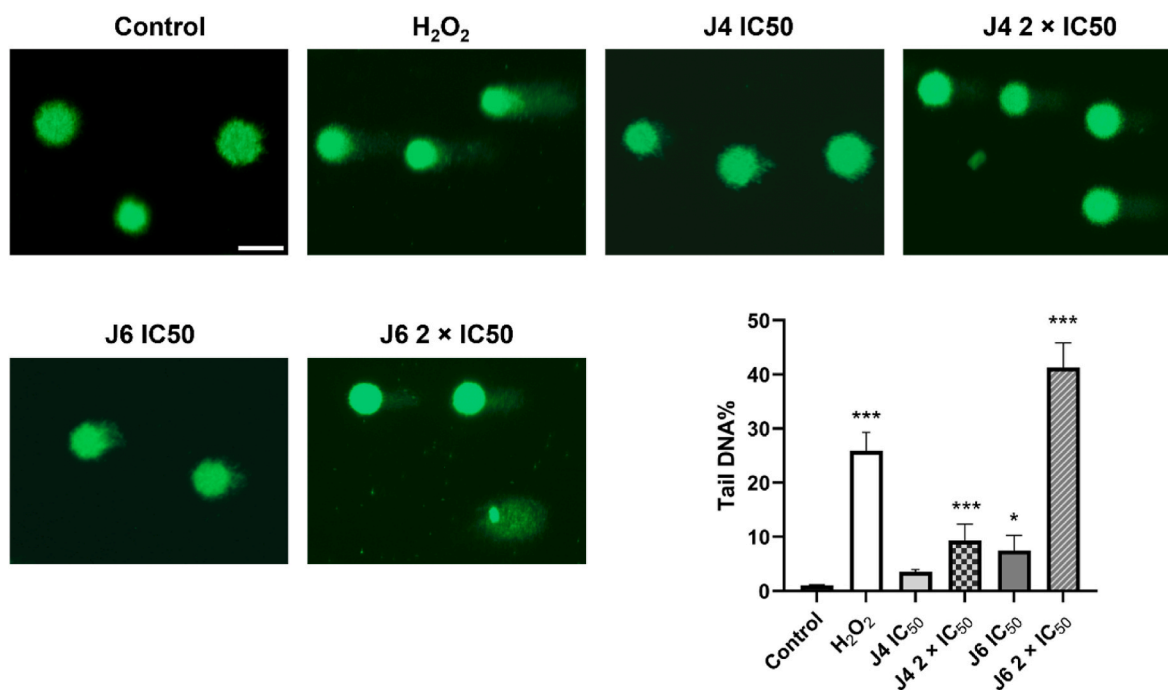


Fig. 9. Detection of DNA damage by the alkaline comet assay. Representative images of CCRF-CEM cells treated with palladium (II)-based compounds J4, J6, or DMSO (control) for 24 h, or H₂O₂ (positive control) for 1 h. Scale bar, 60 μ m. The tail DNA percentage was measured by Image J from 50 randomly represented as mean \pm SEM shown in the bar diagram. Statistical significance (* $p \leq 0.05$, ** $p \leq 0.01$, *** $p \leq 0.0001$) was compared to DMSO.

expression in CCRF-CEM cells was upregulated with J4 and downregulated with J6. The expression level of p62 in CEM/ADR5000 cells was, however, almost equal to untreated samples (Fig. 3). Taken together, J6 may induce autophagy only in CCRF-CEM cells. A crosstalk between autophagy and parthanatos modulated by PARP was reported in rat stria marginal cells (Jiang et al., 2018). However, upon the elevated treated concentration in western blotting, there was no statistical significance observed for these two autophagy biomarkers. Therefore, we concluded that autophagy could not be the major mode of cell death induced by J4 and J6 in CCRF-CEM cells.

Taking a broad look at the field of metal-based agents as chemotherapeutics, they have been designed with a “multitargeted” approach to maximize anticancer activity and to overcome the problem of drug resistance. The utilization of a certain central metal ion can have a significant impact on biological activity since different metals show distinct physicochemical characteristics (Lucaciu et al., 2022). In an endeavor to replace platinum, palladium, gold, and ruthenium are the most studied metals with potential anticancer activity (Ferraro et al., 2022). However, the challenge of designing and synthesizing Pd (II) complexes is their lower kinetic stability, which affects to address their drug targets (Prince et al., 2017). The stability of our Pd (II) complexes containing halogen-substituted Schiff bases and pic have been previously confirmed by LC/MS analysis (Rudbari et al., 2022). Moreover, we also confirmed that there is no cytotoxicity from the original material palladium salt (PdCl₂), and the cytotoxic activity of the Schiff base ligand is inadequate compared with the corresponding Pd (II) complex. Therefore, our drug design strategy with excellent anticancer activity and stability is worthy to be further studied. Generally, the induction of apoptotic cell death pathways has been a main goal to achieve cytotoxicity in designing non-platinum compounds (Ferraro et al., 2022). Similarly, numerous investigations indeed have shown that Pd (II)-based complexes can cause cell death by apoptosis (Ari et al., 2014; Coskun et al., 2013; Keswani et al., 2014). However, dysfunctional apoptosis allows tumor cells to escape from this mode of programmed cell death for uncontrolled proliferation. To the best of our knowledge, our current study is the first to report that Pd (II) complexes can induce parthanatos

as the main cell death pathway. On the other hand, DNA represents the principal target of Pd (II) complexes (Ferraro et al., 2022). It has been reported that DNA binding by Pd (II) complexes causes genetic damage (Bjelogrić et al., 2019). Our single cell electrophoresis observations and upregulated p-histone H2AX expression both supported that J4 and J6 caused DNA damage, which subsequently induced parthanatos.

Another aspect we focused on was the relevance of the multidrug resistance phenotype for our palladium (II) complexes. Drug resistance is a crucial factor leading to the failure of chemotherapy with fatal consequences for patients. Apart from resistance to apoptosis, another major reason is multidrug resistance (MDR), where tumor cells confer resistance to a quantity of functionally and structurally unrelated compounds via the ATP-binding cassette (ABC) transporters. P-glycoprotein (P-gp) is a well-known drug efflux pump, whose overexpression leads to lower efficacy of chemotherapeutics (Li et al., 2016). We previously reported that P-gp-overexpressing CEM/ADR5000 cells were moderately cross-resistant to J4 and J6 (2- to 4-fold) (Rudbari et al., 2022), while they are highly cross-resistant to many clinically established anticancer drugs (100- to 1000-fold) (Efferth et al., 2008). In the present study, we observed that CEM/ADR5000 cells are also able to induce parthanatos upon J4 or J6 treatment. We conclude that at lower concentrations, P-gp is expelling these two compounds, while at higher concentrations the efflux capacity of P-gp might be exhausted leading to parthanatos. Parthanatos may be an alternative strategy to overcome drug resistance if other mechanisms of cell death such as apoptosis or autophagy fail.

5. Conclusion

In conclusion, we demonstrated that two Pd (II) complexes containing double chlorine-/iodine- substituted Schiff base and 2-picolylamine (J4 and J6) induced parthanatos as the major mode of cell death accompanied with a minor contribution of apoptotic cell death in drug-sensitive CCRF-CEM and multidrug-resistant CEM/ADR5000 leukemia cells. Both compounds displayed non-toxic effects on human peripheral mononuclear cells. They induced overactivation of PARP and

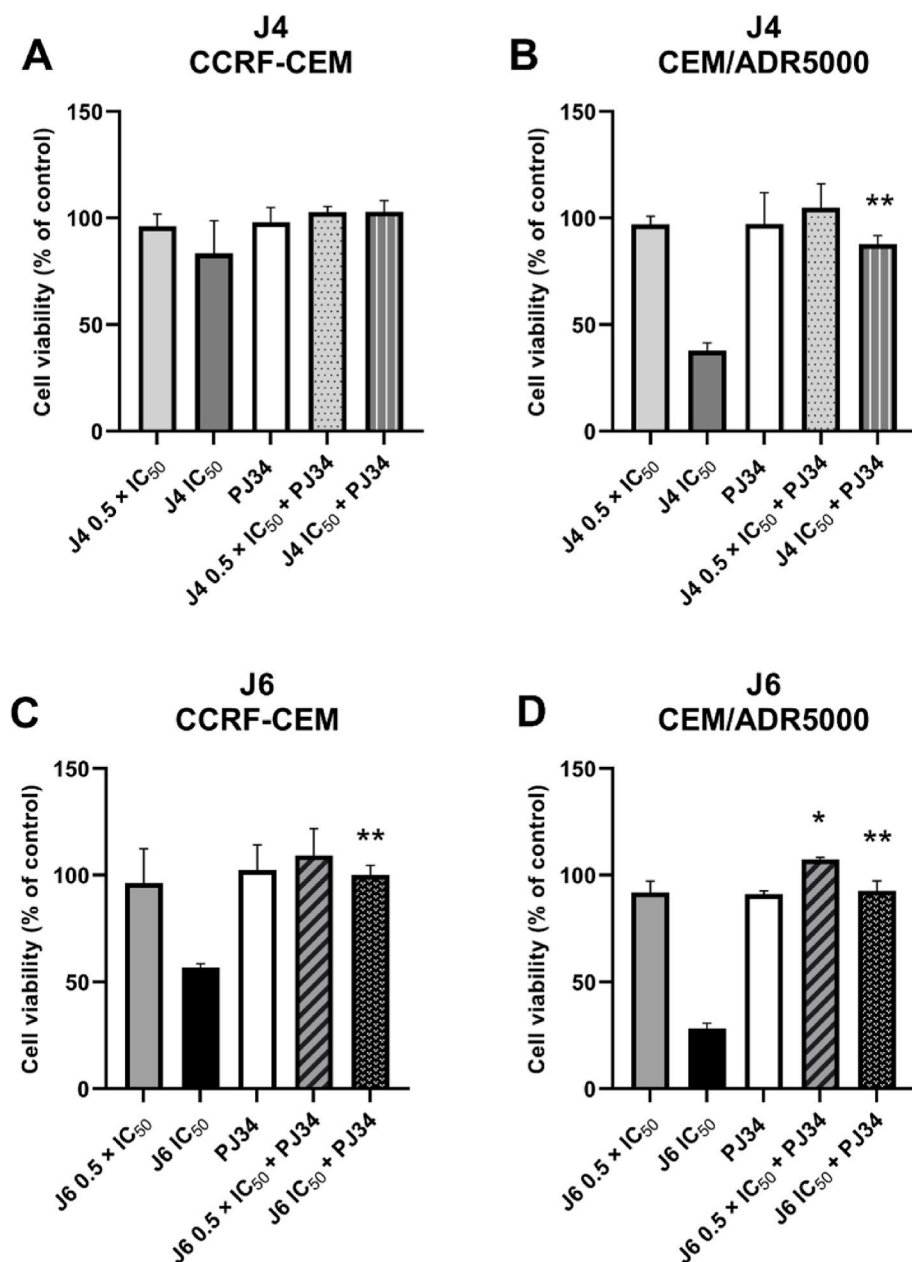


Fig. 10. Cell viability of PARP inhibitor PJ34 in the presence of different concentrations ($0.5 \times IC_{50}$, and IC_{50}) of J4 or J6. (A) CCRF-CEM and (B) ADR/CEM5000 cells treated with J4 or in combination with PJ34. (C) CCRF-CEM and (D) ADR/CEM5000 cells treated with J6 or in combination with PJ34. PJ34 was $10 \mu M$. Bar diagrams were shown as mean value \pm SD from three repetitions). Statistical significance used paired Student's t-test ($*p \leq 0.05$, $**p \leq 0.01$), if compared with J4 or J6 treatment alone.

PAR, nuclear AIF translocation, dissipation of mitochondrial membrane potential, and DNA damage. These effects led to cells dying from parthanatos. Along with our previous biological investigations (Rudbari et al., 2022), J4 and J6 arrest the cell cycle in the G2/M phase and inhibited the proteolytic activity of the proteasome in CCRF-CEM cells. These results present the novel Pd (II) complexes J4 and J6 as promising anticancer candidates. The induction of parthanatos by J4 and J6 implies the possibility of better attacking drug-resistant cancers suffering from the inability to induce other modes of cell death. Our results may encourage further studies on palladium-based drug design, and palladium-based complexes may offer great potential for cancer therapy.

CRediT authorship contribution statement

Min Zhou: Study conception and design, Data collection, Investigation, Validation, Software, Formal analysis, Data curation, Visualization, Project administration, Writing – original draft, preparation, Writing – review & editing. **Joelle C. Boulos:** Data collection,

Investigation, Validation, Writing – review & editing. **Ejlal A. Omer:** Data collection, Investigation, Validation, Writing – review & editing. **Hadi Amiri Rudbari:** Resources, Visualization, Writing – review & editing. **Tanja Schirmeister:** Resources, Writing – review & editing. **Nicola Micale:** Resources, Writing – review & editing. **Thomas Efferth:** Study conception and design, Project administration, Supervision, Writing – review & editing.

Declaration of competing interest

The authors declare that they have no known competing financial interests or personal relationships that could have appeared to influence the work reported in this paper.

Data availability

Data will be made available on request.

Acknowledgements

We thank the IMB Microscopy and Histology Core Facility (Mainz, Germany) for their helpful training and technical support for microscopy-related experiments with the AF7000 widefield fluorescence microscope (founded by DFG grant 212049334) and Stellaris 8 Falcon confocal microscope (founded by the DFG grant 497669232). We also thank the IMB Flow Cytometry Core Facility (Mainz, Germany) for the analysis of mitochondrial membrane potential on BD LSRFortessa SOP. We are grateful for a Ph.D. stipend from the Chinese Scholarship Council to M.Z., the stipend from the Sibylle Kalkhof-Rose-Foundation to J.C.B., and the stipend from the German Academic Exchange Service (DAAD) to E.A.O.

Appendix A. Supplementary data

Supplementary data related to this article can be found at <https://doi.org/10.1016/j.ejphar.2023.175980>.


References

- Abu-Surrah, A.S., Abdalla, M.Y., 2008. Palladium-based chemotherapeutic agents: routes toward complexes with good antitumor activity. *Cancer Ther.* 6, 1–10.
- Alam, M.N., Huq, F., 2016. Comprehensive review on tumour active palladium compounds and structure–activity relationships. *Coord. Chem. Rev.* 316, 36–67.
- Andrabi, S.A., Dawson, T.M., Dawson, V.L., 2008. Mitochondrial and nuclear cross talk in cell death: parthanatos. *Ann. N. Y. Acad. Sci.* 1147, 233–241.
- Andrabi, S.A., Kim, N.S., Yu, S.-W., Wang, H., Koh, D.W., Sasaki, M., Klaus, J.A., Otsuka, T., Zhang, Z., Koehler, R.C., Hurn, P.D., Poirier, G.G., Dawson, V.L., Dawson, T.M., 2006a. Poly(ADP-ribose) (PAR) polymer is a death signal. *Proc. Natl. Acad. Sci. U.S.A.* 103, 18308–18313.
- Andrabi, S.A., Kim, N.S., Yu, S.-W., Wang, H., Koh, D.W., Sasaki, M., Klaus, J.A., Otsuka, T., Zhang, Z., Koehler, R.C., Hurn, P.D., Poirier, G.G., Dawson, V.L., Dawson, T.M., 2006b. Poly(ADP-ribose) (PAR) polymer is a death signal. *Proc. Natl. Acad. Sci. U.S.A.* 103, 18308–18313.
- Ari, F., Cevatemre, B., Armutak, E.I., Aztopal, N., Yilmaz, V.T., Ulukaya, E., 2014. Apoptosis-inducing effect of a palladium(II) saccharinate complex of terpyridine on human breast cancer cells in vitro and in vivo. *Bioorg. Med. Chem.* 22, 4948–4954.
- Ari, F., Ulukaya, E., Sarimahmut, M., Yilmaz, V.T., 2013. Palladium(II) saccharinate complexes with bis(2-pyridylmethyl)amine induce cell death by apoptosis in human breast cancer cells in vitro. *Bioorg. Med. Chem.* 21, 3016–3021.
- Azzouzi, A.R., Vincendeau, S., Barret, E., Cicco, A., Kleinclaus, F., van der Poel, H.G., Stief, C.G., Rassweiler, J., Salomon, G., Solsona, E., Alcaraz, A., Tammela, T.T., Rosario, D.J., Gomez-Veiga, F., Ahlgren, G., Benzaghoul, F., Gaillac, B., Amzal, B., Debruyne, F.M., Fromont, G., Gratzke, C., Emberton, M., 2017. Padeliporfin vascular-targeted photodynamic therapy versus active surveillance in men with low-risk prostate cancer (CLIN1001 PCM301): an open-label, phase 3, randomised controlled trial. *Lancet Oncol.* 18, 181–191.
- Batista de Carvalho, A.L., Medeiros, P.S., Costa, F.M., Ribeiro, V.P., Sousa, J.B., Diniz, C., Marques, M.P., 2016. Anti-invasive and anti-proliferative synergism between docetaxel and a polynuclear Pd-spermine agent. *PLoS One* 11, e0167218.
- Bispo, J.A.B., Pinheiro, P.S., Kobetz, E.K., 2020. Epidemiology and etiology of leukemia and lymphoma. *Cold Spring Harb. Perspect. Med.* 10, a034819.
- Bjelogrić, S.K., Todorović, T.R., Kojić, M., Senčanski, M., Nikolić, M., Višnjevac, A., Arašković, J., Miljković, M., Müller, C.D., Filipović, N.R., 2019. Pd(II) complexes with N-heteroaromatic hydrazone ligands: anticancer activity, in silico and experimental target identification. *J. Inorg. Biochem.* 199, 110758.
- Boulou, J.C., Omer, E.A., Rigano, D., Formisano, C., Chatterjee, M., Leich, E., Klaucek, S. M., Shan, L.-t., Efferth, T., 2023. Cynaropicrin disrupts tubulin and c-Myc-related signaling and induces parthanatos-type cell death in multiple myeloma. *Acta Pharmacol. Sin.* <https://doi.org/10.1038/s41401-023-01117-3>. Online ahead of print.
- Carneiro, T.J., Martins, A.S., Marques, M.P.M., Gil, A.M., 2020. Metabolic aspects of palladium(II) potential anti-cancer drugs. *Front. Oncol.* 10, 590970.
- Chipuk, J.E., Moldoveanu, T., Llambi, F., Parsons, M.J., Green, D.R., 2010. The BCL-2 family reunion. *Mol. Cell* 37, 299–310.
- Coskun, M.D., Ari, F., Oral, A.Y., Sarimahmut, M., Kutlu, H.M., Yilmaz, V.T., Ulukaya, E., 2013. Promising anti-growth effects of palladium(II) saccharinate complex of terpyridine by inducing apoptosis on transformed fibroblasts in vitro. *Bioorg. Med. Chem.* 21, 4698–4705.
- Crowley, L.C., Marfell, B.J., Scott, A.P., Waterhouse, N.J., 2016. Quantitation of apoptosis and necrosis by annexin V binding, propidium iodide uptake, and flow cytometry. *Cold Spring Harb. Protoc.* 2016 <https://doi.org/10.1101/pdb.prot087288>.
- Davis, A.S., Viera, A.J., Mead, M.D., 2014. Leukemia: an overview for primary care. *Am. Fam. Physician* 89, 731–738.
- Dawood, M., Elbadawi, M., Böckers, M., Bringmann, G., Efferth, T., 2020. Molecular docking-based virtual drug screening revealing an oxofluorenyl benzamide and a bromonaphthalene sulfonamide hydroxybenzoic acid as HDAC6 inhibitors with cytotoxicity against leukemia cells. *Biomed. Pharmacother.* 129, 110454.
- De Biasi, S., Gibellini, L., Cossarizza, A., 2015. Uncompensated polychromatic analysis of mitochondrial membrane potential using JC-1 and multilaser excitation. *Curr. Protoc. Cytom.* 72 (7), 32.31–37.32.11.
- Desoize, B., Madoulet, C., 2002. Particular aspects of platinum compounds used at present in cancer treatment. *Crit. Rev. Oncol. Hematol.* 42, 317–325.
- Döhner, H., Wei, A.H., Löwenberg, B., 2021. Towards precision medicine for AML. *Nat. Rev. Clin. Oncol.* 18, 577–590.
- Efferth, T., Konkimalla, V.B., Wang, Y.F., Sauerbrey, A., Meinhardt, S., Zintl, F., Mattern, J., Volm, M., 2008. Prediction of broad spectrum resistance of tumors towards anticancer drugs. *Clin. Cancer Res.* 14, 2405–2412.
- Efferth, T., Sauerbrey, A., Olbrich, A., Gebhart, E., Rauch, P., Weber, H.O., Hengstler, J. G., Halatsch, M.E., Volm, M., Tew, K.D., Ross, D.D., Funk, J.O., 2003. Molecular modes of action of artesunate in tumor cell lines. *Mol. Pharmacol.* 64, 382–394.
- El-Morsy, F.A., Jean-Claude, B.J., Butler, I.S., El-Sayed, S.A., Mostafa, S.I., 2014. Synthesis, characterization and anticancer activity of new zinc(II), molybdate(II), palladium(II), silver(I), rhodium(III), ruthenium(II) and platinum(II) complexes of 5,6-diamino-4-hydroxy-2-mercaptopyrimidine. *Inorg. Chim. Acta.* 423, 144–155.
- Eliasson, M.J., Sampei, K., Mandir, A.S., Hurn, P.D., Traystman, R.J., Bao, J., Pieper, A., Wang, Z.Q., Dawson, T.M., Snyder, S.H., Dawson, V.L., 1997. Poly(ADP-ribose) polymerase gene disruption renders mice resistant to cerebral ischemia. *Nat. Med.* 3, 1089–1095.
- Elmore, S., 2007. Apoptosis: a review of programmed cell death. *Toxicol. Pathol.* 35, 495–516.
- Fatokun, A.A., Dawson, V.L., Dawson, T.M., 2014. Parthanatos: mitochondrial-linked mechanisms and therapeutic opportunities. *Br. J. Pharmacol.* 171, 2000–2016.
- Ferraro, M.G., Piccolo, M., Misso, G., Santamaria, R., Irace, C., 2022. Bioactivity and development of small non-platinum metal-based chemotherapeutics. *Pharmaceutics* 14, 954.
- Finger, P.T., Berson, A., Ng, T., Szechter, A., 2002. Palladium-103 plaque radiotherapy for choroidal melanoma: an 11-year study. *Int. J. Radiat. Oncol. Biol. Phys.* 54, 1438–1445.
- Florea, A.M., Büsselberg, D., 2011. Cisplatin as an anti-tumor drug: cellular mechanisms of activity, drug resistance and induced side effects. *Cancers* 3, 1351–1371.
- Foley, G.E., Lazarus, H., Farber, S., Uzman, B.G., Boone, B.A., McCarthy, R.E., 1965. Continuous culture of human lymphoblasts from peripheral blood of a child with acute leukemia. *Cancer* 18, 522–529.
- Frezza, M., Hindo, S., Chen, D., Davenport, A., Schmitt, S., Tomco, D., Dou, Q.P., 2010. Novel metals and metal complexes as platforms for cancer therapy. *Curr. Pharmaceut. Des.* 16, 1813–1825.
- Ghosh, S., 2019. Cisplatin: the first metal based anticancer drug. *Bioorg. Chem.* 88, 102925.
- Green, D.R., Llambi, F., 2015. Cell death signaling. *Cold Spring Harbor Perspect. Biol.* 7, a006080.
- Greenwald, S.H., Pierce, E.A., 2019. Parthanatos as a cell death pathway underlying retinal disease. *Adv. Exp. Med. Biol.* 1185, 323–327.
- Gump, J.M., Thorburn, A., 2011. Autophagy and apoptosis: what is the connection? *Trends Cell Biol.* 21, 387–392.
- Gyori, B.M., Venkatachalam, G., Thiagarajan, P.S., Hsu, D., Clement, M.V., 2014. OpenComet: an automated tool for comet assay image analysis. *Redox Biol.* 2, 457–465.
- Hanahan, D., Weinberg, R.A., 2011. Hallmarks of cancer: the next generation. *Cell* 144, 646–674.
- Harratz, M.M., Dawson, T.M., Dawson, V.L., 2008. Advances in neuronal cell death 2007. *Stroke* 39, 286–288.
- He, C., Levine, B., 2010. The Beclin 1 interactome. *Curr. Opin. Cell Biol.* 22, 140–149.
- Huang, Y., Ibrado, A.M., Reed, J.C., Bullock, G., Ray, S., Tang, C., Bhalla, K., 1997. Co-expression of several molecular mechanisms of multidrug resistance and their significance for paclitaxel cytotoxicity in human AML HL-60 cells. *Leukemia* 11, 253–257.
- Ilić, D.R., Jevtić, V.V., Radić, G.P., Arsin, K., Ristić, B., Harhaji-Trajković, L., Vuković, N., Sukdolac, S., Klisurić, O., Trajković, V., Trifunović, S.R., 2014. Synthesis, characterization and cytotoxicity of a new palladium(II) complex with a coumarin-derived ligand. *Eur. J. Med. Chem.* 74, 502–508.
- Islam, M.A., Sooro, M.A., Zhang, P., 2018. Autophagic regulation of p62 is critical for cancer therapy. *Int. J. Mol. Sci.* 19, 1405.
- Jang, K.H., Do, Y.J., Son, D., Son, E., Choi, J.S., Kim, E., 2017. AIF-independent parthanatos in the pathogenesis of dry age-related macular degeneration. *Cell Death Dis.* 8, e2526.
- Jänicke, R.U., Ng, P., Sprengart, M.L., Porter, A.G., 1998. Caspase-3 is required for alpha-fodrin cleavage but dispensable for cleavage of other death substrates in apoptosis. *J. Biol. Chem.* 273, 15540–15545.
- Jiang, H.Y., Yang, Y., Zhang, Y.Y., Xie, Z., Zhao, X.Y., Sun, Y., Kong, W.J., 2018. The dual role of poly(ADP-ribose) polymerase-1 in modulating parthanatos and autophagy under oxidative stress in rat cochlear marginal cells of the stria vascularis. *Redox Biol.* 14, 361–370.
- Kadioglu, O., Cao, J., Kosyakova, N., Mrasek, K., Liehr, T., Efferth, T., 2016. Genomic and transcriptomic profiling of resistant CEM/ADR-5000 and sensitive CCRF-CEM leukemia cells for unravelling the full complexity of multi-factorial multidrug resistance. *Sci. Rep.* 6, 36754.
- Kam, T.I., Mao, X., Park, H., Chou, S.C., Karuppagounder, S.S., Umanah, G.E., Yun, S.P., Brahmachari, S., Panicker, N., Chen, R., Andrabi, S.A., Qi, C., Poirier, G.G., Pletnikova, O., Troncoso, J.C., Bekris, L.M., Leverenz, J.B., Pantelyat, A., Ko, H.S., Rosenthal, L.S., Dawson, T.M., Dawson, V.L., 2018. Poly(ADP-ribose) drives pathologic α -synuclein neurodegeneration in Parkinson's disease. *Science* 362, eaat8407.

- Kang, Y.-H., Yi, M.-J., Kim, M.-J., Park, M.-T., Bae, S., Kang, C.-M., Cho, C.-K., Park, I.-C., Park, M.-J., Rhee, C.H., Hong, S.-I., Chung, H.Y., Lee, Y.-S., Lee, S.-J., 2004. Caspase-independent cell death by arsenic trioxide in human cervical cancer cells: reactive oxygen species-mediated poly(ADP-ribose) polymerase-1 activation signals apoptosis-inducing factor release from mitochondria. *Cancer Res.* 64, 8960–8967.
- Kapdi, A.R., Fairlamb, I.J., 2014. Anti-cancer palladium complexes: a focus on PdX₂L₂, palladacycles and related complexes. *Chem. Soc. Rev.* 43, 4751–4777.
- Keswani, T., Chowdhury, S., Mukherjee, S., Bhattacharyya, A., 2014. Palladium(II) complex induces apoptosis through ROS-mediated mitochondrial pathway in human lung adenocarcinoma cell line (A549). *Curr. Sci.* 107, 1711–1719.
- Kielhorn, J., Melber, C., Keller, D., Mangelsdorf, I., 2002. Palladium—a review of exposure and effects to human health. *Int. J. Hyg Environ. Health* 205, 417–432.
- Kimmig, A., Gekeler, V., Neumann, M., Frese, G., Handgretinger, R., Kardos, G., Diddens, H., Niethammer, D., 1990. Susceptibility of multidrug-resistant human leukemia cell lines to human interleukin 2-activated killer cells. *Cancer Res.* 50, 6793–6799.
- Kovala-Demertzi, D., Boccarelli, A., Demertzi, M.A., Coluccia, M., 2007. In vitro antitumor activity of 2-acetyl pyridine 4n-ethyl thiosemicarbazone and its platinum (II) and palladium(II) complexes. *Chemotherapy* 53, 148–152.
- Kumaravel, T.S., Vilhar, B., Faux, S.P., Jha, A.N., 2009. Comet Assay measurements: a perspective. *Cell Biol. Toxicol.* 25, 53–64.
- Lazarević, T., Rilak, A., Bugarić, Z. D., 2017. Platinum, palladium, gold and ruthenium complexes as anticancer agents: current clinical uses, cytotoxicity studies and future perspectives. *Eur. J. Med. Chem.* 142, 8–31.
- Levine, B., Kroemer, G., 2019. Biological functions of autophagy genes: a disease perspective. *Cell* 176, 11–42.
- Levy, J.M.M., Towers, C.G., Thorburn, A., 2017. Targeting autophagy in cancer. *Nat. Rev. Cancer* 17, 528–542.
- Li, W., Zhang, H., Assaraf, Y.G., Zhao, K., Xu, X., Xie, J., Yang, D.H., Chen, Z.S., 2016. Overcoming ABC transporter-mediated multidrug resistance: molecular mechanisms and novel therapeutic drug strategies. *Drug Resist. Updates* 27, 14–29.
- Liang, X.H., Jackson, S., Seaman, M., Brown, K., Kempkes, B., Hibshoosh, H., Levine, B., 1999. Induction of autophagy and inhibition of tumorigenesis by beclin 1. *Nature* 402, 672–676.
- Liang, X.H., Kleeman, L.K., Jiang, H.H., Gordon, G., Goldman, J.E., Berry, G., Herman, B., Levine, B., 1998. Protection against fatal Sindbis virus encephalitis by beclin, a novel Bcl-2-interacting protein. *J. Virol.* 72, 8586–8596.
- Liu, W.J., Ye, L., Huang, W.F., Guo, L.J., Xu, Z.G., Wu, H.L., Yang, C., Liu, H.F., 2016. p62 links the autophagy pathway and the ubiquitin-proteasome system upon ubiquitinated protein degradation. *Cell. Mol. Biol. Lett.* 21, 29.
- Lu, X., Saeed, M.E.M., Hegazy, M.F., Kampf, C.J., Efferth, T., 2020. Chemopreventive property of Sencha tea extracts towards sensitive and multidrug-resistant leukemia and multiple myeloma cells. *Biomolecules* 10, 1000.
- Luciaciu, R.L., Hangan, A.C., Sevastre, B., Oprean, L.S., 2022. Metallo-drugs in cancer therapy: past, present and future. *Molecules* 27, 6485.
- Ma, D., Lu, B., Feng, C., Wang, C., Wang, Y., Luo, T., Feng, J., Jia, H., Chi, G., Luo, Y., Ge, P., 2016. Deoxy podophyllotoxin triggers parthanatos in glioma cells via induction of excessive ROS. *Cancer Lett.* 371, 194–204.
- Mah, L.J., El-Osta, A., Karagiannis, T.C., 2010. γH2AX: a sensitive molecular marker of DNA damage and repair. *Leukemia* 24, 679–686.
- Mahmoud, N., Hegazy, M.-E.F., Wadie, W., Elbadawi, M., Fleischer, E., Klinger, A., Bringmann, G., Khayyal, M.T., Efferth, T., 2022. Naphthoquinone derivatives as P-glycoprotein inducers in inflammatory bowel disease: 2D monolayers, 3D spheroids, and in vivo models. *Pharmacol. Res.* 179, 106233.
- McFarland, S.A., Mandel, A., Dumoulin-White, R., Gasser, G., 2020. Metal-based photosensitizers for photodynamic therapy: the future of multimodal oncology? *Curr. Opin. Chem. Biol.* 56, 23–27.
- Miller, M.A., Askevold, B., Mikula, H., Kohler, R.H., Pirovich, D., Weissleder, R., 2017. Nano-palladium is a cellular catalyst for in vivo chemistry. *Nat. Commun.* 8, 15906.
- Mohammad, R.M., Muqbil, I., Lowe, L., Yedjou, C., Hsu, H.Y., Lin, L.T., Siegelin, M.D., Fimognari, C., Kumar, N.B., Dou, Q.P., Yang, H., Samadi, A.K., Russo, G.L., Spagnuolo, C., Ray, S.K., Chakrabarti, M., Morre, J.D., Coley, H.M., Honoki, K., Fujii, H., Georgakilas, A.G., Amedei, A., Niccolai, E., Amin, A., Ashraf, S.S., Helferich, W.G., Yang, X., Boosani, C.S., Guha, G., Bhakta, D., Ciriolo, M.R., Aquilano, K., Chen, S., Mohammed, S.I., Keith, W.N., Bilsland, A., Halicka, D., Nowshen, S., Azmi, A.S., 2015. Broad targeting of resistance to apoptosis in cancer. *Semin. Cancer Biol.* 35 (Suppl. 1), S78–s103.
- Ndagi, U., Mhlongo, N., Soliman, M.E., 2017. Metal complexes in cancer therapy - an update from drug design perspective. *Drug Des. Dev. Ther.* 11, 599–616.
- Orvig, C., Abrams, M.J., 1999. Medicinal inorganic chemistry: introduction. *Chem. Rev.* 99, 2201–2204.
- Özenver, N., Saeed, M., Demirez, L., Efferth, T., 2018. Aloe-emodin as drug candidate for cancer therapy. *Oncotarget* 9, 17770–17796.
- Prince, S., Mapolie, S., Blanckenberg, A., 2017. Palladium-based anti-cancer therapeutics. In: Schwab, M. (Ed.), *Encyclopedia of Cancer*. Springer Berlin Heidelberg, Berlin, Heidelberg, pp. 3371–3378.
- Qin, Q.-P., Zou, B.-Q., Tan, M.-X., Luo, D.-M., Wang, Z.-F., Wang, S.-L., Liu, Y.-C., 2018. High in vitro anticancer activity of a dinuclear palladium(II) complex with a 2-phenylpyridine ligand. *Inorg. Chem. Commun.* 96, 106–110.
- Reigosa-Chamorro, F., Raposo, L.R., Munín-Cruz, P., Pereira, M.T., Roma-Rodrigues, C., Baptista, P.V., Fernandes, A.R., Vila, J.M., 2021. In vitro and in vivo effect of palladacycles: targeting A2780 ovarian carcinoma cells and modulation of angiogenesis. *Inorg. Chem.* 60, 3939–3951.
- Riccardi, C., Nicoletti, I., 2006. Analysis of apoptosis by propidium iodide staining and flow cytometry. *Nat. Protoc.* 1, 1458–1461.
- Rudbari, H.A., Kordestani, N., Cuevas-Vicario, J.V., Zhou, M., Efferth, T., Correia, I., Schirmeister, T., Barthels, F., Enamullah, M., Fernandes, A.R., 2022. Investigation of the influence of chirality and halogen atoms on the anticancer activity of enantiopure palladium (II) complexes derived from chiral amino-alcohol Schiff bases and 2-picolyamine. *New J. Chem.* 46, 6470–6483.
- Scattolin, T., Bortolamiol, E., Visentin, F., Palazzolo, S., Caligiuri, I., Perin, T., Canzonieri, V., Demitri, N., Rizzolio, F., Togni, A., 2020. Palladium(II)-η(3)-allyl complexes bearing N-trifluoromethyl N-heterocyclic carbenes: a new generation of anticancer agents that restrain the growth of high-grade serous ovarian cancer tumoroids. *Chemistry* 26, 11868–11876.
- Scattolin, T., Voloshkin, V.A., Visentin, F., Nolan, S.P., 2021. A critical review of palladium organometallic anticancer agents. *Cell Rep. Phys. Sci.* 2, 100446.
- Shibuya, S., Watanabe, K., Tsuji, G., Ichihashi, M., Shimizu, T., 2019. Platinum and palladium nanoparticle-containing mixture, PAPANAL, does not induce palladium allergy. *Exp. Dermatol.* 28, 1025–1028.
- Siegel, R.L., Miller, K.D., Fuchs, H.E., Jemal, A., 2022. Cancer Statistics, 2022. *CA Cancer J. Clin.* 72, 7–33.
- Sinha, S., Levine, B., 2008. The autophagy effector Beclin 1: a novel BH3-only protein. *Oncogene* 27 (Suppl. 1), S137–S148.
- Soldani, C., Scovassi, A.L., 2002. Poly(ADP-ribose) polymerase-1 cleavage during apoptosis: an update. *Apoptosis* 7, 321–328.
- Sung, H., Ferlay, J., Siegel, R.L., Laversanne, M., Soerjomataram, I., Jemal, A., Bray, F., 2021. Global Cancer Statistics 2020: GLOBOCAN estimates of incidence and mortality worldwide for 36 cancers in 185 countries. *CA A Cancer J. Clin.* 71, 209–249.
- Susin, S.A., Lorenzo, H.K., Zamzami, N., Marzo, I., Snow, B.E., Brothers, G.M., Mangion, J., Jacotot, E., Costantini, P., Loeffler, M., Larochette, N., Goodlett, D.R., Aebbersold, R., Siderovski, D.P., Pennings, J.M., Kroemer, G., 1999. Molecular characterization of mitochondrial apoptosis-inducing factor. *Nature* 397, 441–446.
- Vojtek, M., Gonçalves-Monteiro, S., Pinto, E., Kalivodová, S., Almeida, A., Marques, M.P.M., Batista de Carvalho, A.L.M., Martins, C.B., Mota-Filipe, H., Ferreira, I., Diniz, C., 2021. Preclinical pharmacokinetics and biodistribution of anticancer dinuclear palladium(II)-spermine complex (Pd(2)Spm) in mice. *Pharmaceuticals* 14, 173.
- Wang, Y., Dawson, V.L., Dawson, T.M., 2009. Poly(ADP-ribose) signals to mitochondrial AIF: a key event in parthanatos. *Exp. Neurol.* 218, 193–202.
- Wang, Y., Kim, N.S., Haince, J.-F., Kang, H.C., David, K.K., Andrabi, S.A., Poirier, G.G., Dawson, V.L., Dawson, T.M., 2011. Poly(ADP-Ribose) (PAR) binding to apoptosis-inducing factor is critical for PAR polymerase-1-dependent cell death (parthanatos). *Sci. Signal.* 4 ra20-ra20.
- Wang, Y., Luo, W., Wang, Y., 2019. PARP-1 and its associated nucleases in DNA damage response. *DNA Repair* 81, 102651.
- Wong, R.S.Y., 2011. Apoptosis in cancer: from pathogenesis to treatment. *J. Exp. Clin. Cancer Res.* 30, 87.
- Yan, G., Elbadawi, M., Efferth, T., 2020. Multiple cell death modalities and their key features (Review). *World Acad Sci J* 2, 39–48.
- Yu, S.W., Andrabi, S.A., Wang, H., Kim, N.S., Poirier, G.G., Dawson, T.M., Dawson, V.L., 2006. Apoptosis-inducing factor mediates poly(ADP-ribose) (PAR) polymer-induced cell death. *Proc. Natl. Acad. Sci. U.S.A.* 103, 18314–18319.
- Yu, S.W., Wang, H., Poitras, M.F., Coombs, C., Bowers, W.J., Federoff, H.J., Poirier, G.G., Dawson, T.M., Dawson, V.L., 2002. Mediation of poly(ADP-ribose) polymerase-1-dependent cell death by apoptosis-inducing factor. *Science* 297, 259–263.
- Zhang, J., Liu, D., Zhang, M., Zhang, Y., 2019. Programmed necrosis in cardiomyocytes: mitochondria, death receptors and beyond. *Br. J. Pharmacol.* 176, 4319–4339.
- Zhao, N., Mao, Y., Han, G., Ju, Q., Zhou, L., Liu, F., Xu, Y., Zhao, X., 2015. YMI55, a survivin suppressant, triggers PARP-dependent cell death (parthanatos) and inhibits esophageal squamous-cell carcinoma xenografts in mice. *Oncotarget* 6, 18445–18459.
- Zhou, M., Boulos, J.C., Klauk, S.M., Efferth, T., 2023. The cardiac glycoside ZINC253504760 induces parthanatos-type cell death and G2/M arrest via downregulation of MEK1/2 phosphorylation in leukemia cells. *Cell Biol. Toxicol.*
- Zhou, Y., Liu, L., Tao, S., Yao, Y., Wang, Y., Wei, Q., Shao, A., Deng, Y., 2021. Parthanatos and its associated components: promising therapeutic targets for cancer. *Pharmacol. Res.* 163, 105299.

Article

Modes of Action of a Novel c-MYC Inhibiting 1,2,4-Oxadiazole Derivative in Leukemia and Breast Cancer Cells

Min Zhou ¹, Joelle C. Boulos ¹, Ejlal A. Omer ¹, Sabine M. Klauck ² and Thomas Efferth ^{1,*} 

¹ Department of Pharmaceutical Biology, Institute of Pharmaceutical and Biomedical Sciences, Johannes Gutenberg University-Mainz, Staudinger Weg 5, 55128 Mainz, Germany

² Division of Cancer Genome Research, German Cancer Research Center (DKFZ), German Cancer Consortium (DKTK), National Center for Tumor Disease (NCT), Im Neuenheimer Feld 460, 69120 Heidelberg, Germany

* Correspondence: efferth@uni-mainz.de; Tel.: +49-6131-392-5751; Fax: +49-6131-392-3752

Abstract: The *c-MYC* oncogene regulates multiple cellular activities and is a potent driver of many highly aggressive human cancers, such as leukemia and triple-negative breast cancer. The oxadiazole class of compounds has gained increasing interest for its anticancer activities. The aim of this study was to investigate the molecular modes of action of a 1,2,4-oxadiazole derivative (ZINC15675948) as a *c-MYC* inhibitor. ZINC15675948 displayed profound cytotoxicity at the nanomolar range in CCRF-CEM leukemia and MDA-MB-231-pcDNA3 breast cancer cells. Multidrug-resistant sublines thereof (i.e., CEM/ADR5000 and MDA-MB-231-BCRP) were moderately cross-resistant to this compound (<10-fold). Molecular docking and microscale thermophoresis revealed a strong binding of ZINC15675948 to *c-MYC* by interacting close to the *c-MYC*/MAX interface. A *c-MYC* reporter assay demonstrated that ZINC15675948 inhibited *c-MYC* activity. Western blotting and qRT-PCR showed that *c-MYC* expression was downregulated by ZINC15675948. Applying microarray hybridization and signaling pathway analyses, ZINC15675948 affected signaling routes downstream of *c-MYC* in both leukemia and breast cancer cells as demonstrated by the induction of DNA damage using single cell gel electrophoresis (alkaline comet assay) and induction of apoptosis using flow cytometry. ZINC15675948 also caused G2/M phase and S phase arrest in CCRF-CEM cells and MDA-MB-231-pcDNA3 cells, respectively, accompanied by the downregulation of CDK1 and p-CDK2 expression using western blotting. Autophagy induction was observed in CCRF-CEM cells but not MDA-MB-231-pcDNA3 cells. Furthermore, microarray-based mRNA expression profiling indicated that ZINC15675948 may target *c-MYC*-regulated ubiquitination, since the novel ubiquitin ligase (ELL2) was upregulated in the absence of *c-MYC* expression. We propose that ZINC15675948 is a promising natural product-derived compound targeting *c-MYC* in *c-MYC*-driven cancers through DNA damage, cell cycle arrest, and apoptosis.

Keywords: 1,2,4-oxadiazole; *c-MYC* inhibitor; leukemia; natural product derivative; oncogenes; triple-negative breast cancer



Citation: Zhou, M.; Boulos, J.C.; Omer, E.A.; Klauck, S.M.; Efferth, T. Modes of Action of a Novel *c-MYC* Inhibiting 1,2,4-Oxadiazole Derivative in Leukemia and Breast Cancer Cells. *Molecules* **2023**, *28*, 5658. <https://doi.org/10.3390/molecules28155658>

Academic Editors: M. Mizerska-Kowalska, Wojciech Płaziński, Sylwia Sowa and Roman Paduch

Received: 16 June 2023

Revised: 19 July 2023

Accepted: 24 July 2023

Published: 26 July 2023



Copyright: © 2023 by the authors. Licensee MDPI, Basel, Switzerland. This article is an open access article distributed under the terms and conditions of the Creative Commons Attribution (CC BY) license (<https://creativecommons.org/licenses/by/4.0/>).

1. Introduction

Cancer is mainly caused by genomic alterations that result from the loss of tumor suppressor genes and the activation of oncogenes [1]. The *MYC* gene is one of the oncogenes that has been described as a master regulator of gene expression in multiple biological processes [2,3]. This gene encodes a family of basic helix-loop-helix zipper (bHLHZip) proteins consisting of *c-MYC*, *N-MYC*, and *L-MYC* [4]. *MYC* acts as a transcription factor that binds to its obligatory partner, *MYC*-associated factor X (MAX). The *MYC*-MAX heterodimer activates a large number of genes by binding to E box sequences (5'-CACGTG-3') within gene promoters and enhancers [5].

MYC-regulated transcription is tightly controlled in non-transformed cells. However, *MYC* is estimated to be overexpressed up to 70% in various human cancer types [6].

MYC contributes to several hallmarks of cancer, including the escape from programmed cell death, promoting sustainable proliferation, genome instability, escape from immunosurveillance, and change of cellular metabolism [7,8]. The major mechanisms of MYC deregulation are gene alternation and the activation of upstream MYC-related signaling pathways (e.g., NOTCH, WNT, and EGFR) [9]. Moreover, MYC is an unstable protein with a short half-life [10], and its stability is also regulated by post-translational modifications [11]. For example, MYC gene amplification largely drives breast carcinogenesis [12], and the chromosomal translocation of the MYC gene contributes to the development of T-cell acute leukemia [13]. In mice with MYC-induced hematological cancers, an inactivation of the MYC transgene led to tumor regression [14]. To date, there is no approved MYC inhibitor, despite several promising MYC inhibitors being investigated in preclinical or clinical studies [8]. Therefore, there is an ongoing quest for novel effective MYC inhibitors for an improvement of cancer therapy with targeted drugs.

Natural products are a promising resource for drug discovery [15]. Oxadiazole represents a five-membered heterocyclic scaffold with one oxygen and two nitrogen atoms. Oxadiazole-based compounds are a rapidly growing field in drug development. They are fundamental pharmacophores due to their stability in aqueous medium and are commonly employed as bioisosteric substitutes [16,17]. Based on the position of oxygen and nitrogen in the ring, oxadiazoles are classified into four regioisomeric structures [18]. In addition, 1,2,4-Oxadiazoles received considerable attention as witnessed by increasing numbers of published studies [19]. The first natural products from the class of 1,2,4-oxadiazoles were phidianidine A and B that were isolated from marine mollusk *Phidiana militaris* by Alder and Hancock [20]. Interestingly, phidianidine A was identified as an antifoulant agent which is a chemical defense of slow-moving marine organisms to deter predators, other colonizers, or competitors [21]. In the past two decades, a great number of 1,2,4-oxadiazole derivatives were synthesized and studied for their pharmacological properties, which exhibit numerous bioactivities, including anti-cancer [22,23], anti-inflammatory [24], anti-bacterial [25], anti-viral [26], anti-malarial [27], anti-diabetic [28], and anti-Alzheimer activities [29]. Zibotentan represents an example of an oxadiazole that reached a clinical phase III trial for the treatment of hormone-resistant prostate carcinoma [30]. Studies revealed that 1,2,4-oxadiazoles derivatives exhibited more powerful anticancer activities than established drugs (e.g., doxorubicin and etoposide) by inhibiting cell proliferation which make them appealing as prospective therapeutic candidates [16,18]. However, the modes of action of 1,2,4-oxadiazoles derivatives in cancer have not been fully understood yet.

Breast cancer is the most common malignancy in females worldwide. Triple-negative breast cancer (TNBC) is characterized by the absence of estrogen (ER)/progesterone (PR) expression and human epidermal growth factor receptor-2 (HER2) amplification [31]. MYC is remarkably elevated in TNBC compared with other breast cancer subtypes. TNBC is highly invasive leading to a poor five-year survival rate and distant recurrence rates [12,32]. On the other hand, acute lymphoblastic leukemia (ALL) is an aggressive hematological cancer frequently appearing in children and adolescents. A multitude of evidence supports the important role of MYC in the initiation and progression of ALL [33].

The aim of this study was to investigate the 1,2,4-oxadiazoles derivative ZINC15675948 as a novel c-MYC inhibitor. We determined the anticancer activity of ZINC15675948 against drug-sensitive and -resistant leukemia (CCRF-CEM and CEM/ADR5000) and triple-negative breast cancer (MDA-MB-231-pcDNA3 and MDA-MB-BCRP) cell lines. The effects of ZINC15675948 were studied by using western blot, qRT-PCR, molecular docking, microscale thermophoresis, and c-MYC reporter assay. By means of microarray hybridization and Ingenuity Pathway Analysis, we explored the underlying modes of action of ZINC15675948 regarding cell cycle, apoptosis, autophagy, and DNA damage. In addition, the interactions of ZINC15675948 with the multidrug-resistance-mediating ATP-binding cassette transporters' P-glycoprotein and breast cancer resistance protein were investigated using molecular docking.

2. Results

2.1. Growth Inhibition Assay

ZINC15675948 exhibited profound cytotoxicity toward both leukemia and breast cancer cell lines using resazurin reduction assays. Doxorubicin was used as a positive control [34]. CCRF-CEM and MDA-MB-231-pcDNA3 cells were extremely sensitive to ZINC15675948 with IC_{50} values of $0.008 \pm 0.001 \mu\text{M}$, and $0.08 \pm 0.004 \mu\text{M}$, respectively. It is interesting that CEM/ADR5000 cells as well as MDA-MB-BCRP cells displayed cross-resistance toward ZINC15675948 (degrees of resistance: 8.37 and 9.0, respectively). The dose-response curves are shown in Figure 1C,D, and the IC_{50} values and degrees of resistance are presented in Table 1.

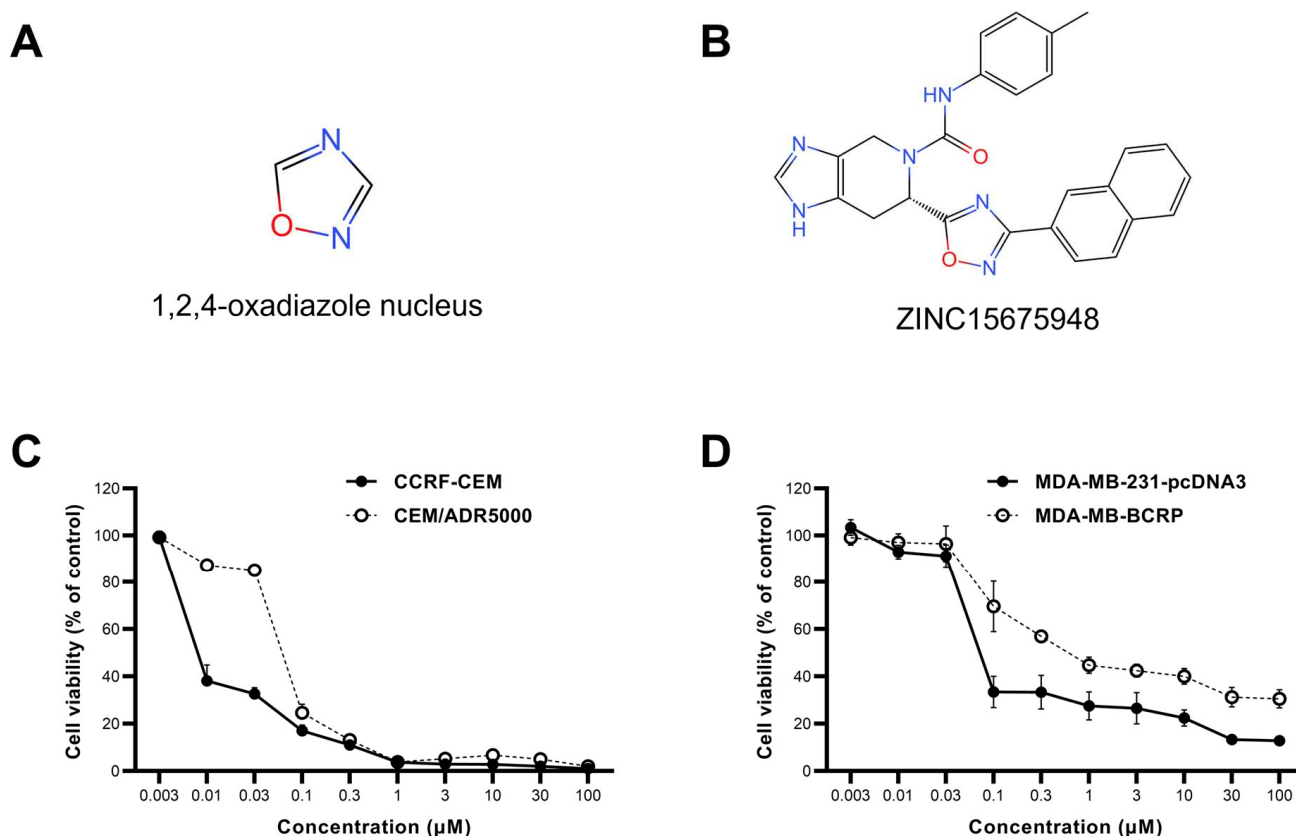


Figure 1. The chemical structure and dose-response curve of ZINC15675948 determined by using the resazurin reduction assay. (A) 1,2,4-Oxadiazole nucleus. (B) Chemical structure of ZINC15675948. (C) Growth inhibition of ZINC15675948 toward leukemia CCRF-CEM and P-glycoprotein-overexpressing CEM/ADR5000 cell lines. (D) Growth inhibition of ZINC15675948 toward triple-negative breast cancer MDA-MB-231-pcDNA3 and BCRP overexpressing MDA-MB-BCRP cell lines. The data were plotted as mean \pm SD from three independent experiments with each of the 6 parallel measurements.

Table 1. Cytotoxicity of ZINC15675948 toward drug-sensitive and -resistant cancer cell lines measured by resazurin reduction assay. CEM/ADR5000 and MDA-MB-BCRP were the two cell lines displaying multidrug-resistant phenotypes by overexpressing P-glycoprotein and BCRP, respectively.

Cell Lines	IC_{50} (μM)	Degree of Resistance
CCRF-CEM	0.008 ± 0.001	8.37
CEM/ADR5000	0.071 ± 0.002	
MDA-MB-231-pcDNA3	0.08 ± 0.004	9
MDA-MB-BCRP	0.72 ± 0.07	

As multidrug-resistant cell lines were cross-resistant to ZINC15675948, further investigations using ZINC15675948 were performed only in CCRF-CEM and MDA-MB-231-pcDNA3 cells.

2.2. Molecular Docking

The oncogene *MYC* is deregulated in various human cancers and drives several cancer-related hallmarks. Despite its unquestionable contribution to cancer development, *MYC* has been regarded as undruggable, and there are only a few *MYC* inhibitors so far [35,36]. The aim of this study was targeting *c-MYC* by ZINC15675948, as demonstrated below with different *in vitro* verifications and pathway analysis of microarray data. To investigate the possible interaction and binding affinity of ZINC15675948 to *c-MYC*, molecular docking was performed using AutoDock 4.2.6. As shown in Figure 2A, the binding site of ZINC15675948 bound to *c-MYC* was almost the same as for the known *MYC*-inhibiting control drugs. ZINC15675948 was particularly near to 10058-F4 and 10074-A4, and Arg925 and Gln927 were two common amino acid residues shown in the interactions, and Gln 927 displayed hydrogen-bonding (Figure 2B–D). Table 2 illustrates that ZINC15675948 displayed a strong binding to *c-MYC*, revealed by a lowest binding energy (LBE) value of -9.91 kcal/mol and a predicted inhibition constant (*pKi*) of 0.05 μ M. In comparison, the binding affinities of known *c-MYC* inhibitors were weak (LBE value of 10058-F4: -4.92 kcal/mol; LBE value of 10074-A4: -6.42 ± 0.01 kcal/mol; LBE value of 10074-G5: -6.96 ± 0.01 kcal/mol).

Table 2. Molecular docking results of ZINC15675948 and known inhibitors 10058-F4, 10074-A4, and 10075-G5 (positive control) to *c-MYC*.

Compound	Lowest Binding Energy (kcal/mol)	<i>pKi</i> (μ M)	Amino Acids Interactions (Residues in H-Bond Bolded)
ZINC15675948	-9.91	0.055	Arg924, Asp926, Gln927 , Tyr949, Ile950, Val953
10058-F4	-4.92	247.03 ± 1.5	Arg925, Gln927 , Pro929, Leu931, Glu932
10074-A4	-6.42 ± 0.01	19.53 ± 0.30	Arg925, Asp926 , Gln927
10074-G5	-6.96 ± 0.01	7.93 ± 0.13	Pro929, Pro930 , Lys945, Ala948

To better understand the cross-resistance of CCRF-CEM and MDA-MB-231-pcDNA3 cells toward ZINC15675948, molecular docking of ZINC15675948 towards P-gp and BCRP was carried out. Table 3 revealed that ZINC15675948 showed high binding affinities to P-gp and BCRP (LBE values: -10.55 ± 0.24 kcal/mol and -11.49 kcal/mol, respectively). The binding site of ZINC15675948 to P-gp was similar to doxorubicin (Figure 3A). They shared the same amino acid with Trp232 and Gln990 on P-gp (Figure 3B,C). ZINC15675948, likewise doxorubicin, bound to the substrate-binding site on P-gp. However, the binding site of ZINC15675948 was similar to both doxorubicin and Ko143 (Figure 3E–H). We further performed a doxorubicin uptake assay (Section 2.11) to pinpoint whether ZINC15675948 is an inhibitor or substrate of P-gp and BCRP.

2.3. Microscale Thermophoresis

To confirm the *in silico* binding of ZINC15675948 to *c-MYC* with an *in vitro* assay, we applied microscale thermophoresis (MST). As shown in Figure 2F, the measurement of the concentration-dependent fluorescence signals revealed an interaction between the fluorescently labeled *c-MYC* protein and ZINC15675948. ZINC15675948 bound to *c-MYC* with a K_d of 1.08 ± 0.1 μ M.

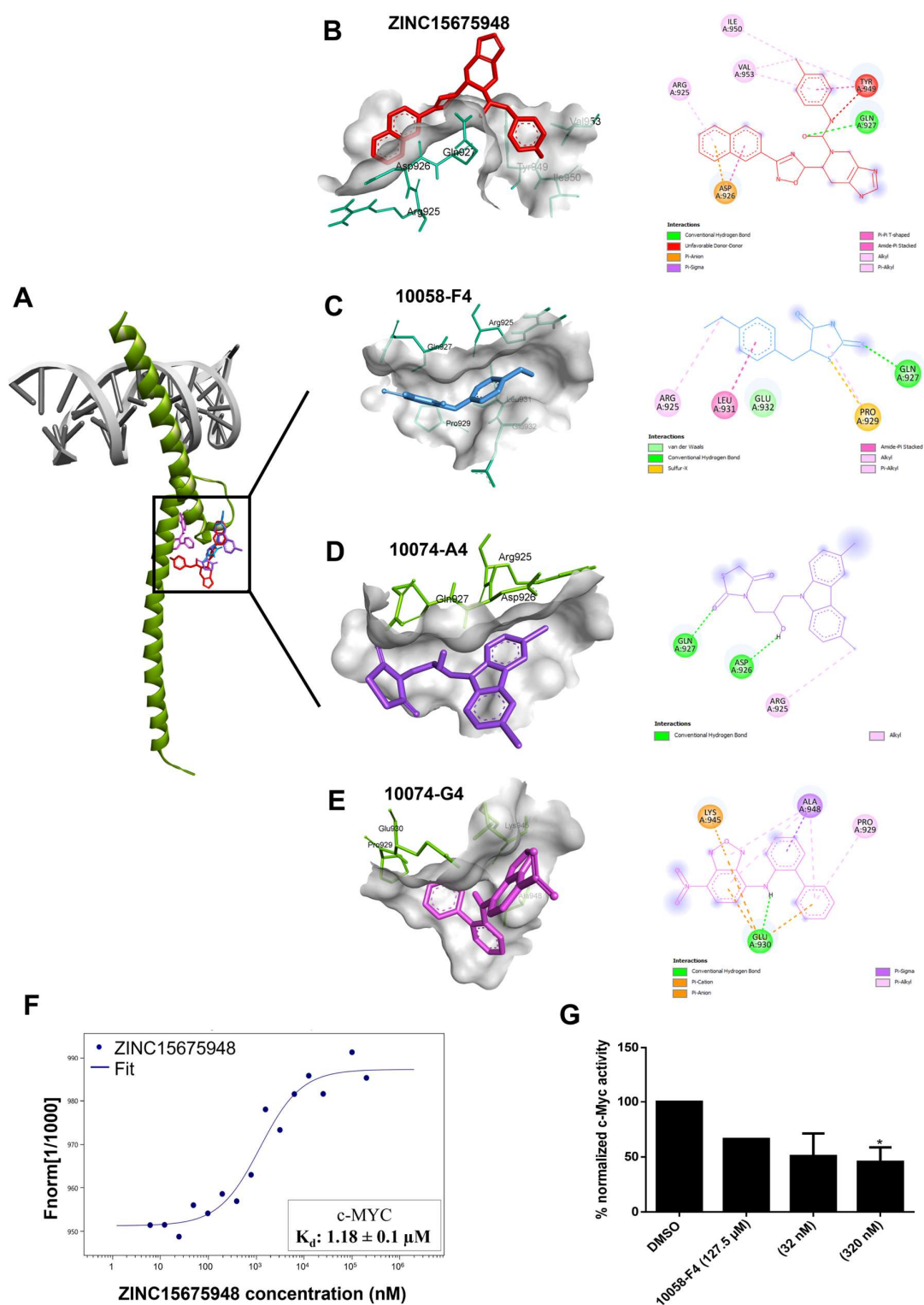


Figure 2. Inhibition of c-MYC by ZINC15675948. (A) In silico molecular docking of ZINC15675948 and three known inhibitors 100F4-58, 10074-A4, and 10074-G5 to c-MYC. (B) Interacting amino acids of ZINC15675948 (red), (C) 10058-F4 (blue), (D) 10074-A4 (purple), (E) 10074-G4 (violet) interacting with c-MYC as visualized by Discovery Studio. (F) Binding kinetics of ZINC15675948 bound to c-MYC obtained by microscale thermophoresis. (G) Inhibition of c-MYC activity by ZINC15675948 as determined by a c-MYC reporter assay. Statistical significance ($* p \leq 0.05$) was compared to DMSO (negative control). All experiments were performed three times independently.

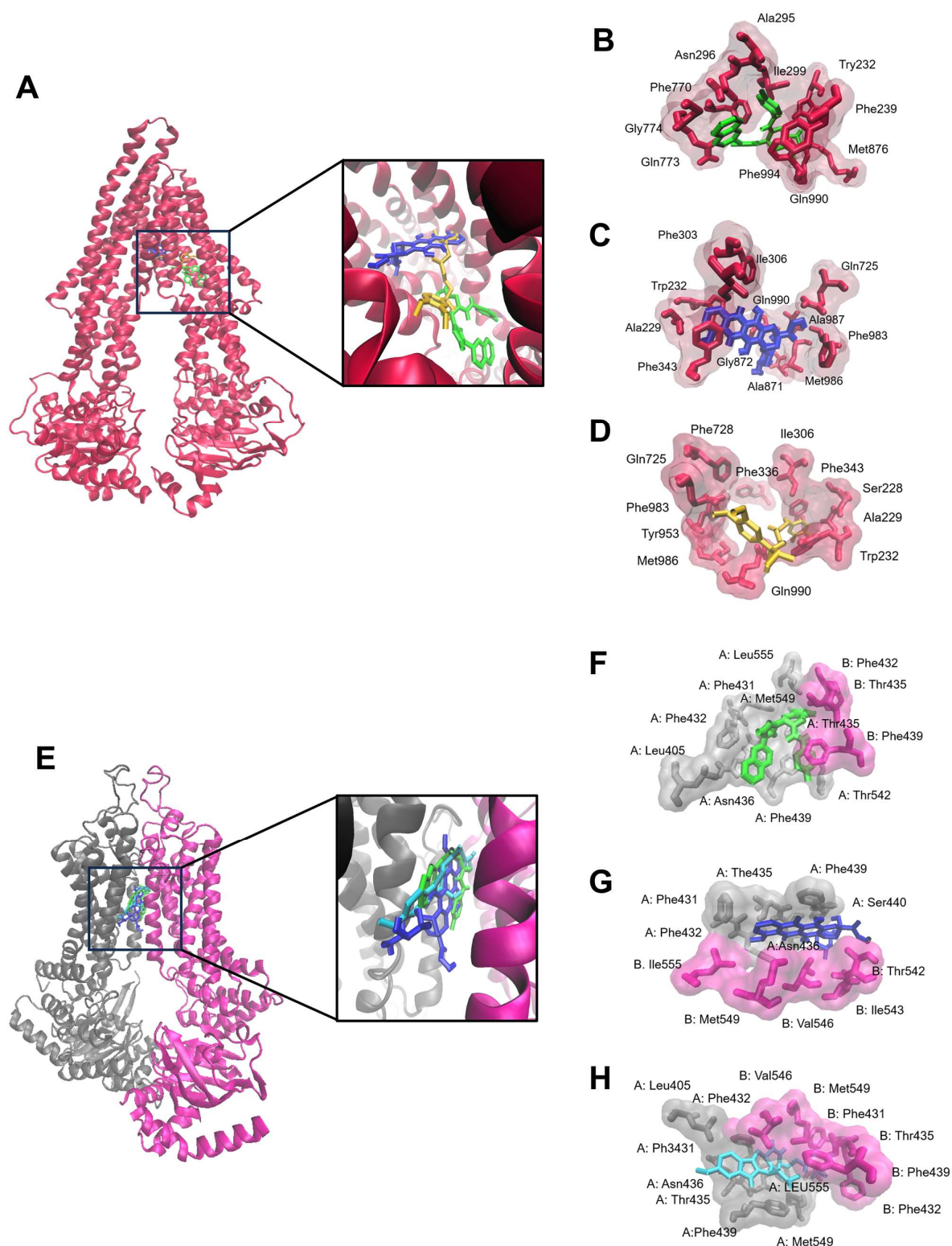


Figure 3. Molecular docking of ZINC15675948 to the ABC transporters (A) P-gp and (E) BCRP. The proteins were presented in a new cartoon format. The ligands were displayed using a dynamic bond format with different colors: ZINC15675948 (green), doxorubicin (blue), verapamil (yellow), and Ko143 (cyan). The binding sites were visualized by P-gp residues that interact with (B) ZINC15675948, (C) doxorubicin, and (D) verapamil, as well as BCRP residues that interact with (F) ZINC15675948, (G) doxorubicin and (H) Ko143, are shown in a QuickSurf format.

Table 3. In silico molecular docking of ZINC15675948 and control drugs (doxorubicin, verapamil, and Ko143) to P-gp and BCRP.

Protein	Compound	Lowest Binding Energy (kcal/mol)	pKi (μM)	Amino Acids Interactions (Residues in H-Bond Bolded)
P-gp	ZINC15675948	−10.55 ± 0.24	0.07 ± 0.01	Trp232, Phe239, Ala295, Asn296, Ile299, Phe770, Gln773 , Gly774, Met876, Gln990, Phe994
	Doxorubicin	−6.42 ± 0.05	147.35 ± 72.62	Ala229, Trp232, Phe303, Ile306, Phe343, Gln725, Ala871, Gly872, Phe983, Met986, Ala987, Gln990
	Verapamil	−7.61 ± 0.31	3.0 ± 1.46	Ser228, Ala229, Trp232, Ile306, Phe336, Phe343, Gln725, Phe728, Tyr953, Phe983, Met986, Gln990
BCRP	ZINC15675948	−11.49 ± 0.01	0.007 ± 0.004	A: Leu405, Phe431, Phe432, Thr435, Asn436, Phe439, Thr542, Met549, Leu555 B: Phe432, Thr435, Phe439
	Doxorubicin	−7.00 ± 0.49	122.79 ± 10.96	A: Phe431, Phe432, The435, Asn436, Phe439, Ser440 B: The542, Ile 543, Val546, Met549, Ile555
	Ko143	−10.24 ± 0.19	0.03 ± 0.01	A: Leu405, Phe431, Phe432, Thr435, Asn436, Phe439, Met549, Leu555 B: Phe431, Phe32, Thr435 , Phe439, Val546, Met549

2.4. c-MYC Reporter Assay

To determine whether the c-MYC activity could be diminished by ZINC15675948 binding, we performed c-MYC reporter assays in HEK293 cells with a transfected c-MYC-luciferase reporter construct. Notably, the c-MYC activity was suppressed by ZINC15675948 in a concentration-dependent manner. A significant inhibition was observed at a concentration of 320 nM (Figure 2G). Surprisingly, 10058-F4 as a positive control only showed a slight inhibition. Therefore, ZINC15675948 indeed inhibited c-MYC activity as consistently also demonstrated with molecular docking, microscale thermophoresis, and as illustrated below by western blotting and qRT-PCR.

2.5. Gene Expression Profile of Cell Lines Using Microarray Analyses

The gene expression measured using mRNA microarray hybridization was filtered by Chipster software (version 3.16.3). A total of 329 and 314 genes were significantly deregulated in CCRF-CEM cells and MDA-MB-231-pcDNA3 cells, respectively, compared with their untreated samples (Supplementary Tables S1 and S2). The deregulated genes were further analyzed by Ingenuity Pathway Analysis (IPA) to predict canonical pathways, networks, and cellular functions and diseases affected by ZIN15675948. Here, we did not observe any potentially impacted canonical pathways. Interestingly, several affected cellular functions were commonly revealed in the two cell lines, including “cell death and survival”, “cell cycle”, “cellular growth and proliferation”, as well as “DNA replication, recombination and repair” (Figure 4). “Cancer” and “hematological disease” were affected correspondingly by ZINC15675948 in CCRF-CEM cells. MDA-MB-231-pcDNA3 cells also showed “cancer” as an important affected disease. Therefore, we further investigated the roles of the cell cycle, apoptosis, autophagy, and DNA damage to verify these microarray-based results by independent other methods.

We further accessed the networks under different cellular functions to unravel the genes that were involved. The IPA-based comparison of untreated and ZINC15675948-treated CCRF-CEM cells indeed also revealed a downregulation of the c-MYC gene as illustrated in Figure 5A,B. These networks are related to cell cycle and cell death, implying that they were downstream and affected by the c-MYC gene. However, the c-MYC gene did not appear in the gene expression profiles of MDA-MB-231-pcDNA3 cells. The cell death network revealed that *MCL-1* and *BAD* were downregulated accompanied by an upregulation of *SQSTM1* (p62) (Figure 5C). Furthermore, Figure 5D shows that the *ELL2* gene was upregulated, which is involved in the proteasomal degradation of c-MYC [37,38].

The tumor suppressor *TP53* was upregulated, which may be a consequence of *c-MYC* downregulation as we will discuss below.



Figure 4. Gene expression profiling as determined by Ingenuity Pathway Analysis (IPA) of CCRF-CEM and MDA-MB-231-pcDNA3 cells upon treatment with the IC_{50} concentration of ZINC15675948 for 24 h. Top cellular functions (red boxes) and diseases (green boxes) affected by ZINC15675948 in (A) CCRF-CEM and (B) MDA-MB-231-pcDNA3 cells. CCRF-CEM.

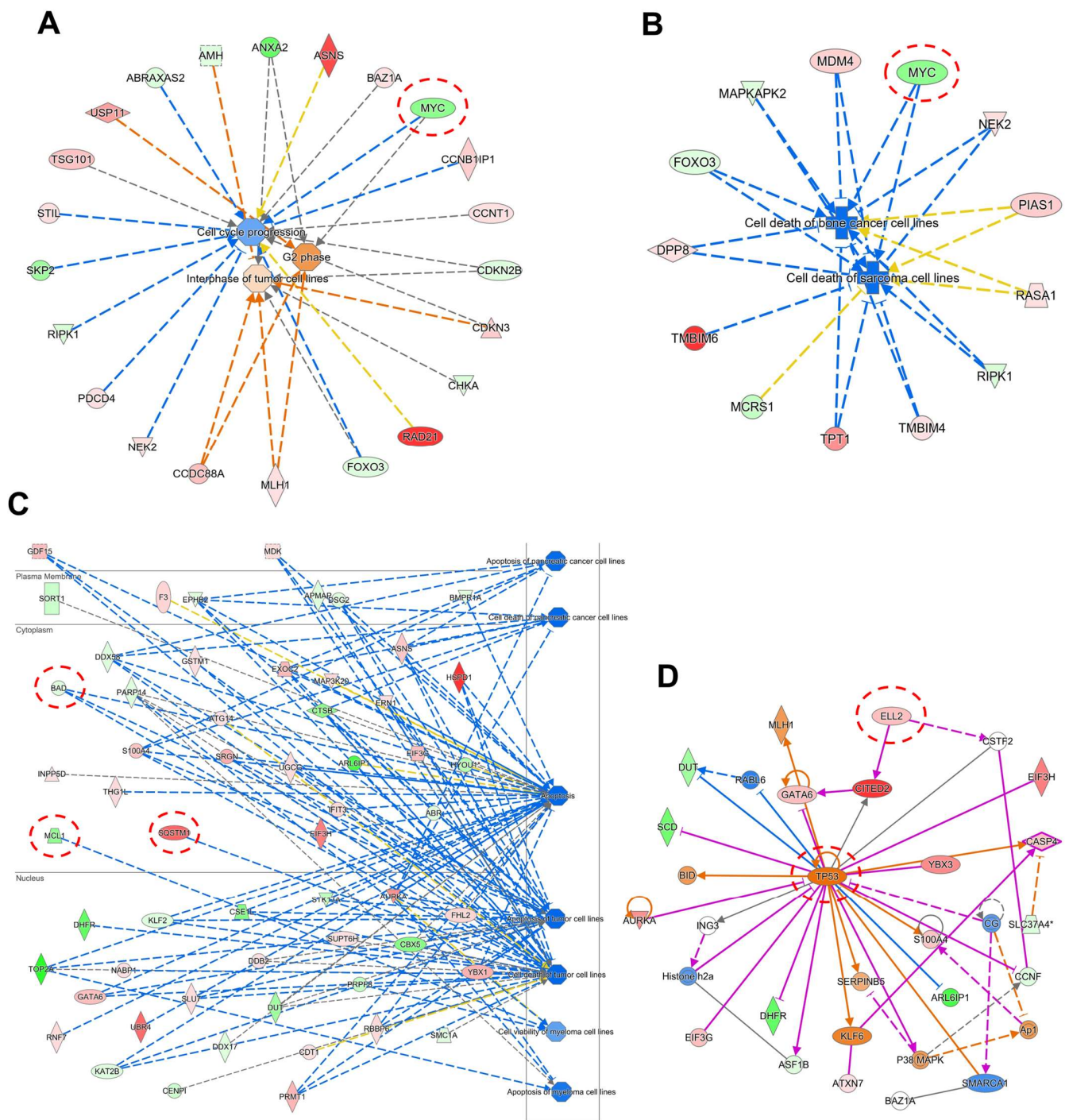


Figure 5. Molecular network generated using IPA software (content version: 51963813) from mRNA microarray hybridization affected by ZINC15675948 in CCRF-CEM and MDA-MB-231-pcDNA3 cells. (A) Cell cycle network in CCRF-CEM cells. The red circle highlights that *c-MYC* was downregulated and related to cell cycle regulation. (B) Cell death network in CCRF-CEM cells. The red circle highlights that *c-MYC* was also downregulated and involved in cell death. (C) Cell cycle network in MDA-MB-231-pcDNA3 cells. The red circles highlight that *SQSTM1* (*p62*) was upregulated, while *MCL-1* and *BAD* were downregulated. (D) The red circles highlight that *TP53* and *ELL2* were upregulated in MDA-MB-231-pcDNA3 cells.

2.6. Quantitative Reverse Transcription PCR (qRT-PCR)

The technical verifications of the results obtained from microarray hybridization were conducted with the top deregulated genes. Two upregulated and downregulated genes

(*RAD21*, *HMGC51*, *PGK1*, and *ATP5MF*) in CCRF-CEM cells, and two upregulated and downregulated genes (*HSPD1*, *CITED2*, *H4C3*, and *DHFR*) in MDA-MB-231-pcDNA3 cells were subjected to perform qRT-PCR (Figure 6A). The Pearson correlation coefficients were calculated between the determined fold change of microarray hybridization and qRT-PCR data. As shown in Figure 6B,C, the r value was 0.98 in CCRF-CEM cells and 0.97 in MDA-MB-231-pcDNA3 cells, confirming a high degree of concordance between these two different methods. Furthermore, the expression level of *c-MYC* was determined by qRT-PCR (Figure 6D). Treatment of ZINC15675948 (IC_{50}) significantly downregulated *c-MYC* ($p \leq 0.05$) in both leukemia and breast cancer cell lines, indicating that ZINC15675948 inhibited *c-MYC* at the gene expression level.

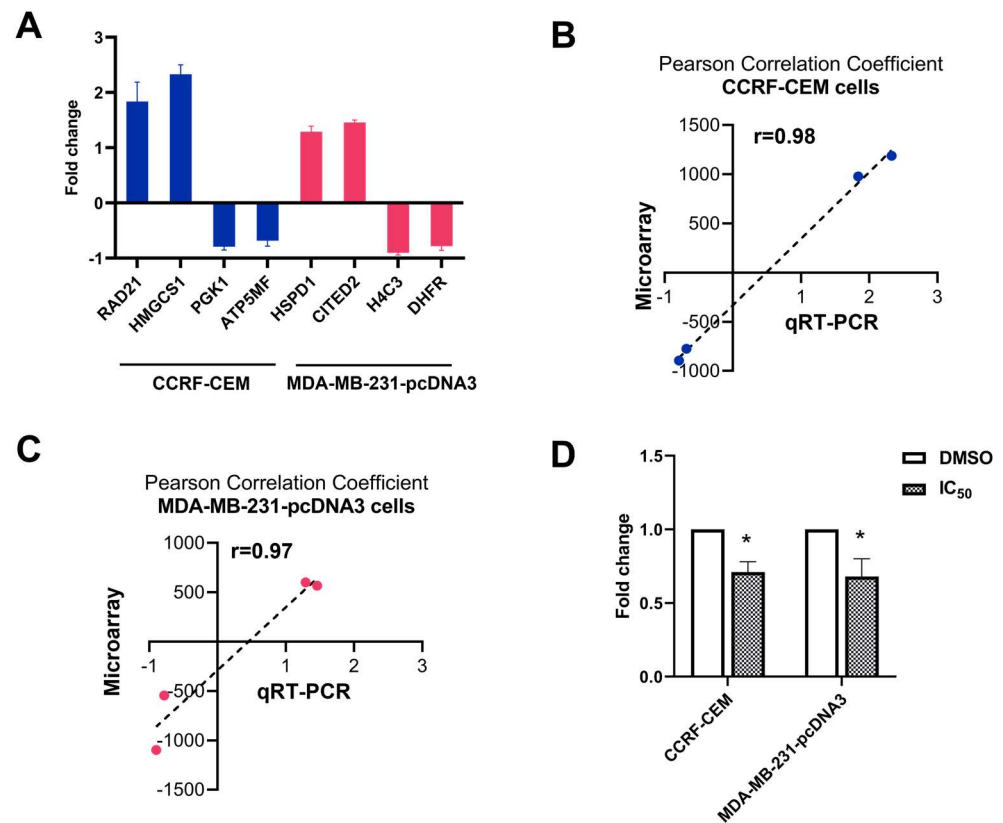


Figure 6. Technical and biological verifications by qRT-PCR analyses in CCRF-CEM and MDA-MB-231-pcDNA3 cells upon treatment with the IC_{50} concentration of ZINC15675948 for 24 h. (A) Technical verifications of the top four deregulated genes in CCRF-CEM cells and MDA-MB-231-pcDNA3 cells, respectively. Linear regressions and Pearson correlation coefficients of microarray and qRT-PCR data obtained in (B) CCRF-CEM cells and (C) MDA-MB-231-pcDNA3 cells. (D) Downregulation of *c-MYC* expression in CCRF-CEM and MDA-MB-231-pcDNA3 cells upon treatment with ZINC15675948. Statistical significance ($* p \leq 0.05$) was compared to control (DMSO). The results are represented as mean values \pm SD of three independent experiments.

2.7. Single Cell Gel Electrophoresis (Alkaline Comet Assay)

As “DNA replication, recombination and repair” appeared in our IPA analysis as “cellular functions” affected by ZINC15675948, we performed alkaline comet assays to detect DNA damage at the level of single cells. Representative images are shown in Figure 7. Compared with non-damaged control cells (DMSO), there was an increase in ZINC15675948-induced comet tails in both CCRF-CEM and MDA-MB-231-pcDNA3 cells, suggesting that DNA was indeed damaged. H_2O_2 as a positive control also led to clearly visible comet tails. The analysis of tails of each 50 cells revealed that ZINC15675948 induced DNA damage in both cell lines in a concentration-dependent manner.

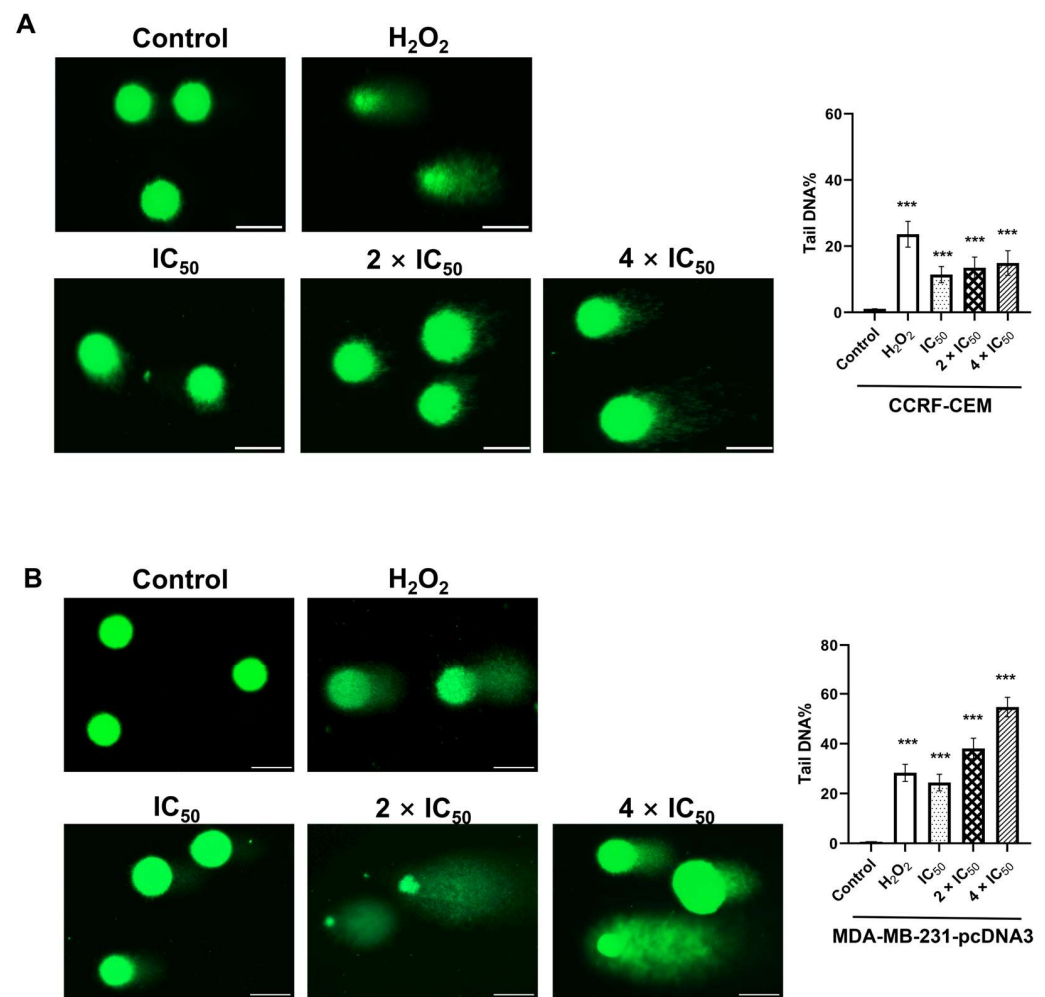


Figure 7. Analysis of DNA damage by single cell gel electrophoreses (alkaline comet assay) induced by ZINC15675948. Representative comet images captured in (A) CCRF-CEM and (B) MDA-MB-231-pcDNA3 cells treated with different concentrations for 24 h. H₂O₂ and DMSO served as positive or negative controls. Scale bar, 50 μ m. The graph showed tail DNA percentage presented as mean values \pm SEM from 50 comets. Statistical significance (***) $p \leq 0.001$ was compared to DMSO.

2.8. Cell Cycle Arrest

The IPA analysis of the microarray data also revealed that cell cycle progression was disturbed by ZINC15675948 in both CCRF-CEM and MDA-MB-231-pcDNA3 cells. Therefore, we investigated the cell cycle distribution by flow cytometry. Figure 8 shows that ZINC15675948 significantly increased the fraction of CCRF-CEM cells in the G2/M phase after treatment for 72 h, which was in a range of 28.25–33.3% at different concentrations compared with DMSO (15.0%). Whereas the S phase fraction of MDA-MB-231-pcDNA3 increased after 24 h. At the highest concentration ($2 \times IC_{50}$), S phase arrest reached 28.1% ($p < 0.01$) compared with DMSO as mock control, which was close to the positive control, cisplatin (36.2%) in MDA-MB-231-pcDNA3 cells. Hence, ZINC15675948 arrested the leukemia cells in the G2/M phase and the breast cancer cells in the S phase of the cell cycle.

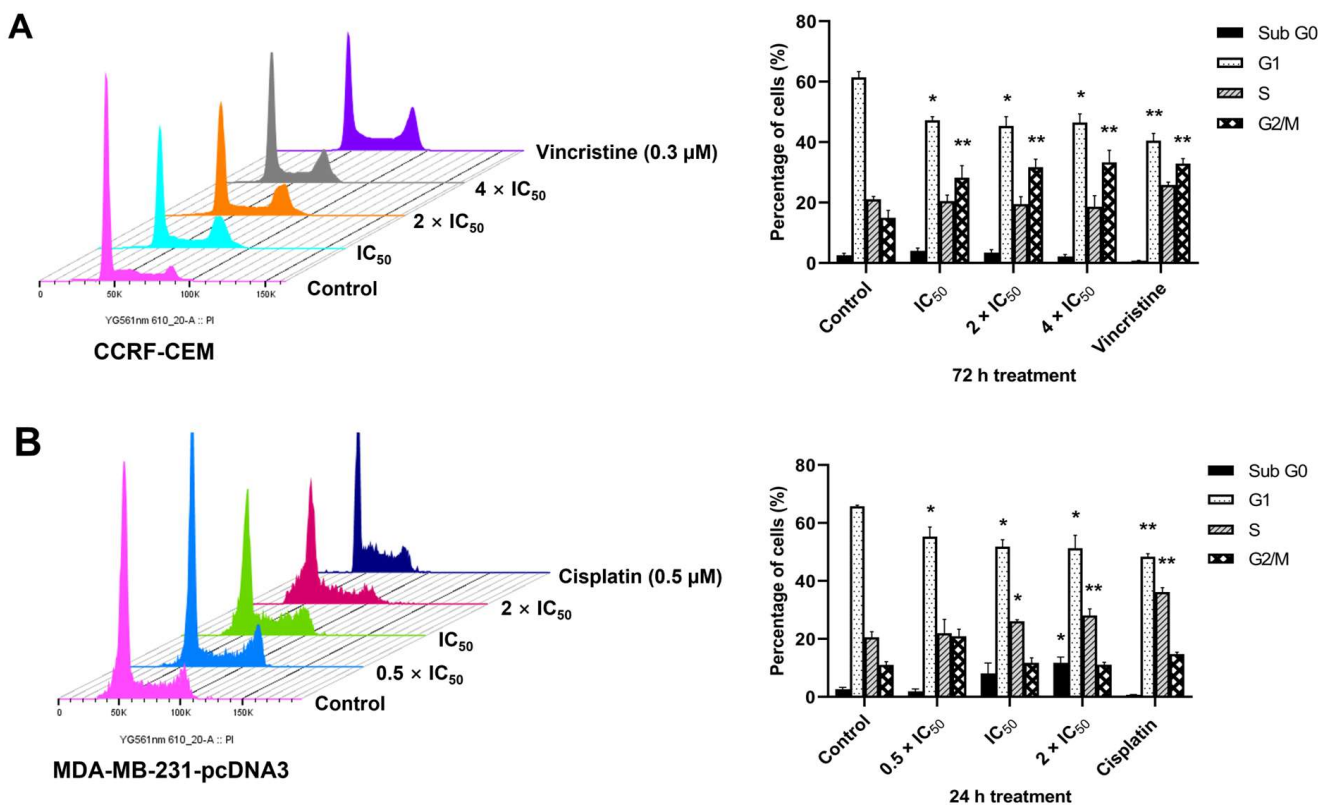


Figure 8. Cell cycle analysis with ZINC15675948. **(A)** Histograms of cell cycle distribution in CCRF-CEM cells upon treatment with different concentrations of ZINC15675948 for 72 h. Vincristine and DMSO were used as positive and negative controls. **(B)** Histograms of cell cycle distribution in MDA-MB-231-pcDNA3 cells upon treatment with ZINC15675948 for 24 h. Cisplatin and DMSO were used as positive and negative controls. The results were represented as mean \pm SD from three independent measurements. Statistical significance was analyzed using Student's *t*-test, * $p < 0.05$, ** $p < 0.01$ compared with DMSO.

2.9. Detection of Apoptosis

As “cell death and survival” was revealed as cellular function in the microarray analysis, we measured apoptosis induction by ZINC15675948 using flow cytometry and annexin V and PI double staining in CCRF-CEM cells and with F2N12S and SYTOX[®] AADvanced[™] dead cell staining in MDA-MB-231-pcDNA3 cells. As shown in Figure 9A, ZINC15675948 induced late apoptosis in CCRF-CEM cells in a time- and concentration-dependent manner. The late apoptotic cells remarkably increased to 41.4% at a concentration of $4 \times IC_{50}$ after 72 h, which was similar to the effect of 5 μ M vincristine (66%). In parallel, ZINC15675948 also induced apoptosis in MDA-MB-231-pcDNA3 cells after 48 h (Figure 9B). Especially, treatment with $4 \times IC_{50}$ resulted in 14.7% apoptotic cells compared to DMSO (5.9%). Therefore, ZINC15675948 significantly induced apoptosis in both cell lines.

2.10. Western Blotting

Western blotting was performed to study the expression of c-MYC and other proteins related to cell cycle and autophagy. CCRF-CEM cells and MDA-MB-231-pcDNA3 cells were treated with ZINC15675948 (IC_{50} , $2 \times IC_{50}$ and $4 \times IC_{50}$) for 24 h. Notably, the protein expression of c-MYC was significantly decreased at all concentrations in CCRF-CEM cells ($p \leq 0.01$). The decrease of c-MYC expression was significant at a concentration of $4 \times IC_{50}$ in MDA-MB-231-pcDNA3 cells ($p = 0.008$) (Figure 10). Therefore, ZINC15675948 inhibited c-MYC expression at the protein level.

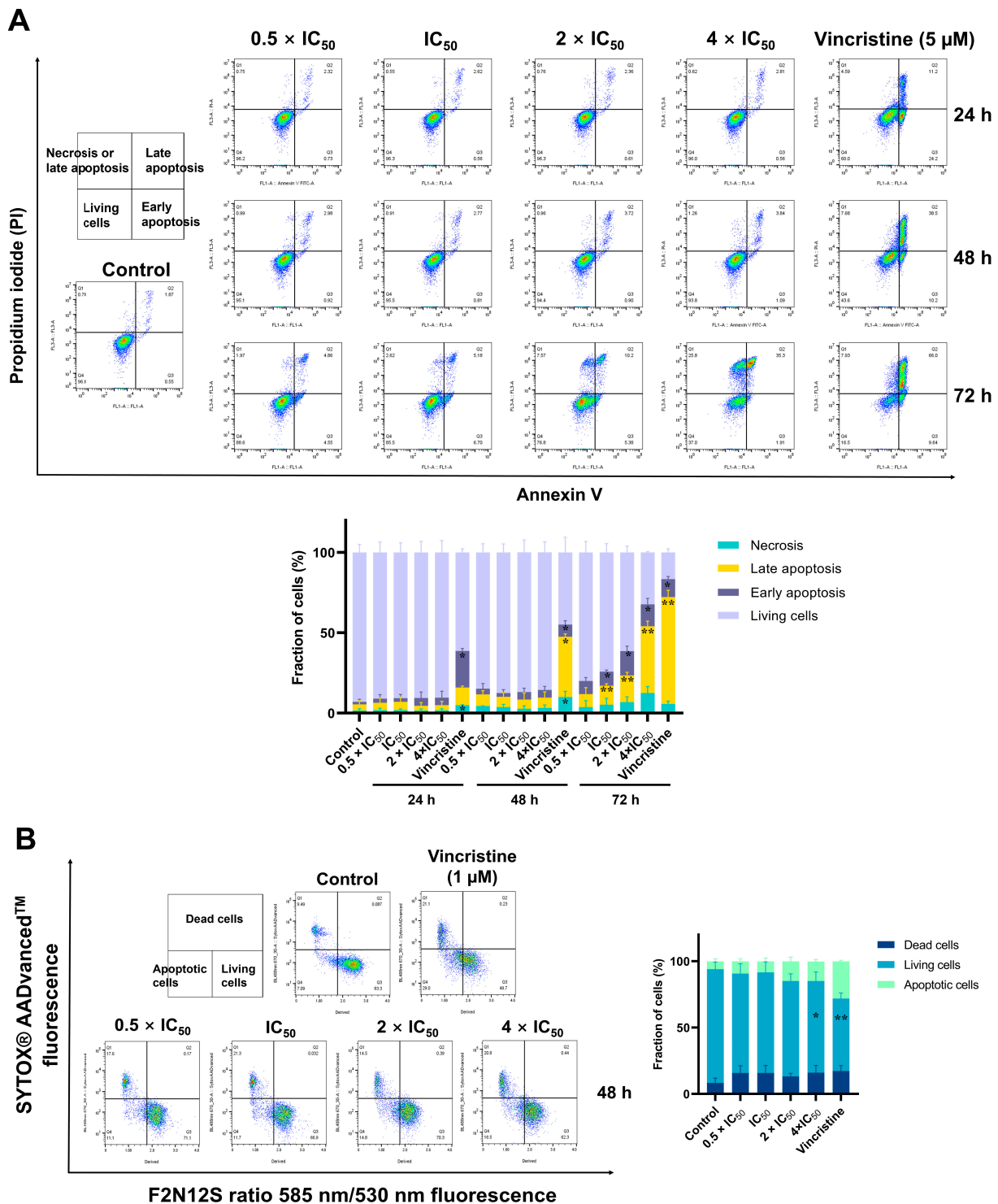


Figure 9. Detection of apoptosis induced by ZINC15675948 by flow cytometry. (A) Histograms of CCRF-CEM cells treated with different concentrations of ZINC15675948 for 24, 48, and 72 h. Vincristine (5 μM) and DMSO served as positive and negative controls. Apoptosis was detected using Annexin V and PI staining. (B) Histograms of MDA-MB-231-pcDNA3 cells treated with different concentrations of ZINC15675948 for 48 h. Vincristine (1 μM) and DMSO served as positive and negative controls. Apoptosis was determined using F2N12S and SYTOX® AADvanced™ dye. The experiments were performed three times independently. Statistical significance was analyzed using Student’s *t*-test, * *p* < 0.05, ** *p* < 0.01 vs. DMSO.

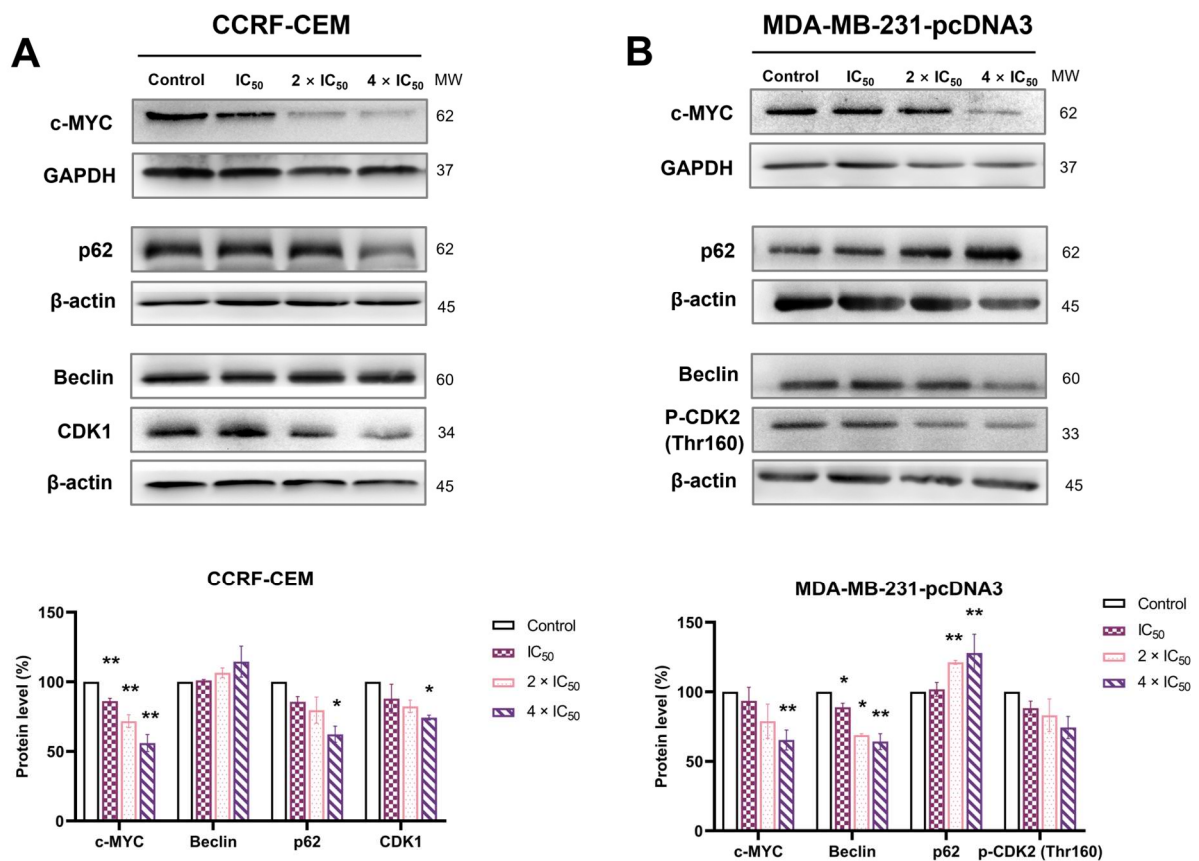


Figure 10. Western blot analysis of c-MYC and proteins involved in cell cycle and autophagy in (A) CCRF-CEM and (B) MDA-MB-231-pcDNA3 cells treated with various concentrations of ZINC15675948 for 24 h. Bands were normalized to GAPDH or β -actin for quantification (mean \pm SEM). Error bars of three repetitions independently were shown. Statistical significance was shown by Student's *t*-test, * $p < 0.05$, ** $p < 0.01$ compared with DMSO untreated cells.

To determine whether autophagy contributes to the “cell death and survival” pathway predicted by IPA, we examined two autophagy biomarkers, Beclin and p62. As shown in Figure 10A, the expression of p62 was significantly downregulated by ZINC15675948 at a concentration of $4 \times \text{IC}_{50}$ in CCRF-CEM cells ($p = 0.02$) with a slightly raised expression of Beclin, while the expression of p62 was significantly upregulated in MDA-MB-231-pcDNA3 cells, which was consistent with p62 gene upregulation found with microarray hybridization. The expression of Beclin was accordingly downregulated (Figure 10B). Therefore, ZINC15675948 induced autophagy in CCRF-CEM cells but not in MDA-MB-231-pcDNA3 cells.

Furthermore, we verified biomarkers of the G2/M and S phases of the cell cycle that were arrested by ZINC15675948 in CCRF-CEM cells and MDA-MB-231-pcDNA3 cells, respectively. Indeed, the expression of CDK1 (indicative for G2/M phase arrest) was downregulated in CCRF-CEM cells, and the expression of phosphorylated CDK2 (Thr160) (indicative for S phase arrest) decreased in MDA-MB-231-pcDNA3 cells.

2.11. Doxorubicin Uptake Assay

Since multidrug-resistant cell lines were cross-resistant to ZINC15675948 in the growth inhibition assay, the uptake assay of doxorubicin using flow cytometry was further carried out in P-gp-overexpressing (CEM/ADR5000) and BCRP-overexpressing (MDA-MB-BCRP) cells to verify the functional role of ZINC15675948 with P-gp and BCRP. As shown in Figure 11A, treatment with positive control verapamil significantly enhanced the ability of CEM/ADR5000 cells to uptake doxorubicin by 3.07-fold ($p = 0.02$). In comparison,

ZINC15675948-treated ADR/CEM5000 cells with three different concentrations did not observe doxorubicin accumulation. In MDA-MB-BCRP cells (Figure 11B), Ko143 as a BCRP inhibitor also remarkably increased doxorubicin uptake ($p = 0.003$), while there was no evidence of ZINC15675948 treatments increasing doxorubicin accumulation in MDA-MB-BCRP cells. Therefore, these results confirmed that ZINC15675948 is a substrate of P-gp and BCRP.

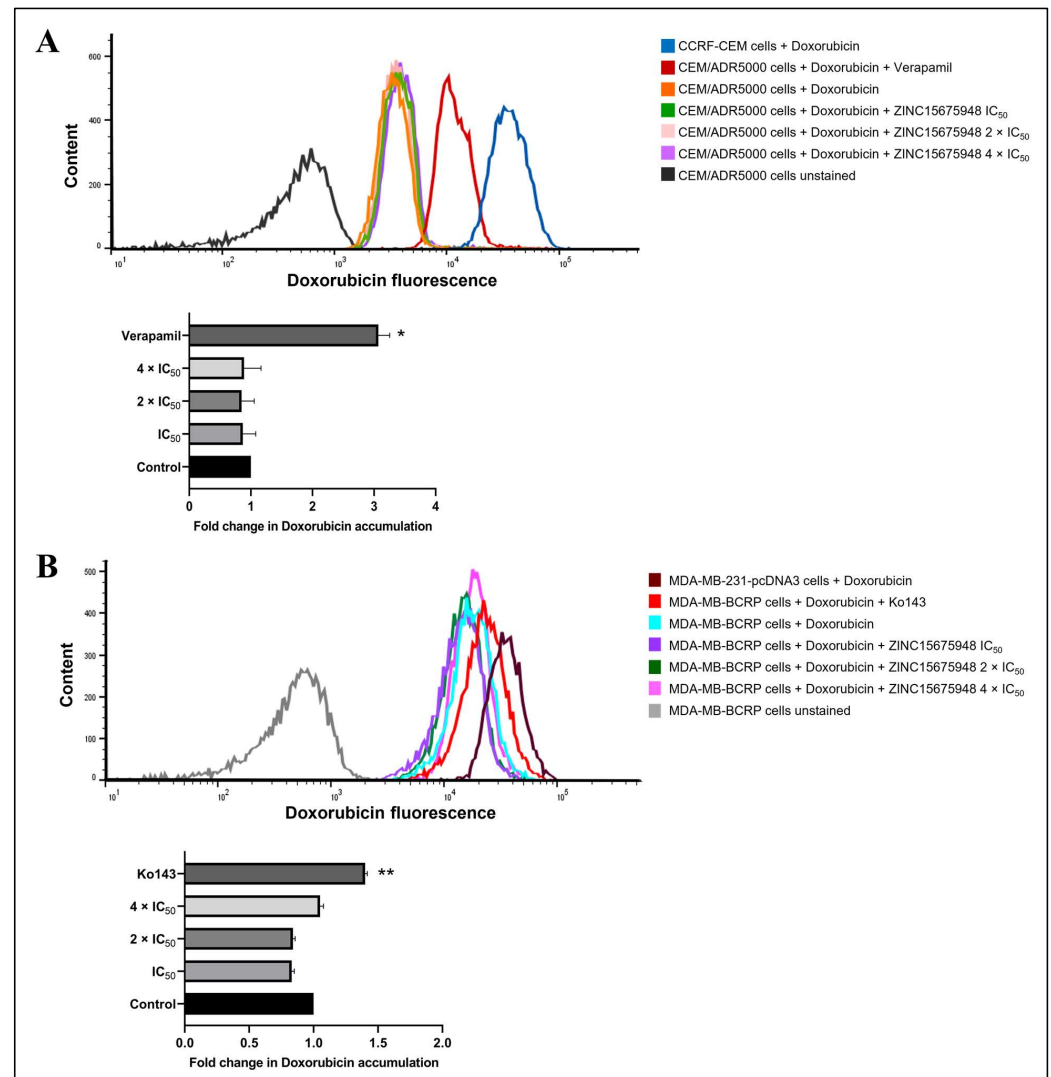


Figure 11. Doxorubicin uptake assay with ZINC15675948. **(A)** Flow cytometric analysis of doxorubicin fluorescence intensity in unstained CEM/ADR5000 cells (autofluorescence, black), CEM/ADR5000 cells treated with doxorubicin (orange), doxorubicin in combination with ZINC15675948 IC₅₀ (green), 2 × IC₅₀ (pink), and 4 × IC₅₀ (violet). CEM/ADR5000 cells treated with doxorubicin in combination with verapamil, a known P-gp inhibitor were used as a positive control. CCRF-CEM cells treated with doxorubicin (blue) were applied as a positive control for doxorubicin uptake. **(B)** Flow cytometric analysis of doxorubicin fluorescence intensity in unstained MDA-MB-BCRP cells (autofluorescence, red-brown), MDA-MB-BCRP cells treated with doxorubicin (cyan), doxorubicin in combination with ZINC15675948 IC₅₀ (purple), 2 × IC₅₀ (green), and 4 × IC₅₀ (pink). MDA-MB-BCRP cells treated with doxorubicin in combination with Ko143 (red), a known BCRP inhibitor was used as a positive control. MDA-MB-231-pcDNA3 cells treated with doxorubicin (grey) were applied as a positive control for doxorubicin uptake. Quantification of fluorescence intensity is shown in the below bar diagram. Three replicates of the experiments were performed, and the results were shown as mean ± SD (* $p \leq 0.05$, ** $p \leq 0.01$, compared with doxorubicin-treated cells alone).

3. Discussion

Over a time period from 1946 to 2019, natural products and their derivatives accounted for a majority of all anticancer drugs [39], suggesting the eminent importance of natural products in drug development. Seeking novel c-MYC inhibitors represents an urgent demand as c-MYC broadly initiates cancer development. A c-MYC deregulation is frequently involved in the carcinogenesis of lymphoblastic leukemia and triple-negative breast cancer [12,33]. Recently, compounds harboring an oxadiazole scaffold efficiently blocked c-MYC activity. The well-known c-MYC inhibitors, 10074-G5, and 10074-A4, are excellent examples [40,41]. The aim of this study was to investigate a natural product derivative of 1,2,4-oxadiazole, ZINC15675948, as a potential c-MYC inhibitor and its modes of action in leukemia and breast cancer cells.

We first demonstrated that ZINC15675948 exhibited profound growth inhibitory activity against leukemia and breast cancer cell lines at nanomolar ranges. Another 1,2,4-oxadiazole derivative with reported strong cytotoxic activities toward leukemia and breast cancer cell lines supported our results [18]. Since CEM/ADR5000 and MDA-MB-BCRP cell lines were cross-resistant to ZINC15675948, we selected the drug-sensitive cell lines CCRF-CEM and MDA-MB-231-pcDNA3 to analyze the molecular mechanisms of this compound.

Next, we addressed the question of whether ZINC15675948 can inhibit c-MYC activity or c-MYC expression. MYC was previously considered as undruggable [42]. Recently, strategies to directly or indirectly inhibit MYC expression with small molecules showed promising results, such as targeting the MYC-MAX interface or disrupting MYC-MAX DNA binding, inducing MYC degradation by ubiquitination protease system, and targeting upstream regulators of MYC [43–45]. In our study, molecular docking revealed that ZINC15675948 displayed even better LBE to c-MYC than the three positive drugs. The binding of ZINC15675948 to c-MYC was close to the MYC-MAX interaction site, similar to 10058-F4, 10074-A4, and 10074-G5, which have been demonstrated to bind to the MYC monomer and inhibit its ability to interact with MAX [46]. It is known that one of the most important properties of oxadiazoles is that they act as hydrogen bond acceptors and thus are stable in water-based medium [19]. Our molecular docking definitely showed that ZINC15675948 interacted with Gln927 as a hydrogen bond. Microscale thermophoresis was correlated well with *in silico* binding, which indicated that ZINC15675948 bound to c-MYC with a K_d value of $1.08 \pm 0.1 \mu\text{M}$. In comparison, 10074-G5 showed the best lowest binding energy of all known c-MYC inhibitors. It bound to MYC with a K_d value of $4.4 \mu\text{M}$ as reported [47]. Meanwhile, the c-MYC reporter assay confirmed that ZINC15675948 showed a better inhibition activity to c-MYC than 10058-F4. Furthermore, the expression of c-MYC was downregulated by ZINC15675948 determined using western blotting and qRT-PCR. Therefore, ZINC15675948 can inhibit c-MYC expression. ZINC15675948 may directly target c-MYC by interfering with the MYC-MAX dimer and thereby affecting c-MYC activity.

In our microarray analysis, c-MYC expression was only downregulated in CCRF-CEM cells but not in MDA-MB-231-pcDNA3 cells by ZINC15675948. However, ZINC15675948 upregulated *ELL2* in MDA-MB-231-pcDNA3 cells. Besides transcriptional and post-transcriptional mechanisms, the stability and activity of c-MYC are regulated by a series of post-translational modifications, including phosphorylation, methylation, acetylation, glycosylation, SUMOylation, proline isomerization, and ubiquitination. The ubiquitination-proteasome pathway is one of the prime mechanisms to degrade c-MYC [10,48]. Several E3 ubiquitin ligases were identified to positively or negatively regulate c-MYC inhibition through degradation [49]. The product of the *ELL* (eleven-nineteen lysine-rich leukemia) gene is a transcription elongation factor that accelerates the transcription elongation process of RNA polymerase II. ELL1 (ELL) is the first identified potential c-MYC suppressor in the ELL family. ELL1 functions as an E3 ubiquitin ligase through a CEYLH region in the C-terminus of the protein and targets c-MYC for proteasomal degradation, which thereby inhibits c-MYC-dependent transcriptional activity and cell proliferation [38]. This CEYLH region shares homology within the ELL family suggesting that ELL2 could also have a similar role as ELL1 in the ubiquitin-proteasomal degradation of c-MYC [37]. Therefore, we assume that

ELL2 ubiquitinated c-MYC protein in MDA-MB-231-pcDNA3 cells, explaining why *c-MYC* mRNA was not downregulated in the microarray analysis. It is worth pointing out that the *c-MYC* activity has been indeed reported to be regulated by ubiquitination [49]. Hence, ZINC15675948 may inhibit *c-MYC* by ubiquitination in MDA-MB-231-pcDNA3 cells.

c-MYC plays a critical role in regulating cell growth, differentiation, cell cycle, apoptosis, metabolism, angiogenesis, DNA repair, immune response, protein translocation, and stem cell formation [6]. However, *c-MYC* activation is not sufficient alone to cause carcinogenesis. Key mediators of *c-MYC*-driven cellular processes such as cell cycle checkpoints, apoptosis regulators, as well as tumor suppressor proteins are also required for tumorigenesis. Therefore, synthetic lethal interactions may provide additional opportunities to indirectly inhibit *c-MYC* [9]. Our microarray hybridization data showed that the “cell cycle”, “cell death and survival” and “DNA damage” functions were affected both in leukemia and breast cancer cells by ZINC15675948.

DNA damage is an important mechanism of cancer chemotherapeutics that is associated with cell cycle arrest and apoptosis to limit cancer progression [50]. Using single cell gel electrophoresis (alkaline comet assay), we observed that ZINC15675948 remarkably caused DNA damage as seen in increased comet tails upon treatment. In line with this result, ZINC15675948 arrested CCRF-CEM cells in the G2/M phase and MDA-MB-231-pcDNA3 cells in the S phase of the cell cycle as determined by flow cytometry. These results were further confirmed by a downregulated expression of CDK1 or p-CDK2 (Thr160) using western blotting, respectively. *c-MYC* overexpression promotes cancer cells to re-enter the cell cycle by activating cyclin-dependent kinases (CDKs) and cyclins [9]. CDK1 represents a core component in mammalian cell division. Inhibition of CDK1 induced *c-MYC*-dependent apoptosis in lymphoblastoid cell lines [51]. CDK2 is activated in the late G1 phase and continues into the S phase. Activation of CDK2 requires phosphorylation of Thr160 [52]. Hence, we conclude that ZINC15675948 treatment resulted in DNA damage and cell cycle arrest as downstream events of *c-MYC* inhibition.

ZINC15675948 significantly induced apoptosis in both leukemia and breast cancer cell lines. Induction of cell death in CCRF-CEM cells was also indicated as a *c-MYC*-dependent event by our IPA analysis due to the downregulated *c-MYC* expression. Although *c-MYC* did not appear in the microarray-based dataset of MDA-MB-231-pcDNA3 cells, *TP53* was upregulated. Evidence for crosstalk of *c-MYC* and p53 networks showed that *c-MYC*-induced apoptosis is dependent on p53 stabilization and activation [53]. In addition, the induction of apoptosis in MDA-MB-231-pcDNA3 cells correlated well with the microarray-based IPA prediction that *MCL-1* and *BAD* (*BCL-xL*) were downregulated. *MCL-1* and *BCL-xL* are members of the anti-apoptotic B-cell lymphoma 2 (*BCL-2*) family. Overexpression of anti-apoptotic genes implies an inhibition of apoptosis and leads to cancer development. A recent study revealed that *c-MYC*-driven human Burkitt lymphoma cells were eradicated by targeting *MCL-1* [54]. Therefore, these data favor the view that ZINC15675948-driven inhibition of *c-MYC* and related signals caused apoptosis.

In addition to apoptosis, autophagy is a type II programmed cell death that might also be relevant for the modes of action of ZINC15675948. Autophagy is a mechanism that transports damaged proteins or organelles to lysosomes for degradation, playing important roles in maintaining energy homeostasis and ensuring cellular materials' quality control [55]. If autophagy is induced, Beclin is recruited to organize the pre-autophagosomal structure that is necessary for autophagosome formation [56]. P62 (SQSTM1) transports ubiquitinated cargoes for autophagic degradation. The activation of autophagy declines the expression of p62 [57]. In this study, we demonstrated that the induction of autophagy by ZINC15675948 was cell line-dependent. ZINC15675948 induced autophagy in CCRF-CEM cells as evidenced by a significantly downregulated expression of p62 and an upregulation of Beclin. Induction of autophagy could result from the suppression of *c-MYC*. These results are supported by our recent report from our group that artemisinin-induced autophagy followed upon *c-MYC* inhibition in CCRF-CEM cells [58]. Autophagy induction was not

observed in MDA-MB-231-pcDNA3 cells, while the upregulated expression of p62 was correlated with that of microarray data.

ATP-binding cassette (ABC) transporters are widely expressed in various tissues protecting them from endogenous molecules and xenobiotics. ABC transporters are involved in the efflux of cytotoxic drugs from cancer cells leading to the multidrug resistance (MDR) phenotype [59] with broad cross-resistance profiles to diverse chemotherapeutics without structural or pharmacological commonalities, including *Vinca* alkaloids, taxanes, anthracyclines, epipodophyllotoxins, and others [60]. Human P-glycoprotein and BCRP are well-known ABC transporters mediating MDR. P-gp is encoded by the *ABCB1/MDR1* gene and is expressed in the normal intestine, kidneys, liver, placenta, brain, and adrenal glands. BCRP is encoded by the *ABCG2* gene and is also expressed in many tissues, including breast, colon, liver, bile, and in brain capillaries [61–63]. P-gp and BCRP confer anticancer drug resistance and were clinically found to correlate with poor diagnosis and survival of cancer patients [64,65]. Cytotoxic agents displaying degrees of cross-resistance above two can be considered as moderate substrates of ABC transporters, while high degrees of resistance (>1000) can also be observed in MDR cells [66,67]. P-gp overexpressing CEM/ADR5000 cells were 8.37 times more cross-resistant to ZINC15675948, while BCRP overexpressing cells were nine times more resistant to ZINC15675948 compared to their sensitive cell lines, indicating that ZINC15675948 was moderately cross-resistant to P-g and BCRP. Using molecular docking, we observed that ZINC15675948 bound at the substrate binding site on P-gp, but its binding site on BCRP is ambiguous concerning the substrate or inhibitor pockets. In the further doxorubicin uptake assay, our data confirmed that ZINC15675948 failed to block the efflux. Therefore, there was no intracellular accumulation of doxorubicin, which can be taken as a further hint that ZINC15675948 is a substrate of P-gp and BCRP. This finding is consistent with our recent report [68]. Future structure-activity relationship (SAR) investigations of derivatives of ZINC15675948 can be carried out to search for more therapeutically promising P-gp and BCRP inhibitors.

4. Materials and Methods

4.1. Compounds

The compound ZINC15675948 (IUPAC name: (6S)-N-(4-methylphenyl)-6-(3-naphthalen-2-yl-1,2,4-oxadiazol-5-yl)-3,4,6,7-tetrahydroimidazo [4,5-c]pyridine-5-carboxamide) (C₂₆H₂₂N₆O₂) was purchased from Glentham Life Sciences (Corsham, United Kingdom) (Ref: 44011662 GLS05772). The structure of the 1,2,4-oxadiazole nucleus and ZINC15675948 is shown (Figure 1A,B). The stock solution was prepared with dimethyl sulfoxide (DMSO) at a concentration of 20 mM and stored at −20 °C until use. Since DMSO was the solvent of the compound, DMSO was used as a negative control in all experiments. DMSO was added at the same volume as the highest concentration of ZINC15675948 in the cells, which was less than 1% of the total medium.

4.2. Cell Culture

The cell lines investigated in this study were reported previously [69,70]. The drug-sensitive CCRF-CEM and multidrug-resistant CEM/ADR5000 leukemia cell lines were cultivated in complete RPMI 1640 medium (Invitrogen, Darmstadt, Germany). The two breast cancer cell lines transduced with the control vector (MDA-MB-231-pcDNA3) or with a cDNA for the breast cancer resistance protein BCRP (MDA-MB-231-BCRP clone 23) were maintained in DMEM medium (Invitrogen, Darmstadt, Germany). Both media were supplemented with 10% fetal bovine serum (FBS) (Invitrogen) and 1% penicillin (100 µg/mL)-streptomycin (100 µg/mL) (Invitrogen). Cells were cultured at 37 °C in a humidified air incubator (90%) containing 5% CO₂. In addition, CEM/ADR5000 cells were continuously treated with 5000 ng/mL doxorubicin every two weeks to maintain the overexpression of P-glycoprotein. The gene expression profiles of CEM/ADR5000 cells were previously described in [71–73]. MDA-MB-231-BCRP clone 23 cells were treated with 800 ng/mL geneticin (Sigma-Aldrich, Darmstadt, Germany) every two weeks.

4.3. Growth Inhibition Assay

The resazurin reduction assay was used to access the effect of growth inhibition of ZINC15675948 [74]. The non-fluorescent dye resazurin is metabolically converted to the fluorescent dye resorufin by living cells [75]. Briefly, the CCRF-CEM and CEM/ADR5000 suspension cells were seeded into 96-well plates (1×10^4 cells/well) and then directly treated with 10 concentrations of ZINC15675948 in a range of 0.3–100 μ M, respectively, in a total volume of 200 μ L. MDA-MB-231-pcDNA3 and MDA-MB-231-BCRP clone 23 cells were seeded into 96 well plates (5×10^3 cells/well) overnight and treated in the same series of concentrations as in leukemia cells with ZINC15675948 on the following day. After 72 h incubation, 20 μ L of 0.01% resazurin (Promega, Germany) were added to each well and incubated for 4 h at 37 °C. The resazurin fluorescence was detected using an Infinite M2000 Pro™ plate reader (Tecan, Crailsheim, Germany) at Ex/Em = 550 nm/590 nm wavelength. Relative cell viability was calculated in comparison to the DMSO-treated control. The final concentration of DMSO was 0.5%. The growth inhibition was accessed according to the effectiveness in inhibiting cell proliferation by half and was expressed as half-maximal inhibitory concentration (IC₅₀) values. All IC₅₀ values were expressed as mean \pm standard deviation (SD). This experiment was repeated three times independently with six wells for each concentration. The figures were analyzed using GraphPad Prism Software (version 9.0.2) (GraphPad Software Inc., San Diego, CA, USA).

4.4. Molecular Docking

In silico molecular docking was performed using the AutoDock 4.2.6 software (The Scripps Research Institute, CA, USA). The protocol was recently described by us [69]. The SDF format of ZINC15675948 was downloaded from ZINC 15 database (<https://zinc15.docking.org/> accessed on 20 October 2019). ZINC15675948 was considered to perform molecular docking to P-glycoprotein (P-gp, *MDR1*, *ABCB1*) and the breast cancer resistance protein (BCRP, *ABCG2*), since growth inhibition of ZINC15675948 was determined in P-gp- or BCRP-overexpressing multidrug-resistant cell lines. The 3D structures of c-MYC (PDB code: 1NKP), P-gp (PDB code: 6QEX) and BCRP (PDB code: 6FFC) were downloaded from the RCSB Protein Data Bank (<http://www.rcsb.org/>, accessed on 20 October 2019) as PDB files. The known c-MYC inhibitors 10058-F4, 10074-A4 and 10074-G5 were used as positive control drugs to compare their affinity and binding mode with ZINC15675948 [76]. C-MYC was covered with grid box for the defined docking mode. The center of the grid box was set at x = 67.083, y = 64.481, and z = 42.943 with a spacing of 0.397 and with a number of grid points of 68 in x, 64 in y, and 72 in z). Doxorubicin as a known substrate of P-gp and BCRP was used as a control drug. Verapamil and Ko143 are inhibitors of P-gp or BCRP, respectively. Both were also used as control drugs. The grid boxes of P-gp and BCRP were placed around the drug-binding site [74]. Hydrogens were added to each protein structure, missing atoms were checked. The Lamarckian GA (4.2) was applied as an algorithm for 250 runs and 25,000,000 energy evaluations for each cycle. Docking was performed three times independently and the predicted inhibition constants were obtained from the docking log files (dlg). VMD (Visual Molecular Dynamics) software (version 1.9.3) (University of Illinois at Urbana Champaign, Champaign, IL, USA) and Discovery Studio Visualizer software (version v.21.1.0.20298) (Dassault Systems Biovia Corp, San Diego, CA, USA) were used as visualization tools to generate figures and gain a deeper understanding of the binding modes that were calculated from docking.

4.5. Microscale Thermophoresis

Microscale thermophoresis (MST) was performed with human recombinant c-MYC protein and ZINC15675948. The protein was purchased from Abcam (Cambridge, UK) with a concentration of 0.5 mg/mL (ab169901). C-MYC was labeled with Monolith Protein Labeling Kit RED-NHS 2nd Generation (Nano Temper Technologies GmbH, Munich, Germany) according to the manufacturer's instructions. The final concentration of c-MYC after labeling was 595 nM. ZINC15675948 was diluted from 400 μ M to a series

of concentrations in assay buffer (50 mM Tris buffer (pH 7.4) containing 10 mM MgCl₂, 150 mM NaCl, and 0.05% Tween-20). The labeled protein and diluted compounds were mixed (1:1). After 30 min incubation in the dark at room temperature, the fluorescence signal was measured on a Monolith NT.115 instrument (Nano Temper Technologies) with Monolith NT.115 standard capillaries. The MST with ZINC15675948 was performed with 70% LED power and 10% MST power. Fitting curved and dissociation constant (K_d) values were calculated with MO. Affinity Analysis software (version 2.2.4) (Nano Temper Technologies). The measurements were repeated three times independently.

4.6. c-MYC Reporter Assay

A signal MYC reporter assay (Qiagen, Germantown, MD, USA) was used to determine the impact of ZINC15675948 on c-MYC activity as we described recently [58]. Briefly, a c-MYC-luciferase reporter construct was transfected into human embryonic kidney HEK293 cells and incubated according to the manufacturer's instructions. Subsequently, cells were treated with two concentrations ($4 \times IC_{50}$ in CCRF-CEM or MDA-MB-231-pcDNA3) of ZINC15675948 (32 nM and 320 nM) and DMSO (negative control) or of the known c-MYC inhibitor 10058-F4 (positive control) for 48 h. A Dual-glo[®] Luciferase Reporter Assay System (Promega, Madison, WI, USA) was applied for the measurement of c-MYC promoter activity. Renilla and firefly luciferase luminescence were measured using an Infinite M2000 Pro[™] plate reader (Tecan, Crailsheim, Germany).

4.7. Gene Expression Profiles

Total mRNA was isolated using the InviTrap[®] Spin Universal RNA Mini Kit (Invitex Molecular, Berlin, Germany). CCRF-CEM (1×10^6 cells/well) and MDA-MB-231-pcDNA3 cells (5×10^5 cells/well) were treated with DMSO as a solvent control and ZINC15675948 for 24 h in duplicate. ZINC15675948 was applied with a concentration according to the IC_{50} value (CCRF-CEM cells: 0.008 μ M, MDA-MB-231-pcDNA3 cells: 0.08 μ M). The RNA concentrations were determined using NanoDrop1000 (PEQLAB, Erlangen, Germany). Afterwards, quality control of total RNA, probe labeling, hybridization, scanning and data analysis of the samples were performed at the Genomics and Proteomics Core Facility of the German Cancer Research Center (DKFZ, Heidelberg, Germany). Affymetrix GeneChips[®] with human Clariom[™] S assays (Affymetrix, Santa Clara, CA, USA) were applied for microarray hybridizations as previously described in detail [34].

4.8. Pathway Analysis of Microarray Data

The Chipster software (<http://chipster.csc.fi/>, accessed on 20 October 2019) (The Finnish IT Center for Science CSC, Espoo, Finland) was used to filter a set of differentially expressed genes acquired from microarray hybridization [77]. The Empirical Bayes *t*-test ($p < 0.05$) was applied to access the deregulated genes between DMSO and ZINC15675948-treated groups (accessed in July 2021). The filtered genes were analyzed with the Ingenuity Pathway Analysis (IPA) software (Qiagen, Redwood City, CA, USA) (content version 51963813) by the core analysis tool to determine the cellular functions and networks affected by drug treatment (accessed in August 2021).

4.9. Quantitative Real-Time Reverse Transcription PCR

The same total RNA samples (DMSO control and IC_{50}) used for the microarray analyses were also used for qRT-PCR experiments [78]. One microgram RNA was converted to cDNA using the LunaScript[®] RT SuperMix Kit cDNA Synthesis Kit (New England Bio Labs, Darmstadt, Germany) according to the manufacturer's instructions. All PCR primers were designed using the NCBI Primer-BLAST (<https://www.ncbi.nlm.nih.gov/tools/primer-blast/>) website and purchased from Eurofins genomics (Ebersberg, Germany) (<https://eurofinsgenomics.eu/en/dna-rna-oligonucleotides/optimised-application-oligos/pcr-primers/>) (accessed in September 2021). The primer sequences are shown in Table 4. The *GAPDH* gene served as an internal control. The reaction mix-

ture contained 4 μL master mix ($5 \times$ Hot Start Taq EveGreen[®] qPCR Mix (no Rox) (Axon Labortechnik, Kaiserslautern, Germany), 1 μL forward or reversed primer (250 nM final concentration), 13 μL nuclease-free water (Thermo Fisher), and 1 μL cDNA converted from 300 ng RNA. The qRT-PCR was performed on CFX384 Touch Real-Time PCR Detection System (Bio-Rad, Munich, Germany) using the 384-well plate. The initial denaturation of qRT-PCR was at 95 °C for 10 min followed by 40 cycles including strand separation at 95 °C for 15 s, annealing at 57.5 °C for 40 s and extension at 72 °C for 1 min. CFX Manager Software (version 3.1) was used to generate the C_q values. The fold-change of gene expression was calculated using comparative $2^{-\Delta\Delta CT}$ method as reported in the literature [79]. Specifically, for the DMSO control sample, the data of the target gene are presented as fold change in gene expression normalized to *GAPDH* gene. For the sample treat with the IC_{50} of the compound, the evaluation of $2^{-\Delta\Delta CT}$ after normalization to *GAPDH* gene reveals the fold change of the target gene in gene expression relative to the untreated control.

Table 4. The sequence (5'→3') of qRT-PCR primers.

Gene Symbol	Forward Primer	Reverse Primer
<i>RAD21</i>	GAGTCAGCTATGCCTCCACC	TGGAGGTTCTCTGGGGGAA
<i>HMGCS1</i>	CTTTCGTGGCTCACTCCCTT	GTTTCCTCCTTCGGGCACA
<i>PGK1</i>	TGTGTGGAATGGTCCTGTGG	TGGCTTTCACCACCTCATCC
<i>ATP5MF</i>	CGGACACCAGGACTCCAAAA	GGACTGAAGTCCCAGCATCAA
<i>CITED2</i>	GGCGAAGCTGGGGAATAACA	AATCAGCCCTCTCATCTCTG
<i>HSPD1</i>	GCCGCCCCGCAGAAAT	AAGCCCGAGTGAGATGAGGA
<i>H4C3</i>	CAGGGCATTACAAAACCGGC	GTGCTCCGTATAGGTGACGG
<i>DHFR</i>	GCCACCGCTCAGGAATGAAT	AGGTTGTGGTCATTCTCTGGAA
<i>c-MYC</i>	ACACTAACATCCCACGCTCTG	CTCGCTAAGGCTGGGGAAAG
<i>GAPDH</i>	ATGAATGGGCAGCCGTTAGG	AGCATCACCCGGAGGAGAAA

4.10. Single Cell Gel Electrophoresis (Alkaline Comet Assay)

DNA damage was detected by alkaline comet assay using the OxiSelect[™] Comet Assay Kit (Cell Biolabs/Biocat, Heidelberg, Germany) as described in [78]. The alkaline comet assay is a sensitive method for monitoring the migration of DNA fragments from nuclei under alkaline conditions. It detects DNA single- and double-strand breaks at a cellular level [50]. Briefly, CCRF-CEM cells (1×10^6 cells/well) were seeded into a 6-well plate and treated with different concentrations of ZINC15675948 (IC_{50} , $2 \times IC_{50}$ and $4 \times IC_{50}$) and DMSO as a negative control for 24 h. MDA-MB-231-pcDNA3 cells (5×10^5 cells/well) were first seeded for 24 h to allow adhesion and then incubated with the same treatments for 24 h. Both cell lines were treated with H_2O_2 (50 μM) as a positive control for 30 min [80]. Cells were harvested and centrifuged at $3000 \times g$ for 10 min and were suspended in 1 mL cold PBS. Next, 1×10^5 cells were counted and mixed with agarose at 37 °C at a ratio of 1:6 and then spread on a comet slide. The following steps were conducted in the dark. Slides were left at 4 °C for 30 min to solidify and then immersed in pre-chilled lysis solution (NaCl 14.6 g, EDTA solution 20 mL, $10 \times$ lysis solution, pH 10.0, fulfill to 100 mL with distilled water, stored at 4 °C) for 1 h at 4 °C. Afterwards, slides were immersed in pre-chilled alkaline electrophoresis solution buffer (NaOH 12 g, EDTA solution 2 mL, fulfill to 100 mL with distilled water, stored at 4 °C) for 40 min. Next, electrophoresis was performed for 20 min at 20 V with alkaline electrophoresis solution buffer. Subsequently, slides were transferred into pre-chilled distilled water for 2×5 min for washing, followed by immersion in 70% ethanol for 5 min. After slides were dry, Vista Green DNA dye was diluted in TE buffer (Tris 121.14 mg, EDTA 200 μL , pH 7.5, fulfill to 100 mL distilled water) at a ratio of 1:1000. Then 100 μL diluted Vista Green DNA dye was added to each sample. DNA damage was captured by EVOS digital inverted microscope (Life Technologies GmbH, Darmstadt, Germany). At least 50 comets of each treatment were analyzed by Imaged J software (version 1.53q) using a plugin OpenComet (National

University of Singapore, Singapore). The tail DNA percentage was used as a parameter of DNA damage [81,82].

4.11. Cell Cycle Arrest

CCRF-CEM cells (1×10^6 cells/well) were seeded into a 6-well-plate and treated with ZINC15675948 at concentrations of IC_{50} , $2 \times IC_{50}$ or $4 \times IC_{50}$, DMSO (negative control), or vincristine (positive control, $0.3 \mu\text{M}$) (University Hospital Pharmacy, Mainz, Germany) for 72 h. MDA-MB-231-pcDNA3 cells (3×10^5 cells/well) were seeded and on the second day treated with ZINC15675948 at concentrations of $0.5 \times IC_{50}$, IC_{50} or $2 \times IC_{50}$, and DMSO (negative control) and cisplatin (positive control, $0.5 \mu\text{M}$) (University Hospital Pharmacy) for 24 h. The cells were harvested and centrifuged with cold PBS (4°C) twice (1500 rpm for 5 min). Ice-cold ethanol (80%) was used for fixation. Samples were kept at -20°C at least for 24 h. Afterwards, cells were spun down from the ethanol by centrifugation at 4000 rpm for 10 min and washed twice with cold PBS. Before measurement, the cells were resuspended with 500 μL cold PBS containing 20 g/mL RNase (Roche Diagnostics, Mannheim, Germany) and incubated at room temperature for 30 min, followed by staining with 50 $\mu\text{g}/\text{mL}$ propidium iodide (PI) (Sigma-Aldrich). After 15 min incubation in the dark at 4°C , CCRF-CEM cells were analyzed on a BD Accuri™ C6 Flow Cytometer (Becton-Dickinson, Heidelberg, Germany). MDA-MB-231-pcDNA3 cells were analyzed on a BD LSRFortessa SORP (Becton Dickinson, Heidelberg, Germany). The cells were gated firstly using FSC-A/SSC-A gate in linear scale, 10^4 cells were recorded. Then doublets were removed using FL2-A/FL2-H gate also in linear scale. The DNA histogram was generated using FL2-A/histogram properties. All the experiments were repeated three times independently. The cell cycle distributions were analyzed by the FlowJo software (version 10.8.1) (Celeza, Olten, Switzerland) [34].

4.12. Detection of Apoptosis in Suspension Cells

Annexin V-FITC apoptosis kit (Bio Version/Biocat, Heidelberg, Germany) was applied to detect apoptosis in suspension cells [83]. CCRF-CEM cells (1×10^6 cells/well) were seeded in a 6-well plate, then treated with different concentrations (IC_{50} , $2 \times IC_{50}$ or $4 \times IC_{50}$) of ZINC15675948, DMSO (negative control), or vincristine (positive control, $5 \mu\text{M}$), and incubated for 24, 48, or 72 h. The cells were harvested, washed with cold PBS and $1 \times$ binding buffer (Bio Version), respectively. Afterwards, the cells were stained with 52.5 μL annexin V master mix (2.5 μL annexin V, 50 μL $1 \times$ binding buffer) (Bio Version), and incubated at 4°C in the dark for 15 min. Then cells were stained with 440 μL PI master mix (10 μL PI, 430 μL $1 \times$ binding buffer) (Bio Version). The detection was performed on a BD Accuri™ C6 Flow Cytometer (Becton-Dickinson) and 2×10^4 cells were recorded for each sample. Four different cell populations were obtained from flow cytometer, including living cells: annexin (−)/PI (−), early apoptosis: annexin (+)/PI (−), late apoptosis: annexin (+)/PI (+), and necrosis: annexin (−)/PI (+). The data were analyzed using FlowJo software (version 10.8.1) (Celeza). The experiments were repeated in triplicate.

4.13. Detection of Apoptosis in Adherent Cells

MDA-MB-231-pcDNA3 adherent cells generally need trypsinization for cell-harvesting, which may result in false positive results by applying the Annexin V-FITC apoptosis kit. Therefore, the Violet Ratiometric Membrane Asymmetry Prob/Dead Cell Apoptosis Kit (Thermo Fisher Scientific, Darmstadt, Germany) was alternatively utilized to detect apoptosis in adherent cells [84]. Furthermore, 4'-N,N-diethylamino-6-(N,N,N dodecylmethylamino-sulfopropyl)-methyl-3-hydroxyflavone (F2N12S) is a novel fluorescent probe to monitor the lipid composition on the plasma membrane in the early stage of apoptosis. SYTOX® AADvanced™ can pass through the cell membrane only in necrosis or late apoptosis. Briefly, 1×10^5 MDA-MB-231-pcDNA3 cells were seeded in a 6-well plate overnight and then treated with different concentrations ($0.5 \times IC_{50}$, IC_{50} , $2 \times IC_{50}$ or

$4 \times IC_{50}$) of ZINC1565948, DMSO (negative control), or vincristine (positive control, 1 μ M). After the incubation for 48 h, cells were detached using 500 μ L Accutase (Thermo Fisher Scientific, Darmstadt, Germany) at room temperature and then washed with 1 mL cold Hank's balanced salt solution (HBSS, 4 $^{\circ}$ C) twice. Cells were suspended with 1 mL HBSS. Subsequently, 1 μ L F2N12S solution was added to each sample at a final concentration of 200 nM. Another 1 μ L SYTOX[®] AADvanced[™] dead cell stain solution was added at a final concentration of 1 μ M. Samples were incubated at room temperature for 5 min and then analyzed using a BD LSRFortessa SORP (Becton Dickinson). The F2N12S was excited at 405 nm, and the emissions were collected with orange fluorescence (585/15 bandpass filter) and green fluorescence (530/30 bandpass filter). A ratio of the orange fluorescence channel to the green fluorescence channel was set as a derive parameter. The SYTOX[®] AADvanced[™] dead cell stain was excited at 488 nm, and the emission was collected with a 670/30 bandpass filter. The detections were repeated three times independently. The data were analyzed by the FlowJo software (version 10.8.1) (Celeza).

4.14. Protein Analyses by SDS-PAGE and Immunoblotting

CCRF-CEM cells (6,000,000 cells/flask) and MDA-MB-231-pcDNA3 cells (500,000 cells/well) were treated with varying concentrations of ZINC15675948 (IC_{50} , $2 \times IC_{50}$, or $4 \times IC_{50}$) or DMSO as a negative control. After 24 h incubation, the cells were harvested and washed with PBS. Then 100 μ L of ice-cold M-PER Mammalian Protein Extraction Reagent (Thermo Fisher Scientific, Darmstadt, Germany) containing 1% Halt Protease Inhibitor Cocktail and phosphatase inhibitor (Thermo Fisher Scientific) were added to each sample. The cell lysis solutions were shaken for 30 min at 4 $^{\circ}$ C and centrifuged at $14,000 \times g$ for 15 min at 4 $^{\circ}$ C. The supernatants were harvested, and the protein concentrations were measured with NanoDrop1000 (PEQLAB, Erlangen, Germany).

Each protein sample of 30 mg was electrophoresed on 10% SDS-polyacrylamide gels and transferred to polyvinylidene difluoride (Ruti[®]-PVDF) membranes (Millipore Corporation, Billerica, MA, USA) at 250 mA for 90 min. The membranes were washed with Tris-buffered saline containing 0.1% Tween-20 (TBST) for 5 min and then blocked in 5% bovine serum albumin in TBST for 1 h at room temperature. Afterward, the membranes were washed with TBST for 3×5 min and incubated with diluted primary antibody at 4 $^{\circ}$ C overnight as follows: c-MYC antibody (1:1000, Cell Signaling Technology, Frankfurt a. M., Germany), p62, SQSTM1 polyclonal antibody (1:1000, Proteintech, Planegg-Martinsried, Germany), Beclin 1 polyclonal antibody (1:1000, Proteintech), CDK1 (1:1000, Cell Signaling Technology), Phospho-CDK2 (Thr160) (1:1000, Cell Signaling Technology), GAPDH (1:1000, Cell Signaling Technology), or β -actin (1:1000, Cell Signaling Technology). After washing with TBST for 3×5 min, the membranes were incubated with diluted secondary antibody anti-rabbit IgG, HRP-linked antibody (1:2000, Cell Signaling Technology) for 1 h at room temperature. Finally, Horseradish peroxidase (HRP) substrate (Luminata[™] Classico, Merck Millipore, Schwalbach, Germany) was added to membranes in the dark. The Alpha Innotech FluorChem Q system (Biozym, Oldendorf, Germany) was used for band detection. The quantification was carried out using Image J software (version 1.53q) (National Institute of Health, Bethesda, MD, USA). All the experiments were repeated at least three times independently.

4.15. Doxorubicin Uptake Assay

Doxorubicin is a substrate of P-gp. P-gp-overexpressing CEM/ADR5000 cells were seeded in 12-well plates (10^4 cells/well). Doxorubicin was obtained from the University Hospital Pharmacy (Mainz, Germany) and used at a concentration of 10 μ M in all samples. In parallel, different concentrations of ZINC15675948 (IC_{50} , $2 \times IC_{50}$ or $4 \times IC_{50}$) were combined with doxorubicin treatment. Verapamil (20 μ M; Sigma-Aldrich) was applied as a positive control for P-gp inhibition. Unstained CEM/ADR5000 cells were used as a negative control. In comparison, non-P-gp-expressing CCRF-CEM cells were used as a positive control for doxorubicin uptake. After 3 h incubation at 37 $^{\circ}$ C, cells were centrifuged

to discard the old medium and resuspended in 1 mL PBS. The doxorubicin fluorescence assay was carried out on a BD Accuri™ C6 Flow Cytometer (Becton-Dickinson) by blue laser at excitation 488 nm and emission 530 nm. In each sample, 3000 cells were counted. Dead cells and debris were removed by gating the cells in forward vs. side scatter, and forward-area vs. forward-height scatter, respectively. All experiments were performed in triplicate. The protocol has been described by us in [74].

MDA-MB-231-pcDNA3 and MDA-MB-BCRP (5000 cells/well) were seeded into 12-well plates. Doxorubicin treatment was combined with ZINC15675948 (IC_{50} , $2 \times IC_{50}$ or $4 \times IC_{50}$). Ko143 (200 nM; Sigma-Aldrich) was used as a positive control for BCRP inhibition. The negative control is unstaining cells. Non-BCRP-overexpressing MDA-MB-231-pcDNA cells were applied as a positive control of doxorubicin uptake. After 24-h incubation at 37 °C, the samples were washed and measured as described above.

5. Conclusions

In conclusion, ZINC15675948 displayed remarkable cytotoxicity in CCRF-CEM and MDA-MB-231-pcDNA3 cells. ZINC15675948 bound to the c-MYC/MAX interface and inhibited c-MYC activity and expression. The inhibition of c-MYC in MDA-MB-231-pcDNA3 cells involved ubiquitination. By means of microarray-based mRNA expression profiling, we verified that ZINC15675948 induced DNA damage and apoptosis in both cell lines as downstream effects of c-MYC inhibition. ZINC15675948 caused G2/M phase cell cycle arrest in CCRF-CEM cells and S phase arrest in MDA-MB-231-pcDNA3 cells. ZINC15675948 also induced autophagy in CCRF-CEM cells. Furthermore, ZINC15675948 was a substrate of two ABC transporters, P-gp and BCRP. These results illustrate that ZINC15675948 is a promising inhibitor of c-MYC worth further development as a novel anticancer drug.

Supplementary Materials: The following supporting information can be downloaded at: <https://www.mdpi.com/article/10.3390/molecules28155658/s1>, Table S1: Deregulated gene expression upon treatment of CCRF-CEM leukemia cells with the IC_{50} concentration of ZINC15675948 for 24 h; Table S2: Deregulated gene expression upon treatment of MDA-MB-231-pcDNA3 breast cancer cells with the IC_{50} concentration of ZINC15675948 for 24 h.

Author Contributions: Conceptualization, M.Z., S.M.K. and T.E.; Data curation, M.Z., J.C.B. and S.M.K.; Formal analysis, M.Z.; Investigation, M.Z., J.C.B., E.A.O. and S.M.K.; Methodology, M.Z., J.C.B., E.A.O. and S.M.K.; Project administration, T.E.; Software, M.Z., J.C.B., E.A.O. and S.M.K.; Supervision, T.E.; Validation, M.Z., J.C.B. and E.A.O.; Visualization, M.Z., J.C.B. and E.A.O.; Writing—original draft, M.Z.; Writing—review & editing, M.Z., S.M.K. and T.E. All authors have read and agreed to the published version of the manuscript.

Funding: This research received no external funding.

Institutional Review Board Statement: Not applicable.

Informed Consent Statement: Not applicable.

Data Availability Statement: The authors declare that the data supporting the findings of this study are available within the paper.

Acknowledgments: We are appreciative of the expression profiling service provided by the Microarray Unit of the Genomics and Proteomics Core Facility, German Cancer Research Center (DKFZ). We thank the Flow Cytometry Core Facility at the Institute of Molecular Biology (IMB, Mainz, Germany) for their helpful training and technical support for the usage of BD LSRFortessa SORP, which was applied for the detection of cell cycle and apoptosis in adherent cells. We are grateful for a stipend of the Chinese Scholarship Council to M.Z., the stipend of the Sibylle Kalkhof-Rose-Foundation to J.C.B., and the stipend of the German Academic Exchange Service (DAAD) to E.A.O.

Conflicts of Interest: The authors declare no conflict of interest.

Sample Availability: Samples of the compound ZINC15675948 are available upon reasonable request.

Abbreviations

ABC, ATP-binding cassette transporter; ALL, acute lymphoblastic leukemia; BCRP, breast cancer resistance protein; CDK, cyclin-dependent kinases; DMSO, dimethyl sulfoxide; ELL, eleven-nineteen lysine-rich leukemia gene, elongation factor for RNA polymerase II; FBS, fetal bovine serum; HBSS, Hank's balanced salt solution; IC₅₀, half-maximal inhibitory concentration; IPA, Ingenuity Pathway Analysis; K_d, dissociation constant; LBE, lowest binding energy; MAX, MYC-associated factor X; MDR, multidrug resistance; MST, microscale thermophoresis; PBS, phosphate buffered saline; P-gp, P-glycoprotein; TNBC, triple-negative breast cancer.

References

1. Bishop, J.M. Molecular themes in oncogenesis. *Cell* **1991**, *64*, 235–248. [[CrossRef](#)] [[PubMed](#)]
2. Dang, C.V. MYC on the path to cancer. *Cell* **2012**, *149*, 22–35. [[CrossRef](#)] [[PubMed](#)]
3. Lourenco, C.; Resetca, D.; Redel, C.; Lin, P.; MacDonald, A.S.; Ciaccio, R.; Kenney, T.M.G.; Wei, Y.; Andrews, D.W.; Sunnerhagen, M.; et al. MYC protein interactors in gene transcription and cancer. *Nat. Rev. Cancer* **2021**, *21*, 579–591. [[CrossRef](#)] [[PubMed](#)]
4. Albiñ, A.; Johnsen, J.I.; Henriksson, M.A. MYC in oncogenesis and as a target for cancer therapies. *Adv. Cancer Res.* **2010**, *107*, 163–224. [[CrossRef](#)]
5. Sammak, S.; Hamdani, N.; Gorrec, F.; Allen, M.D.; Freund, S.M.V.; Bycroft, M.; Zinzalla, G. Crystal structures and nuclear magnetic resonance studies of the apo form of the c-MYC: MAX bHLHZip complex reveal a helical basic region in the absence of DNA. *Biochemistry* **2019**, *58*, 3144–3154. [[CrossRef](#)]
6. Duffy, M.J.; O'Grady, S.; Tang, M.; Crown, J. MYC as a target for cancer treatment. *Cancer Treat. Rev.* **2021**, *94*, 102154. [[CrossRef](#)]
7. Gabay, M.; Li, Y.; Felsher, D.W. MYC activation is a hallmark of cancer initiation and maintenance. *Cold Spring Harb. Perspect. Med.* **2014**, *4*, a014241. [[CrossRef](#)]
8. Llombart, V.; Mansour, M.R. Therapeutic targeting of “undruggable” MYC. *eBioMedicine* **2022**, *75*, 103756. [[CrossRef](#)]
9. Dhanasekaran, R.; Deutzmann, A.; Mahauad-Fernandez, W.D.; Hansen, A.S.; Gouw, A.M.; Felsher, D.W. The MYC oncogene—The grand orchestrator of cancer growth and immune evasion. *Nat. Rev. Clin. Oncol.* **2022**, *19*, 23–36. [[CrossRef](#)]
10. Sears, R.C. The life cycle of C-myc: From synthesis to degradation. *Cell Cycle* **2004**, *3*, 1133–1137. [[CrossRef](#)]
11. Dingar, D.; Tu, W.B.; Resetca, D.; Lourenco, C.; Tamachi, A.; De Melo, J.; Houlahan, K.E.; Kalkat, M.; Chan, P.K.; Boutros, P.C.; et al. MYC dephosphorylation by the PP1/PNUTS phosphatase complex regulates chromatin binding and protein stability. *Nat. Commun.* **2018**, *9*, 3502. [[CrossRef](#)] [[PubMed](#)]
12. Fallah, Y.; Brundage, J.; Allegakoen, P.; Shajahan-Haq, A.N. MYC-driven pathways in breast cancer subtypes. *Biomolecules* **2017**, *7*, 53. [[CrossRef](#)] [[PubMed](#)]
13. Boxer, L.M.; Dang, C.V. Translocations involving c-myc and c-myc function. *Oncogene* **2001**, *20*, 5595–5610. [[CrossRef](#)] [[PubMed](#)]
14. Felsher, D.W.; Bishop, J.M. Reversible tumorigenesis by MYC in hematopoietic lineages. *Mol. Cell* **1999**, *4*, 199–207. [[CrossRef](#)] [[PubMed](#)]
15. Atanasov, A.G.; Zotchev, S.B.; Dirsch, V.M.; Orhan, I.E.; Banach, M.; Rollinger, J.M.; Barreca, D.; Weckwerth, W.; Bauer, R.; Bayer, E.A.; et al. Natural products in drug discovery: Advances and opportunities. *Nat. Rev. Drug Discov.* **2021**, *20*, 200–216. [[CrossRef](#)]
16. Hassan, A.; Khan, A.H.; Saleem, F.; Ahmad, H.; Khan, K.M. A patent review of pharmaceutical and therapeutic applications of oxadiazole derivatives for the treatment of chronic diseases (2013–2021). *Expert Opin. Ther. Pat.* **2022**, *32*, 969–1001. [[CrossRef](#)]
17. Camci, M.; Karali, N. Bioisosterism: 1,2,4-oxadiazole rings. *ChemMedChem* **2023**, *18*, e202200638. [[CrossRef](#)]
18. Atmaram, U.A.; Roopan, S.M. Biological activity of oxadiazole and thiaziazole derivatives. *Appl. Microbiol. Biotechnol.* **2022**, *106*, 3489–3505. [[CrossRef](#)]
19. Dhameiliya, T.M.; Chudasma, S.J.; Patel, T.M.; Dave, B.P. A review on synthetic account of 1,2,4-oxadiazoles as anti-infective agents. *Mol. Divers.* **2022**, *26*, 2967–2980. [[CrossRef](#)]
20. Carbone, M.; Li, Y.; Irace, C.; Mollo, E.; Castelluccio, F.; Di Pascale, A.; Cimino, G.; Santamaria, R.; Guo, Y.-W.; Gavagnin, M. Structure and cytotoxicity of phidianidines A and B: First finding of 1,2,4-oxadiazole system in a marine natural product. *Org. Lett.* **2011**, *13*, 2516–2519. [[CrossRef](#)] [[PubMed](#)]
21. Labriere, C.; Elumalai, V.; Staffansson, J.; Cervin, G.; Le Norcy, T.; Denardou, H.; Réhel, K.; Moodie, L.W.K.; Hellio, C.; Pavia, H.; et al. Phidianidine A and synthetic analogues as naturally inspired marine antifoulants. *J. Nat. Prod.* **2020**, *83*, 3413–3423. [[CrossRef](#)]
22. Shamsi, F.; Hasan, P.; Queen, A.; Hussain, A.; Khan, P.; Zeya, B.; King, H.M.; Rana, S.; Garrison, J.; Alajmi, M.F.; et al. Synthesis and SAR studies of novel 1,2,4-oxadiazole-sulfonamide based compounds as potential anticancer agents for colorectal cancer therapy. *Bioorg. Chem.* **2020**, *98*, 103754. [[CrossRef](#)]
23. Caneschi, W.; Enes, K.B.; Carvalho de Mendonça, C.; de Souza Fernandes, F.; Miguel, F.B.; da Silva Martins, J.; Le Hyaric, M.; Pinho, R.R.; Duarte, L.M.; Leal de Oliveira, M.A.; et al. Synthesis and anticancer evaluation of new lipophilic 1,2,4 and 1,3,4-oxadiazoles. *Eur. J. Med. Chem.* **2019**, *165*, 18–30. [[CrossRef](#)]
24. Mohamed, M.F.A.; Marzouk, A.A.; Nafady, A.; El-Gamal, D.A.; Allam, R.M.; Abu-Rahma, G.E.-D.A.; El Subbagh, H.I.; Moustafa, A.H. Design, synthesis and molecular modeling of novel aryl carboximidamides and 3-aryl-1,2,4-oxadiazoles derived from indomethacin as potent anti-inflammatory iNOS/PGE2 inhibitors. *Bioorg. Chem.* **2020**, *105*, 104439. [[CrossRef](#)]

25. Il'in, M.V.; Sysoeva, A.A.; Bolotin, D.S.; Novikov, A.S.; Suslonov, V.V.; Rogacheva, E.V.; Kraeva, L.A.; Kukushkin, V.Y. Aminonitrone as highly reactive bifunctional synthons. An expedient one-pot route to 5-amino-1,2,4-triazoles and 5-amino-1,2,4-oxadiazoles—Potential antimicrobials targeting multi-drug resistant bacteria. *New J. Chem.* **2019**, *43*, 17358–17366. [[CrossRef](#)]
26. Kim, J.; Shin, J.S.; Ahn, S.; Han, S.B.; Jung, Y.-S. 3-Aryl-1,2,4-oxadiazole derivatives active against human rhinovirus. *ACS Med. Chem. Lett.* **2018**, *9*, 667–672. [[CrossRef](#)]
27. Dos Santos Filho, J.M.; de Queiroz, E.S.D.M.A.; Macedo, T.S.; Teixeira, H.M.P.; Moreira, D.R.M.; Challal, S.; Wolfender, J.L.; Queiroz, E.F.; Soares, M.B.P. Conjugation of N-acylhydrazone and 1,2,4-oxadiazole leads to the identification of active antimalarial agents. *Bioorg. Med. Chem.* **2016**, *24*, 5693–5701. [[CrossRef](#)]
28. Mohammad, B.D.; Baig, M.S.; Bhandari, N.; Siddiqui, F.A.; Khan, S.L.; Ahmad, Z.; Khan, F.S.; Tagde, P.; Jeandet, P. Heterocyclic compounds as dipeptidyl peptidase-IV inhibitors with special emphasis on oxadiazoles as potent anti-diabetic agents. *Molecules* **2022**, *27*, 6001. [[CrossRef](#)] [[PubMed](#)]
29. Wang, M.; Liu, T.; Chen, S.; Wu, M.; Han, J.; Li, Z. Design and synthesis of 3-(4-pyridyl)-5-(4-sulfamido-phenyl)-1,2,4-oxadiazole derivatives as novel GSK-3 β inhibitors and evaluation of their potential as multifunctional anti-Alzheimer agents. *Eur. J. Med. Chem.* **2021**, *209*, 112874. [[CrossRef](#)] [[PubMed](#)]
30. Nelson, J.B.; Fizazi, K.; Miller, K.; Higano, C.; Moul, J.W.; Akaza, H.; Morris, T.; McIntosh, S.; Pemberton, K.; Gleave, M. Phase 3, randomized, placebo-controlled study of zibotentan (ZD4054) in patients with castration-resistant prostate cancer metastatic to bone. *Cancer* **2012**, *118*, 5709–5718. [[CrossRef](#)] [[PubMed](#)]
31. Engebraaten, O.; Vollan, H.K.M.; Børresen-Dale, A.L. Triple-negative breast cancer and the need for new therapeutic targets. *Am. J. Pathol.* **2013**, *183*, 1064–1074. [[CrossRef](#)] [[PubMed](#)]
32. Yin, L.; Duan, J.J.; Bian, X.W.; Yu, S.C. Triple-negative breast cancer molecular subtyping and treatment progress. *Breast Cancer Res.* **2020**, *22*, 61. [[CrossRef](#)] [[PubMed](#)]
33. Li, Q.; Pan, S.; Xie, T.; Liu, H. MYC in T-cell acute lymphoblastic leukemia: Functional implications and targeted strategies. *Blood Sci.* **2021**, *3*, 65–70. [[CrossRef](#)] [[PubMed](#)]
34. Hegazy, M.F.; Dawood, M.; Mahmoud, N.; Elbadawi, M.; Sugimoto, Y.; Klauck, S.M.; Mohamed, N.; Efferth, T. 2 α -Hydroxyalantolactone from *Pulicaria undulata*: Activity against multidrug-resistant tumor cells and modes of action. *Phytomedicine* **2021**, *81*, 153409. [[CrossRef](#)]
35. Beaulieu, M.E.; Soucek, L. Finding MYCure. *Mol. Cell. Oncol.* **2019**, *6*, e1618178. [[CrossRef](#)]
36. Whitfield, J.R.; Soucek, L. The long journey to bring a Myc inhibitor to the clinic. *J. Cell Biol.* **2021**, *220*, e202103090. [[CrossRef](#)]
37. Ghobrial, A.; Flick, N.; Daly, R.; Hoffman, M.; Milcarek, C. ELL2 influences transcription elongation, splicing, Ig secretion and growth. *J. Mucosal Immunol. Res.* **2019**, *3*, 112.
38. Chen, Y.; Zhou, C.; Ji, W.; Mei, Z.; Hu, B.; Zhang, W.; Zhang, D.; Wang, J.; Liu, X.; Ouyang, G.; et al. ELL targets c-Myc for proteasomal degradation and suppresses tumour growth. *Nat. Commun.* **2016**, *7*, 11057. [[CrossRef](#)]
39. Newman, D.J.; Cragg, G.M. Natural products as sources of new drugs over the nearly four decades from 01/1981 to 09/2019. *J. Nat. Prod.* **2020**, *83*, 770–803. [[CrossRef](#)]
40. Yap, J.L.; Wang, H.; Hu, A.; Chauhan, J.; Jung, K.Y.; Gharavi, R.B.; Prochownik, E.V.; Fletcher, S. Pharmacophore identification of c-Myc inhibitor 10074-G5. *Bioorg. Med. Chem. Lett.* **2013**, *23*, 370–374. [[CrossRef](#)]
41. Hammoudeh, D.I.; Follis, A.V.; Prochownik, E.V.; Metallo, S.J. Multiple independent binding sites for small-molecule inhibitors on the oncoprotein c-Myc. *J. Am. Chem. Soc.* **2009**, *131*, 7390–7401. [[CrossRef](#)]
42. Massó-Vallés, D.; Soucek, L. Blocking Myc to treat cancer: Reflecting on two decades of omomyc. *Cells* **2020**, *9*, 883. [[CrossRef](#)] [[PubMed](#)]
43. Han, H.; Jain, A.D.; Truica, M.I.; Izquierdo-Ferrer, J.; Anker, J.F.; Lysy, B.; Sagar, V.; Luan, Y.; Chalmers, Z.R.; Unno, K.; et al. Small-molecule MYC inhibitors suppress tumor growth and enhance immunotherapy. *Cancer Cell* **2019**, *36*, 483–497. [[CrossRef](#)] [[PubMed](#)]
44. Boike, L.; Cioffi, A.G.; Majewski, F.C.; Co, J.; Henning, N.J.; Jones, M.D.; Liu, G.; McKenna, J.M.; Tallarico, J.A.; Schirle, M.; et al. Discovery of a functional covalent ligand targeting an intrinsically disordered cysteine within MYC. *Cell Chem. Biol.* **2021**, *28*, 4–13. [[CrossRef](#)] [[PubMed](#)]
45. Panda, D.; Saha, P.; Das, T.; Dash, J. Target guided synthesis using DNA nano-templates for selectively assembling a G-quadruplex binding c-MYC inhibitor. *Nat. Commun.* **2017**, *8*, 16103. [[CrossRef](#)]
46. Michel, J.; Cuchillo, R. The impact of small molecule binding on the energy landscape of the intrinsically disordered protein C-myc. *PLoS ONE* **2012**, *7*, e41070. [[CrossRef](#)]
47. Follis, A.V.; Hammoudeh, D.I.; Wang, H.; Prochownik, E.V.; Metallo, S.J. Structural rationale for the coupled binding and unfolding of the c-Myc oncoprotein by small molecules. *Chem. Biol.* **2008**, *15*, 1149–1155. [[CrossRef](#)]
48. Farrell, A.S.; Sears, R.C. MYC degradation. *Cold Spring Harb. Perspect. Med.* **2014**, *4*, a014365. [[CrossRef](#)]
49. Chen, Y.; Sun, X.-X.; Sears, R.C.; Dai, M.-S. Writing and erasing MYC ubiquitination and SUMOylation. *Genes Dis.* **2019**, *6*, 359–371. [[CrossRef](#)]
50. Lu, Y.; Liu, Y.; Yang, C. Evaluating In Vitro DNA Damage Using Comet Assay. *J. Vis. Exp.* **2017**, *128*, e56450. [[CrossRef](#)]
51. Goga, A.; Yang, D.; Tward, A.D.; Morgan, D.O.; Bishop, J.M. Inhibition of CDK1 as a potential therapy for tumors over-expressing MYC. *Nat. Med.* **2007**, *13*, 820–827. [[CrossRef](#)]
52. Gu, Y.; Rosenblatt, J.; Morgan, D.O. Cell cycle regulation of CDK2 activity by phosphorylation of Thr160 and Tyr15. *EMBO J.* **1992**, *11*, 3995–4005. [[CrossRef](#)]

53. Kurbegovic, A.; Trudel, M. The master regulators Myc and p53 cellular signaling and functions in polycystic kidney disease. *Cell. Signal.* **2020**, *71*, 109594. [[CrossRef](#)] [[PubMed](#)]
54. Kelly, G.L.; Grabow, S.; Glaser, S.P.; Fitzsimmons, L.; Aubrey, B.J.; Okamoto, T.; Valente, L.J.; Robati, M.; Tai, L.; Fairlie, W.D.; et al. Targeting of MCL-1 kills MYC-driven mouse and human lymphomas even when they bear mutations in p53. *Genes Dev.* **2014**, *28*, 58–70. [[CrossRef](#)] [[PubMed](#)]
55. Li, X.; He, S.; Ma, B. Autophagy and autophagy-related proteins in cancer. *Mol. Cancer* **2020**, *19*, 12. [[CrossRef](#)]
56. Kang, R.; Zeh, H.J.; Lotze, M.T.; Tang, D. The Beclin 1 network regulates autophagy and apoptosis. *Cell Death Differ.* **2011**, *18*, 571–580. [[CrossRef](#)]
57. Liu, W.J.; Ye, L.; Huang, W.F.; Guo, L.J.; Xu, Z.G.; Wu, H.L.; Yang, C.; Liu, H.F. p62 links the autophagy pathway and the ubiquitin–proteasome system upon ubiquitinated protein degradation. *Cell Mol. Biol. Lett.* **2016**, *21*, 29. [[CrossRef](#)] [[PubMed](#)]
58. Elbadawi, M.; Boulos, J.C.; Dawood, M.; Zhou, M.; Gul, W.; ElSohly, M.A.; Klauck, S.M.; Efferth, T. The novel artemisinin dimer isoniazide ELI-XXIII-98-2 induces c-MYC inhibition, DNA damage, and autophagy in leukemia cells. *Pharmaceutics* **2023**, *15*, 1107. [[CrossRef](#)]
59. Li, W.; Zhang, H.; Assaraf, Y.G.; Zhao, K.; Xu, X.; Xie, J.; Yang, D.H.; Chen, Z.S. Overcoming ABC transporter-mediated multidrug resistance: Molecular mechanisms and novel therapeutic drug strategies. *Drug Resist. Updates* **2016**, *27*, 14–29. [[CrossRef](#)]
60. Robey, R.W.; Pluchino, K.M.; Hall, M.D.; Fojo, A.T.; Bates, S.E.; Gottesman, M.M. Revisiting the role of ABC transporters in multidrug-resistant cancer. *Nat. Rev. Cancer* **2018**, *18*, 452–464. [[CrossRef](#)]
61. Tiwari, A.K.; Sodani, K.; Dai, C.L.; Ashby, C.R., Jr.; Chen, Z.S. Revisiting the ABCs of multidrug resistance in cancer chemotherapy. *Curr. Pharm. Biotechnol.* **2011**, *12*, 570–594. [[CrossRef](#)]
62. Doyle, L.; Ross, D.D. Multidrug resistance mediated by the breast cancer resistance protein BCRP (ABCG2). *Oncogene* **2003**, *22*, 7340–7358. [[CrossRef](#)]
63. Silva, R.; Vilas-Boas, V.; Carmo, H.; Dinis-Oliveira, R.J.; Carvalho, F.; de Lourdes Bastos, M.; Remião, F. Modulation of P-glycoprotein efflux pump: Induction and activation as a therapeutic strategy. *Pharmacol. Ther.* **2015**, *149*, 1–123. [[CrossRef](#)]
64. Szakács, G.; Paterson, J.K.; Ludwig, J.A.; Booth-Genthe, C.; Gottesman, M.M. Targeting multidrug resistance in cancer. *Nat. Rev. Drug Discov.* **2006**, *5*, 219–234. [[CrossRef](#)]
65. Modi, A.; Roy, D.; Sharma, S.; Vishnoi, J.R.; Pareek, P.; Elhence, P.; Sharma, P.; Purohit, P. ABC transporters in breast cancer: Their roles in multidrug resistance and beyond. *J. Drug Target.* **2022**, *30*, 927–947. [[CrossRef](#)] [[PubMed](#)]
66. Hall, M.D.; Handley, M.D.; Gottesman, M.M. Is resistance useless? Multidrug resistance and collateral sensitivity. *Trends Pharmacol. Sci.* **2009**, *30*, 546–556. [[CrossRef](#)] [[PubMed](#)]
67. Efferth, T.; Konkimalla, V.B.; Wang, Y.F.; Sauerbrey, A.; Meinhardt, S.; Zintl, F.; Mattern, J.; Volm, M. Prediction of broad spectrum resistance of tumors towards anticancer drugs. *Clin. Cancer Res.* **2008**, *14*, 2405–2412. [[CrossRef](#)]
68. Saeed, M.E.M.; Boulos, J.C.; Elhaboub, G.; Rigano, D.; Saab, A.; Loizzo, M.R.; Hassan, L.E.A.; Sugimoto, Y.; Piacente, S.; Tundis, R.; et al. Cytotoxicity of cucurbitacin E from *Citrullus colocynthis* against multidrug-resistant cancer cells. *Phytomedicine* **2019**, *62*, 152945. [[CrossRef](#)] [[PubMed](#)]
69. Saeed, M.E.M.; Mahmoud, N.; Sugimoto, Y.; Efferth, T.; Abdel-Aziz, H. Molecular determinants of sensitivity or resistance of cancer cells toward sanguinarine. *Front. Pharmacol.* **2018**, *9*, 136. [[CrossRef](#)]
70. Doyle, L.A.; Yang, W.; Abruzzo, L.V.; Krogmann, T.; Gao, Y.; Rishi, A.K.; Ross, D.D. A multidrug resistance transporter from human MCF-7 breast cancer cells. *Proc. Natl. Acad. Sci. USA* **1998**, *95*, 15665–15670. [[CrossRef](#)]
71. Kadioglu, O.; Cao, J.; Kosyakova, N.; Mrasek, K.; Liehr, T.; Efferth, T. Genomic and transcriptomic profiling of resistant CEM/ADR-5000 and sensitive CCRF-CEM leukaemia cells for unravelling the full complexity of multi-factorial multidrug resistance. *Sci. Rep.* **2016**, *6*, 36754. [[CrossRef](#)]
72. Efferth, T.; Sauerbrey, A.; Olbrich, A.; Gebhart, E.; Rauch, P.; Weber, H.O.; Hengstler, J.G.; Halatsch, M.E.; Volm, M.; Tew, K.D.; et al. Molecular modes of action of artesunate in tumor cell lines. *Mol. Pharmacol.* **2003**, *64*, 382–394. [[CrossRef](#)]
73. Kimmig, A.; Gekeler, V.; Neumann, M.; Frese, G.; Handgretinger, R.; Kardos, G.; Diddens, H.; Niethammer, D. Susceptibility of multidrug-resistant human leukemia cell lines to human interleukin 2-activated killer cells. *Cancer Res.* **1990**, *50*, 6793–6799.
74. Abdelfatah, S.; Böckers, M.; Asensio, M.; Kadioglu, O.; Klinger, A.; Fleischer, E.; Efferth, T. Isopetasin and S-isopetasin as novel P-glycoprotein inhibitors against multidrug-resistant cancer cells. *Phytomedicine* **2021**, *86*, 153196. [[CrossRef](#)]
75. O'Brien, J.; Wilson, I.; Orton, T.; Pognan, F. Investigation of the Alamar Blue (resazurin) fluorescent dye for the assessment of mammalian cell cytotoxicity. *Eur. J. Biochem.* **2000**, *267*, 5421–5426. [[CrossRef](#)]
76. Yin, X.; Giap, C.; Lazo, J.S.; Prochownik, E.V. Low molecular weight inhibitors of Myc-Max interaction and function. *Oncogene* **2003**, *22*, 6151–6159. [[CrossRef](#)]
77. Kallio, M.A.; Tuimala, J.T.; Hupponen, T.; Klemelä, P.; Gentile, M.; Scheinin, I.; Koski, M.; Käki, J.; Korpelainen, E.I. Chipster: User-friendly analysis software for microarray and other high-throughput data. *BMC Genom.* **2011**, *12*, 507. [[CrossRef](#)] [[PubMed](#)]
78. Zhou, M.; Boulos, J.C.; Klauck, S.M.; Efferth, T. The cardiac glycoside ZINC253504760 induces parthanatos-type cell death and G₂/M arrest via downregulation of MEK1/2 phosphorylation in leukemia cells. *Cell Biol. Toxicol.* **2023**, 1–27. [[CrossRef](#)] [[PubMed](#)]
79. Livak, K.J.; Schmittgen, T.D. Analysis of relative gene expression data using real-time quantitative PCR and the 2^{-ΔΔCT} method. *Methods* **2001**, *25*, 402–408. [[CrossRef](#)] [[PubMed](#)]
80. Benhusein, G.M.; Mutch, E.; Aburawi, S.; Williams, F.M. Genotoxic effect induced by hydrogen peroxide in human hepatoma cells using comet assay. *Libyan J. Med.* **2010**, *5*, 4637. [[CrossRef](#)]

81. Gyori, B.M.; Venkatachalam, G.; Thiagarajan, P.S.; Hsu, D.; Clement, M.V. OpenComet: An automated tool for comet assay image analysis. *Redox Biol.* **2014**, *2*, 457–465. [[CrossRef](#)] [[PubMed](#)]
82. Collins, A.R. The comet assay for DNA damage and repair. *Mol. Biotechnol.* **2004**, *26*, 249–261. [[CrossRef](#)] [[PubMed](#)]
83. Crowley, L.C.; Marfell, B.J.; Scott, A.P.; Waterhouse, N.J. Quantitation of apoptosis and necrosis by annexin V binding, propidium iodide uptake, and flow cytometry. *Cold Spring Harb. Protoc.* **2016**, *2016*, 953–957. [[CrossRef](#)] [[PubMed](#)]
84. Shynkar, V.V.; Klymchenko, A.S.; Kunzelmann, C.; Duportail, G.; Muller, C.D.; Demchenko, A.P.; Freyssinet, J.-M.; Mely, Y. Fluorescent biomembrane probe for ratiometric detection of apoptosis. *J. Am. Chem. Soc.* **2007**, *129*, 2187–2193. [[CrossRef](#)] [[PubMed](#)]

Disclaimer/Publisher’s Note: The statements, opinions and data contained in all publications are solely those of the individual author(s) and contributor(s) and not of MDPI and/or the editor(s). MDPI and/or the editor(s) disclaim responsibility for any injury to people or property resulting from any ideas, methods, instructions or products referred to in the content.

Curriculum Vitae of Min Zhou

Date of birth: 29 January 1994; Place of birth: Kunming, China;

E-mail: minzhou1@uni-mainz.de;

Phone: +49(0)15257225218

Address: Staudinger Weg 5, 55128 Mainz, Germany



Education

- **Johannes Gutenberg-Universität Mainz**, Mainz, Germany
Ph. D candidate for Pharmaceutical Biology, October 2019-present, expected defense: October 2023
 Supervisor: Prof. Dr. Thomas Efferth
- **Kunming Institute of Botany, University Chinese Academy of Sciences (UCAS)**, Kunming and Beijing, China
Master, Ethnobotany, 2016-2019
 Supervisor: Prof. Xuefei Yang
- **Yunnan Agricultural University**, Kunming, China
Bachelor, Land Resource Management, 2012-2016

Research experience

- Ph.D. candidate: Prof. Dr. Thomas Efferth's group, Johannes Gutenberg-Universität Mainz
 - 1) Molecular mode of action and parthanatic cell death of a novel cardiac glycoside compound targets **MEK1/2** in leukemia cells.
 - 2) Molecular mode of action of a 1,2,4-oxadiazole derivate targets **c-MYC** in leukemia and triple-negative breast cancer cells.
 - 3) **Parthanatic cell death** of synthesized palladium (II) -based compounds to overcome anti-apoptosis and anti-autophagy in leukemia cells.
- Master student: Prof. Xuefei Yang's group, Kunming Institute of Botany, Chinese Academy of Sciences
 - 1) Ethnobotany research, nutritional and functional evaluation on **edible flowers** in Yunnan, China.
 - 2) Traditional medicine in Myanmar: isolation of potential **anti-diabetic** compounds from medical plants
 - 3) Traditional Tibetan herbal medicine and Ethnobotany: verification of plant extracts against **anti-cold stress** in *Caenorhabditis elegans*.

Awards, Honors & Activities

- Special Award of Best Poster Presentation, 7th Cancer World Congress, Palermo, Italy, 2023.
- Special Award of Best Flash Oral Presentation, 6th Cancer World Congress, Lisbon, Portugal, 2022.
- Outstanding Performance Award, 5th Youth Forum, Kunming Institute of Botany, Kunming, China,

2019.

- Honours Student, University of Chinese Academy of Sciences, Beijing, China, 2017.
- Merit Award, 11th Student Academic and Scientific Works Competition, Yunnan Agricultural University, Kunming, China, 2015.
- Outstanding Volunteers, 1st China-South Asia Exposition, Kunming, China, 2015.

Personal Skills

Laboratory skills	Software and analysis	Language
<ul style="list-style-type: none"> • Cell culture (leukemia, breast, colon, kidney, glioblastoma, osteosarcoma cancer cells) • Cell growth inhibition assay • Isolation of peripheral blood mononuclear cells • Western blotting • PCR • qRT-PCR • Single cell electrophoresis • Wound healing assay • Immunofluorescence microscopy • Flow cytometry (cell cycle, apoptosis, ROS, mitochondrial membrane potential) • Luciferase assay • mRNA and DNA extraction • Bioinformatical evaluation of microarray hybridization • Mycoplasma detection 	<ul style="list-style-type: none"> • Ingenuity Pathway Analysis • Chipster • Autodock • Pyrx Virtual Screening • Prism-GraphPad • Origin • Image J • R programming • Swiss target prediction • String protein-protein interaction network • Visual Molecular Dynamics • FlowJo • ArcGIS • Motif Enrichment Analysis 	<ul style="list-style-type: none"> • Chinese (native) • English • German (Level: A2.2)

Scholarships

- Doctoral Scholarship, Chinese Scholarship Council, 48 months, October 2019-September 2023
- Exchange Student Scholarship, Kagoshima University (Japan), 2 weeks, 2015.
- The First Prize Scholarship, Yunnan Agricultural University, 12 months, 2013.

Teaching experience

- Pharmacological Biology III, Johannes Gutenberg-Universität Mainz, 2020-present
 - 1) Responsible for Quality control: Identification of *Panax ginseng* by PCR;
 - 2) Quantitative analytics of caraway oil.

Conference

- 1) 7th Cancer World Congress, Palermo, Italy, May 28th - 30th, 2023. (Awarded with Best Poster Presentation of Young Researcher)
- 2) 6th Cancer World Congress, Lisbon, Portugal, September 28th - 30th, 2022. (Awarded with Best Flash Oral Presentation of Young Researcher)
- 3) 9th National Symposium on Ethnobotany and 8th Asia-Pacific Forum on Ethnobotany, Huhhot, China, July 16-18 2016.

Book chapters and contributions

- Common Research Methods in Ethnobotany. Chapter: Relative importance values. Zhejiang Education Publishing House, 2018 (Writing).
- Typical Vegetables in Myanmar, Press of University of Science and Technology of China, 2018. (Collection of plant information and photographs).